Phenotyping cardiometabolic disease with magnetic resonance techniques

Paiman, E.H.M.

Elisabeth H.M. Paiman

PHENOTYPING

Cardiometabolic Disease

with Magnetic Resonance Techniques

Phenotyping Cardiometabolic Disease with Magnetic Resonance Techniques

Elisabeth Helena Maria Paiman

Phenotyping Cardiometabolic Disease with Magnetic Resonance Techniques

Cover design: E.H.M. Paiman & Optima Grafische Communicatie
Lay-out: E.H.M. Paiman
Printed by: Optima Grafische Communicatie
ISBN: 978-94-6361-449-8

Phenotyping Cardiometabolic Disease with Magnetic Resonance Techniques

Proefschrift

ter verkrijging van
de graad van Doctor aan de Universiteit Leiden,
op gezag van Rector Magnificus prof. mr. C.J.J.M. Stolker,
volgens besluit van het College voor Promoties
te verdedigen op donderdag 1 oktober 2020
klokke 15.00 uur

door

Elisabeth Helena Maria Paiman
geboren te Leiderdorp
in 1988

Promotor	Prof. dr. H.J. Lamb
Copromotores	Dr. ir. R.J. van der Geest Dr. I.M. Jazet
Leden promotiecommissie	Dr. R.N. Planken (Amsterdam UMC) Prof. dr. S. Middeldorp (Amsterdam UMC) Prof. dr. H. Pijl

The work described in this thesis was performed at the department of Radiology, Leiden University Medical Center, Leiden, the Netherlands. Research was financially supported by the Cardio Vascular Imaging Group (CVIG), Leiden, the Netherlands. Part of this work was funded by NWO Domain Applied and Engineering Sciences, grant number 12899. Another part of the research described in this thesis was financially supported by Novo Nordisk A/S, Bagsvaerd, Denmark. Financial support by the Dutch Heart Foundation for the publication of this thesis is gratefully acknowledged. Additional financial support for the printing of this thesis was kindly provided by Medis Medical Imaging Systems bv.

TABLE OF CONTENTS

CHAPTER

General introduction and outline

GENERAL INTRODUCTION AND OUTLINE

Over the past decades, the number of individuals with type 2 diabetes has been growing worldwide (1,2), which is largely driven by the increasing prevalence of obesity (3-5). Type 2 diabetes is a major health concern, as it is related to several conditions, including heart failure (6,7) and coronary heart disease (8,9). Despite remarkable advances in cardiovascular prevention and treatment, heart disease remains a common cause of death and an important contributor to health loss globally (10,11).

The aim of the studies in this thesis was to gain more insight into diabetic cardiomyopathy and the cardiometabolic actions of type 2 diabetes medication by using magnetic resonance techniques (Part I). In addition, we aimed to contribute to improving cardiovascular risk stratification in individuals who received hematopoietic stem cell transplantation in childhood, which is associated with cardiometabolic disease later in life (Part II), and in patients with ischemic heart disease, who have an increased susceptibility of ventricular arrhythmia (Part III).

Phenotypic Characterization with Magnetic Resonance Techniques

In this thesis, we used a variety of magnetic resonance methods for the phenotypic characterization of cardiometabolic disease. Whereas the concept 'phenotype' initially referred to the outward appearance of an organism (12), today, this term has also been adopted to describe the manifestation of disease as characterized by radiologic imaging techniques (13). The disease phenotype is the result of a complex interaction between genetic predisposition and environmental conditions, including socioeconomic, occupational and behavioral factors. Starting from the mid-twentieth century, there has been an increasing awareness of the relationship between health behavior and disease, especially in cardiovascular medicine. For example, in 1953, the first study was published on the relation of physical activity to coronary heart disease (14). With the growing evidence of the role of modifiable risk factors (15), contemporary cardiology has expanded its focus beyond treatment to include prevention and early detection of disease. As part of personalized medicine, there is more and more interest in both genotypic and phenotypic characterization, which may help to identify high-risk groups for cardiometabolic diseases and to select appropriate treatment strategies for specific patient populations (16).

Whereas medical research in the fifteenth century was more or less confined to human anatomy (17), the area of physiology started to develop in the mid-ninetieth century (18). In the last hundred years, research in the field of cell and molecular biology has resulted in important insights in human biological processes (18). At present, organ-based but also system-wise thinking is part of medical reasoning (19). Interestingly, in view of the super specialization of medical disciplines, some argue that doctors should also have a generalist approach to medical care (20). For example, obesity and type 2 diabetes are closely related to cardiovascular health

and, in this respect, holistic thinking beyond the highly specialized fields of, for example, internal medicine, cardiology and radiology may be beneficial for patient outcome.

The studies in this thesis were performed in the department of Radiology and were in close collaboration with the department of Internal Medicine. We used several cardiovascular magnetic resonance techniques including 2D and 4D flow imaging, feature tracking cine imaging, T1 mapping and proton-magnetic resonance spectroscopy (^{1}H-MRS). With these methods, it is possible to assess anatomical structures but also organ function and tissue characteristics (21). As such, the thought behind this thesis was that imaging-based phenotyping in radiology might contribute to insights into mechanisms of diseases in the field of internal medicine.

Part I Type 2 Diabetes

Type 2 diabetes has become a major public health challenge, as its prevalence is increasing worldwide due to lifestyle changes related to economic development, rapid urbanization and population aging (2). Whereas type 2 diabetes was affecting 4.7% of the global population in 1980, the world prevalence had risen to 8.5% by 2014 (1).

Although obesity, unhealthy diet and physical inactivity are strong risk factors for the development of type 2 diabetes (22-25), type 2 diabetes is most likely to represent a complex interplay between genetic susceptibility and environmental factors. In the United States, highest prevalences of type 2 diabetes have been reported among Hispanic, Asian and African American individuals (22.6%, 21.8% and 20.6%, respectively, compared with 11.3% in individuals of European descent) (26), whereas in the Netherlands, the highest prevalence of type 2 diabetes has been documented among South Asian Surinamese (16.7% (35-44 years) and 35.0% (45-60 years), as compared with 4.2% and 8.2%, respectively, among ethnic Dutch) (27). Although environmental conditions, for example cultural and socioeconomic factors, vary between ethnic groups, the disparities in type 2 diabetes prevalence may be in part explained by genetic predisposition (28). Proposed mechanisms for the increased risk of type 2 diabetes among South Asian ethnicities comprise a susceptibility to visceral rather than subcutaneous fat storage, a high mitochondrial efficiency, an intrauterine disadvantageous environment and low vitamin D serum levels, in combination with lifestyle factors including a high carbohydrate diet and insufficient physical activity (29).

In the Framingham Heart Study in 1974, for the first time, the association between type 2 diabetes and congestive heart failure, independent of other cardiovascular risk factors, was documented in a large, population-based study (6). The risk of congestive heart failure associated with type 2 diabetes was approximately two to five times increased for men and women, respectively (6). Similarly, other observations have reported rate ratios of incident heart failure of 1.85–2.5 in individuals with compared to those without type 2 diabetes (7,30). Furthermore, a recent study including 1.9 million people has shown that heart failure is a

common initial presentation of cardiovascular disease in type 2 diabetes, accounting for 14.1% of the first cardiovascular manifestations (31). Likewise, another study in older patients with type 2 diabetes has demonstrated that heart failure often develops in the absence of ischemic heart disease (among the individuals who developed heart failure, 27.2% had no preceding of concomitant vascular event and 36.8% had no prior coronary artery disease), and, importantly, heart failure hospitalization in type 2 diabetes patients was associated with high mortality, also in individuals without coronary artery disease (the annual mortality rate after heart failure hospitalization was 21.3% and 24.6% in type 2 diabetes patients with and without preceding vascular disease, respectively) (32). In this context, it has been argued that there should be more attention to heart failure as complication of type 2 diabetes, also in the absence of ischemic cardiomyopathy (33).

Heart failure in type 2 diabetes patients without prior myocardial infarction is characterized by preserved ejection fraction, and is preceded by progressive diastolic dysfunction (34). Heart failure with preserved ejection fraction (HFpEF) in patients with type 2 diabetes is considered to be multifactorial, resulting from coronary atherosclerosis, high blood pressure, extracellular fluid volume expansion and, possibly, diabetic cardiomyopathy (35). The concept 'diabetic cardiomyopathy' has been introduced to refer to the direct detrimental effect of type 2 diabetes on the myocardium, independent of other conditions such as coronary artery disease or hypertension (36), but there is no agreed definition (34). Molecular mechanisms which have been implicated in diabetic cardiomyopathy comprise coronary microvascular dysfunction, chronic inflammation, disturbed insulin and renin-angiotensin-aldosterone signaling, lipotoxicity, altered substrate metabolism, impaired calcium handling, mitochondrial dysfunction, modification of structural proteins by advanced glycation end-products, and perturbations in cell homeostatic processes including apoptosis, autophagy and endoplasmic reticulum stress (37,38).

Although diabetic cardiomyopathy has been recognized as a distinct clinical entity (39), the pathogenesis is still incompletely understood and the phenotypic characterization remains to be elucidated (40,41). Also, until recently, there were no glucose-lowering agents with cardioprotective effects to reduce the risk of heart failure in type 2 diabetes patients (42,43). In Part I, we explored the imaging features of diabetic cardiomyopathy and investigated the effects of an antidiabetic agent with potentially beneficial effects on intrinsic myocardial function.

Chapter 2

The difficulty in characterizing diabetic cardiomyopathy is the strong association between obesity and type 2 diabetes, with approximately 80 percent of the type 2 diabetes patients being obese (44). Therefore, the separation of the cardiovascular effects of type 2 diabetes, obesity or other factors associated with type 2 diabetes and obesity is challenging (45). The population-based Netherlands Epidemiology of Obesity (NEO) study from Leiden was designed

to disentangle the pathways leading to common disease in obesity (46). In Chapter 2, we examined the role of insulin resistance in cardiovascular remodeling in individuals with obesity from the NEO cohort. Strength of this study was the assessment of specific adiposity metrics rather than overall measures of obesity (eg, body weight), which enabled the adjustment for the confounding effects of adipose tissue.

Chapter 3

In the population-based study in Chapter 2, we evaluated standard magnetic resonance parameters of cardiac structure and function. Nonetheless, magnetic resonance also allows for the assessment of myocardial steatosis (47) and diffuse fibrosis (48), as well as cardiac strain as a more sensitive measure of systolic function (49), which were examined in Chapter 3. It has been hypothesized that these myocardial tissue characteristics may be affected in type 2 diabetes, preceding abnormalities in diastolic function (50,51).

Furthermore, there has been limited research on the putative differences in diabetic cardiomyopathy among different type 2 diabetes patient groups, although the pathogenesis of type 2 diabetes and type 2 diabetes-related cardiovascular disease seems different in South Asian compared with other ethnicities (29,52,53). It is known that individuals of South Asian descent have a high risk of developing coronary heart disease, which is not completely explained by excess cardiometabolic risk factors (54). Furthermore, in South Asians, type 2 diabetes increases the mortality of ischemic heart disease nearly threefold, while in Europeans, the excess mortality related to type 2 diabetes estimates 1.5-fold (55). Likewise, previous findings indicate that the etiology of HFpEF in type 2 diabetes may be distinct in South Asian compared with other ethnic groups. For example, it has been demonstrated that the impact of type 2 diabetes on cardiac function is worse in South Asians than in Europeans (56). Furthermore, the population attributable risk of type 2 diabetes for HFpEF appears to be higher among South Asians, as type 2 diabetes is threefold more common in HFpEF patients of South Asian than in those of European origin (56). Also, type 2 diabetes has been reported to have a more adverse impact on heart failure hospitalization and mortality in individuals of South Asian than those of European ethnicity (57). Thus far, it has not been demonstrated that the treatment of type 2 diabetes or the prevention of type 2 diabetes-related cardiovascular disease should be different in South Asians. Nonetheless, because of the disparities in cardiometabolic profile between ethnic groups, current guidelines take ethnicity into account in recommendations for cardiovascular risk management and screening for type 2 diabetes (58). For example, body mass index (BMI) cut points to define overweight are lower for South Asians (BMI >23 kg/m^2 instead of BMI >25 kg/m^2) (59,60). Also, screening for type 2 diabetes is justified above 35 years among South Asians, compared with screening at the age of 45 years and older in other ethnic groups (27).

In the area of The Hague, a large percentage of the type 2 diabetes population is of Surinamese Hindustani descent. In Chapter 3, we aimed to characterize diabetic

cardiomyopathy by using various magnetic resonance techniques, and, additionally, in view of the ethnic differences regarding type 2 diabetes and diabetic heart failure, we compared the cardiovascular remodeling characteristics between Dutch South Asian and Dutch European type 2 diabetes groups.

Chapter 4 and 5

In recent years, several types of antidiabetic agents have been introduced including liraglutide. Liraglutide is a long-acting, glucagon-like peptide 1 (GLP-1) receptor agonist, which, in contrast to native GLP-1, is resistant to degradation by dipeptidyl peptidase 4 (DPP-4) (61). Liraglutide influences blood glucose levels through several mechanisms, including increase of glucose-dependent insulin secretion, decrease of postprandial glucagon, slowed gastric emptying and reduced food intake (62). Because of the excess cardiovascular burden in type 2 diabetes patients and the concerns about potentially higher cardiovascular risks associated with certain antidiabetic agents, since 2008, authorities have mandated cardiovascular safety trials to secure the approval of novel glucose-lowering drugs (63). In the months that we started with the liraglutide study in Leiden, the results of such a cardiovascular safety trial (the LEADER trial) were published. The LEADER trial reported that liraglutide compared to placebo added to standard care is beneficial for cardiovascular mortality in patients with type 2 diabetes and high cardiovascular risk, presumably because of anti-atherosclerotic effects (64). In addition, in prior preclinical and clinical studies, liraglutide proved to exert pleiotropic favorable effects on blood pressure, lipids, inflammation and other metabolic factors (62). However, the effect of liraglutide on intrinsic myocardial function in type 2 diabetes patients with asymptomatic heart failure remained to be addressed.

Previously in Leiden, the effect of the antidiabetic agent pioglitazone on diastolic function has been investigated (65). This thesis reports the results of a similar trial on the effect of liraglutide on diastolic function in type 2 diabetes patients of South Asian descent living in the Netherlands, whereas a parallel study was performed in Dutch European type 2 diabetes patients (66). In Chapter 4, we described the metabolic effects of liraglutide (effects on ectopic fat accumulation and glucose regulation), and in Chapter 5, we assessed the cardiovascular actions of liraglutide (effects on cardiac diastolic and systolic function, aortic stiffness, myocardial triglyceride content and myocardial extracellular volume) in Dutch South Asian type 2 diabetes patients.

Part II Pediatric Hematopoietic Stem Cell Transplantation

Chapter 6

As the long-term survival after pediatric hematopoietic stem cell transplantation has been improved drastically, current research is aimed at enhancing quality of life (67,68). From previous studies it is known that pre-transplant or transplant-related therapies in childhood

are associated with several risks in adulthood, including endocrine and cardiovascular disease (69,70). In Chapter 6, we aimed to find early magnetic resonance-derived features which may be used to select patients at high cardiovascular risk who may require frequent follow-up.

Part III Ischemic Heart Disease

Chapter 7 and 8

In Part I, we examined diastolic dysfunction as complication of obesity and type 2 diabetes. However, metabolically unhealthy individuals have an increased susceptibility of developing HFpEF, but they are also at risk of heart failure with reduced ejection fraction (HFrEF). Although the clinical expression of HFpEF and HFrEF is similar (symptoms of dyspnea, fatigue, exercise intolerance and signs of edema), HFpEF and HFrEF are two separate entities with distinct pathogeneses and epidemiologic differences (71). In general, HFrEF (or systolic heart failure) is caused by coronary artery disease, whereas hypertension, obesity and type 2 diabetes are frequent conditions in HFpEF (or diastolic heart failure) (40,72). In Part III, we addressed ischemic heart disease and heart failure after myocardial infarction.

In Chapter 7, we reviewed the currently available cardiovascular magnetic resonance techniques, with special attention given to the protocols without use of gadolinium-based contrast material. Late gadolinium enhancement (LGE) imaging is an important technique for the clinical evaluation of myocardial scar (73). Interestingly, native T1 mapping may evolve as a non-contrast alternative for myocardial tissue characterization in ischemic heart disease (74).

An important risk in patients with prior myocardial infarction and low ejection fraction is sudden death due to ventricular arrhythmia, but also non-sudden death due to decompensated HFrEF (75). In Chapter 8, we retrospectively evaluated the cardiac magnetic resonance examinations of patients with ischemic heart disease and implantable cardioverter defibrillator (ICD) therapy. We hypothesized that left ventricular function parameters, which are known to be associated with cardiac remodeling, may be used as risk stratifiers for ventricular arrhythmia and decompensated heart failure in post-infarct patients with highly depressed systolic function. In this hypothesis-generating study we assessed the associations between systolic and diastolic strain parameters and the risk of appropriate ICD therapy and all-cause mortality, as surrogate markers of ventricular arrhythmia and decompensated heart failure, respectively.

OBJECTIVES

The general aim of the studies presented in this thesis was to characterize cardiovascular remodeling associated with metabolic disturbances, using various magnetic resonance techniques. It was hypothesized that imaging-based phenotyping may contribute to a better understanding of cardiometabolic disease and help to identify patients at increased cardiovascular risk. We investigated the cardiovascular phenotype in relation to type 2 diabetes and in response to treatment with liraglutide (Part I), after hematopoietic stem cell transplantation (Part II) and in ischemic heart disease (Part III).

REFERENCES

1. NCD Risk Factor Collaboration. Worldwide trends in diabetes since 1980: a pooled analysis of 751 population-based studies with 4.4 million participants. Lancet 2016;387(10027):1513-1530.
2. Zheng Y, Ley SH, Hu FB. Global aetiology and epidemiology of type 2 diabetes mellitus and its complications. Nat Rev Endocrinol 2018;14(2):88-98.
3. NCD Risk Factor Collaboration. Worldwide trends in body-mass index, underweight, overweight, and obesity from 1975 to 2016: a pooled analysis of 2416 population-based measurement studies in 128.9 million children, adolescents, and adults. Lancet 2017;390(10113):2627-2642.
4. Ng M, Fleming T, Robinson M, et al. Global, regional, and national prevalence of overweight and obesity in children and adults during 1980-2013: a systematic analysis for the Global Burden of Disease Study 2013. Lancet 2014;384(9945):766-781.
5. Kahn SE, Hull RL, Utzschneider KM. Mechanisms linking obesity to insulin resistance and type 2 diabetes. Nature 2006;444(7121):840-846.
6. Kannel WB, Hjortland M, Castelli WP. Role of diabetes in congestive heart failure: the Framingham study. Am J Cardiol 1974;34(1):29-34.
7. He J, Ogden LG, Bazzano LA, Vupputuri S, Loria C, Whelton PK. Risk factors for congestive heart failure in US men and women: NHANES I epidemiologic follow-up study. Arch Intern Med 2001;161(7):996-1002.
8. Emerging Risk Factors Collaboration, Sarwar N, Gao P, et al. Diabetes mellitus, fasting blood glucose concentration, and risk of vascular disease: a collaborative meta-analysis of 102 prospective studies. Lancet 2010;375(9733):2215-2222.
9. Alexander CM, Landsman PB, Teutsch SM. Diabetes mellitus, impaired fasting glucose, atherosclerotic risk factors, and prevalence of coronary heart disease. Am J Cardiol 2000;86(9):897-902.
10. Roth GA, Johnson C, Abajobir A, et al. Global, Regional, and National Burden of Cardiovascular Diseases for 10 Causes, 1990 to 2015. J Am Coll Cardiol 2017;70(1):1-25.
11. GBD Disease and Injury Incidence and Prevalence Collaborators. Global, regional, and national incidence, prevalence, and years lived with disability for 354 diseases and injuries for 195 countries and territories, 1990-2017: a systematic analysis for the Global Burden of Disease Study 2017. Lancet 2018;392(10159):1789-1858.
12. Johannsen W. The Genotype Conception of Heredity. The American Naturalist 1911;45(531):129-159.
13. Bycroft C, Freeman C, Petkova D, et al. The UK Biobank resource with deep phenotyping and genomic data. Nature 2018;562(7726):203-209.
14. Morris JN, Heady JA, Raffle PA, Roberts CG, Parks JW. Coronary heart-disease and physical activity of work. Lancet 1953;262(6796):1111-1120; concl.
15. Yusuf S, Hawken S, Ounpuu S, et al. Effect of potentially modifiable risk factors associated with myocardial infarction in 52 countries (the INTERHEART study): case-control study. Lancet 2004;364(9438):937-952.
16. UK Biobank data on 500,000 people paves way to precision medicine. Nature 2018;562(7726):163-164.
17. Standring S. A brief history of topographical anatomy. J Anat 2016;229(1):32-62.
18. Morriss-Kay G. The Journal of Anatomy: origin and evolution. J Anat 2016;229(1):2-31.
19. Kaplan DM. Perspective: Whither the problem list? Organ-based documentation and deficient synthesis by medical trainees. Acad Med 2010;85(10):1578-1582.
20. Rimmer A. The UK needs more generalists, but where will they come from? BMJ 2017;356:j1116.
21. Salerno M, Sharif B, Arheden H, et al. Recent Advances in Cardiovascular Magnetic Resonance: Techniques and Applications. Circ Cardiovasc Imaging 2017;10(6).
22. Juonala M, Magnussen CG, Berenson GS, et al. Childhood adiposity, adult adiposity, and cardiovascular risk factors. N Engl J Med 2011;365(20):1876-1885.
23. Hu FB, Manson JE, Stampfer MJ, et al. Diet, lifestyle, and the risk of type 2 diabetes mellitus in women. N Engl J Med 2001;345(11):790-797.
24. Nettleton JA, Steffen LM, Ni H, Liu K, Jacobs DR, Jr. Dietary patterns and risk of incident type 2 diabetes in the Multi-Ethnic Study of Atherosclerosis (MESA). Diabetes Care 2008;31(9):1777-1782.
25. Auchincloss AH, Diez Roux AV, Mujahid MS, Shen M, Bertoni AG, Carnethon MR. Neighborhood

resources for physical activity and healthy foods and incidence of type 2 diabetes mellitus: the Multi-Ethnic study of Atherosclerosis. Arch Intern Med 2009;169(18):1698-1704.
26. Menke A, Casagrande S, Geiss L, Cowie CC. Prevalence of and Trends in Diabetes Among Adults in the United States, 1988-2012. JAMA 2015;314(10):1021-1029.
27. Bindraban NR, van Valkengoed IG, Mairuhu G, et al. Prevalence of diabetes mellitus and the performance of a risk score among Hindustani Surinamese, African Surinamese and ethnic Dutch: a cross-sectional population-based study. BMC Public Health 2008;8:271.
28. Chen L, Magliano DJ, Zimmet PZ. The worldwide epidemiology of type 2 diabetes mellitus--present and future perspectives. Nat Rev Endocrinol 2011;8(4):228-236.
29. Bakker LE, Sleddering MA, Schoones JW, Meinders AE, Jazet IM. Pathogenesis of type 2 diabetes in South Asians. Eur J Endocrinol 2013;169(5):R99-R114.
30. Nichols GA, Gullion CM, Koro CE, Ephross SA, Brown JB. The incidence of congestive heart failure in type 2 diabetes: an update. Diabetes Care 2004;27(8):1879-1884.
31. Shah AD, Langenberg C, Rapsomaniki E, et al. Type 2 diabetes and incidence of cardiovascular diseases: a cohort study in 1.9 million people. Lancet Diabetes Endocrinol 2015;3(2):105-113.
32. Khan H, Kalogeropoulos AP, Zannad F, et al. Incident heart failure in relation to vascular disease: insights from the Health, Aging, and Body Composition Study. Eur J Heart Fail 2014;16(5):526-534.
33. Bell DS. Heart failure: the frequent, forgotten, and often fatal complication of diabetes. Diabetes Care 2003;26(8):2433-2441.
34. Seferovic PM, Petrie MC, Filippatos GS, et al. Type 2 diabetes mellitus and heart failure: a position statement from the Heart Failure Association of the European Society of Cardiology. Eur J Heart Fail 2018;20(5):853-872.
35. Boudina S, Abel ED. Diabetic cardiomyopathy revisited. Circulation 2007;115(25):3213-3223.
36. Rubler S, Dlugash J, Yuceoglu YZ, Kumral T, Branwood AW, Grishman A. New type of cardiomyopathy associated with diabetic glomerulosclerosis. Am J Cardiol 1972;30(6):595-602.
37. Paulus WJ, Tschope C. A novel paradigm for heart failure with preserved ejection fraction: comorbidities drive myocardial dysfunction and remodeling through coronary microvascular endothelial inflammation. J Am Coll Cardiol 2013;62(4):263-271.
38. Bugger H, Abel ED. Molecular mechanisms of diabetic cardiomyopathy. Diabetologia 2014;57(4):660-671.
39. Richardson P, McKenna W, Bristow M, et al. Report of the 1995 World Health Organization/ International Society and Federation of Cardiology Task Force on the Definition and Classification of cardiomyopathies. Circulation 1996;93(5):841-842.
40. Seferovic PM, Paulus WJ. Clinical diabetic cardiomyopathy: a two-faced disease with restrictive and dilated phenotypes. Eur Heart J 2015;36(27):1718-1727, 1727a-1727c.
41. Marwick TH, Ritchie R, Shaw JE, Kaye D. Implications of Underlying Mechanisms for the Recognition and Management of Diabetic Cardiomyopathy. J Am Coll Cardiol 2018;71(3):339-351.
42. Hupfeld C, Mudaliar S. Navigating the "MACE" in Cardiovascular Outcomes Trials and decoding the relevance of Atherosclerotic Cardiovascular Disease benefits versus Heart Failure benefits. Diabetes Obes Metab 2019;21(8):1780-1789.
43. Gilbert RE, Krum H. Heart failure in diabetes: effects of anti-hyperglycaemic drug therapy. Lancet 2015;385(9982):2107-2117.
44. Scheen AJ, Van Gaal LF. Combating the dual burden: therapeutic targeting of common pathways in obesity and type 2 diabetes. Lancet Diabetes Endocrinol 2014;2(11):911-922.
45. Wang J, Song Y, Wang Q, Kralik PM, Epstein PN. Causes and characteristics of diabetic cardiomyopathy. Rev Diabet Stud 2006;3(3):108-117.
46. de Mutsert R, den Heijer M, Rabelink TJ, et al. The Netherlands Epidemiology of Obesity (NEO) study: study design and data collection. Eur J Epidemiol 2013;28(6):513-523.
47. de Heer P, Bizino MB, Lamb HJ, Webb AG. Parameter optimization for reproducible cardiac (1) H-MR spectroscopy at 3 Tesla. J Magn Reson Imaging 2016;44(5):1151-1158.
48. Taylor AJ, Salerno M, Dharmakumar R, Jerosch-Herold M. T1 Mapping: Basic Techniques and Clinical Applications. JACC Cardiovasc Imaging 2016;9(1):67-81.
49. Schuster A, Hor KN, Kowallick JT, Beerbaum P, Kutty S. Cardiovascular Magnetic Resonance Myocardial Feature Tracking: Concepts and Clinical Applications. Circ Cardiovasc Imaging 2016;9(4):e004077.
50. Ng AC, Delgado V, Bertini M, et al. Myocardial steatosis and biventricular strain and strain

rate imaging in patients with type 2 diabetes mellitus. Circulation 2010;122(24):2538-2544.
51. Shah RV, Abbasi SA, Neilan TG, et al. Myocardial tissue remodeling in adolescent obesity. J Am Heart Assoc 2013;2(4):e000279.
52. Barnett AH, Dixon AN, Bellary S, et al. Type 2 diabetes and cardiovascular risk in the UK south Asian community. Diabetologia 2006;49(10):2234-2246.
53. Patel SA, Shivashankar R, Ali MK, et al. Is the "South Asian Phenotype" Unique to South Asians?: Comparing Cardiometabolic Risk Factors in the CARRS and NHANES Studies. Glob Heart 2016;11(1):89-96 e83.
54. Tillin T, Hughes AD, Mayet J, et al. The relationship between metabolic risk factors and incident cardiovascular disease in Europeans, South Asians, and African Caribbeans: SABRE (Southall and Brent Revisited) -- a prospective population-based study. J Am Coll Cardiol 2013;61(17):1777-1786.
55. Forouhi NG, Sattar N, Tillin T, McKeigue PM, Chaturvedi NJD. Do known risk factors explain the higher coronary heart disease mortality in South Asian compared with European men? Prospective follow-up of the Southall and Brent studies, UK. 2006;49(11):2580-2588.
56. Park CM, Tillin T, March K, et al. Hyperglycemia has a greater impact on left ventricle function in South Asians than in Europeans. Diabetes Care 2014;37(4):1124-1131.
57. Bank IEM, Gijsberts CM, Teng TK, et al. Prevalence and Clinical Significance of Diabetes in Asian Versus White Patients With Heart Failure. JACC Heart Fail 2017;5(1):14-24.
58. American Diabetes Association. 2. Classification and Diagnosis of Diabetes: Standards of Medical Care in Diabetes-2020. Diabetes Care 2020;43(Suppl 1):S14-S31.
59. Razak F, Anand SS, Shannon H, et al. Defining obesity cut points in a multiethnic population. Circulation 2007;115(16):2111-2118.
60. Tillin T, Sattar N, Godsland IF, Hughes AD, Chaturvedi N, Forouhi NG. Ethnicity-specific obesity cut-points in the development of Type 2 diabetes - a prospective study including three ethnic groups in the United Kingdom. Diabet Med 2015;32(2):226-234.
61. Lee YS, Jun HS. Anti-diabetic actions of glucagon-like peptide-1 on pancreatic beta-cells. Metabolism 2014;63(1):9-19.
62. Drucker DJ. The Cardiovascular Biology of Glucagon-like Peptide-1. Cell Metab 2016;24(1):15-30.
63. Cefalu WT, Kaul S, Gerstein HC, et al. Cardiovascular Outcomes Trials in Type 2 Diabetes: Where Do We Go From Here? Reflections From a Diabetes Care Editors' Expert Forum. 2018;41(1):14-31.
64. Marso SP, Daniels GH, Brown-Frandsen K, et al. Liraglutide and Cardiovascular Outcomes in Type 2 Diabetes. N Engl J Med 2016;375(4):311-322.
65. van der Meer RW, Rijzewijk LJ, de Jong HW, et al. Pioglitazone improves cardiac function and alters myocardial substrate metabolism without affecting cardiac triglyceride accumulation and high-energy phosphate metabolism in patients with well-controlled type 2 diabetes mellitus. Circulation 2009;119(15):2069-2077.
66. Bizino MB, Jazet IM, Westenberg JJM, et al. Effect of liraglutide on cardiac function in patients with type 2 diabetes mellitus: randomized placebo-controlled trial. Cardiovasc Diabetol 2019;18(1):55.
67. Pulte D, Gondos A, Brenner H. Trends in 5- and 10-year survival after diagnosis with childhood hematologic malignancies in the United States, 1990-2004. J Natl Cancer Inst 2008;100(18):1301-1309.
68. Chima RS, Daniels RC, Kim MO, et al. Improved outcomes for stem cell transplant recipients requiring pediatric intensive care. Pediatr Crit Care Med 2012;13(6):e336-342.
69. Uderzo C, Pillon M, Corti P, et al. Impact of cumulative anthracycline dose, preparative regimen and chronic graft-versus-host disease on pulmonary and cardiac function in children 5 years after allogeneic hematopoietic stem cell transplantation: a prospective evaluation on behalf of the EBMT Pediatric Diseases and Late Effects Working Parties. Bone Marrow Transplant 2007;39(11):667-675.
70. Lipshultz SE, Adams MJ, Colan SD, et al. Long-term cardiovascular toxicity in children, adolescents, and young adults who receive cancer therapy: pathophysiology, course, monitoring, management, prevention, and research directions: a scientific statement from the American Heart Association. Circulation 2013;128(17):1927-1995.
71. Borlaug BA, Redfield MM. Diastolic and systolic heart failure are distinct phenotypes within the heart failure spectrum. Circulation 2011;123(18):2006-2013; discussion 2014.
72. Pfeffer MA, Shah AM, Borlaug BA. Heart Failure With Preserved Ejection Fraction In Perspective. Circ Res 2019;124(11):1598-1617.
73. Kim RJ, Chen EL, Lima JA, Judd RM. Myocardial Gd-DTPA kinetics determine

MRI contrast enhancement and reflect the extent and severity of myocardial injury after acute reperfused infarction. Circulation 1996;94(12):3318-3326.
74. Messroghli DR, Walters K, Plein S, et al. Myocardial T1 mapping: application to patients with acute and chronic myocardial infarction. Magn Reson Med 2007;58(1):34-40.
75. Al-Khatib SM, Stevenson WG, Ackerman MJ, et al. 2017 AHA/ACC/HRS Guideline for Management of Patients With Ventricular Arrhythmias and the Prevention of Sudden Cardiac Death: A Report of the American College of Cardiology/American Heart Association Task Force on Clinical Practice Guidelines and the Heart Rhythm Society. J Am Coll Cardiol 2018;72(14):e91-e220.

CHAPTER

2

The role of insulin resistance in the relation of visceral, abdominal subcutaneous and total body fat to cardiovascular function

Paiman EHM, de Mutsert R, Widya RL, Rosendaal FR, Jukema JW, Lamb HJ

Nutr Metab Cardiovasc Dis. 2020; in press. doi: 10.1016/j.numecd.2020.07.011

ABSTRACT

Background

The separate cardiovascular effects of type 2 diabetes and adiposity remain to be examined. This study aimed to investigate the role of insulin resistance in the relations of visceral (VAT), abdominal subcutaneous (aSAT) adipose tissue and total body fat (TBF) to cardiovascular remodeling.

Methods

In this cross-sectional analysis of the population-based Netherlands Epidemiology of Obesity study, 914 middle-aged individuals (46% men) were included. Participants underwent magnetic resonance imaging. Standardized linear regression coefficients (95%CI) were calculated, adjusted for potential confounding factors.

Results

All fat depots and insulin resistance (HOMA-IR), separate from VAT and TBF, were associated with lower mitral early and late peak filling rate ratios (E/A): -0.04 (-0.09;0.01) per SD (54 cm^2) VAT; -0.05 (-0.10;0.00) per SD (94 cm^2) aSAT; -0.09 (-0.16;-0.02) per SD (8%) TBF; -0.11 (-0.17;-0.05) per 10-fold increase in HOMA-IR, whereas VAT and TBF were differently associated with left ventricular (LV) end-diastolic volume: -8.9 (-11.7;-6.1) mL per SD VAT; +5.4 (1.1;9.7) mL per SD TBF. After adding HOMA-IR to the model to evaluate the mediating role of insulin resistance, change in E/A was -0.02 (-0.07;0.04) per SD VAT; -0.03 (-0.08;0.02) per SD aSAT; -0.06 (-0.13;0.01) per SD TBF, and change in LV end-diastolic volume was -7.0 (-9.7;-4.3) mL per SD VAT. In women, adiposity but not HOMA-IR was related to higher aortic arch pulse wave velocity.

Conclusion

Insulin resistance was associated with reduced diastolic function, separately from VAT and TBF, and partly mediated the associations between adiposity depots and lower diastolic function.

Highlights

- We examined the separate relations of HOMA-IR and body fat to cardiac remodeling.
- All adipose tissue depots were associated with reduced diastolic function.
- Visceral but not total body fat was related to a smaller left ventricular volume.
- HOMA-IR was linked to diastolic dysfunction, separately from body fat.
- HOMA-IR mediated the relation of body fat to diastolic dysfunction.

INTRODUCTION

Type 2 diabetes, in the absence of significant coronary artery disease, hypertension or other potential etiologies, is associated with myocardial remodeling (1). This concept is referred to as diabetic cardiomyopathy (2). Although diabetic cardiomyopathy has been recognized as a distinct clinical entity (3), its phenotypic characterization remains unclear (1). One of the difficulties in phenotyping diabetic cardiomyopathy is the strong association between obesity and type 2 diabetes (4). Due to their coexistence, it is challenging to isolate the contribution of type 2 diabetes and obesity to cardiovascular remodeling.

Obesity has been related to a variety of alterations in left ventricular (LV) morphology and function, vascular function and hemodynamics (5-9). Interestingly, visceral (VAT) and subcutaneous (SAT) adipose tissue are metabolically distinct and show differential incidence rates of cardiovascular disease (10). VAT in particular secretes proinflammatory and proatherogenic cytokines including tumor necrosis factor-alpha and interleukin-6 (11), whereas VAT produces less adiponectin, which protects the heart from adverse remodeling (12). Particularly VAT may predispose to type 2 diabetes, as low adiponectin levels and chronic inflammation are considered to mediate the effects of obesity in the pathogenesis of insulin resistance (13). Of importance, VAT and SAT appear to be differently associated with cardiac structure and hemodynamics (9,14). Overall obesity and SAT have been related to increases in LV dimensions and cardiac output, presumably as a result of intravascular volume expansion (9,14,15). In contrast, VAT has been associated with reduced LV end-diastolic volume and increased LV mass, possibly due to the release of prohypertrophic adipokines (9,14,16). Furthermore, previous large-scale studies have reported associations of type 2 diabetes with LV functional impairments, particularly diastolic dysfunction, but also with increased cardiac mass (17-21). Although VAT has been related to impaired diastolic function as well (22), a direct causal link between type 2 diabetes and diastolic dysfunction is supported by alterations in cardiac metabolism associated with insulin resistance (23-27). In contrast, LV morphological changes in type 2 diabetes may be explained predominantly by hemodynamic mechanisms associated with increased body size and altered body composition (9,28). Previously, only a few population-based studies have assessed imaging-based metrics of VAT and SAT in addition to generalized measures of obesity, when examining LV structure and function in obese individuals (9,14,29), but the association of type 2 diabetes with cardiovascular remodeling, separate from adipose tissue, remains to be investigated.

Furthermore, it has been demonstrated that not merely type 2 diabetes but rather the insulin resistance continuum has adverse effects on cardiac structure and function (17,18,30-33). As such, assessment of the role of insulin resistance in adipose tissue-related cardiovascular remodeling in the general population may contribute to the phenotypic characterization of diabetic cardiomyopathy. Thus far, the relation of insulin resistance to cardiovascular remodeling, independent of the body fat depots, has not been examined in a population-

based cohort, whereas adjustment for overall obesity may not fully separate the cardiovascular effects of insulin resistance and VAT.

The aim of this study was to investigate the role of insulin resistance in the associations of VAT, abdominal SAT (aSAT) and total body fat (TBF) with cardiovascular remodeling, assessed by LV mass and dimensions, systolic and diastolic function, stroke volume, cardiac output and aortic stiffness, using magnetic resonance imaging (MRI), in the middle-aged general population. As depicted in **Figure 1**, this implies 1) assessment of the relation of insulin resistance to cardiovascular parameters after adjusting for potential confounding by adiposity, and 2) examination of the attenuation of the association of adiposity with cardiovascular parameters after adding insulin resistance as a potential mediator to the regression models. Our hypothesis is that insulin resistance is associated with reduced diastolic function, separately from VAT and TBF, and that insulin resistance is a mediator in the relation of adiposity to reduced diastolic function.

METHODS

Study design and study population

The Netherlands Epidemiology of Obesity (NEO) study is a prospective, population-based cohort study in 6,671 individuals (34). Between 2008 and 2012, men and women aged between 45 and 65 years, with a self-reported body mass index (BMI) of 27 kg/m^2 or higher, from Leiden and the surrounding area were invited to participate. To obtain a reference distribution of BMI, men and women from Leiderdorp in the same age range were invited irrespective of their BMI. A random subset of the participants underwent MRI. The Medical Ethics Committee of Leiden University Medical Center approved the study protocol. All participants provided written informed consent.

The present study is a cross-sectional analysis of the baseline measurements of the NEO study. Participants included those who underwent cardiac and abdominal MRI. Exclusion criteria were use of glucose-lowering medication (oral hypoglycemic agents or insulin) in the month before study visit and a history of cardiovascular disease (congestive heart failure, myocardial infarction, angina pectoris and/or heart rhythm abnormalities). Participants with missing data were excluded.

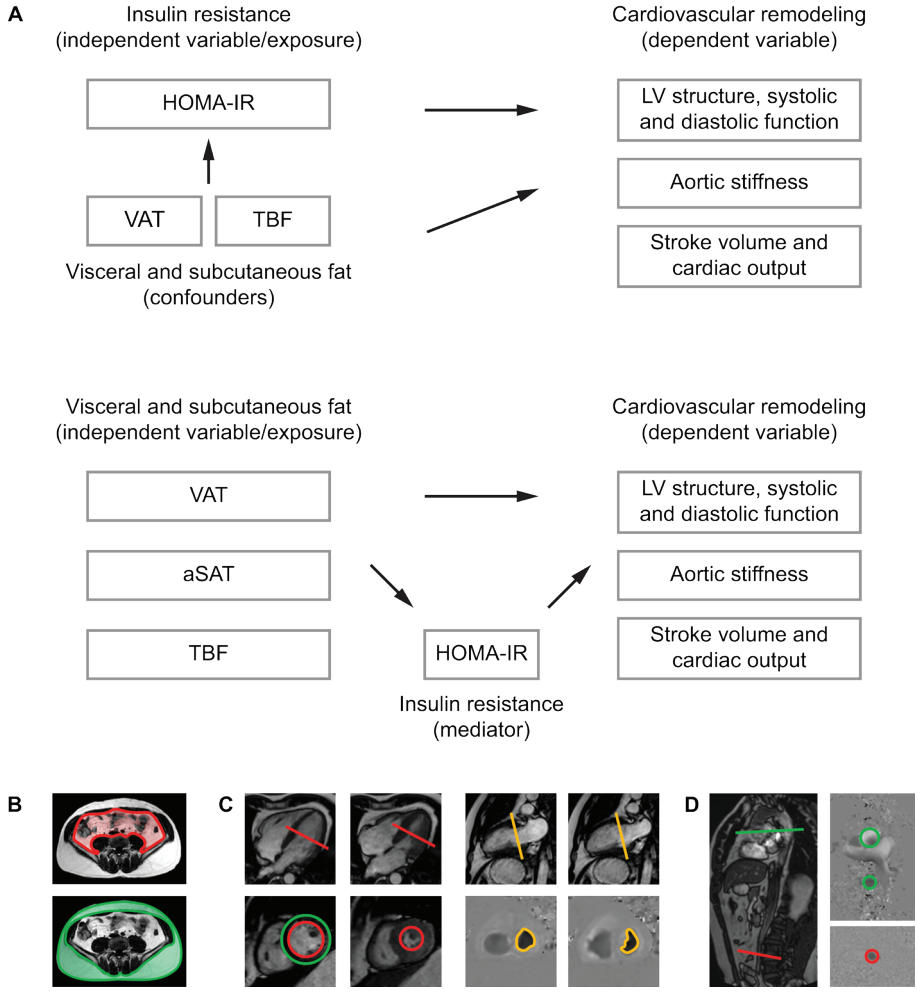

Figure 1. Study aim and MRI-derived adiposity and cardiovascular parameters. (**A**) This study sought to examine the role of HOMA-IR in the associations of VAT, aSAT and TBF with cardiovascular remodeling, assessed by LV mass and dimensions, systolic and diastolic function, stroke volume, cardiac output and aortic stiffness. (**B**) VAT (***upper image***) and aSAT (***lower image***) were assessed on transverse slices at the level of the fifth lumbar vertebra. (**C**) LV systolic function was quantified as the LV ejection fraction, derived from short-axis cine MRI. LV structure was assessed by measurement of LV mass and end-diastolic volumes (***left panel***). LV diastolic function was examined by calculating the ratio of the early and late diastolic flow rates across the mitral valve, using velocity-encoded MRI (***right panel***). (**D**) Aortic stiffness was quantified as the velocity of the systolic pulse wave, from ascending aorta to distal abdominal aorta, using velocity-encoded MRI. Abbreviations: aSAT: abdominal subcutaneous adipose tissue, HOMA-IR: homeostatic model assessment of insulin resistance, LV: left ventricular, TBF: total body fat, VAT: visceral adipose tissue.

Data collection

Self-reported ethnicity was categorized into white and other, education into low and high (higher vocational school, university and postgraduate education) and tobacco smoking into never (reference), former and current smoker. Physical activity was expressed in metabolic equivalents of task (MET)-hours per week. Data on the frequency, duration and intensity of physical activity during leisure time was collected using the Short Questionnaire to Assess Health-enhancing physical activity (SQUASH). In women, the use of hormones (contraceptives or hormone replacement therapy) was grouped into current and no use of estrogens and menopausal state into postmenopausal (reference), peri- and premenopausal. Data on anthropometry and blood pressure and blood samples were obtained in the morning after an overnight fast of at least ten hours. Hypertension was defined as systolic blood pressure ≥ 140 mmHg and/or diastolic blood pressure ≥ 90 mmHg, and/or use of antihypertensive drugs (35). Fasting glucose and insulin were examined using an enzymatic colorimetric assay (Roche Modular P800 Analyzer, Roche Diagnostics, Mannheim, Germany) and a two-site chemiluminescent immunometric assay (Siemens Immulite 2500, Siemens Healthcare Diagnostics, Breda), respectively. Details on the data collection can be found elsewhere (34).

Insulin resistance, adiposity and cardiovascular parameters

We used the homeostatic model assessment of insulin resistance (HOMA-IR). HOMA-IR was calculated according to: fasting glucose (in mmol/L) multiplied by fasting insulin (in mU/L), divided by 22.5 (36,37).

The MRI studies were at the same morning as the clinical data collection. Abdominal and cardiac MRI was performed on a 1.5 Tesla MR scanner (Philips Medical Systems, Best, the Netherlands). The MRI data were analyzed using MASS and FLOW (Leiden University Medical Center, Leiden, the Netherlands).

VAT and aSAT were quantified as the mean area on three transverse images at the level of the fifth lumbar vertebra. Such cross-sectional single-slice areas strongly correlate with the total VAT and aSAT volumes (38). We estimated the TBF percentage using the Tanita bio-impedance balance (TBF-310; Tanita International Division, Yiewsley, United Kingdom). Lean body mass was calculated from body weight and TBF percentage.

LV mass was evaluated in the end-diastolic phase. LV stroke volume was defined as the difference between end-diastolic volume and end-systolic volume. Similarly to several previous studies, LV mass and volumes were adjusted for lean body mass (9,39,40). LV concentricity was defined as the LV mass-to-volume ratio. We calculated the LV ejection fraction by dividing stroke volume by end-diastolic volume, multiplied by 100%, and cardiac output by multiplying stroke volume by heart rate. Diastolic function was assessed using the ratio of the mitral early and late peak filling rate (E/A ratio). We examined the aortic pulse wave velocity (PWV), as a measure of aortic stiffness, for the total aorta and regionally for the aortic arch and descending aorta. Details on the image acquisition are provided as **Supplementary Material**.

Statistical analyses

In the NEO study, individuals with a BMI of 27 kg/m^2 or higher were oversampled. For a correct representation of the associations in the general population, individuals were weighted toward the BMI distribution of participants from the Leiderdorp municipality, whose BMI distribution was similar to the BMI distribution of the Dutch general population, to adjust for the oversampling of individuals with a BMI of 27 kg/m^2 or higher (34).

Baseline characteristics were expressed as mean and standard deviation (SD), median and interquartile range, or percentage. We performed standardized linear regression analysis to assess the associations of VAT, aSAT, TBF and HOMA-IR with cardiovascular parameters. We used the standard deviation of the adiposity parameters and the normally-distributed log-transform of HOMA-IR. Regression coefficients were calculated for the total population and for men and women separately. Sex interaction was examined by assessment of the sex interaction coefficients. Similarly to others (9), we assessed the relation of insulin resistance and adipose tissue to LV mass and dimensions by adjusting for lean body mass, which is a stronger correlate for cardiac structure than body surface area or height$^{2.7}$ (39,40).

In the first model, the standardized linear regression coefficients with 95% confidence intervals (95%CI) for the associations between adiposity and cardiovascular parameters were calculated with adjustment for the potential confounding factors age, sex, ethnicity, education, smoking, physical activity, use of hormones and menopause, in addition to hypertension and lean body mass. As adiposity parameters are highly correlated (41), the first model was additionally adjusted for either VAT or TBF. The coefficients of VAT were adjusted for TBF and vice versa, as VAT is closely related to overall obesity. The coefficients of aSAT were adjusted for VAT, as the abdominal fat depots are strongly associated. In contrast, the coefficients of aSAT were not adjusted for TBF, as in general TBF mainly consists of subcutaneous fat.

In the second model, the mediating role of insulin resistance in the association between adiposity and cardiovascular parameters was evaluated, by adding HOMA-IR to the first model, after assessment of the mediator conditions (42,43). First, we evaluated the independent association between HOMA-IR and cardiovascular parameters, by adjusting for adiposity (VAT and TBF), age, sex, ethnicity, education, smoking, physical activity, use of hormones, menopause, hypertension and lean body mass. Second, we calculated the interaction coefficients between adipose tissue (VAT, aSAT and TBF) and HOMA-IR to rule out exposure-mediator interaction, whereas the relations between the fat depots and insulin resistance were confirmed previously (44). Third, we assessed the mediating role of HOMA-IR by visual inspection of the change in regression coefficient of the adiposity parameter after adding HOMA-IR to the model. Mediation by HOMA-IR was supported if the regression coefficient was fully or partly attenuated towards the null. ***P*** values <0.05 were considered to indicate significant interaction. Stata Statistical Software (release 14; StataCorp, College Station, TX) was used for the statistical analyses.

RESULTS

Baseline characteristics

In total, 6,671 participants were included in the NEO study. Cardiac MRI was acquired in a subsample of 1,207 participants. Data on both systolic and diastolic function and aortic PWV were available in 1,163 individuals. After exclusion of n=87 participants due to technical errors in systolic and/or diastolic cardiac MRI and/or aortic PWV (n=48 for systolic cardiac MRI, n=20 for diastolic cardiac MRI, n=22 for aortic PWV), consecutively n=59 because of use of glucose-lowering medication, n=65 because of a history of cardiac disease and n=38 due to missing data, the total number of participants was 914.

Table 1. Demographic, clinical and biochemical characteristics by BMI categories

	Normal weight BMI < 25 kg/m²	Overweight BMI 25-30 kg/m²	Obese BMI ≥ 30 kg/m²
Proportion of study population	42%	45%	13%
Demographic			
Age, y	55 (4)	55 (6)	56 (11)
Sex, % men	34	58	46
Ethnicity, % white	98	96	94
Education, % high	55	45	32
Median physical activity, hours/week	37.6 (16.5, 57.8)	30.2 (18.3, 47.3)	28.0 (13.3, 46.0)
Clinical			
Postmenopausal, % (women)	58	58	64
Current use of hormones, % (women)	8	12	5
Tobacco smoking, %			
Current smoker	10	14	14
Ever smoker	40	45	52
Never smoker	50	41	34
Heart rate, bpm	63 (5)	64 (11)	67 (18)
Systolic blood pressure, mmHg	129 (11)	131 (17)	135 (30)
Diastolic blood pressure, mmHg	82 (6)	85 (11)	87 (18)
Use of antihypertensive drugs, %	12	19	33
Hypertension, %	39	46	64
Use of lipid-lowering medication, %	3	9	13
Biochemical			
Fasting glucose, mmol/L	5.1 (0.3)	5.5 (0.9)	5.8 (1.5)
HbA1c, %	5.2 (0.1)	5.3 (0.4)	5.5 (0.8)
Median fasting insulin, mU/L	6.0 (4.4, 9.0)	8.9 (6.0, 12.8)	14.1 (9.9, 20.7)
Median HOMA-IR, units	1.4 (1.0, 2.1)	2.1 (1.4, 3.1)	3.4 (2.4, 5.2)
Fasting triglycerides, mg/dL	1.0 (0.3)	1.4 (0.8)	1.7 (1.8)

Table 1. Demographic, clinical and biochemical characteristics by BMI categories

	Normal weight BMI < 25 kg/m²	Overweight BMI 25-30 kg/m²	Obese BMI ≥ 30 kg/m²
Fasting total cholesterol, mmol/L	5.7 (0.5)	5.8 (1.1)	5.7 (1.9)
Fasting HDL cholesterol, mmol/L	1.7 (0.2)	1.5 (0.4)	1.3 (0.6)
Fasting LDL cholesterol, mmol/L	3.5 (0.5)	3.7 (1.0)	3.6 (1.7)

Data are means (SD) or medians (interquartile ranges). Results are based on analyses weighted toward the BMI distribution of the general population (n=914). Please note that the absolute number of individuals in each BMI category is not provided because of the weighted analysis. Abbreviations: HbA1c: glycated hemoglobin, HOMA-IR: homeostatic model assessment of insulin resistance. Due to missing values, for heart rate: n=904, HbA1c: n=910.

The study population (46% men) had a mean age (SD) of 55 (6) years, BMI of 25.9 (3.9) kg/m^2, VAT of 113 (58) cm^2 (men) and 67 (40) cm^2 (women), aSAT: 208 (77) cm^2 (men) and 260 (98) cm^2 (women), TBF: 25 (5)% (men) and 36 (6)% (women), LV mass: 96 (25) g, LV end-diastolic volume: 148 (32) mL, LV concentricity: 0.66 (0.13), LV ejection fraction: 64 (6)%, E/A ratio: 1.33 (0.46), aortic PWV: 6.6 (1.4) m/s, cardiac output: 6.2 (1.4) L/min and HOMA-IR: 2.4 (2.0). Baseline characteristics stratified by BMI are shown in **Table 1 and 2**. In contrast to aortic arch PWV, which was obtained in all participants (n=914), total aortic PWV and descending aortic PWV was available in 911 and 832 participants, respectively. Baseline characteristics of the excluded participants were similar to those of the included study population (43% men, mean age (SD): 56 (6), BMI: 26.4 (4.6) kg/m^2).

Table 2. Adiposity and cardiovascular characteristics by BMI categories

	Normal weight BMI < 25 kg/m²	Overweight BMI 25-30 kg/m²	Obese BMI ≥ 30 kg/m²
Adiposity			
Median BMI, kg/m^2	22.6 (21.5, 23.8)	26.8 (25.8, 27.9)	32.3 (31.0, 34.5)
Waist circumference, cm			
Men	89 (3)	99 (6)	113 (12)
Women	77 (3)	91 (8)	105 (15)
Hip circumference, cm			
Men	98 (2)	105 (4)	113 (10)
Women	96 (3)	106 (5)	118 (14)
Waist/hip ratio			
Men	0.90 (0.02)	0.94 (0.05)	1.00 (0.09)
Women	0.81 (0.03)	0.86 (0.06)	0.90 (0.11)
Body weight, kg			
Men	75.9 (4.3)	88.5 (8.0)	106.4 (17.7)
Women	62.2 (3.2)	75.0 (7.8)	92.0 (18.0)

Table 2. Adiposity and cardiovascular characteristics by BMI categories

	Normal weight BMI < 25 kg/m²	Overweight BMI 25-30 kg/m²	Obese BMI ≥ 30 kg/m²
Lean body mass, kg			
Men	61.0 (3.4)	65.8 (5.7)	71.2 (12.5)
Women	42.0 (1.4)	45.5 (3.2)	49.6 (6.4)
TBF, %			
Men	20 (2)	26 (3)	33 (8)
Women	32 (2)	39 (4)	46 (6)
VAT, cm^2			
Men	75 (17)	120 (50)	178 (109)
Women	45 (13)	77 (33)	128 (90)
aSAT, cm^2			
Men	155 (20)	210 (52)	331 (142)
Women	193 (30)	294 (56)	435 (170)
Cardiovascular MRI			
LV end-diastolic volume, mL	138 (16)	154 (33)	160 (59)
LV end-systolic volume, mL	50 (7)	56 (17)	60 (31)
LV mass, g	88 (11)	101 (26)	104 (54)
LV concentricity, g/mL	0.65 (0.06)	0.66 (0.14)	0.66 (0.26)
LV ejection fraction, %	64 (3)	64 (6)	63 (11)
E/A ratio	1.39 (0.25)	1.31 (0.50)	1.17 (0.61)
LV stroke volume, mL	88 (10)	98 (22)	100 (37)
LV cardiac output, L	5.9 (0.7)	6.4 (1.4)	6.7 (2.6)
Aortic PWV, m/s			
Total aorta	6.7 (0.9)	6.6 (1.2)	6.7 (2.1)
Aortic arch	6.5 (1.1)	6.6 (2.3)	6.8 (4.0)
Descending aorta	7.0 (1.3)	6.8 (1.8)	6.9 (2.9)

Data are means (SD) or medians (interquartile ranges). Abbreviations: aSAT: abdominal subcutaneous adipose tissue, E/A ratio: ratio of mitral early and late peak filling rate, LV: left ventricular, LV concentricity: LV mass-to-volume ratio, PWV: pulse wave velocity, TBF: total body fat, VAT: visceral adipose tissue. Results are based on analyses weighted toward the BMI distribution of the general population (n=914). Due to missing values, for PWV total aorta: n=911, PWV descending aorta: n=832.

Adiposity and cardiovascular parameters

The regression coefficients for the relation of adiposity to cardiovascular parameters, in the total population and in men and women separately are presented in **Supplemental Table 1** and **Table 3**, respectively. In the total population (**Supplemental Table 1**), VAT as compared with TBF was differently associated with most of the cardiovascular parameters, except for LV diastolic function. In general, the associations between aSAT and the cardiovascular parameters were weaker than for VAT and TBF. VAT was associated with a smaller LV end-diastolic volume (-8.9 (-11.7;-6.1) mL per SD VAT) and reduced stroke volume and cardiac output, whereas for TBF those parameters were higher (LV end-diastolic volume: +5.4 (1.1;9.7) mL per SD TBF). There were no associations between aSAT and LV end-diastolic volume and cardiac output.

For VAT, the reduction in LV end-diastolic volume was paralleled by a small decrease in LV mass (-3.3 (-5.1;-1.6) g per SD VAT) and therefore, LV concentricity was slightly higher (+0.02 (0.00;0.03) per SD VAT). For TBF, the increase in LV end-diastolic volume was larger than the slight increase in LV mass (+0.6 (-1.7;2.9) g/mL per SD TBF). As a result, TBF was associated with a slightly lower LV concentricity (-0.02 (-0.04;0.00) g/mL per SD TBF). Results were generally similar in the analyses with indexing to height$^{2.7}$ instead of adjusting for lean body mass (**Supplemental Table 2**).

The aSAT- and TBF-related changes in LV end-diastolic volume and/or stroke volume resulted in small changes in LV ejection fraction. Of importance, all fat parameters were or tended to be associated with a small reduction in E/A ratio: -0.04 (-0.09;0.01) per SD VAT; -0.05 (-0.10;0.00) per SD aSAT; -0.09 (-0.16;-0.02) per SD TBF. In the total population, the regression coefficients for the associations between the adiposity parameters and total and regional aortic PWV were all around zero.

Sex differences were present in the association of TBF and aSAT with LV mass and LV concentricity and in the relation of adiposity to aortic arch PWV (**Table 3** and **Figure 2**). TBF tended to be related to a higher LV mass in men, but not in women (***P*** interaction=0.04), and aSAT was associated with a lower LV mass in women, but not in men (***P*** interaction=0.01). As a result, the differential relation of VAT versus TBF and aSAT with LV concentricity (higher versus lower LV concentricity, respectively) was more pronounced in women than in men. Furthermore, VAT, aSAT and TBF were associated with a higher aortic arch PWV in women, but not in men (***P*** interaction=0.001, 0.048 and 0006, respectively).

Table 3. Associations of HOMA-IR, VAT, aSAT and TBF with cardiovascular parameters, stratified by sex

	Adjusted standardized difference in cardiovascular parameters (95%CI)		
	Men (46%)	**Women (54%)**	***P* interaction**
LV structure			
LV mass, g			
Log HOMA-IR	-3.6 (-7.2 to 0.1)	-5.0 (-7.9 to -2.1)	0.09
VAT (SD: 54 cm^2)	-3.4 (-5.7 to -1.2)	-4.2 (-7.2 to -1.2)	0.06
aSAT (SD: 94 cm^2)	0.2 (-2.3 to 2.8)	-4.0 (-6.0 to -2.0)	0.01
TBF (SD: 8%)	2.6 (-1.4 to 6.5)	0.6 (-2.3 to 3.7)	0.04
LV end-diastolic volume, mL			
Log HOMA-IR	-10.5 (-15.2 to -5.9)	-6.4 (-10.4 to -2.5)	0.6
VAT (SD: 54 cm^2)	-7.6 (-11.3 to -3.9)	-11.1 (-15.1 to -7.1)	0.2
aSAT (SD: 94 cm^2)	2.5 (-1.7 to 6.6)	-3.0 (-6.2 to 0.2)	0.3
TBF (SD: 8%)	6.4 (0.1 to 12.7)	4.3 (-2.3 to 10.9)	0.4
LV concentricity, g/mL			
Log HOMA-IR	0.03 (0.00 to 0.05)	-0.01 (-0.03 to 0.01)	0.02
VAT (SD: 54 cm^2)	0.01 (-0.01 to 0.03)	0.02 (0.00 to 0.05)	0.8
aSAT (SD: 94 cm^2)	-0.01 (-0.03 to 0.01)	-0.02 (-0.03 to 0.00)	0.4
TBF (SD: 8%)	-0.01 (-0.04 to 0.02)	-0.02 (-0.05 to 0.01)	0.4
LV function			
LV ejection fraction, %			
Log HOMA-IR	0.7 (-0.5 to 1.8)	-0.5 (-1.5 to 0.5)	0.3
VAT (SD: 54 cm^2)	0.4 (-0.5 to 1.2)	-0.3 (-1.4 to 0.8)	0.7
aSAT (SD: 94 cm^2)	-0.3 (-1.2 to 0.6)	-0.9 (-1.7 to -0.2)	0.5
TBF (SD: 8%)	-1.3 (-2.6 to 0.0)	-0.4 (-1.5 to 0.6)	0.6
E/A ratio			
Log HOMA-IR	-0.17 (-0.27 to -0.07)	-0.04 (-0.12 to 0.03)	0.2
VAT (SD: 54 cm^2)	-0.01 (-0.08 to 0.06)	-0.09 (-0.16 to -0.02)	0.3
aSAT (SD: 94 cm^2)	-0.06 (-0.13 to 0.00)	-0.04 (-0.11 to 0.04)	0.7
TBF (SD: 8%)	-0.12 (-0.22 to -0.02)	-0.07 (-0.18 to 0.05)	0.8
Aortic stiffness			
Total aorta, m/s			
Log HOMA-IR	0.1 (-0.1 to 0.4)	-0.1 (-0.3 to 0.2)	0.9
VAT (SD: 54 cm^2)	-0.1 (-0.2 to 0.1)	0.1 (-0.2 to 0.4)	0.3
aSAT (SD: 94 cm^2)	0.1 (-0.1 to 0.3)	-0.1 (-0.3 to 0.1)	0.6
TBF (SD: 8%)	0.1 (-0.2 to 0.3)	-0.1 (-0.4 to 0.2)	0.7

Table 3. Associations of HOMA-IR, VAT, aSAT and TBF with cardiovascular parameters, stratified by sex

	Adjusted standardized difference in cardiovascular parameters (95%CI)		
	Men (46%)	**Women (54%)**	***P* interaction**
Aortic arch, m/s			
Log HOMA-IR	0.0 (-0.5 to 0.5)	-0.1 (-0.6 to 0.3)	0.3
VAT (SD: 54 cm^2)	-0.1 (-0.5 to 0.2)	0.3 (0.0 to 0.6)	0.001
aSAT (SD: 94 cm^2)	0.0 (-0.3 to 0.3)	0.1 (-0.1 to 0.4)	0.048
TBF (SD: 8%)	0.0 (-0.5 to 0.5)	0.3 (0.0 to 0.7)	0.006
Descending aorta, m/s			
Log HOMA-IR	0.2 (-0.1 to 0.6)	-0.2 (-0.5 to 0.2)	0.3
VAT (SD: 54 cm^2)	-0.1 (-0.3 to 0.1)	0.0 (-0.5 to 0.6)	0.8
aSAT (SD: 94 cm^2)	0.1 (-0.1 to 0.4)	-0.2 (-0.5 to 0.1)	0.1
TBF (SD: 8%)	0.1 (-0.2 to 0.4)	-0.2 (-0.7 to 0.3)	0.5
Hemodynamics			
Stroke volume, mL			
Log HOMA-IR	-5.3 (-8.7 to -1.9)	-4.6 (-7.3 to -1.9)	0.9
VAT (SD: 54 cm^2)	-4.3 (-6.8 to -1.9)	-7.5 (-10.2 to -4.8)	0.2
aSAT (SD: 94 cm^2)	0.9 (-1.9 to 3.7)	-3.4 (-5.4 to -1.3)	0.3
TBF (SD: 8%)	2.0 (-2.2 to 6.1)	1.9 (-2.2 to 6.1)	0.7
Cardiac output, mL			
Log HOMA-IR	181 (-76 to 438)	-144 (-371 to 84)	0.2
VAT (SD: 54 cm^2)	-126 (-308 to 56)	-321 (-519 to -122)	0.9
aSAT (SD: 94 cm^2)	71 (-126 to 267)	-128 (-280 to 23)	1.0
TBF (SD: 8%)	125 (-158 to 407)	264 (-10 to 537)	0.4

Results represent regression coefficients per 10-fold increase in HOMA-IR or per SD of measure of adiposity and are corrected for age, ethnicity, education, smoking, physical activity, use of hormone therapy, menopausal state, hypertension, lean body mass and adiposity (HOMA-IR is adjusted for VAT and TBF, VAT is adjusted for TBF, and aSAT and TBF are adjusted for VAT). ***P*** values for interaction by sex. Abbreviations: aSAT: abdominal subcutaneous adipose tissue, E/A ratio: ratio of mitral early and late peak filling rate, log HOMA-IR: log-transformation of the homeostatic model assessment of insulin resistance, LV: left ventricular, LV concentricity: LV mass-to-volume ratio, PWV: pulse wave velocity, TBF: total body fat, VAT: visceral adipose tissue. Results are based on analyses weighted toward the BMI distribution of the general population (n=914). Due to missing values, for PWV total aorta: n=911, PWV descending aorta: n=832.

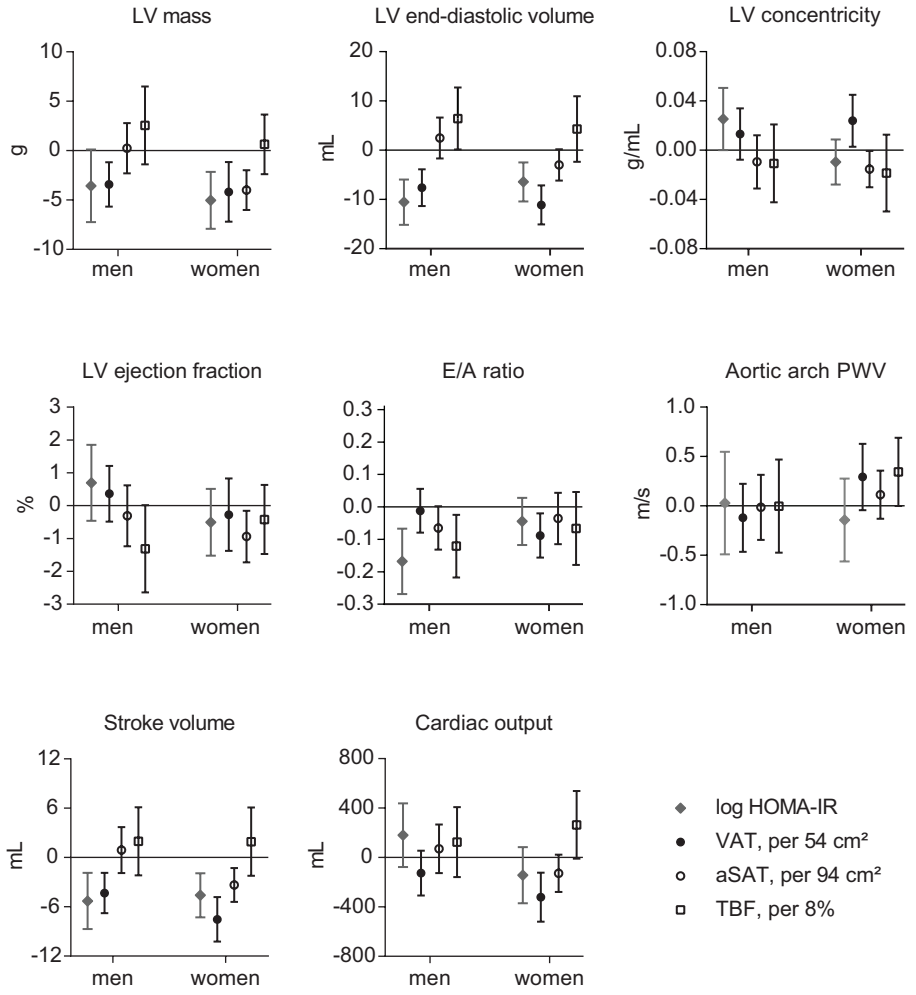

Figure 2. Associations of HOMA-IR, VAT, aSAT and TBF with cardiovascular parameters for men and women. Adjusted standardized regression coefficients (95%CI) in men and women for the association of HOMA-IR (log-transformation) (=***solid diamond***), VAT (SD: 54 cm^2) (=***solid circle***), aSAT (SD: 94 cm^2) (=***open circle***) and TBF (SD: 8%) (=***open square***) with cardiovascular parameters (after adjustment for potential confounding factors, see Table 3). Abbreviations: aSAT: abdominal subcutaneous adipose tissue, E/A ratio: ratio of mitral early and late peak filling rate, HOMA-IR: homeostatic model assessment of insulin resistance, LV: left ventricular, LV concentricity: LV mass-to-volume ratio, PWV: pulse wave velocity, TBF: total body fat, VAT: visceral adipose tissue.

Table 4. Mediating role of HOMA-IR in the associations of VAT, aSAT and TBF with cardiovascular parameters

	Adjusted standardized difference in cardiovascular parameters (95%CI	
	Model 1: adjusted for confounding factors	**Model 2: model 1 + adjusted for insulin resistance**
LV end-diastolic volume, mL		
VAT (SD: 54 cm^2)	-8.9 (-11.7 to -6.1)	-7.0 (-9.7 to -4.3)
aSAT (SD: 94 cm^2)	-0.5 (-2.9 to 1.8)	0.4 (-1.8 to 2.7)
TBF (SD: 8%)	5.4 (1.1 to 9.7)	7.5 (3.1 to 11.9)
Stroke volume, mL		
VAT (SD: 54 cm^2)	-5.6 (-7.5 to -3.7)	-4.4 (-6.2 to -2.6)
aSAT (SD: 94 cm^2)	-1.4 (-2.9 to 0.2)	-0.8 (-2.4 to 0.8)
TBF (SD: 8%)	2.2 (-0.5 to 4.9)	3.5 (0.6 to 6.3)
E/A ratio		
VAT (SD: 54 cm^2)	-0.04 (-0.09 to 0.01)	-0.02 (-0.07 to 0.04)
aSAT (SD: 94 cm^2)	-0.05 (-0.10 to 0.00)	-0.03 (-0.08 to 0.02)
TBF (SD: 8%)	-0.09 (-0.16 to -0.02)	-0.06 (-0.13 to 0.01)

Results represent regression coefficients per SD of measure of adiposity. Model 1: adjusted for age, sex, ethnicity, education, smoking, physical activity, use of hormone therapy, menopausal state, hypertension, lean body mass and adiposity (VAT is adjusted for TBF, and aSAT and TBF are adjusted for VAT). Model 2: model 1 + adjusted for HOMA-IR. For abbreviations, see Table 3.

Mediating role of insulin resistance

In the total population (**Supplemental Table 1**), HOMA-IR was associated with a lower E/A ratio and smaller LV end-diastolic volume (-0.11 (-0.17;-0.05) and -8.5 (-11.5;-5.5) mL per 10-fold increase in HOMA-IR, respectively), paralleled by a reduction in LV mass, a slightly higher LV concentricity, and a reduced stroke volume. Results were similar when indexing to $height^{2.7}$ instead of accounting for lean body mass (**Supplemental Table 2**). In contrast, HOMA-IR was not associated with LV ejection fraction, cardiac output or aortic PWV. In the analyses stratified by sex (**Table 3** and **Figure 2**), HOMA-IR was associated with a higher LV concentricity in men, but not in women (***P*** interaction=0.02).

As HOMA-IR appeared to be related to a lower E/A ratio and smaller LV dimensions, similarly in men and women, HOMA-IR was included as a mediating variable in the models on the association of adiposity with E/A ratio, LV end-diastolic volume and stroke volume, after ruling out exposure-mediator interaction (***P*** interaction >0.2 for all associations). As shown in **Table 4** and **Figure 3**, HOMA-IR attenuated the association between the fat depots and E/A ratio, and between VAT and LV end-diastolic volume and stroke volume.

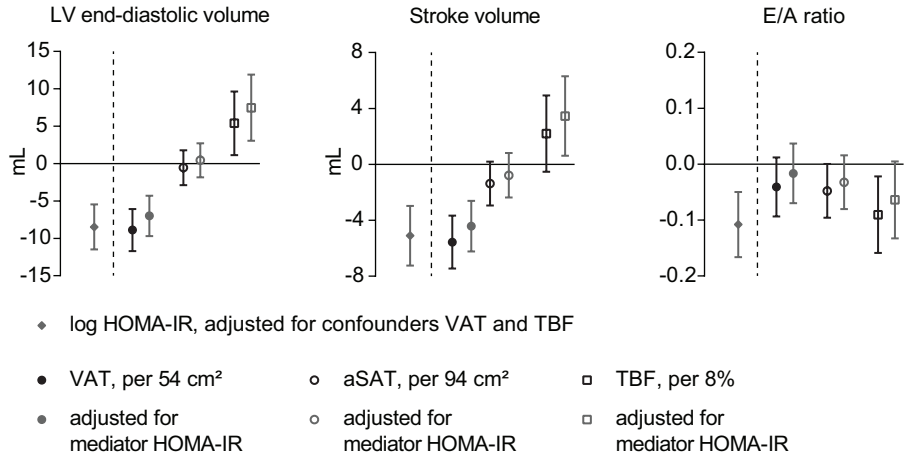

Figure 3. Mediating role of HOMA-IR in the associations of VAT, aSAT and TBF with cardiovascular parameters. Adjusted standardized regression coefficients (95%CI) in the total population for the association of HOMA-IR (log-transformation) (=***solid diamond***) and VAT (SD: 54 cm^2) (=***solid circle***), aSAT (SD: 94 cm^2) (=***open circle***) and TBF (SD: 8%) (=***open square***) with cardiovascular parameters. Regression coefficients for adiposity are presented after adjustment for potential confounding factors (model 1, see Table 4) (***each left bar, in black***) and after adding HOMA-IR as a mediator to the model (model 2, see Table 4) (***each right bar, in gray***). For abbreviations, see Figure 2.

DISCUSSION

In previous studies, the separate effects of insulin resistance, visceral and subcutaneous fat in obesity-related cardiovascular remodeling have not been fully disentangled. In this population-based study including middle-aged men and women without use of glucose-lowering medication and no history of cardiovascular disease, insulin resistance was associated with a lower diastolic function, independently of VAT and TBF; in contrast, insulin resistance was not associated with systolic function and aortic stiffness. Furthermore, insulin resistance partly mediated the relations of VAT, aSAT and TBF to reduced diastolic function as well as the relationship of VAT to a smaller LV end-diastolic volume. Interestingly, all fat depots were associated with a lower diastolic function, while VAT and TBF demonstrated distinct associations with LV dimensions. In this population-based study, the differential association between VAT versus TBF fat with LV structure and dimensions (higher versus lower LV concentricity, respectively) was more pronounced in women than in men, and all adiposity parameters were associated with a higher aortic arch PWV in women, but not in men.

Insulin resistance

Our results expand current literature on the relation of insulin resistance, abnormal glucose metabolism and type 2 diabetes to diastolic dysfunction (17,18,32,33,45). Several large-scale

studies have described reduced diastolic function in association with abnormalities in glucose regulation; for example, the Strong Heart Study reported a lower Doppler E/A ratio in non-diabetic, non-hypertensive individuals with impaired fasting glucose and/or impaired glucose tolerance than in those with normal glucose tolerance (17), and the ARIC (Atherosclerosis Risk In the Community) study demonstrated higher echocardiography-derived LV filling pressures associated with glycemic status (normal, prediabetes or type 2 diabetes), independent of BMI (18). Whereas BMI is less complex, expensive and time consuming than direct adipose tissue measures, it is an inaccurate metric of excess body fat and visceral adiposity (46). Therefore, the cardiovascular effects of insulin resistance and VAT might not be fully disentangled by adjustment for BMI. Importantly, this study confirms the relation of insulin resistance to reduced diastolic function in the middle-aged general population, separately from VAT and TBF. Also, our study allows for the appreciation of the relative contribution of insulin resistance, in comparison with adipose tissue, to impairments in diastolic function.

Unlike the findings of previous population-based studies (7,8,17-21,29-31), in our study, insulin resistance was not associated with increased cardiac mass but neither was adiposity, which might be attributable to the lower degree of obesity in our population (BMI of ~25.9 kg/m2). Interestingly, several population-based studies have reported an increasing LV mass with worsening abnormalities in glucose metabolism, particularly in women (18,19,47,48). In view of these previous findings, our observation of a higher LV concentricity with increasing HOMA-IR in men, but not in women, is remarkable. However, it should be noted that this HOMA-IR-related increase in LV concentricity in men was without an increase in LV mass. Also, we did not observe sex differences in the associations of HOMA-IR with LV end-diastolic volume and LV mass, which prevents us from drawing definitive conclusions regarding sex-related differences in the impact of HOMA-IR on LV concentric remodeling.

Proposed mechanisms for reduced diastolic function in insulin-resistant individuals comprise abnormalities in myocardial energetics and calcium homeostasis (25,26,49). Interestingly, the contribution of metabolic processes to impairments in diastolic function may be larger as compared with LV geometric remodeling (25). Insulin resistance has been shown to alter the myocardial substrate preference, which is associated with adenosine triphosphate (ATP) shortage (23,24). Diastolic rather than systolic function has been demonstrated to be primarily affected by energy shortage (26). Additionally, altered myocardial tissue characteristics, including collagen deposition and triglyceride accumulation, may increase myocardial stiffness and contribute to impaired LV relaxation (50,51), although the association between insulin resistance and impaired diastolic function has been shown to be independent of myocardial fibrosis (52). In our study, insulin resistance and VAT were also associated with a smaller LV end-diastolic volume. Interestingly, a recent study in type 2 diabetes patients described a link between cardiac steatosis and phosphocreatine (PCr)-to-ATP ratios and concentric LV remodeling, suggesting a role for myocardial lipotoxicity and energetic status in type 2 diabetes-related LV morphologic changes (51).

Adipose tissue

The various fat depots were differently associated with LV dimensions and hemodynamics. TBF was related to a higher cardiac output, presumably due to increased metabolic demands (53), whereas VAT was associated with lower blood flow rates. This divergent association of VAT and SAT with LV morphology and hemodynamic parameters is in keeping with the UK Biobank data (14), the Dallas Heart Study (9) and the MESA (Multi-Ethnic Study of Atherosclerosis) (29,30). VAT in particular may attract macrophages and this chronic low-grade inflammatory state may cause endothelial dysfunction (11). In our study, VAT was associated with a smaller LV end-diastolic volume and higher LV concentricity, particularly in women. Accordingly, it has been previously shown that cardiac adaptations to obesity are more severe in women, which might be attributable to sex differences in biological factors associated with adipose tissue (54).

Interestingly, in the UK Biobank study (14), women showed a stronger relation of VAT to increased total vascular stiffness as compared with men. In our study, adiposity-related aortic arch stiffening was present in women, but not in men. In addition to hyperleptinemia, increased circulating inflammatory markers and local inflammation of perivascular fat (8,55), in some studies, insulin resistance has been implicated in obesity-related aortic stiffening (56,57); however, a mediating role of HOMA-IR in the relation of adiposity to increased aortic stiffness was not supported by our data. While age- and hypertension-related aortic stiffening is thought to be due to progressive declines in elastin primarily in the proximal aorta (58), the mechanisms by which adiposity might impair total and regional vascular function remain to be elucidated and in particular the impact of sex may warrant further research.

Implications

In our population, the observed reductions in diastolic function were small, as MRI-derived E/A ratio values in normal diastolic function range from 0.8 to 1.5 (59). Also, insulin resistance did not completely mediate the associations between adipose tissue and reduced diastolic function, which implies that other factors including inflammation, increased leptin and autonomic dysfunction are likely to may play a role in the pathogenesis of diastolic dysfunction in obesity (60,61). Nonetheless, the results of this study confirm that insulin resistance, separate from adipose tissue, is associated with reduced diastolic function, thereby supporting that diastolic dysfunction is indeed a characteristic of diabetic cardiomyopathy. Furthermore, concentric remodeling has been associated with an increased susceptibility of heart failure events (62). In this context, our results reaffirm the clinical importance of differentiating visceral and subcutaneous adiposity, as VAT but not TBF was associated with a smaller LV end-diastolic volume.

Limitations

Some limitations need to be addressed. The cross-sectional design does not allow to draw conclusions on causality, neither on the direction of the associations. Also, our study may not

have sufficient power to draw conclusions on sex differences in obesity-related cardiovascular remodeling, as the observed changes in cardiovascular parameters related to adiposity and insulin resistance were small. We excluded individuals using type 2 diabetes medication, who may have the largest impairments in diastolic function, because glucose-lowering drugs may influence insulin resistance or modify the relation of insulin resistance to cardiovascular parameters (37). Furthermore, we used HOMA-IR as a feasible alternative for the hyperinsulinemic euglycemic clamp, which is considered the gold standard for whole-body insulin resistance. HOMA-IR is widely used in epidemiologic studies and corresponds well to estimates of insulin resistance in clamp studies (63). Interestingly, advanced PET/MR protocols which enable the measurement of tissue-specific insulin sensitivity may help to gain more insight into the association of myocardial insulin resistance with cardiac remodeling (64). In the NEO study, diastolic function is derived from MRI. MRI values for the E/A ratio are highly reproducible and strongly correlate with echocardiography measurements (65-67). However, in clinical patients, the diagnosis of diastolic dysfunction is based on echocardiography, using multiple diastolic function parameters, in combination with the evaluation for signs or symptoms of congestive heart failure (68). For example, we did not have data on left atrial size, which can be used as a measure of chronic diastolic dysfunction. Furthermore, we examined LV ejection fraction, whereas systolic strain is considered a more sensitive measure for LV contractility (18,20). Accordingly, in the Strong Heart Study, insulin resistance was related to lower systolic strain and reduced measures of myocardial mechano-energetic efficiency, whereas LV ejection fraction was unaltered (69).

CONCLUSION

In this cross-sectional population-based imaging study in middle-aged men and women, we document that insulin resistance has a mediating role in the relation between adipose tissue and a lower E/A ratio and between VAT and a smaller LV end-diastolic volume. All fat depots including VAT, aSAT and TBF were related to reduced diastolic function, whereas VAT but not TBF was associated with smaller LV dimensions. We assessed specific adiposity metrics rather than excess body weight. The present study demonstrates that insulin resistance is associated with a lower E/A ratio and a smaller LV end-diastolic volume, separately from VAT and TBF, supporting reduced diastolic function and smaller LV dimensions as adiposity-independent characteristics of insulin resistance-related cardiovascular remodeling, in the middle-aged general population.

ACKNOWLEDGEMENTS

We express our gratitude to all individuals who participate in the Netherlands Epidemiology of Obesity (NEO) study. We are grateful to all participating general practitioners for inviting eligible participants. We furthermore thank P.R. van Beelen and all research nurses for data collection, P.J. Noordijk and her team for sample handling and storage, and I. de Jonge for data management.

FUNDING

This project was funded by the 'Cardio Vascular Imaging Group (CVIG)', Leiden University Medical Center (Leiden, the Netherlands). The NEO study is supported by the participating Departments, the Division and the Board of Directors of the Leiden University Medical Center, and by the Leiden University, Research Profile Area 'Vascular and Regenerative Medicine'.

REFERENCES

1. Seferovic PM, Paulus WJ. Clinical diabetic cardiomyopathy: a two-faced disease with restrictive and dilated phenotypes. Eur Heart J 2015;36(27):1718-1727, 1727a-1727c.
2. Rubler S, Dlugash J, Yuceoglu YZ, Kumral T, Branwood AW, Grishman A. New type of cardiomyopathy associated with diabetic glomerulosclerosis. Am J Cardiol 1972;30(6):595-602.
3. Richardson P, McKenna W, Bristow M, et al. Report of the 1995 World Health Organization/ International Society and Federation of Cardiology Task Force on the Definition and Classification of cardiomyopathies. Circulation 1996;93(5):841-842.
4. Mokdad AH, Ford ES, Bowman BA, et al. Prevalence of obesity, diabetes, and obesity-related health risk factors, 2001. JAMA 2003;289(1):76-79.
5. Lauer MS, Anderson KM, Kannel WB, Levy D. The impact of obesity on left ventricular mass and geometry. The Framingham Heart Study. JAMA 1991;266(2):231-236.
6. Heckbert SR, Post W, Pearson GD, et al. Traditional cardiovascular risk factors in relation to left ventricular mass, volume, and systolic function by cardiac magnetic resonance imaging: the Multiethnic Study of Atherosclerosis. J Am Coll Cardiol 2006;48(11):2285-2292.
7. Brunner EJ, Shipley MJ, Ahmadi-Abhari S, et al. Adiposity, obesity, and arterial aging: longitudinal study of aortic stiffness in the Whitehall II cohort. Hypertension 2015;66(2):294-300.
8. Britton KA, Wang N, Palmisano J, et al. Thoracic periaortic and visceral adipose tissue and their cross-sectional associations with measures of vascular function. Obesity (Silver Spring) 2013;21(7):1496-1503.
9. Neeland IJ, Gupta S, Ayers CR, et al. Relation of regional fat distribution to left ventricular structure and function. Circ Cardiovasc Imaging 2013;6(5):800-807.
10. Neeland IJ, Turer AT, Ayers CR, et al. Body fat distribution and incident cardiovascular disease in obese adults. J Am Coll Cardiol 2015;65(19):2150-2151.
11. Hamdy O, Porramatikul S, Al-Ozairi E. Metabolic obesity: the paradox between visceral and subcutaneous fat. Curr Diabetes Rev 2006;2(4):367-373.
12. Ziemke F, Mantzoros CS. Adiponectin in insulin resistance: lessons from translational research. Am J Clin Nutr 2010;91(1):258S-261S.
13. Li S, Shin HJ, Ding EL, van Dam RM. Adiponectin levels and risk of type 2 diabetes: a systematic review and meta-analysis. JAMA 2009;302(2):179-188.
14. van Hout MJP, Dekkers IA, Westenberg JJM, Schalij MJ, Scholte A, Lamb HJ. The impact of visceral and general obesity on vascular and left ventricular function and geometry: a cross-sectional magnetic resonance imaging study of the UK Biobank. Eur Heart J Cardiovasc Imaging 2019.
15. Wade KH, Chiesa ST, Hughes AD, et al. Assessing the causal role of body mass index on cardiovascular health in young adults: Mendelian randomization and recall-by-genotype analyses. Circulation 2018;138(20):2187-2201.
16. Cho DH, Kim MN, Joo HJ, Shim WJ, Lim DS, Park SM. Visceral obesity, but not central obesity, is associated with cardiac remodeling in subjects with suspected metabolic syndrome. Nutr Metab Cardiovasc Dis 2019;29(4):360-366.
17. Capaldo B, Di Bonito P, Iaccarino M, et al. Cardiovascular Characteristics in Subjects With Increasing Levels of Abnormal Glucose Regulation The Strong Heart Study. Diabetes Care 2013;36(4):992-997.
18. Skali H, Shah A, Gupta DK, et al. Cardiac structure and function across the glycemic spectrum in elderly men and women free of prevalent heart disease: the Atherosclerosis Risk In the Community study. Circ Heart Fail 2015;8(3):448-454.
19. Galderisi M, Anderson KM, Wilson PW, Levy D. Echocardiographic evidence for the existence of a distinct diabetic cardiomyopathy (the Framingham Heart Study). Am J Cardiol 1991;68(1):85-89.
20. Devereux RB, Roman MJ, Paranicas M, et al. Impact of diabetes on cardiac structure and function: the strong heart study. Circulation 2000;101(19):2271-2276.
21. Bertoni AG, Goff DC, Jr., D'Agostino RB, Jr., et al. Diabetic cardiomyopathy and subclinical cardiovascular disease: the Multi-Ethnic Study of Atherosclerosis (MESA). Diabetes Care 2006;29(3):588-594.
22. Sawada N, Daimon M, Kawata T, et al. The

Significance of the Effect of Visceral Adiposity on Left Ventricular Diastolic Function in the General Population. Sci Rep 2019;9(1):4435.
23. Rider OJ, Cox P, Tyler D, Clarke K, Neubauer S. Myocardial substrate metabolism in obesity. Int J Obes (Lond) 2013;37(7):972-979.
24. Rijzewijk LJ, van der Meer RW, Lamb HJ, et al. Altered myocardial substrate metabolism and decreased diastolic function in nonischemic human diabetic cardiomyopathy: studies with cardiac positron emission tomography and magnetic resonance imaging. J Am Coll Cardiol 2009;54(16):1524-1532.
25. Rayner JJ, Banerjee R, Holloway CJ, et al. The relative contribution of metabolic and structural abnormalities to diastolic dysfunction in obesity. Int J Obes (Lond) 2018;42(3):441-447.
26. Rider OJ, Francis JM, Ali MK, et al. Effects of catecholamine stress on diastolic function and myocardial energetics in obesity. Circulation 2012;125(12):1511-1519.
27. von Bibra H, St John Sutton M. Diastolic dysfunction in diabetes and the metabolic syndrome: promising potential for diagnosis and prognosis. Diabetologia 2010;53(6):1033-1045.
28. Chinali M, de Simone G, Roman MJ, et al. Impact of obesity on cardiac geometry and function in a population of adolescents: the Strong Heart Study. J Am Coll Cardiol 2006;47(11):2267-2273.
29. Abbasi SA, Hundley WG, Bluemke DA, et al. Visceral adiposity and left ventricular remodeling: The Multi-Ethnic Study of Atherosclerosis. Nutr Metab Cardiovasc Dis 2015;25(7):667-676.
30. Shah RV, Abbasi SA, Heydari B, et al. Insulin resistance, subclinical left ventricular remodeling, and the obesity paradox: MESA (Multi-Ethnic Study of Atherosclerosis). J Am Coll Cardiol 2013;61(16):1698-1706.
31. Velagaleti RS, Gona P, Chuang ML, et al. Relations of insulin resistance and glycemic abnormalities to cardiovascular magnetic resonance measures of cardiac structure and function: the Framingham Heart Study. Circ Cardiovasc Imaging 2010;3(3):257-263.
32. Stahrenberg R, Edelmann F, Mende M, et al. Association of glucose metabolism with diastolic function along the diabetic continuum. Diabetologia 2010;53(7):1331-1340.
33. Fontes-Carvalho R, Ladeiras-Lopes R, Bettencourt P, Leite-Moreira A, Azevedo A. Diastolic dysfunction in the diabetic continuum: association with insulin resistance, metabolic syndrome and type 2 diabetes. Cardiovasc Diabetol 2015;14:4.
34. de Mutsert R, den Heijer M, Rabelink TJ, et al. The Netherlands Epidemiology of Obesity (NEO) study: study design and data collection. Eur J Epidemiol 2013;28(6):513-523.
35. Williams B, Mancia G, Spiering W, et al. 2018 ESC/ESH Guidelines for the management of arterial hypertension. Eur Heart J 2018;39(33):3021-3104.
36. Matthews DR, Hosker JP, Rudenski AS, Naylor BA, Treacher DF, Turner RC. Homeostasis model assessment: insulin resistance and beta-cell function from fasting plasma glucose and insulin concentrations in man. Diabetologia 1985;28(7):412-419.
37. Wallace TM, Levy JC, Matthews DR. Use and abuse of HOMA modeling. Diabetes Care 2004;27(6):1487-1495.
38. Schweitzer L, Geisler C, Pourhassan M, et al. What is the best reference site for a single MRI slice to assess whole-body skeletal muscle and adipose tissue volumes in healthy adults? Am J Clin Nutr 2015;102(1):58-65.
39. Bella JN, Devereux RB, Roman MJ, et al. Relations of left ventricular mass to fat-free and adipose body mass: the strong heart study. The Strong Heart Study Investigators. Circulation 1998;98(23):2538-2544.
40. Daniels SR, Kimball TR, Morrison JA, Khoury P, Witt S, Meyer RA. Effect of lean body mass, fat mass, blood pressure, and sexual maturation on left ventricular mass in children and adolescents. Statistical, biological, and clinical significance. Circulation 1995;92(11):3249-3254.
41. Seidell JC, Bouchard C. Visceral fat in relation to health: is it a major culprit or simply an innocent bystander? Int J Obes Relat Metab Disord 1997;21(8):626-631.
42. Richiardi L, Bellocco R, Zugna D. Mediation analysis in epidemiology: methods, interpretation and bias. Int J Epidemiol 2013;42(5):1511-1519.
43. Robins JM, Greenland S. Identifiability and exchangeability for direct and indirect effects. Epidemiology 1992;3(2):143-155.
44. de Mutsert R, Gast K, Widya R, et al. Associations of Abdominal Subcutaneous and Visceral Fat with Insulin Resistance and Secretion Differ Between Men and Women: The Netherlands Epidemiology of Obesity Study. Metab Syndr Relat Disord 2018;16(1):54-63.
45. From AM, Scott CG, Chen HH. The development

of heart failure in patients with diabetes mellitus and pre-clinical diastolic dysfunction a population-based study. J Am Coll Cardiol 2010;55(4):300-305.
46. Ortega FB, Lavie CJ, Blair SN. Obesity and Cardiovascular Disease. Circ Res 2016;118(11):1752-1770.
47. Rutter MK, Parise H, Benjamin EJ, et al. Impact of glucose intolerance and insulin resistance on cardiac structure and function: sex-related differences in the Framingham Heart Study. Circulation 2003;107(3):448-454.
48. Ilercil A, Devereux RB, Roman MJ, et al. Relationship of impaired glucose tolerance to left ventricular structure and function: The Strong Heart Study. Am Heart J 2001;141(6):992-998.
49. Lebeche D, Davidoff AJ, Hajjar RJ. Interplay between impaired calcium regulation and insulin signaling abnormalities in diabetic cardiomyopathy. Nat Clin Pract Cardiovasc Med 2008;5(11):715-724.
50. Wong TC, Piehler KM, Kang IA, et al. Myocardial extracellular volume fraction quantified by cardiovascular magnetic resonance is increased in diabetes and associated with mortality and incident heart failure admission. Eur Heart J 2014;35(10):657-664.
51. Levelt E, Mahmod M, Piechnik SK, et al. Relationship Between Left Ventricular Structural and Metabolic Remodeling in Type 2 Diabetes. Diabetes 2016;65(1):44-52.
52. Ladeiras-Lopes R, Moreira HT, Bettencourt N, et al. Metabolic Syndrome Is Associated With Impaired Diastolic Function Independently of MRI-Derived Myocardial Extracellular Volume: The MESA Study. Diabetes 2018;67(5):1007-1012.
53. Collis T, Devereux RB, Roman MJ, et al. Relations of stroke volume and cardiac output to body composition: the strong heart study. Circulation 2001;103(6):820-825.
54. De Simone G, Devereux RB, Chinali M, et al. Sex differences in obesity-related changes in left ventricular morphology: the Strong Heart Study. J Hypertens 2011;29(7):1431-1438.
55. Rider OJ, Tayal U, Francis JM, et al. The effect of obesity and weight loss on aortic pulse wave velocity as assessed by magnetic resonance imaging. Obesity (Silver Spring) 2010;18(12):2311-2316.
56. Webb DR, Khunti K, Silverman R, et al. Impact of metabolic indices on central artery stiffness: independent association of insulin resistance and glucose with aortic pulse wave velocity. Diabetologia 2010;53(6):1190-1198.
57. Poon AK, Meyer ML, Tanaka H, et al. Association of insulin resistance, from mid-life to late-life, with aortic stiffness in late-life: the Atherosclerosis Risk in Communities Study. Cardiovasc Diabetol 2020;19(1):11.
58. Safar ME, Levy BI, Struijker-Boudier H. Current perspectives on arterial stiffness and pulse pressure in hypertension and cardiovascular diseases. Circulation 2003;107(22):2864-2869.
59. Westenberg JJ. CMR for Assessment of Diastolic Function. Curr Cardiovasc Imaging Rep 2011;4(2):149-158.
60. Paulus WJ, Tschope C. A novel paradigm for heart failure with preserved ejection fraction: comorbidities drive myocardial dysfunction and remodeling through coronary microvascular endothelial inflammation. J Am Coll Cardiol 2013;62(4):263-271.
61. Fontes-Carvalho R, Pimenta J, Bettencourt P, Leite-Moreira A, Azevedo A. Association between plasma leptin and adiponectin levels and diastolic function in the general population. Expert Opin Ther Targets 2015;19(10):1283-1291.
62. Zile MR, Gottdiener JS, Hetzel SJ, et al. Prevalence and significance of alterations in cardiac structure and function in patients with heart failure and a preserved ejection fraction. Circulation 2011;124(23):2491-2501.
63. Bonora E, Targher G, Alberiche M, et al. Homeostasis model assessment closely mirrors the glucose clamp technique in the assessment of insulin sensitivity: studies in subjects with various degrees of glucose tolerance and insulin sensitivity. Diabetes Care 2000;23(1):57-63.
64. Johansson E, Lubberink M, Heurling K, et al. Whole-Body Imaging of Tissue-specific Insulin Sensitivity and Body Composition by Using an Integrated PET/MR System: A Feasibility Study. Radiology 2018;286(1):271-278.
65. Ashrafpoor G, Bollache E, Redheuil A, et al. Age-specific changes in left ventricular diastolic function: a velocity-encoded magnetic resonance imaging study. Eur Radiol 2015;25(4):1077-1086.
66. Buss SJ, Krautz B, Schnackenburg B, et al. Classification of diastolic function with phase-contrast cardiac magnetic resonance imaging: validation with echocardiography and age-related reference values. Clin Res Cardiol 2014;103(6):441-450.
67. Rathi VK, Doyle M, Yamrozik J, et al. Routine evaluation of left ventricular diastolic function

by cardiovascular magnetic resonance: a practical approach. J Cardiovasc Magn Reson 2008;10:36.
68. Nagueh SF, Smiseth OA, Appleton CP, et al. Recommendations for the Evaluation of Left Ventricular Diastolic Function by Echocardiography: An Update from the American Society of Echocardiography and the European Association of Cardiovascular Imaging. J Am Soc Echocardiogr 2016;29(4):277-314.
69. Mancusi C, de Simone G, Best LG, et al. Myocardial mechano-energetic efficiency and insulin resistance in non-diabetic members of the Strong Heart Study cohort. Cardiovasc Diabetol 2019;18(1):56.

SUPPLEMENTARY MATERIAL

Image acquisition

VAT and aSAT were assessed by acquiring three transverse images at the level of the fifth lumbar vertebra, using a turbo spin-echo protocol, with imaging parameters: repetition/echo time (TR/TE) 300/20 ms, flip angle (FA) 90°, slice thickness 10 mm, slice gap 2 mm.

For LV structure and systolic function, the LV was imaged in short-axis orientation using electrocardiographically (ECG)-gated breath-hold balanced steady-state free precession (bSSFP), with imaging parameters: TR/TE 3.4/1.7 ms, FA 35º, slice thickness 10 mm, no slice gap, field of view (FOV) 400x400 mm, matrix size 256x256.

To determine diastolic function, an ECG-gated gradient echo sequence with velocity encoding over the mitral valve was used, with imaging parameters: TR/TE 6.5/1 ms, FA 20°, slice thickness 8 mm, FOV 350x350 mm, matrix size 256x256, velocity-encoding gradient 150 cm/s, number of phases 40.

Aortic PWV was derived from retrospectively ECG-gated gradient echo sequences with velocity-encoding (200 cm/s), acquired perpendicular to the ascending and proximal descending aorta and distal descending aorta (just above the aortic bifurcation). Aortic PWV was calculated by dividing the aortic path length by the transit time of the arrival of the systolic wave front, as previously described (1).

REFERENCES

1. Widya RL, de Mutsert R, Westenberg JJM, Gast KB, den Heijer M, le Cessie S, et al. Is Hepatic Triglyceride Content Associated with Aortic Pulse Wave Velocity and Carotid Intima-Media Thickness? The Netherlands Epidemiology of Obesity Study. Radiology 2017;285:73-82.

Supplemental Table 1. Associations of HOMA-IR, VAT, aSAT and TBF with cardiovascular parameters in the total population

	Standardized difference in cardiovascular parameters (95%CI)	
	Crude	**Adjusted**
LV structure		
LV mass, g		
Log HOMA-IR	-4.0 (-6.0 to -2.0)	-4.1 (-6.4 to -1.9)
VAT (SD: 54 cm^2)	-1.9 (-3.2 to -0.5)	-3.3 (-5.1 to -1.6)
aSAT (SD: 94 cm^2)	-2.4 (-3.6 to -1.3)	-2.5 (-4.0 to -1.0)
TBF (SD: 8%)	-0.8 (-2.2 to 0.6)	0.6 (-1.7 to 2.9)
LV end-diastolic volume, mL		
Log HOMA-IR	-8.6 (-11.4 to -5.8)	-8.5 (-11.5 to -5.5)
VAT (SD: 54 cm^2)	-6.1 (-8.3 to -4.0)	-8.9 (-11.7 to -6.1)
aSAT (SD: 94 cm^2)	0.8 (-1.1 to 2.7)	-0.5 (-2.9 to 1.8)
TBF (SD: 8%)	3.5 (1.2 to 5.8)	5.4 (1.1 to 9.7)
LV concentricity, g/mL		
Log HOMA-IR	0.02 (0.01 to 0.04)	0.01 (-0.01 to 0.02)
VAT (SD: 54 cm^2)	0.03 (0.02 to 0.04)	0.02 (0.00 to 0.03)
aSAT (SD: 94 cm^2)	-0.02 (-0.03 to -0.01)	-0.01 (-0.03 to 0.00)
TBF (SD: 8%)	-0.04 (-0.05 to -0.03)	-0.02 (-0.04 to 0.00)
LV function		
LV ejection fraction, %		
Log HOMA-IR	-0.2 (-0.9 to 0.4)	0.0 (-0.8 to 0.8)
VAT (SD: 54 cm^2)	-0.3 (-0.8 to 0.1)	0.1 (-0.6 to 0.7)
aSAT (SD: 94 cm^2)	-0.5 (-0.9 to -0.1)	-0.7 (-1.2 to -0.1)
TBF (SD: 8%)	0.1 (-0.4 to 0.5)	-0.8 (-1.6 to 0.0)
E/A ratio		
Log HOMA-IR	-0.18 (-0.24 to -0.12)	-0.11 (-0.17 to -0.05)
VAT (SD: 54 cm^2)	-0.12 (-0.16 to -0.08)	-0.04 (-0.09 to 0.01)
aSAT (SD: 94 cm^2)	-0.04 (-0.08 to 0.00)	-0.05 (-0.10 to 0.00)
TBF (SD: 8%)	-0.05 (-0.09 to 0.00)	-0.09 (-0.16 to -0.02)
Aortic stiffness		
Total aorta, m/s		
Log HOMA-IR	0.2 (0.0 to 0.4)	0.0 (-0.1 to 0.2)
VAT (SD: 54 cm^2)	0.1 (0.0 to 0.2)	0.0 (-0.1 to 0.1)
aSAT (SD: 94 cm^2)	0.0 (-0.1 to 0.1)	0.0 (-0.2 to 0.1)
TBF (SD: 8%)	0.2 (0.0 to 0.3)	0.0 (-0.2 to 0.1)

Supplemental Table 1. Associations of HOMA-IR, VAT, aSAT and TBF with cardiovascular parameters in the total population

	Standardized difference in cardiovascular parameters (95%CI)	
	Crude	**Adjusted**
Aortic arch, m/s		
Log HOMA-IR	0.2 (0.0 to 0.4)	0.0 (-0.4 to 0.3)
VAT (SD: 54 cm^2)	0.2 (0.1 to 0.4)	0.0 (-0.3 to 0.2)
aSAT (SD: 94 cm^2)	0.1 (-0.1 to 0.2)	0.1 (-0.1 to 0.3)
TBF (SD: 8%)	0.1 (-0.1 to 0.3)	0.2 (-0.1 to 0.5)
Descending aorta, m/s		
Log HOMA-IR	0.2 (-0.1 to 0.4)	0.1 (-0.2 to 0.3)
VAT (SD: 54 cm^2)	0.1 (-0.1 to 0.2)	0.0 (-0.2 to 0.2)
aSAT (SD: 94 cm^2)	0.0 (-0.1 to 0.2)	-0.1 (-0.3 to 0.1)
TBF (SD: 8%)	0.2 (0.1 to 0.4)	-0.1 (-0.5 to 0.2)
Hemodynamics		
Stroke volume, mL		
Log HOMA-IR	-5.4 (-7.4 to -3.5)	-5.1 (-7.2 to -3.0)
VAT (SD: 54 cm^2)	-4.1 (-5.6 to -2.6)	-5.6 (-7.5 to -3.7)
aSAT (SD: 94 cm^2)	-0.3 (-1.6 to 1.0)	-1.4 (-2.9 to 0.2)
TBF (SD: 8%)	1.6 (0.0 to 3.2)	2.2 (-0.5 to 4.9)
Cardiac output, mL		
Log HOMA-IR	-24 (-172 to 124)	-30 (-210 to 150)
VAT (SD: 54 cm^2)	-115 (-227 to -2)	-223 (-359 to -88)
aSAT (SD: 94 cm^2)	34 (-57 to 125)	-13 (-121 to 94)
TBF (SD: 8%)	155 (37 to 273)	242 (66 to 419)

Results represent regression coefficients per 10-fold increase in HOMA-IR or per SD of measure of adiposity. In the left column, regression coefficients for LV structure and volumes (LV mass, LV end-diastolic volume, LV stroke volume and cardiac output) are corrected for lean body mass. In the right column, regression coefficients are corrected for age, sex, ethnicity, education, smoking, physical activity, use of hormone therapy, menopausal state, hypertension, lean body mass and adiposity (HOMA-IR is adjusted for VAT and TBF, VAT is adjusted for TBF, and aSAT and TBF are adjusted for VAT). Abbreviations: aSAT: abdominal subcutaneous adipose tissue, E/A ratio: ratio of mitral early and late peak filling rate, log HOMA-IR: log-transformation of the homeostatic model assessment of insulin resistance, LV: left ventricle, LV concentricity: LV mass-to-volume ratio, PWV: pulse wave velocity, TBF: total body fat, VAT: visceral adipose tissue. All analyses are weighted towards the BMI distribution of the general population (n=914). Due to missing values, for PWV total aorta: n=911, PWV descending aorta: n=832.

Supplemental Table 2. Associations of HOMA-IR, VAT, aSAT and TBF with LV mass and volumes indexed to height$^{2.7}$

	Standardized difference in cardiovascular parameters (95%CI)	
	Crude	**Adjusted**
LV mass/height$^{2.7}$, g/m$^{2.7}$		
Log HOMA-IR	0.1 (-0.5 to 0.7)	-0.8 (-1.4 to -0.2)
VAT (SD: 54 cm^2)	1.0 (0.6 to 1.3)	-0.2 (-0.7 to 0.3)
aSAT (SD: 94 cm^2)	-0.1 (-0.4 to 0.2)	0.3 (0.0 to 0.7)
TBF (SD: 8%)	-0.7 (-1.0 to -0.4)	0.6 (-0.1 to 1.3)
LV end-diastolic volume/height$^{2.7}$, L/m$^{2.7}$		
Log HOMA-IR	-0.8 (-1.6 to -0.1)	-1.6 (-2.5 to -0.8)
VAT (SD: 54 cm^2)	0.0 (-0.5 to 0.5)	-1.0 (-1.7 to -0.3)
aSAT (SD: 94 cm^2)	1.0 (0.5 to 1.5)	1.4 (0.8 to 1.9)
TBF (SD: 8%)	0.7 (0.2 to 1.2)	2.1 (0.9 to 3.3)
Stroke volume/height$^{2.7}$, mL/m$^{2.7}$		
Log HOMA-IR	-0.6 (-1.1 to -0.1)	-1.0 (-1.6 to -0.4)
VAT (SD: 54 cm^2)	-0.1 (-0.4 to 0.2)	-0.6 (-1.1 to -0.2)
aSAT (SD: 94 cm^2)	0.5 (0.1 to 0.8)	0.6 (0.2 to 1.0)
TBF (SD: 8%)	0.4 (0.1 to 0.8)	1.0 (0.3 to 1.8)
Cardiac output/height$^{2.7}$, mL/m$^{2.7}$		
Log HOMA-IR	28 (-7 to 63)	-1 (-41 to 40)
VAT (SD: 54 cm^2)	14 (-9 to 36)	-18 (-50 to 13)
aSAT (SD: 94 cm^2)	44 (22 to 65)	45 (20 to 70)
TBF (SD: 8%)	42 (19 to 65)	79 (32 to 125)

Results represent regression coefficients per 10-fold increase in HOMA-IR or per SD of measure of adiposity. Adjusted regression coefficients are corrected for age, sex, ethnicity, education, smoking, physical activity, use of hormone therapy, menopausal state, hypertension, lean body mass and adiposity (HOMA-IR is adjusted for VAT and TBF, VAT is adjusted for TBF, and aSAT and TBF are adjusted for VAT). For abbreviations, see Supplemental Table 1.

CHAPTER

Phenotyping diabetic cardiomyopathy in Europeans and South Asians

Paiman EHM, van Eyk HJ, Bizino MB, Dekkers IA, de Heer P, Smit JWA, Jazet IM, Lamb HJ

Cardiovasc Diabetol. 2019 Oct 11;18(1):133. doi: 10.1186/s12933-019-0940-z

ABSTRACT

Background

The pathogenesis and cardiovascular impact of type 2 diabetes (T2D) may be different in South Asians compared with other ethnic groups. The phenotypic characterization of diabetic cardiomyopathy remains debated and little is known regarding differences in T2D-related cardiovascular remodeling across ethnicities. We aimed to characterize the differences in left ventricular (LV) function and structure, myocardial tissue characteristics and aortic stiffness between T2D patients and controls and to assess the differences in T2D-related cardiovascular remodeling between South Asians and Europeans.

Methods

T2D patients and controls of South Asian and European descent underwent 3 Tesla cardiovascular magnetic resonance imaging (CMR) and cardiac proton magnetic resonance spectroscopy (^{1}H-MRS). Differences in cardiovascular parameters between T2D patients and controls were examined using ANCOVA and were reported as mean (95%CI). Ethnic group comparisons in the association of T2D with cardiovascular remodeling were made by adding the interaction term between ethnicity and diabetes status to the model.

Results

A total of 131 individuals were included (54 South Asians (50.1±8.7 years, 33% men, 33 patients vs. 21 controls) and 77 Europeans (58.8±7.0 years, 56% men, 48 patients vs. 29 controls)). The transmitral early and late filling rate ratio (E/A) was lower in T2D patients compared with controls, in South Asians (-0.20 (-0.36;-0.03), ***P***=0.021) and Europeans (-0.20 (-0.36;-0.04), ***P***=0.017), whereas global longitudinal strain and aortic pulse wave velocity were similar. South Asian T2D patients had a higher LV mass (+22 g (15;30), ***P***<0.001) (***P*** for interaction by ethnicity=0.005) with a lower extracellular volume fraction (-1.9% (-3.4;-0.4), ***P***=0.013) (***P*** for interaction=0.114), whilst European T2D patients had a higher myocardial triglyceride content (+0.59% (0.35;0.84), ***P***=0.001) than their control group (***P*** for interaction=0.002).

Conclusion

Diabetic cardiomyopathy was characterized by impaired LV diastolic function in South Asians and Europeans. Increased LV mass was solely observed among South Asian T2D patients, whereas differences in myocardial triglyceride content between T2D patients and controls were only present in the European cohort. The diabetic cardiomyopathy phenotype may differ between subsets of T2D patients, for example across ethnicities, and tailored strategies for T2D management may be required.

BACKGROUND

Type 2 diabetes (T2D), independent of other cardiovascular risk factors, is associated with an increased risk of heart failure (1). South Asians, who represent 20% of the world's population, are at particular risk of developing T2D (2,3). Individuals of South Asian descent appear to have a metabolically disadvantageous phenotype with a relatively high total body fat percentage (4,5). Also, the metabolic sensitivity to excess fat mass may be more pronounced among South Asians compared with other ethnic groups, as indicated by increased insulin resistance at similar adiposity levels (6,7). In individuals of South Asian descent, the release of adipose tissue metabolites may be disturbed (8). Also, in South Asians in particular, excess fat mass may cause a state of chronic inflammation (9). Importantly, the impact of T2D on cardiac function may be greater among South Asians compared with Europeans (10). However, most previous studies on diabetic cardiomyopathy were performed in white populations or ethnicity was not reported (11-13). Little is known regarding the differences in the diabetic cardiomyopathy phenotype across ethnicities, whereas increased insight into the ethnic-specific cardiovascular consequences may guide the development of tailored strategies for the management of T2D.

By using cardiovascular magnetic resonance (CMR), the impact of T2D on the left ventricle (LV) can be characterized on a functional, structural and myocardial tissue level. Strain echocardiography studies have shown that not merely LV diastolic function, which may be most susceptible to myocardial energy depletion, but also LV systolic function might be impaired (14). The introduction of feature tracking has enabled the assessment of both longitudinal and circumferential strain based on standard cine images, which can be considered more sensitive measures of myocardial contractility compared with LV ejection fraction (15). Myocardial diffuse fibrosis, as the result of hyperglycemia and systemic inflammation in T2D, may be an early hallmark of LV remodeling, preceding functional impairments (16). Also, myocardial steatosis has been proposed as an important contributing factor to both LV structural and functional remodeling in patients with T2D (12-14). In this study, we aimed to characterize the differences in CMR-derived LV systolic and diastolic function, LV structure and myocardial tissue characteristics and aortic stiffness between T2D patients and controls and to assess the differences in T2D-related cardiovascular remodeling between South Asians and Europeans.

METHODS

Study population

This is a single-center, cross-sectional study. The data of the T2D patients of European and South Asian origin (i.e. Hindustani Surinamese, Indian, Pakistani, Bangladeshi or Sri Lankan) were derived from the baseline measurements of two previous randomized controlled trials (ClinicalTrials.gov NCT01761318 (17) and NCT02660047 (18), respectively). In addition, healthy

controls of European and South Asian descent in the same age range and with a similar sex distribution as compared with the T2D patients were prospectively enrolled. Ethnicity was based on self-identified origin and self-reported origin of both biological parents and their ancestors. Written informed consent was obtained prior to inclusion. The study complied with the revised Declaration of Helsinki and was approved by the institutional review board (Leiden University Medical Center, Leiden, the Netherlands).

All T2D patients were obese (body mass index (BMI) ≥25 kg/m^2 for Europeans and ≥23 kg/m^2 for South Asians) and used metformin, sulfonylurea derivatives and/or insulin. Initially, the inclusion criteria for the European and South Asian study population were similar. However, due to the insufficient number of eligible patients, the inclusion criteria for the South Asian T2D patients were adjusted. For the European and South Asian T2D patients, respectively, age ranged from 18-70 and 18-75 year, glycated hemoglobin (HbA1c) was ≥52.5 and <86.5 mmol/mol (≥7.0 and ≤10.0%) and ≥47.5 and <96.5 mmol/mol (≥6.5 and ≤11.0%), systolic and diastolic blood pressure was <150/85 mmHg and <180/110 mmHg, estimated glomerular filtration rate (eGFR) was >60 ml/min/1.73m^2 and >30 ml/min/1.73m^2, no history of significant coronary artery disease for the European T2D group (significant coronary artery disease was defined as: a history of coronary artery bypass grafting and/or percutaneous coronary intervention or significant coronary artery stenosis proven by coronary angiography or non-invasive imaging), and no acute coronary accident in the preceding 30 days for the South Asian T2D group. Main exclusion criteria were: any contra-indication for contrast-enhanced CMR and heart failure New York Heart Association class III-IV. All T2D patients were screened for abnormalities on rest echocardiography (ECG). For the present study, all T2D patients with significant coronary artery disease or valvular disease were excluded.

The healthy controls were recruited by advertisements in Leiden University Medical Center (Leiden, the Netherlands) and in local newspapers. Individuals aged 40-70 years without a history of cardiovascular disease, no medication use and no contra-indications for contrast-enhanced CMR were eligible for participation in the healthy control group. Exclusion criteria were: prediabetes or diabetes (fasting glucose ≥6.1 mmol/L, 2-h glucose after 75 glucose ≥7.8 mmol/L or HbA1c ≥39 mmol/mol (≥5.7%)), metabolic syndrome (≥2 of the following criteria: systolic and diastolic blood pressure blood pressure ≥140/90 mmHg; triglycerides ≥1.7 mmol/L; HDL-cholesterol <0.9 mmol/L for men or <1.0 mmol/L for women; obesity (BMI ≥30 kg/m^2) or abdominal obesity (waist/hip ratio: >0.9 for men or >0.85 for women or high waist circumference: ≥102 cm for men or ≥88 cm for women (Europeans); ≥90 cm for men or ≥80 cm for women (South Asians))), abnormalities upon physical examination, laboratory assessment (blood count, liver and kidney function) or rest ECG.

Data collection

Study participants were included after a screening visit. Clinical and CMR examinations were scheduled either in the morning or evening, after an overnight or 6 hour fast, respectively

(for T2D patients, the insulin dose was adjusted and other glucose-lowering medication was temporarily discontinued). Smoking status was self-reported and was categorized as currently vs. previously or never. Blood pressure was measured in seated position on the right arm after rest, using a validated automatic oscillometric device (SureSigns VS3 Vital signs monitor, Philips, Best, the Netherlands) and was the mean of two consecutive measurements. HbA1c was examined with ion-exchange high-performance liquid chromatography (HPLC; Tosoh G8, Sysmex Nederland B.V., Etten-Leur, the Netherlands). Lipid levels were assessed on a Modular P800 analyzer (Roche Diagnostics, Mannheim, Germany) with calculation of low-density protein (LDL)-cholesterol according to the Friedewald formula. The total body fat percentage was derived from bioelectrical impedance analysis (BIA; Bodystat 1500, Bodystart Ltd., Douglas, United Kingdom).

CMR acquisition and analysis

CMR scans were acquired using a 3 Tesla MR scanner with a dStream Torso anterior coil and a FlexCoverage posterior coil, with up to 32 coil elements for signal reception (Ingenia, Philips, Best, the Netherlands).

VAT and abdominal SAT

Visceral and abdominal subcutaneous adipose tissue (VAT and abdominal SAT) were assessed on 2-point Dixon water-fat separated transverse images of the abdomen. VAT and abdominal SAT were semi-automatically measured based on pixel intensity thresholding on three reformatted transverse slices at the level of the fourth and fifth lumbar vertebrae, with slice thickness of 10 mm and slice gap of 12 mm (repetition time (TR) 3.5 ms, first/second echo time (TE) 1.19/2.3 ms, flip angle (FA) 10°, field of view (FOV) 500x365 mm^2, acquired voxel size 1.60x1.70 mm^2, slice thickness 4 mm, slice gap -2 mm, number of slices 140). VAT and abdominal SAT were quantified as the mean area in squared centimeters of all three slices (MASS version 2015-EXP, Leiden University Medical Center, Leiden, the Netherlands).

LV systolic and diastolic function

LV function was examined on breath-hold ECG-triggered short-axis and 2-, 3- and 4-chamber long-axis cine balanced steady-state free precession (TE/TR 1.5/3.0 ms, FA 45°, FOV 350x350 mm^2 (4-chamber) and 400x352 mm^2 (short-axis), acquired voxel size 2.0x1.6 mm^2 (4-chamber) and 1.5x1.5 mm^2 (short-axis), slice thickness 8 mm, number of phases 30 (4-chamber) and 35 (short-axis)) and free-breathing ECG-gated whole-heart gradient-echo 4D velocity-encoded MR (venc 150 cm/s, TE/TR 4.6/9.0 ms, FA 10°, FOV 360x360 mm^2, acquired voxel size 3.0x3.0 mm^2, slice thickness 3 mm, number of slices 41, number of phases 30, sensitivity encoding (SENSE) factor 2).

LV systolic function parameters included LV ejection fraction measured on short-axis cines (MASS version 2015-EXP, Leiden University Medical Center, Leiden, the Netherlands)

and global longitudinal and circumferential strain (GLS and GCS) derived from long-axis and short-axis cines using feature tracking (QStrain 2.0, Medis Suite 3.0, Medis medical imaging systems, Leiden, the Netherlands). LV contours were semi-automatically drawn in the short-axis images in the end-diastolic and end-systolic phase, to quantify the end-diastolic LV mass, LV end-diastolic and end-systolic volumes, LV stroke volume, ejection fraction, cardiac output and cardiac index. GLS was the average of the peak systolic strain on 2-, 3- and 4-chamber cines. GCS was the peak systolic strain in the mid-ventricular short-axis cines.

LV diastolic strain parameters included the global longitudinal early peak diastolic strain rate (GLSR-E) (average of the early peak diastolic strain rate in 2-, 3- and 4-chamber view) and the global circumferential early peak diastolic strain rate (GCSR-E) (the early peak diastolic strain rate in the mid-ventricular short-axis cines). LV diastolic function parameters derived from 4D velocity-encoded MR included the ratio of the transmitral early (E) and late (A) peak filling rate (E/A ratio), the peak deceleration slope of the E wave (Edec), the estimated LV filling pressure (the ratio of the transmitral early peak velocity and the early peak diastolic mitral septal tissue velocity (Ea) measured on 4-chamber cines) and the estimated LV compliance (the ratio of LV end-diastolic volume and the estimated LV filling pressure) (19). The transmitral flow rate curves were constructed after retrospective mitral valve tracking, perpendicular to the streamlines of inflow across the mitral valve, at the location of peak flow velocity, with correction for through-plane motion of the LV myocardial wall (MASS version 2015-EXP, Leiden University Medical Center, Leiden, the Netherlands) (20,21).

Aortic stiffness

Aortic stiffness was quantified by the aortic pulse wave velocity, which was derived from a double-oblique aorta scout view and two free-breathing 2D velocity-encoded MR scans at the level of the ascending and abdominal aorta (venc 200 cm/s and 150 cm/s, respectively; TE/TR 2.5/4.4 ms, FA 20°, FOV 350x282 mm^2, slice thickness 8 mm, acquired voxel size 2.8x2.8 mm^2, temporal resolution 10 ms). The aortic pulse wave velocity was calculated by dividing the distance between ascending and abdominal aorta by the transit time of the systolic wave front (MASS version 2015-EXP, Leiden University Medical Center, Leiden, the Netherlands and in-house developed software) (22).

Myocardial steatosis

Myocardial steatosis was examined using ECG-triggered, respiratory-navigated cardiac proton-magnetic resonance spectroscopy (^{1}H-MRS) in a voxel of 40x15x25 mm^3 in the mid-ventricular septum, using a high permittivity pad on the thorax (TE 35 ms, TR 3.5 or 9 seconds (water-suppressed and non-water suppressed acquisition, respectively), acquired samples 2048 (spectral resolution 0.73 Hz/sample), number of signal averages 64 or 6 (water-suppressed and non-water suppressed acquisition, respectively)) (23). Starting values for the fit of the acquired spectrum were: triglyceride methyl (CH_3) 0.9 ppm, triglyceride methylene $(CH_2)^n$ 1.3 ppm, COO-

CH_2 2.05 ppm, creatine 3.05 ppm, trimethylamines (TMA) 3.25 ppm. The myocardial triglyceride content was quantified as the amplitude of $(CH_2)^n$ divided by the amplitude of unsuppressed water, multiplied by 100%) (24) (in-house developed software and the Java-based MR user interface, jMRUI v5.0; MRUI Consortium) (25,26).

Myocardial diffuse fibrosis

Myocardial diffuse fibrosis was quantified using native and post-contrast modified Look-Locker inversion recovery (MOLLI) T1 mapping, obtained in short-axis orientation at the mid-ventricular level (TE/TR 1.1/2.3 ms, FA 20°, FOV 350x300 mm^2, slice thickness 8 mm, acquired voxel size 2.1x2.1 mm^2, SENSE factor 2). Post-contrast T1 mapping was acquired 20-25 minutes after administration of 0.15 mmol gadoterate meglumine (0.5 mmol/mL Dotarem; Guerbet Villepinte, France) per kilogram of body weight. Because of ongoing optimization of the T1 mapping protocols throughout the study, native and post-contrast MOLLI acquisition schemes were adjusted (for the European T2D patients: 3b(3b)3b(3b)5b and 3b(3b)3b(3b)5b; for the European controls: 3b(3s)3b(3s)5b and 3b(3s)3b(3s)5b; for the South Asian T2D patients and controls: 5s(3s)3s and 4s(1s)3s(1s)2s, respectively). T1 relaxation times were measured in the mid-ventricular septum, after manual correction for motion (QMap 2.2.18, Medis Suite 3.0, Medis medical imaging systems, Leiden, the Netherlands).

Statistical analysis

Clinical characteristics, adiposity and cardiovascular parameters were presented for the T2D and control group, for Europeans and South Asians separately, and were expressed as means ± SD, medians (interquartile ranges) or numbers (percentages). We assessed the differences in clinical characteristics and cardiovascular parameters between T2D patients and controls, for Europeans and South Asians, using the Student's t-test or the Fisher's exact test, and reported the differences in adiposity parameters as means (95%CI). Differences in cardiovascular parameters between T2D patients and controls, for South Asians and Europeans, were further examined using ANCOVA with adjustment for age, sex, systolic and diastolic blood pressure and smoking status (currently vs. never or formerly). Ethnic group comparisons in the association of T2D with cardiovascular remodeling were made by adding the interaction term between ethnicity and diabetes status to the model (10). We assessed the normal distribution of the data visually. All statistical tests were two-sided and $P<0.05$ was considered significant. Statistical analyses were performed using SPSS 23 (IBM Corp, New York, United States).

RESULTS

Clinical characteristics and adiposity parameters

In the present study, 48 of the 50 European T2D patients who participated in the trial NCT01761318 (17) were included (n=1 was excluded because of type 1 diabetes and n=1 was excluded because of missing CMR data due to claustrophobia). South Asian T2D patients with age >65 years who participated in the trial NCT02660047 (18) were excluded in this study, as we were unable to enroll South Asian healthy controls in this age category due to the high prevalence of cardiometabolic risk factors among older South Asian individuals. In the current study, 33 of the 47 South Asian T2D patients were included (n=6 were excluded because of age >65 years, subsequently n=6 were excluded due to significant coronary artery disease and n=2 due to mitral valve insufficiency and/or stenosis on CMR).

Table 1. Clinical characteristics and adiposity parameters

	Europeans		South Asians	
	T2D (n=48)	**Controls (n=29)**	**T2D (n=33)**	**Controls (n=21)**
Age, years	59.5 ± 6.6	57.6 ± 7.8	51.3 ± 9.0	48.3 ± 8.1
Men, no. (%)	28 (58%)	15 (52%)	12 (36%)	6 (29%)
Current smoker, no. (%)	9 (19%)	1 (3%)	5 (15%)	3 (14%)
BSA, m^2	2.1 ± 0.2*	1.9 ± 0.2	1.9 ± 0.2*	1.7 ± 0.2
BMI, kg/m^2	32 ± 4*	24 ± 3	30 ± 4*	24 ± 3
Waist circumference, cm	110 ± 9*	87 ± 9	101 ± 10*	82 ± 7
Men	109 ± 8	91 ± 7	103 ± 8	86 ± 8
Women	112 ± 10	82 ± 9	100 ± 11	81 ± 7
Waist-hip ratio	1.03 ± 0.07*	0.88 ± 0.08	0.96 ± 0.09*	0.86 ± 0.07
Men	1.05 ± 0.06	0.93 ± 0.04	1.00 ± 0.08	0.93 ± 0.05
Women	1.00 ± 0.07	0.83 ± 0.07	0.94 ± 0.08	0.84 ± 0.07
Systolic blood pressure, mmHg	141 ± 15*	126 ± 12	141 ± 21*	124 ± 14
Diastolic blood pressure, mmHg	87 ± 9*	80 ± 8	85 ± 11	80 ± 12
Heart rate, beats/min	71 ± 12*	59 ± 9	69 ± 12*	61 ± 8
Triglycerides, mmol/L	2.2 ± 1.3*	1.0 ± 0.4	1.9 ± 1.5*	0.9 ± 0.3
Total cholesterol, mmol/L	4.8 ± 1.0*	5.7 ± 1.1	4.4 ± 1.0*	5.4 ± 0.8
HDL-cholesterol, mmol/L	1.3 ± 0.3*	1.9 ± 0.5	1.2 ± 0.3*	1.6 ± 0.3
LDL-cholesterol, mmol/L	2.6 ± 0.9*	3.3 ± 1.0	2.2 ± 0.9*	3.4 ± 0.7
Glycated hemoglobin, mmol/mol	65.5 ± 10.8*	35.5 ± 2.7	66.2 ± 11.3*	35.5 ± 2.4
Serum creatinine, µmol/L	70 ± 18	76 ± 14	67 ± 17	73 ± 18
Urinary ACR, mg/mmol	0.7 (0.0; 2.7)	–	1.9 (0.5; 6.4)	–
Microalbuminuria, no. (%)	9 (19%)	–	10 (30%)	–
Macroalbuminuria, no. (%)	1 (2%)	–	3 (9%)	–

Table 1. Clinical characteristics and adiposity parameters

	Europeans		South Asians	
	T2D (n=48)	Controls (n=29)	T2D (n=33)	Controls (n=21)
Diabetes duration, years	10.7 ± 6.2	–	15.1 ± 9.4	–
Metformin, no. (%)	48 (100%)	–	32 (97%)	–
Insulin, no. (%)	31 (65%)	–	23 (70%)	–
Insulin dose, units/day	44 (32; 94)	–	78 (45; 108)	–
Lipid lowering drugs, no. (%)	39 (81%)	–	25 (76%)	–
Antihypertensive drugs, no. (%)	37 (77%)	–	20 (61%)	–
ACE-inhibitors, no. (%)	17 (35%)	–	8 (24%)	–
Total body fat, %	36.7 ± 9.3*	26.9 ± 7.3	37.3 ± 9.1*	32.3 ± 7.1
Men	29.7 ± 3.6	21.9 ± 3.1	27.3 ± 4.9	23.3 ± 4.2
Women	46.4 ± 5.0	32.2 ± 6.7	42.5 ± 5.7	36.0 ± 4.0
Abdominal SAT, cm^2	346 ± 125*	200 ± 69	344 ± 128*	248 ± 109
Men	277 ± 93	173 ± 55	309 ± 109	204 ± 109
Women	442 ± 97	228 ± 73	364 ± 136	265 ± 107
VAT, cm^2	207 ± 75*	76 ± 34	152 ± 48*	73 ± 30
Men	214 ± 63	89 ± 31	158 ± 49	94 ± 19
Women	197 ± 89	62 ± 32	148 ± 48	65 ± 29

Means ± SD, medians (interquartile range) or numbers (percentages) are presented. * *P*<0.05 vs. controls. Microalbuminuria and macroalbuminuria: urinary albumin/creatinine ratio (ACR) 3-30 mg/mmol and >30 mg/mmol, respectively. Missing values: n=1 for total body fat in the South Asian T2D group. Abbreviations: ACE: angiotensin-converting enzyme; ACR: albumin/creatinine ratio; BMI: body mass index; BSA: body surface area; HDL and LDL: high-density and low-density lipoprotein; VAT and SAT: visceral and subcutaneous adipose tissue.

In total, the present study comprised 131 individuals (n=81 patients with T2D and n=50 healthy controls). In the European cohort (n=77), 48 patients (mean ± SD age: 59.5 ± 6.6 years, diabetes duration: 10.7 ± 6.2 years, 28 (58%) men) and 29 controls (mean ± SD age: 57.6 ± 7.8 years, diabetes duration: 15.1 ± 9.4 years, 15 (52%) men) were included. The South Asian study population (n=54) consisted of 33 patients (51.3 ± 9.0 years, 12 (36%) men) and 21 controls (48.3 ± 8.1 years, 6 (29%) men). Baseline characteristics are presented in **Table 1**. Whereas the T2D and healthy control groups were similar according to age and sex distribution for both the South Asian and European cohort, the South Asian compared with the European study population was younger (50.1 ± 8.7 vs. 58.8 ± 7.0 years, *P*<0.001) and consisted of more women (18/54 (33%) vs. 43/77 (56%) men, *P*=0.013). The European and South Asian control groups were similar regarding smoking status (*P*=0.297), systolic and diastolic blood pressure (*P*=0.467 and 0.973, respectively), triglycerides (*P*=0.582), total cholesterol (*P*=0.285), LDL-cholesterol (*P*=0.848) and HbA1c (*P*=0.925), except that high-density lipoprotein (HDL)-cholesterol was lower among the South Asians (*P*=0.010). For the South Asian as compared with the European

T2D patients, diabetes duration was longer (*P*=0.012), the daily insulin dose tended to be higher (*P*=0.056), the urinary albumin/creatinine ratio was higher (*P*=0.045) and total cholesterol was lower (*P*=0.046), whereas HbA1c was similar (*P*=0.801).

In both the European and South Asian populations, obesity and adipose tissue parameters, blood pressure, cholesterol and glycemic levels were higher in the T2D compared with the control group (**Table 1**). Differences in obesity and adipose tissue parameters between the T2D and control group in the European and South Asian population were 7.8 (6.1 to 9.5) kg/m^2 and 6.2 (4.1 to 8.3) kg/m^2 for BMI, 24 (20 to 28) cm and 19 (14 to 24) cm for waist circumference, 0.15 (0.11 to 0.18) vs. 0.10 (0.05 to 0.14) for waist-hip ratio, 9.8 (5.8 to 13.8)% and 5.0 (0.3 to 9.7)% for total body fat percentage, 131 (102 to 160) cm^2 and 79 (55 to 102) cm^2 for VAT and 146 (96 to 197) cm^2 and 96 (28 vs. 164) cm^2 for abdominal SAT, respectively.

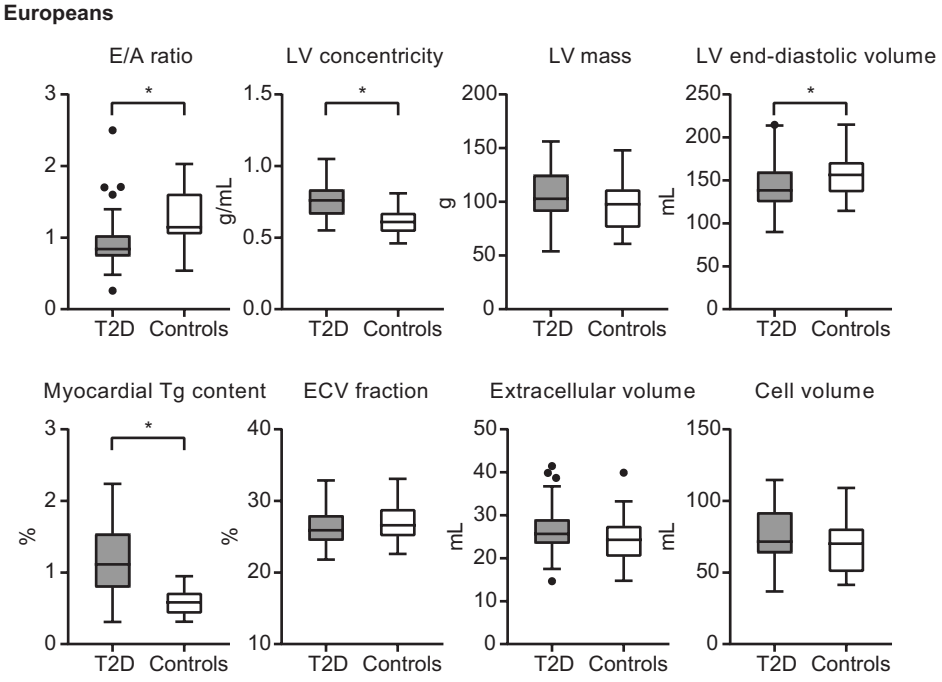

Figure 1. Cardiovascular parameters (boxplots depicting median, interquartile ranges and outliers) in European T2D patients (n=48) and controls (n=29) (* *P*<0.05). In European T2D patients, the E/A ratio was lower than in the controls, LV concentricity was higher in parallel with a lower LV end-diastolic volume, and the myocardial triglyceride content was higher. Abbreviations: E/A: transmitral early to late filling rate ratio; ECV: extracellular volume; LV: left ventricular; Tg: triglyceride.

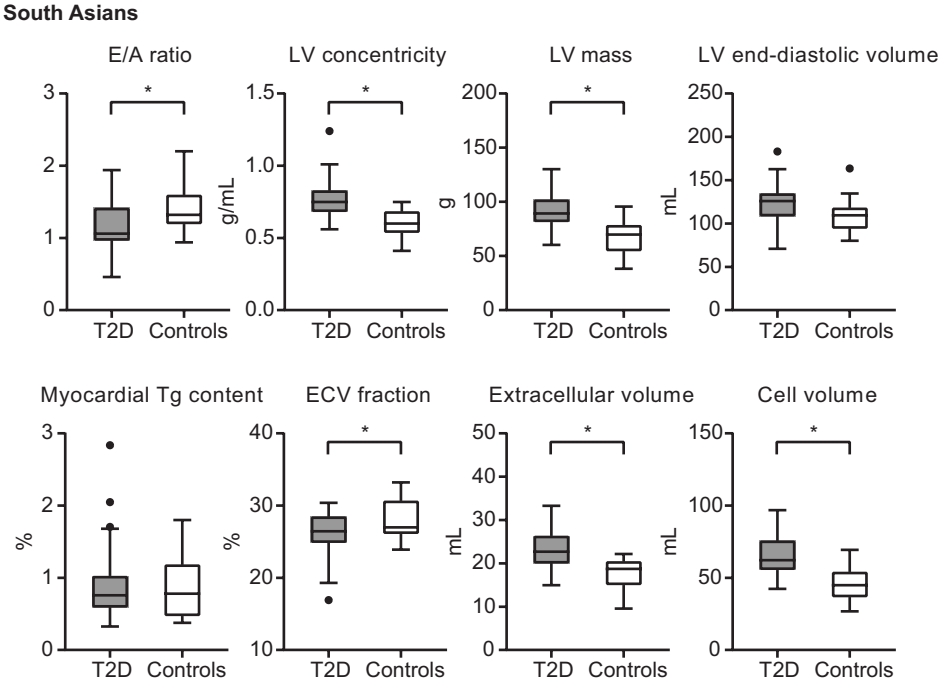

Figure 2. Cardiovascular parameters (boxplots depicting median, interquartile ranges and outliers) in South Asian T2D patients (n=33) compared with controls (n=21) (* $P<0.05$). In South Asian T2D patients, the E/A ratio was lower than in the controls and LV concentricity was higher in parallel with a higher LV mass. As both the LV extracellular volume and myocardial cell volume were higher, the ECV fraction was slightly lower in South Asian T2D patients than in controls. Abbreviations as in Figure 1.

Association between T2D and cardiovascular parameters in Europeans and South Asians

In univariable analyses, for both Europeans and South Asians, T2D patients as compared with controls had LV structural alterations (higher LV concentricity), with impairments in LV diastolic function (lower E/A ratio and higher LV filling pressure) and aortic stiffness (higher aortic pulse wave velocity) (**Table 2 and 3**). The E dec peak, Ea, LV compliance and GLS were impaired in the T2D patients compared with the controls among Europeans but not among South Asians. Cardiovascular parameters for the T2D patients and controls are presented in **Figure 1-3.**

Table 2. Cardiovascular parameters in Europeans

	T2D (n=48)	Controls (n=29)
LV diastolic function		
E, mL/s	326 ± 97	352 ± 55
A, mL/s	366 ± 71*	301 ± 75
E/A ratio	0.93 ± 0.38*	1.24 ± 0.36
E dec peak, mL/s2 x10-3	-2.7 ± 1.0*	-3.2 ± 0.7
Ea, cm/s	5.9 ± 1.7*	7.7 ± 1.9
Estimate of LV filling pressure, mmHg	7.6 ± 2.6*	5.1 ± 1.7
Estimate of LV compliance, mL/mmHg	21.3 ± 9.4*	33.4 ± 11.2
GLSR-E, 1/s	0.78 ± 0.23	0.87 ± 0.28
GCSR-E, 1/s	1.15 ± 0.37	1.22 ± 0.37
LV systolic function		
Ejection fraction, %	55 ± 5	56 ± 6
GLS, %	-19.3 ± 2.7*	-21.1 ± 3.3
GCS, %	-26.1 ± 4.5	-26.5 ± 3.9
Hemodynamics		
Stroke volume, mL	78 ± 17*	88 ± 17
Cardiac output, L/min	5.4 ± 1.0	5.2 ± 1.1
Cardiac index, L/min/m2	2.5 ± 0.4*	2.7 ± 0.5
Aorta stiffness		
Aortic pulse wave velocity, m/s	8.5 ± 2.2*	7.5 ± 1.5
LV structure		
End-diastolic volume, mL	142 ± 29*	156 ± 26
Mass, g	107 ± 23	96 ± 24
Concentricity, g/mL	0.76 ± 0.12*	0.61 ± 0.09
Myocardial tissue characteristics		
Myocardial Tg content, %	1.19 ± 0.53*	0.58 ± 0.18
Native T1, ms	1197 ± 44*	1230 ± 28
Extracellular volume fraction, %	26.3 ± 2.5	26.9 ± 2.7
Extracellular volume, mL	27 ± 6	24 ± 5
Cell volume, mL	75 ± 18	67 ± 18

Means ± SD. * P<0.05 vs. controls. Missing values in the T2D group: n=1 for all flow-derived LV diastolic function parameters, n=3 E dec peak, n=1 GLSR-E, n=1 aortic pulse wave velocity, n=1 myocardial Tg content, n=4 native T1, n=5 extracellular volume, cell volume, fibrosis volume; in the control group: n=1 for all flow-derived LV diastolic function parameters. Abbreviations: Ea: early peak diastolic mitral septal tissue velocity; E and A: transmitral early and late filling rate; E dec peak: peak deceleration slope of E; GLS and GLSR-E: global longitudinal strain and early peak diastolic strain rate, GCS and GCSR-E: global circumferential strain and early peak diastolic strain rate; LV: left ventricular; Tg: triglyceride.

Table 3. Cardiovascular parameters in South Asians

	T2D (n=33)	Controls (n=21)
LV diastolic function		
E, mL/s	339 ± 109	333 ± 67
A, mL/s	302 ± 64*	242 ± 54
E/A ratio	1.15 ± 0.37*	1.42 ± 0.36
E dec peak, mL/s2 x10-3	-2.9 ± 1.2	-3.2 ± 0.7
Ea, cm/s	5.9 ± 2.0	6.8 ± 1.9
Estimate of LV filling pressure, mmHg	6.9 ± 3.0*	5.0 ± 1.6
Estimate of LV compliance, mL/mmHg	20.5 ± 9.0	24.0 ± 7.7
GLSR-E, 1/s	0.88 ± 0.22	0.98 ± 0.16
GCSR-E, 1/s	1.32 ± 0.34	1.31 ± 0.24
LV systolic function		
Ejection fraction, %	58 ± 6	60 ± 5
GLS, %	-20.4 ± 2.8	-21.7 ± 1.7
GCS, %	-27.6 ± 4.3	-27.6 ± 3.4
Hemodynamics		
Stroke volume, mL	70 ± 14	66 ± 12
Cardiac output, L/min	4.8 ± 1.0*	4.0 ± 0.7
Cardiac index, L/min/m2	2.5 ± 0.4	2.3 ± 0.3
Aorta stiffness		
Aortic pulse wave velocity, m/s	7.9 ± 2.0*	6.5 ± 1.1
LV structure		
End-diastolic volume, mL	123 ± 25	110 ± 19
Mass, g	93 ± 20*	66 ± 15
Concentricity, g/mL	0.77 ± 0.14*	0.60 ± 0.10
Myocardial tissue characteristics		
Myocardial Tg content, %	0.93 ± 0.54	0.84 ± 0.43
Native T1, ms	1255 ± 37	1263 ± 42
Extracellular volume fraction, %	26.2 ± 3.0*	28.2 ± 2.6
Extracellular volume, mL	23 ± 5*	18 ± 4
Cell volume, mL	66 ± 16*	45 ± 11

Means ± SD. * P<0.05 vs. controls. Missing values in the T2D group: n=1 native T1 and extracellular volume, cell volume, fibrosis volume; in the control group: n=1 for myocardial Tg content. For abbreviations see Table 2.

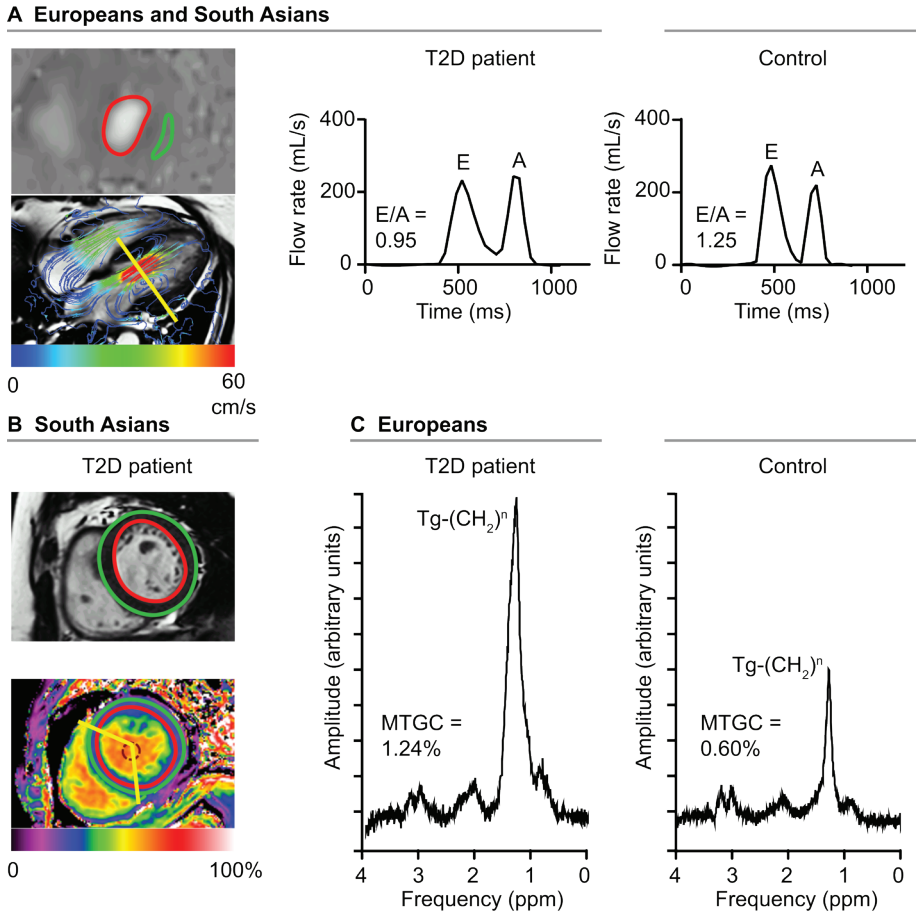

Figure 3. Diabetic cardiomyopathy phenotype in Europeans and South Asians. (**A**) Impaired LV diastolic function, as indicated by a lower ratio of the transmitral early and late filling rate (E/A) was identified as a common characteristic of diabetic cardiomyopathy in Europeans and South Asians. The E/A ratio was measured using 4D velocity-encoded MR after retrospective mitral valve tracking and through-plane motion correction (***left image***). An example of the transmitral flow rate curve in a T2D patient (South Asian 62-year-old woman with E/A: 0.95) and healthy control (South Asian 57-year-old women with E/A: 1.25) is provided (***right images***). (**B**) In South Asian but not in European T2D patients the LV mass, measured on short-axis cine (***upper image***), was higher than in the control group and the extracellular volume fraction, measured in the mid-ventricular septum using T1 mapping (***lower image***), was decreased. In the presented South Asian T2D patient, LV mass was 97 g and extracellular volume fraction was 27%. (**C**) Among Europeans but not among South Asians the myocardial triglyceride content was different for T2D patients compared with controls. An example of cardiac proton-magnetic resonance spectroscopy (^{1}H-MRS) in a 45-year-old woman with T2D (***left image***) and in a 48-year-old non-diabetic woman (***right image***) of European descent is provided (myocardial triglyceride content (MTGC): 1.24% and 0.60%, respectively).

Table 4. Association between T2D and cardiovascular parameters

	Adjusted mean difference (95%CI) between T2D patients and controls		
	Europeans (n=77)	**South Asians (n=54)**	***P* for interaction by ethnicity**
LV diastolic function			
E/A	-0.20 (-0.36, -0.04)	-0.20 (-0.36, -0.03)	0.480
E dec peak, mL/s^2 x10^{-3}	0.35 (-0.13, 0.83)	-0.03 (-0.54, 0.49)	0.576
Ea, cm/s	-1.1 (-1.9, -0.4)	-0.4 (-1.4, 0.6)	0.095
LV filling pressure, mmHg	2.3 (1.0, 3.6)	1.0 (-0.4, 2.4)	0.300
LV compliance, mL/mmHg	-12.9 (-18.6, -7.2)	-1.5 (-6.1, 3.1)	0.008
LV systolic function			
GLS, %	0.6 (-0.9, 2.1)	1.3 (-0.2, 2.8)	0.708
Hemodynamics			
Stroke volume, mL	-10 (-19, -1)	3 (-4, 11)	0.007
Cardiac output, L/min	0.3 (-0.3, 0.8)	0.8 (0.3, 1.3)	0.067
Cardiac index, L/min/m^2	-0.2 (-0.4, 0.0)	0.1 (-0.1, 0.3)	0.012
Aortic stiffness			
Aortic pulse wave velocity, m/s	0.2 (-0.8, 1.2)	0.6 (-0.2, 1.4)	0.761
LV structure			
End-diastolic volume, mL	-20 (-34, -7)	11 (0, 22)	0.001
Mass, g	-1 (-11, 8)	22 (15, 30)	0.005
Concentricity, g/mL	0.10 (0.04, 0.15)	0.14 (0.07, 0.21)	0.574
Myocardial tissue characteristics			
Myocardial Tg content, %	0.59 (0.35, 0.84)	0.10 (-0.20, 0.41)	0.002
Native T1, ms	-25 (-47, -3)	-6 (-31, 18)	0.078
Extracellular volume fraction, %	1.0 (-0.3, 2.2)	-1.9 (-3.4, -0.4)	0.114
Extracellular volume, mL	-1 (-2, 4)	4 (2, 7)	0.071
Cell volume, mL	-3 (-10, 4)	17 (12, 23)	0.003

Adjusted mean difference (95%CI) with correction for age, sex, ethnicity, smoking status (currently vs. never or previously), systolic and diastolic blood pressure. ***P*** value for the interaction by ethnicity in the association between diabetes status and each cardiovascular parameter. For details on missing values see Table 2 and 3. For abbreviations see Table 2.

In multivariable analyses, in both European and South Asian patients the E/A ratio remained lower and LV concentricity persisted to be higher compared with controls, but there were no differences in the E dec peak, GLS or aortic pulse wave velocity (**Table 4**). Furthermore, in multivariable analyses, the LV filling pressure was increased or tended to be higher in European and South Asian T2D patients, respectively, compared with their controls. In European but not in South Asian patients, additionally, Ea and LV compliance were lower in comparison with their controls (***P***=0.095 and 0.008 for interaction by ethnicity, respectively). In European T2D patients

the stroke volume was reduced, with a slight decrease in cardiac index, whereas in South Asian T2D patients cardiac index was preserved in comparison with their control groups (*P*=0.012 for interaction by ethnicity). In European T2D patients the LV concentricity was increased in parallel with lower end-diastolic volumes (*P*=0.001 for interaction by ethnicity), whereas in South Asian T2D patients the increased LV concentricity was in parallel with a higher LV mass (*P*=0.005 for interaction by ethnicity). In South Asian but not in European T2D patients compared with their controls, the myocardial cell and extracellular volumes were higher (*P*=0.003 and 0.071 for interaction by ethnicity, respectively). Because of a larger increase in the myocardial cell volume than in the extracellular volume, the extracellular volume fraction was slightly lower in the South Asian T2D patients than in the controls (*P*=0.114 for interaction by ethnicity). In European but not South Asian T2D patients, the myocardial triglyceride content was higher and native T1 was lower in comparison with their controls (*P*=0.002 and 0.078 for interaction by ethnicity, respectively)

DISCUSSION

In both Europeans and South Asians, the E/A ratio was lower in relation to T2D, whereas global systolic and diastolic strain parameters and aortic pulse wave velocity were similar in the T2D patients and controls in multivariable analysis. Furthermore, South Asian T2D patients had a higher LV mass with a lower extracellular volume fraction, whilst European T2D patients had a higher myocardial triglyceride content than their control group.

LV functional and structural remodeling in T2D

In our study, in both the European and South Asian population, T2D was associated with reduced LV diastolic function and increased LV concentricity. LV diastolic function in T2D may be impaired due to disturbances in myocardial substrate utilization and myocardial energetics (11,27). More recently, the pro-inflammatory state in T2D has been proposed as an important contributing factor to the increased diastolic LV stiffness (28). LV diastolic function may be most susceptible to energy shortage (29), whereas abnormalities in LV systolic function may develop once myocardial energetics are substantially disturbed. Furthermore, in our study, T2D was not associated with an increase in aortic stiffness, although oxidative stress due to hyperglycemia and vascular inflammation have been related to impairments in aortic function (30,31). Possibly, aortic stiffening, similar as LV systolic dysfunction, may arise in more advanced T2D.

The prevalence of diastolic dysfunction in asymptomatic T2D patients has been reported to be at least 50% (32). Notably, several studies have indicated that GLS, in addition to diastolic function parameters, may be impaired in T2D patients (14,33-35). Also, abnormalities in GLS have been demonstrated even in T2D patients with normal diastolic function and, in this regard, some argue that reduced LV longitudinal contractility rather than diastolic dysfunction should

be regarded as the first marker of diabetic cardiomyopathy (36). Nonetheless, in multivariable analysis, we did not observe a reduction in GLS in T2D patients as compared with controls, neither in the European nor in the South Asian population.

Importantly, the increased LV concentricity in European T2D patients was due to a reduction in LV end-diastolic volume, whereas the higher LV concentricity among South Asian T2D patients was related to an increase in LV mass. These observations imply that the higher LV concentricity in T2D may be the result of impaired LV diastolic function (with therefore incomplete LV relaxation, reduced LV filling and lower LV end-diastolic volumes) and/or LV hypertrophic remodeling (37). In the Multi-Ethnic Study of Atherosclerosis (MESA) study, the relationships of T2D and impaired fasting glucose to LV mass, end-diastolic volume and stroke volume differed between white, black, Hispanic and Chinese individuals (38). Similar to our study, the MESA study reported a lower LV end-diastolic volume in white T2D patients, whereas an increased LV mass in relation to T2D, after adjustment for demographic and anthropomorphic factors, was solely observed in the black and Hispanic groups (38). Notably, it has been suggested that LV hypertrophy in T2D may be partly due to excessive sympathetic activity, driven by insulin resistance (39). In this regard, we speculate that LV mass was increased in South Asian but not in European T2D patients, in part because of the slightly higher degree of insulin resistance. Furthermore, population studies have shown that South Asian individuals are susceptible of developing T2D at younger age than other ethnic groups (40). Accordingly, in our study, the diabetes duration was longer for the South Asian compared with the European population. The difference in diabetes duration may have contributed to the increased LV mass as observed in the South Asian but not in the European T2D patients.

A previous community-based study reported that T2D may be more detrimental for cardiac function among South Asians compared with other ethnic groups (10). Nevertheless, in our study, the degree of LV diastolic dysfunction seemed to be slightly higher for the European than for the South Asian T2D patients, as indicated by the lower Ea and LV compliance and significantly higher LV filling pressure in relation to T2D in the European but not in the South Asian cohort. Obesity as well as T2D has been shown to be associated with LV diastolic dysfunction (41,42). The relatively high degree of adiposity in the European T2D patients in comparison with their controls may have accounted for the slightly higher degree of LV diastolic dysfunction than in the South Asian T2D patients.

Role of myocardial steatosis in diabetic cardiomyopathy

Both in imaging studies in T2D patients and in histological studies in diabetic mice, T2D has been demonstrated to be associated with myocardial steatosis (13,43-45). Myocardial lipid overstorage is presumed to induce LV diastolic impairments due to the lipotoxic effects of intermediates such as diacylglycerol and ceramide (44-46). Also, ectopic fat accumulation in the myocardium may reflect altered substrate utilization due to insulin resistance, with an increase in fatty acid oxidation (11,27). In keeping with previous findings, we observed a two-

fold increase in myocardial triglyceride content in T2D patients as compared with healthy controls within the European cohort (13). Interestingly, the myocardial triglyceride content seemed to be increased in the healthy controls of South Asian descent compared with those of European origin, to similar levels as in the T2D patients, despite the strict screening for both T2D and prediabetes. Myocardial triglyceride content in South Asians as compared with Europeans has been previously assessed in young men and middle-aged overweight men, where no differences were found despite the observed higher systemic insulin resistance in those studies (47,48). Presumably, myocardial and systemic insulin sensitivity may not be necessarily interrelated. Accordingly, in a previous study on the relation between myocardial triglyceride content and LV diastolic function in healthy controls, increasing age, but not whole-body insulin resistance, correlated with myocardial steatosis and reduced LV diastolic function (49). Also, it has to be noted that myocardial triglyceride content in non-diabetic individuals reflects the rate of fatty acid uptake as well as oxidation, and may therefore be dependent on many other factors in addition to myocardial insulin sensitivity, for example the amount of circulating fatty acids, dietary carbohydrate intake, plasma glucose availability and muscular glycogen stores (50). Although our data reaffirm the potential role of myocardial steatosis in diabetic cardiomyopathy, our results suggest that myocardial triglyceride accumulation may be present in non-diabetic individuals as well as T2D patients.

Role of diffuse fibrosis in diabetic cardiomyopathy

Previously, myocardial diffuse fibrosis as indicated by an increased extracellular volume fraction has been demonstrated in obese adolescents with or without T2D, independent of blood pressure (16). Interestingly, in a recent population-based study, the extracellular volume fraction was found to be reduced in T2D patients (51). It has been suggested that antihypertensive medication, especially angiotensin-converting enzyme (ACE) inhibitors, may regress myocardial fibrotic remodeling in response to hypertension (52). Our South Asian but not European T2D study population had an increased LV mass, paralleled by a reduced extracellular volume fraction. A majority of the patients were prescribed antihypertensive drugs, with almost halve of them using ACE-inhibitors. This may explain the considerable increase in myocardial cell volume in response to increased LV afterload, with only a slight increase of the LV extracellular volume. Although myocardial diffuse fibrosis may contribute to LV functional impairments in the early stages of T2D, our results suggest that the extracellular volume fraction may not be necessarily increased in patients with longstanding T2D with concomitant antihypertensive medication use.

Limitations

Due to the cross-sectional design of our study, we cannot address issues of causality in the association of T2D and cardiovascular parameters. Our work should be considered a hypothesis-generating study and larger prospective studies are required to confirm the differential impact

of T2D on LV structure between Europeans and South Asians. Due to the relatively low sample size, we could not perform subgroup analyses, for example by sex. It has been recognized that T2D in women may be more detrimental for cardiac function as compared with men (53). The South Asian as compared with the European study population was younger and, importantly, consisted of more women. Possibly, this may have introduced bias. Furthermore, there is a well-established relation between insulin resistance and high blood pressure (54,55), which impedes the recruitment of T2D patients without hypertension. In this regard, to assess the relation of T2D to cardiovascular remodeling separately from hypertension, we adjusted for systolic and diastolic blood pressure; nonetheless, we cannot exclude residual confounding. Ideally, diabetic cardiomyopathy is studied in the absolute absence of coronary artery disease. However, a cardiac stress test was not part of our screening procedure. Furthermore, findings of previous studies indicate that several coexisting factors affect myocardial remodeling in individuals with T2D. For example, it has been demonstrated that cardiac dysfunction is worse in obese T2D patients than in individuals with T2D but without overweight (56). Also, nutrition may interfere with the process of myocardial inflammation and fibrosis in T2D (57). Therefore, differences in body weight and potential differences in diet between the T2D patients and controls may have partly confounded the observed relation of T2D to myocardial remodeling.

CONCLUSIONS

LV diastolic dysfunction was identified as a common characteristic of diabetic cardiomyopathy among South Asians and Europeans. Importantly, increased LV mass was solely observed among South Asian T2D patients, whereas differences in myocardial triglyceride content between T2D patients and controls were only present in the European cohort. This study comprised detailed phenotyping of cardiovascular remodeling in T2D patients, in both Europeans and South Asians. Our results suggest that the diabetic cardiomyopathy phenotype may differ between subsets of T2D patients, for example across ethnicities. Therefore, further research on tailored strategies for T2D management may be warranted.

ACKNOWLEDGEMENTS

We are grateful to all participating patients. We thank all physicians and nurses from Leiden University Medical Center (Leiden, the Netherlands) and Haaglanden Medical Center (The Hague, the Netherlands) for inviting eligible patients, P.J. van den Boogaard for the support in the CMR acquisition and B. Ladan-Eygenraam for the assistance in the clinical data collection.

REFERENCES

1. Marwick TH, Ritchie R, Shaw JE, Kaye D. Implications of Underlying Mechanisms for the Recognition and Management of Diabetic Cardiomyopathy. J Am Coll Cardiol 2018;71(3):339-351.
2. Tillin T, Hughes AD, Mayet J, et al. The relationship between metabolic risk factors and incident cardiovascular disease in Europeans, South Asians, and African Caribbeans: SABRE (Southall and Brent Revisited) -- a prospective population-based study. J Am Coll Cardiol 2013;61(17):1777-1786.
3. Kanaya AM, Wassel CL, Mathur D, et al. Prevalence and correlates of diabetes in South asian indians in the United States: findings from the metabolic syndrome and atherosclerosis in South asians living in america study and the multi-ethnic study of atherosclerosis. Metab Syndr Relat Disord 2010;8(2):157-164.
4. Shah AD, Kandula NR, Lin F, et al. Less favorable body composition and adipokines in South Asians compared with other US ethnic groups: results from the MASALA and MESA studies. Int J Obes (Lond) 2016;40(4):639-645.
5. Gujral UP, Vittinghoff E, Mongraw-Chaffin M, et al. Cardiometabolic Abnormalities Among Normal-Weight Persons From Five Racial/Ethnic Groups in the United States: A Cross-sectional Analysis of Two Cohort Studies. Ann Intern Med 2017;166(9):628-636.
6. Nightingale CM, Rudnicka AR, Owen CG, et al. Influence of adiposity on insulin resistance and glycemia markers among U.K. Children of South Asian, black African-Caribbean, and white European origin: child heart and health study in England. Diabetes Care 2013;36(6):1712-1719.
7. Flowers E, Lin F, Kandula NR, et al. Body Composition and Diabetes Risk in South Asians: Findings From the MASALA and MESA Studies. Diabetes Care 2019;42(5):946-953.
8. Abate N, Chandalia M, Snell PG, Grundy SM. Adipose tissue metabolites and insulin resistance in nondiabetic Asian Indian men. J Clin Endocrinol Metab 2004;89(6):2750-2755.
9. Forouhi NG, Sattar N, McKeigue PM. Relation of C-reactive protein to body fat distribution and features of the metabolic syndrome in Europeans and South Asians. Int J Obes Relat Metab Disord 2001;25(9):1327-1331.
10. Park CM, Tillin T, March K, et al. Hyperglycemia has a greater impact on left ventricle function in South Asians than in Europeans. Diabetes Care 2014;37(4):1124-1131.
11. Rijzewijk LJ, van der Meer RW, Lamb HJ, et al. Altered myocardial substrate metabolism and decreased diastolic function in nonischemic human diabetic cardiomyopathy: studies with cardiac positron emission tomography and magnetic resonance imaging. J Am Coll Cardiol 2009;54(16):1524-1532.
12. Levelt E, Mahmod M, Piechnik SK, et al. Relationship Between Left Ventricular Structural and Metabolic Remodeling in Type 2 Diabetes. Diabetes 2016;65(1):44-52.
13. Rijzewijk LJ, van der Meer RW, Smit JW, et al. Myocardial steatosis is an independent predictor of diastolic dysfunction in type 2 diabetes mellitus. J Am Coll Cardiol 2008;52(22):1793-1799.
14. Ng AC, Delgado V, Bertini M, et al. Myocardial steatosis and biventricular strain and strain rate imaging in patients with type 2 diabetes mellitus. Circulation 2010;122(24):2538-2544.
15. Schuster A, Hor KN, Kowallick JT, Beerbaum P, Kutty S. Cardiovascular Magnetic Resonance Myocardial Feature Tracking: Concepts and Clinical Applications. Circ Cardiovasc Imaging 2016;9(4):e004077.
16. Shah RV, Abbasi SA, Neilan TG, et al. Myocardial tissue remodeling in adolescent obesity. J Am Heart Assoc 2013;2(4):e000279.
17. Bizino MB, Jazet IM, Westenberg JJM, et al. Effect of liraglutide on cardiac function in patients with type 2 diabetes mellitus: randomized placebo-controlled trial. Cardiovasc Diabetol 2019;18(1):55.
18. van Eyk HJ, Paiman EHM, Bizino MB, et al. A double-blind, placebo-controlled, randomised trial to assess the effect of liraglutide on ectopic fat accumulation in South Asian type 2 diabetes patients. Cardiovasc Diabetol 2019;18(1):87.
19. Paelinck BP, de Roos A, Bax JJ, et al. Feasibility of tissue magnetic resonance imaging: a pilot study in comparison with tissue Doppler imaging and invasive measurement. J Am Coll Cardiol 2005;45(7):1109-1116.
20. Westenberg JJ, Roes SD, Ajmone Marsan N, et al. Mitral valve and tricuspid valve blood flow: accurate quantification with 3D velocity-encoded MR imaging with retrospective valve tracking. Radiology 2008;249(3):792-800.
21. Brandts A, Bertini M, van Dijk EJ, et al. Left ventricular diastolic function assessment from

three-dimensional three-directional velocity-in encoded MRI with retrospective valve tracking. J Magn Reson Imaging 2011;33(2):312-319.
22. Grotenhuis HB, Westenberg JJ, Steendijk P, et al. Validation and reproducibility of aortic pulse wave velocity as assessed with velocity-encoded MRI. J Magn Reson Imaging 2009;30(3):521-526.
23. de Heer PM, Bizino MBMD, Versluis MJP, Webb AGP, Lamb HJMDP. Improved Cardiac Proton Magnetic Resonance Spectroscopy at 3 T Using High Permittivity Pads. Investigative Radiology 2016;51(2):134-138.
24. Rial B, Robson MD, Neubauer S, Schneider JE. Rapid quantification of myocardial lipid content in humans using single breath-hold 1H MRS at 3 Tesla. Magn Reson Med 2011;66(3):619-624.
25. Naressi A, Couturier C, Devos JM, et al. Java-based graphical user interface for the MRUI quantitation package. MAGMA 2001;12(2-3):141-152.
26. Naressi A, Couturier C, Castang I, de Beer R, Graveron-Demilly D. Java-based graphical user interface for MRUI, a software package for quantitation of in vivo/medical magnetic resonance spectroscopy signals. Comput Biol Med 2001;31(4):269-286.
27. Diamant M, Lamb HJ, Groeneveld Y, et al. Diastolic dysfunction is associated with altered myocardial metabolism in asymptomatic normotensive patients with well-controlled type 2 diabetes mellitus. J Am Coll Cardiol 2003;42(2):328-335.
28. Paulus WJ, Tschope C. A novel paradigm for heart failure with preserved ejection fraction: comorbidities drive myocardial dysfunction and remodeling through coronary microvascular endothelial inflammation. J Am Coll Cardiol 2013;62(4):263-271.
29. Rider OJ, Francis JM, Ali MK, et al. Effects of catecholamine stress on diastolic function and myocardial energetics in obesity. Circulation 2012;125(12):1511-1519.
30. Gulsin GS, Swarbrick DJ, Hunt WH, et al. Relation of Aortic Stiffness to Left Ventricular Remodeling in Younger Adults With Type 2 Diabetes. Diabetes 2018;67(7):1395-1400.
31. van der Meer RW, Diamant M, Westenberg JJ, et al. Magnetic resonance assessment of aortic pulse wave velocity, aortic distensibility, and cardiac function in uncomplicated type 2 diabetes mellitus. J Cardiovasc Magn Reson 2007;9(4):645-651.
32. Boyer JK, Thanigaraj S, Schechtman KB, Perez JE. Prevalence of ventricular diastolic dysfunction asymptomatic, normotensive patients with diabetes mellitus. Am J Cardiol 2004;93(7):870-875.
33. Ng AC, Delgado V, Bertini M, et al. Findings from left ventricular strain and strain rate imaging in asymptomatic patients with type 2 diabetes mellitus. Am J Cardiol 2009;104(10):1398-1401.
34. Fang ZY, Yuda S, Anderson V, Short L, Case C, Marwick TH. Echocardiographic detection of early diabetic myocardial disease. J Am Coll Cardiol 2003;41(4):611-617.
35. Ernande L, Bergerot C, Girerd N, et al. Longitudinal myocardial strain alteration is associated with left ventricular remodeling in asymptomatic patients with type 2 diabetes mellitus. J Am Soc Echocardiogr 2014;27(5):479-488.
36. Ernande L, Bergerot C, Rietzschel ER, et al. Diastolic dysfunction in patients with type 2 diabetes mellitus: is it really the first marker of diabetic cardiomyopathy? J Am Soc Echocardiogr 2011;24(11):1268-1275 e1261.
37. Zile MR, Baicu CF, Gaasch WH. Diastolic heart failure--abnormalities in active relaxation and passive stiffness of the left ventricle. N Engl J Med 2004;350(19):1953-1959.
38. Bertoni AG, Goff DC, Jr., D'Agostino RB, Jr., et al. Diabetic cardiomyopathy and subclinical cardiovascular disease: the Multi-Ethnic Study of Atherosclerosis (MESA). Diabetes Care 2006;29(3):588-594.
39. Masuo K, Rakugi H, Ogihara T, Esler MD, Lambert GW. Cardiovascular and renal complications of type 2 diabetes in obesity: role of sympathetic nerve activity and insulin resistance. Curr Diabetes Rev 2010;6(2):58-67.
40. Tillin T, Sattar N, Godsland IF, Hughes AD, Chaturvedi N, Forouhi NG. Ethnicity-specific obesity cut-points in the development of Type 2 diabetes - a prospective study including three ethnic groups in the United Kingdom. Diabet Med 2015;32(2):226-234.
41. Shah AS, Khoury PR, Dolan LM, et al. The effects of obesity and type 2 diabetes mellitus on cardiac structure and function in adolescents and young adults. Diabetologia 2011;54(4):722-730.
42. Levelt E, Pavlides M, Banerjee R, et al. Ectopic and Visceral Fat Deposition in Lean and Obese Patients With Type 2 Diabetes. J Am Coll Cardiol 2016;68(1):53-63.
43. McGavock JM, Lingvay I, Zib I, et al. Cardiac steatosis in diabetes mellitus: a 1H-magnetic resonance spectroscopy study. Circulation 2007;116(10):1170-1175.

44. Christoffersen C, Bollano E, Lindegaard ML, et al. Cardiac lipid accumulation associated with diastolic dysfunction in obese mice. Endocrinology 2003;144(8):3483-3490.
45. Atkinson LL, Kozak R, Kelly SE, Onay Besikci A, Russell JC, Lopaschuk GD. Potential mechanisms and consequences of cardiac triacylglycerol accumulation in insulin-resistant rats. Am J Physiol Endocrinol Metab 2003;284(5):E923-930.
46. Zhou YT, Grayburn P, Karim A, et al. Lipotoxic heart disease in obese rats: implications for human obesity. Proc Natl Acad Sci U S A 2000;97(4):1784-1789.
47. van Schinkel LD, Bakker LE, Jonker JT, et al. Functional and metabolic imaging of the cardiovascular system in young healthy South Asians and Caucasians unveils early differences. Diabetes Care 2013;36(10):e178-179.
48. Van Schinkel LD, Bakker LE, Jonker JT, et al. Cardiovascular flexibility in middle-aged overweight South Asians vs. white Caucasians: response to short-term caloric restriction. Nutr Metab Cardiovasc Dis 2015;25(4):403-410.
49. van der Meer RW, Rijzewijk LJ, Diamant M, et al. The ageing male heart: myocardial triglyceride content as independent predictor of diastolic function. Eur Heart J 2008;29(12):1516-1522.
50. Lamb HJ, Smit JW, van der Meer RW, et al. Metabolic MRI of myocardial and hepatic triglyceride content in response to nutritional interventions. Curr Opin Clin Nutr Metab Care 2008;11(5):573-579.
51. Storz C, Hetterich H, Lorbeer R, et al. Myocardial tissue characterization by contrast-enhanced cardiac magnetic resonance imaging in subjects with prediabetes, diabetes, and normal controls with preserved ejection fraction from the general population. Eur Heart J Cardiovasc Imaging 2018;19(6):701-708.
52. Cao Y, Zeng W, Cui Y, et al. Increased myocardial extracellular volume assessed by cardiovascular magnetic resonance T1 mapping and its determinants in type 2 diabetes mellitus patients with normal myocardial systolic strain. Cardiovasc Diabetol 2018;17(1):7.
53. Kannel WB, McGee DL. Diabetes and cardiovascular disease. The Framingham study. JAMA 1979;241(19):2035-2038.
54. Ferrannini E, Buzzigoli G, Bonadonna R, et al. Insulin resistance in essential hypertension. N Engl J Med 1987;317(6):350-357.
55. Eckel RH, Grundy SM, Zimmet PZ. The metabolic syndrome. Lancet 2005;365(9468):1415-1428.
56. Suto M, Tanaka H, Mochizuki Y, et al. Impact of overweight on left ventricular function in type 2 diabetes mellitus. Cardiovasc Diabetol 2017;16(1):145.
57. Waldman M, Cohen K, Yadin D, et al. Regulation of diabetic cardiomyopathy by caloric restriction is mediated by intracellular signaling pathways involving 'SIRT1 and PGC-1alpha'. Cardiovasc Diabetol 2018;17(1):111.

CHAPTER

4

A double-blind, placebo-controlled, randomized trial to assess the effect of liraglutide on ectopic fat accumulation in South Asian type 2 diabetes patients

van Eyk HJ,* Paiman EHM,* Bizino MB, de Heer P, Geelhoed-Duijvestijn PH, Kharagjitsingh AV, Smit JWA, Lamb HJ, Rensen PCN, Jazet IM

* shared first author

Cardiovasc Diabetol. 2019 Jul 9;18(1):87. doi: 10.1186/s12933-019-0890-5

ABSTRACT

Background

South Asians have a high risk to develop type 2 diabetes, which may be related to substantial ectopic fat deposition. Since glucagon-like peptide-1 analogues can reduce ectopic fat accumulation, the aim of the present study was to assess the effect of treatment with liraglutide for 26 weeks on ectopic fat deposition and HbA1c in South Asian patients with type 2 diabetes.

Methods

In a placebo-controlled trial, 47 South Asian patients with type 2 diabetes were randomly assigned to treatment with liraglutide (1.8 mg/day) or placebo added to standard care. At baseline and after 26 weeks of treatment we assessed abdominal subcutaneous, visceral, epicardial and paracardial adipose tissue volume using MRI. Furthermore, myocardial and hepatic triglyceride content were examined with proton magnetic resonance spectroscopy.

Results

In the intention-to-treat analysis, liraglutide decreased body weight compared to placebo (-3.9 ± 3.6 kg ***vs*** -0.6 ± 2.2 kg; mean change from baseline (liraglutide ***vs*** placebo): -3.5 kg; 95%CI [-5.3, -1.8]) without significant effects on the different adipose tissue compartments. HbA1c was decreased in both groups without between group differences. In the per-protocol analysis, liraglutide did decrease visceral adipose tissue volume compared to placebo (-23 ± 27 cm^2 ***vs*** –2 ± 17 cm^2; mean change from baseline (liraglutide ***vs*** placebo): -17 cm^2; 95%CI [-32, -3]). Furthermore, HbA1c was decreased by liraglutide compared to placebo (-1.0 ± 0.8% (-10.5 ± 9.1 mmol/mol) ***vs*** (-0.6 ± 0.8% (-6.1 ± 8.8 mmol/mol), with a between group difference (mean change from baseline (liraglutide ***vs*** placebo): -0.6% (-6.5 mmol/mol); 95%CI [-1.1, -0.1 (-11.5, -1.5)]. Interestingly, the decrease of visceral adipose tissue volume was associated with the reduction of HbA1c (β: 0.165 mmol/mol (0.015%) per 1 cm^2 decrease of visceral adipose tissue volume; 95%CI [0.062, 0.267 (0.006, 0.024%)]).

Conclusion

While the intention-to-treat analysis did not show effects of liraglutide on ectopic fat and HbA1c, per-protocol analysis showed that liraglutide decreases visceral adipose tissue volume, which was associated with improved glycaemic control in South Asians.

Trial registration: NCT02660047 (clinicaltrials.gov). Registered 21 January 2016

INTRODUCTION

South Asians are at high risk to develop type 2 diabetes in comparison with other populations, with an estimated prevalence of type 2 diabetes of 8.5% in the adult population (1). Furthermore, South Asians tend to develop type 2 diabetes at a young age and at a low BMI (2). Notably, at a BMI of 21 kg/m^2 South Asians show similar distributions of variables for glucose metabolism as white Caucasians at a BMI of 30 kg/m^2 (3). The underlying cause of the increased risk to develop type 2 diabetes remains largely unknown, but an increased amount of ectopic fat is likely to play a role (4). It is well known that central obesity, but also increased accumulation of ectopic fat in liver (5) and muscle (6) play an important role in development of insulin resistance and type 2 diabetes (7). Interestingly, several studies have shown that, compared to Europids with a similar BMI, South Asians have more visceral adipose tissue (8,9) and a higher intrahepatic triglyceride content (10,11). Ectopic fat accumulation increases insulin resistance and metabolic risk (12,13), but may also contribute to remodelling of the heart and to diastolic dysfunction (14). Therefore, interventions focussed on reducing ectopic fat accumulation could be an effective approach to reduce insulin resistance and improve glycaemic control in this population.

Glucagon-like peptide-1 (GLP-1) analogues are prescribed to patients with type 2 diabetes to improve glycaemic control and induce weight loss (15,16). The reduction in body weight is primarily the result of a reduction in fat mass, but this reduction does not seem to occur homogeneously in different adipose tissue depots in the body (17,18). Recently, it has been shown that liraglutide, a GLP-1 analogue, reduces hepatic steatosis in patients with non-alcoholic steatohepatitis (19). Furthermore, previous studies investigating the effect of GLP-1 analogues on different fat depots, have shown that while both subcutaneous and visceral adipose tissue are reduced, the decrease of visceral adipose tissue (17,20), and epicardial fat (18,21) is even more pronounced. However, in another study mainly subcutaneous adipose tissue was reduced after treatment, while visceral adipose tissue was not affected (22). Several studies have recently suggested that subcutaneous adipose tissue does not increase the risk to develop diabetes and might even possess protective properties (23,24). Visceral adipose tissue, however, is causally linked to insulin resistance (25). Apparently, conflicting data have been reported with respect to the effect of GLP-1 analogues on the various adipose depots in the general population. Since it is unclear to what extent different adipose tissue compartments are affected by weight loss induced by treatment with GLP-1 analogues, it is important to further investigate the effects of treatment with GLP-1 analogues on the different fat depots, especially since reduction of ectopic adipose tissue would be more beneficial than reduction of subcutaneous adipose tissue.

Since South Asians have a specific body fat distribution, with high amounts of visceral adipose tissue (8,9), effects of a GLP-1 analogue on ectopic fat depots, and subsequently effects on glycaemic control, could be pronounced especially in this population. Therefore, the aim of

the present study was to assess the effect of treatment with liraglutide for 26 weeks on ectopic fat deposition and HbA1c in South Asian patients with type 2 diabetes.

METHODS

Study overview and study population

This study is a 26-week, prospective, randomised, double-blind, clinical trial. Patients from South Asian descent, i.e. individuals with two South Asian parents, with type 2 diabetes were recruited via advertisements and from the outpatient clinics of the Leiden University Medical Center (LUMC, Leiden, the Netherlands), general practitioners, and local hospitals. A screening visit was performed prior to inclusion to assess eligibility for participation. We included subjects with BMI ≥23 kg/m^2, aged 18-74 years, with an HbA1c ≥6.5% and ≤11.0% (≥47.5 and ≤96.4 mmol/mol). Concomitant treatment with metformin, sulfonylurea derivatives and insulin was optional, although the dosage of all glucose-lowering medication needed to be stable for at least 3 months prior to participation. Main exclusion criteria were use of other glucose-lowering therapy than mentioned above or presence of renal disease, congestive heart failure New York Heart Association (NYHA) classification III-IV, uncontrolled hypertension (systolic blood pressure >180 mmHg and/or diastolic blood pressure >110 mmHg) or an acute coronary or cerebrovascular accident within 30 days prior to study inclusion. Furthermore, patients with any contra-indication for contrast-enhanced MRI were excluded. The trial was conducted in accordance with the principles of the revised Declaration of Helsinki. Written informed consent was obtained from all subjects before inclusion. The trial was approved by the local ethics committee and conducted at the LUMC, and was registered at clinicaltrials.gov (NCT01761318).

Study design

At baseline, participants were randomised to receive treatment with liraglutide (Victoza®) or placebo (both provided by Novo Nordisk A/S, Bagsvaerd, Denmark) by block randomisation with block size of 4 and stratification 1:1 for sex and insulin use. During the study, all participants, study investigators and outcome assessors were blinded to treatment allocation. The starting dose of the study medication was 0.6 mg per day, which was titrated in two weeks to a maximum dose of 1.8 mg per day, if tolerated. If necessary in case of adverse events, the dose was reduced. During trial participation, a weekly telephone call was scheduled to discuss blood glucose management and adverse events, and at week 4 and week 12 participants visited the study center for routine blood tests and clinical measurements. In addition to study medication, participants received treatment according to current clinical guidelines to achieve optimal glycaemic control and regulation of blood pressure and cholesterol levels.

Data collection

After inclusion, participants visited the study center at baseline and after 26 weeks of treatment, after ≥6 h of fasting, for medical history assessment, standard physical examination, collection of venous blood samples and MRI. All blood samples were centrifuged and stored at -80°C until analysis. Plasma total cholesterol, HDL-cholesterol and triglyceride concentrations were measured on a Modular P800 analyser (Roche Diagnostics, Mannheim, Germany). LDL-cholesterol was calculated according to the Friedewald formula (26). HbA1c was assessed with ion-exchange high-performance liquid chromatography (HPLC; Tosoh G8, Sysmex Nederland B.V., Etten-Leur, the Netherlands). Body composition and lean body mass was assessed using bioelectrical impedance analysis (BIA; Bodystat 1500, Bodystart Ltd., Douglas, UK).

MRI for adipose tissue volume

A 3.0 Tesla MRI scanner (Ingenia, Philips Healthcare, Best, the Netherlands) was used, with a dStream Torso anterior coil and a FlexCoverage posterior coil in the table top (in total up to 32 coil elements for signal reception). To assess visceral and abdominal subcutaneous adipose tissue volumes, 2-point Dixon water-fat separated transverse images were obtained of the abdomen during one breath-hold, with the following parameters: repetition time (TR) 3.5 ms, first/second echo time (TE1/TE2) 1.19/2.3 ms, flip angle (FA) 10°, field of view (FOV) 500x365 mm^2, acquired voxel size 1.60x1.70 mm^2, slice thickness 4 mm, slice gap -2 mm, and number of slices 140.

For quantification of epicardial and paracardial fat, ECG-triggered fat-selective images, using a multi-shot turbo spin-echo sequence with spectral pre-saturation with inversion recovery (SPIR) for water suppression, were acquired in 4-chamber view orientation at end-diastole, during one breath-hold, with imaging parameters: TR/TE 1000/11 ms, FA 90°, FOV 280x223 mm^2, acquired voxel size 1.09x1.12 mm^2, and slice thickness 4 mm.

MR images were analysed in MASS Research Software V2018-EXP (Leiden University Medical Center, the Netherlands). For assessment of visceral and abdominal subcutaneous adipose tissue volume, three transverse slices were reformatted, at the level of the fourth and fifth lumbar vertebrae, with slice thickness of 10 mm and slice gap of 12 mm. In each slice, the outer borders of visceral and subcutaneous adipose tissue were manually outlined, and the areas were automatically calculated based on pixel intensity thresholding. Subsequently, visceral and abdominal subcutaneous adipose tissue volume were quantified as the mean area in squared centimeters of all three slices. Similarly, epicardial and paracardial fat (between outer wall of the myocardium and visceral pericardium and between visceral and parietal pericardium, respectively) were assessed. Epicardial and paracardial fat were measured in 4 chamber view orientation, in the region surrounding the left and right ventricles, below the level of the atrioventricular valves.

Proton magnetic resonance spectroscopy for myocardial and hepatic triglyceride content

Myocardial and hepatic triglyceride content were examined with proton magnetic resonance spectroscopy (^{1}H-MRS) (27). Spectra were acquired using single voxel point resolved spectroscopy (PRESS), with first order volume B0 pencil beam shimming, respiratory navigator (trigger and track), and multiply optimized insensitive suppression train (MOIST) suppression (bandwidth 190 Hz) for the water-suppressed acquisitions. Parameters were as follows: TR 3.5 or 9 seconds (water-suppressed and non-water-suppressed acquisition, respectively), TE 35 ms, bandwidth 1500 Hz and acquired samples 2048 (spectral resolution 0.73 Hz/sample). Cardiac ^{1}H-MRS additionally used ECG-triggering (R-top trigger delay 200 ms) and acquired in the midventricular septum (voxel size 40x15x25 mm^3, shim volume 50x25x35 mm^3, number of signal averages (NSA) of water-suppressed and non-water-suppressed acquisition 64 and 6, respectively). A high permittivity pad was placed on the thorax at the location of the heart to improve signal-to-noise ratio (28). Hepatic ^{1}H-MRS was obtained in the liver parenchyma, avoiding the inclusion of blood vessels or subcutaneous fat (voxel size 20x20x20 mm^3, shim volume 35x35x35 mm^3, NSA of water-suppressed and non-water-suppressed acquisition 32 and 8, respectively). The voxels were planned at the same location for the baseline and follow-up measurements.

The spectral raw data were processed using an in-house developed script (MATLAB R2015a (MathWorks, Massachusetts, United States). The raw data were phase-, frequency- and eddy current-corrected, if required. Individual signal averages were analysed and signal averages exceeding the 95% confidence interval were considered outliers and were excluded. Reconstructed data were further analysed in the Java-based Magnetic Resonance User Interface (jMRUI v5.0; MRUI Consortium). For the water-suppressed signals, the Hankel-Lanczos filter was applied to remove residual water. The spectra were fitted using the AMARES algorithm, with the assumption of Gaussian line shapes. Prior knowledge for the fit included the following starting values: triglyceride-methyl (CH_3) 0.9 ppm, triglyceride-methylene (CH_2) 1.3 ppm, COO-CH_2 2.05 ppm, creatine 3.05 ppm, trimethylamines (TMA) 3.25 ppm, with soft constraints for the linewidth of the fit of each signal. The first-order phase was fixed to zero. Myocardial and hepatic lipid-to-water ratios were quantified as the signal of triglyceride methylene divided by the unsuppressed water signal, multiplied by 100% (29).

Statistical analyses

The main outcome measure of this study was the effect of liraglutide on cardiac function and sample size calculation was based on this outcome measure as described previously (30). In this manuscript, we report on secondary outcome measures. Data are shown as means ± SD, or as median (interquartile range) when not normally distributed. Within-group changes were assessed using paired t-tests. We performed an ANCOVA to assess between-group differences with treatment included as fixed effect and the baseline value as a covariate. The intention-

to-treat analysis included data of all participants who were randomised and started study medication. The per-protocol analysis included only participants who adhered to the assigned medication, i.e. used ≥80% of prescribed study medication. A *P*-value <0.05 was considered statistically significant. Statistical analyses were performed using SPSS version 23.0 for Windows (IBM Corporation, Chicago, IL).

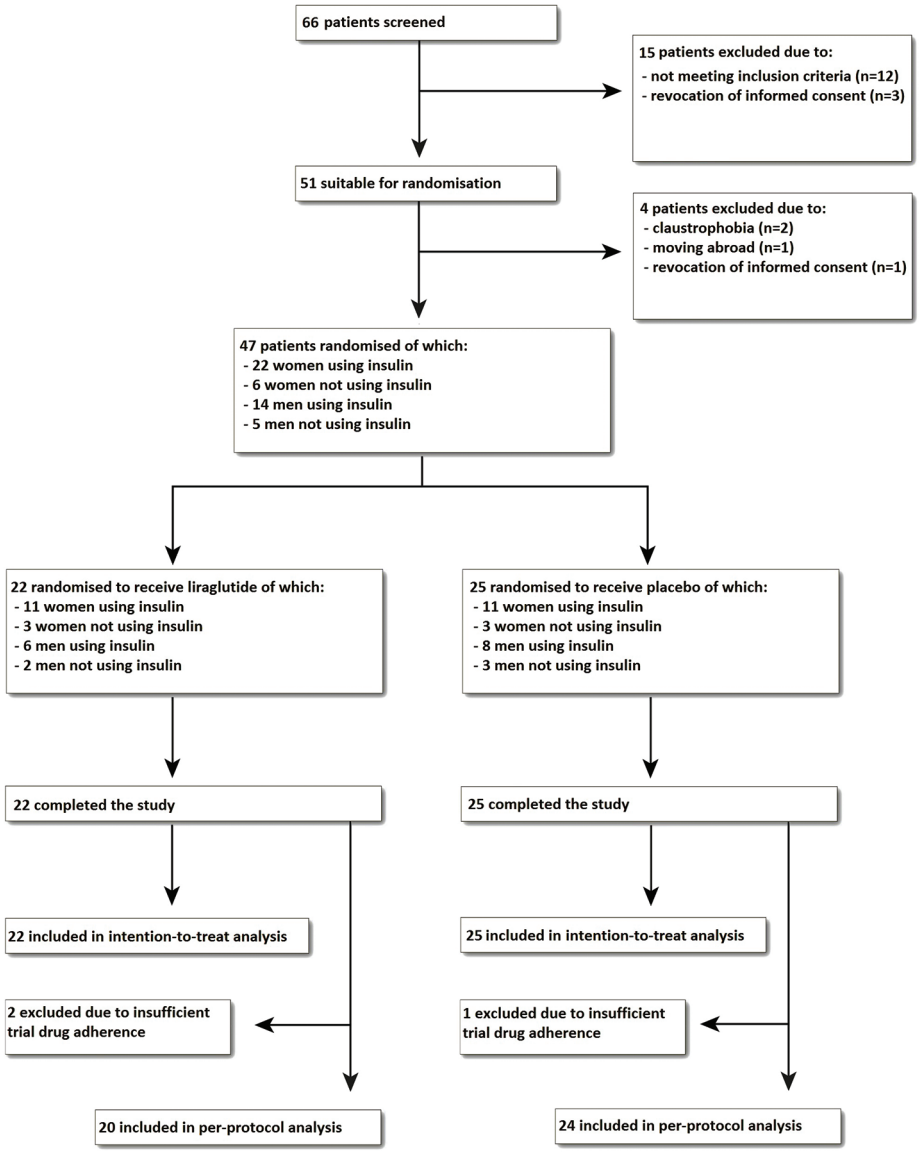

Figure 1. Trial flow diagram.

RESULTS

Population characteristics

As shown in the trial flow diagram in **Figure 1**, 51 patients were included after screening, of whom 4 were excluded before randomisation. Between July 2015 and December 2016, 22 patients were randomised to receive liraglutide and 25 to receive placebo. All randomised patients finished the study and were included in the intention-to-treat analysis. During the study, 19 participants (86.4%) of the liraglutide group and 24 participants (96.0%) of the placebo group used the standard dose of 1.8 mg/day, while in the rest of the participants the maximally tolerated dose was 1.2 mg/day. In the liraglutide group, participants used on average 95.4 ± 8.1% of the prescribed cumulative dose, and in the placebo group the participants used 98.7 ± 5.2%. One participant of the liraglutide group used <80% of the prescribed cumulative dose, and of two participants (one allocated to receive placebo and one to receive liraglutide) adherence could not be calculated, due to missing (empty) medication pens. These participants were included in the intention-to-treat analysis but not in the per-protocol analysis. One serious adverse event (admission for symptoms of acute coronary syndrome) occurred in the placebo group. In the liraglutide group compared to the placebo group, more participants reported nausea (73 ***vs*** 40%) and vomiting (27 ***vs*** 8%) at least once during study participation. As shown in **Table 1**, baseline characteristics of the participants in both treatment groups were balanced. Individuals were 55 ± 11 years old in the liraglutide group, ***vs*** 55 ± 9 years in the placebo group, with a body weight of 81.9 ± 11.0 ***vs*** 77.8 ± 12.4 kg and BMI of 30.4 ± 3.8 ***vs*** 28.6 ± 4.0 kg/m^2, respectively.

Table 1. Baseline characteristics of study participants.

Characteristic	Liraglutide (n= 22)	Placebo (n=25)
Demographics		
Age (year)	55 ± 11	55 ± 9
Sex (no. (%))		
Male	8 (36%)	11 (44%)
Female	14 (64%)	14 (56%)
Diabetes duration (years)	19 ± 10	17 ± 10
Concomitant drug use		
Metformin (no. (%))	22 (100%)	23 (92%)
Metformin dose (g/day)	1.8 ± 0.7	1.7 ± 0.6
Sulfonylurea (no. (%))	3 (14%)	5 (20%)
Insulin (no. (%))	17 (77%)	19 (76%)
Insulin dose (units/day)	77 ± 34	67 ± 30
Lipid-lowering drugs (statin and/or other), no. (%)	17 (77%)	20 (80%)

Table 1. Baseline characteristics of study participants.

Characteristic	Liraglutide (n= 22)	Placebo (n=25)
Clinical parameters		
Body weight (kg)	81.9 ± 11.0	77.8 ± 12.4
BMI (kg/m^2)	30.4 ± 3.8	28.6 ± 4.0
Waist circumference (cm)	104 ± 8	98 ± 10
Hip circumference (cm)	104 ± 7	104 ± 9
Waist-hip ratio	1.00 ± 0.07	0.95 ± 0.09
Lean body mass (kg)	51.6 ± 10.6	48.9 ± 11.2
Lean body mass (%)	62.8 ± 8.4	63.1 ± 9.8
Metabolic factors		
HbA1c (mmol/mol)	65 ± 10	70 ± 12
HbA1c (%)	8.1 ± 0.9	8.6 ± 1.1
Total cholesterol (mmol/L)	3.95 ± 0.65	4.46 ± 1.10
HDL-cholesterol (mmol/L)	1.24 ± 0.33	1.21 ± 0.30
LDL-cholesterol (mmol/L)	2.00 ± 0.65	2.21 ± 0.97
Triglycerides (mmol/L)	1.55 ± 0.86	2.08 ± 1.80
Adipose tissue compartments		
Subcutaneous AT (cm^2)	315 ± 97	326 ± 141
Visceral AT (cm^2)	187 ± 57	149 ± 49
Epicardial AT (cm^2)	10 ± 3	9 ± 3
Paracardial AT (cm^2)	12 ± 4	9 ± 4
Hepatic TGC (%)	6.9 ± 6.3	11.8 ± 10.9
Myocardial TGC (%)	0.9 ± 0.4	1.0 ± 0.6

Results are presented as n (%) or mean ± SD. n=47. Missing data in liraglutide group: n=1 for epicardial adipose tissue volume and paracardial adipose tissue volume. Missing data in placebo group: n=1 for lean body mass (kg and %), epicardial adipose tissue volume and myocardial triglyceride content. AT: adipose tissue, TGC: triglyceride content.

Table 2. Clinical parameters, metabolic factors and adipose tissue compartment changes from baseline after 26 weeks of treatment in the intention-to-treat analysis.

Characteristic	Mean ± SD change from baseline to 26 weeks		Mean [95%CI] changes from baseline (liraglutide *vs* placebo)	*P* value
	Liraglutide (n=22)	Placebo (n=25)		
Clinical parameters				
Body weight (kg)	-3.9 ± 3.6	-0.6 ± 2.2	-3.5 [-5.3, -1.8]	<0.001
BMI (kg/m^2)	-1.5 ± 1.4	-0.2 ± 0.8	-1.4 [-2.0, -0.7]	<0.001
Waist circumference (cm)	-5 ± 4	0 ± 4	-5 [-8, -2)	<0.001
Hip circumference (cm)	-4 ± 5	-2 ± 3	-2 [-5, 0]	0.067
Waist-hip ratio	-0.01 ± 0.04	0.02 ± 0.05	-0.01 [-0.04, 0.01]	0.312
Lean body mass (kg)	-2.3 ± 2.3	0.4 ± 2.9	-2.7 [-4.3, -1.1]	0.001
Lean body mass (%)	0.2 ± 1.7	0.8 ± 2.7	-0.6 [-1.9, 0.8]	0.403
Metabolic factors				
HbA1c (mmol/mol)	-8.5 ± 11.2	-6.8 ± 9.3	-4.0 [-9.7, 1.6]	0.156
HbA1c (%)	-0.8 ± 1.0	-0.6 ± 0.8	-0.4 [-0.9, 0.1]	0.156
Total cholesterol (mmol/L)	0.24 ± 1.09	-0.42 ± 0.82	0.52 [-0.05, 1.09]	0.073
HDL-cholesterol (mmol/L)	-0.04 ± 0.12	-0.05 ± 0.12	0.02 [-0.05, 0.09]	0.657
LDL-cholesterol (mmol/L)	0.15 ± 0.74	-0.14 ± 0.74	0.22 [-0.20, 0.63]	0.296
Triglycerides (mmol/L)	0.28 ± 1.25	-0.38 ± 1.30	0.40 [-0.24, 1.04]	0.214
Adipose tissue compartments				
Subcutaneous AT (cm^2)	-24 ± 37	-10 ± 37	-15 [-37, 6]	0.158
Visceral AT (cm^2)	-20 ± 29	-2 ± 17	-13 [-27, 1]	0.074
Epicardial AT (cm^2)	0 ± 2	1 ± 1	-1 [-2, 0]	0.232
Paracardial AT (cm^2)	-1 ± 3	0 ± 3	-1 [-2, 1]	0.494
Hepatic TGC (%)	-1.2 ± 4.1	-3.3 ± 5.4	0.4 [-1.9, 2.8]	0.704
Myocardial TGC (%)	0.1 ± 0.5	-0.1 ± 0.6	0.2 [-0.1, 0.5]	0.157

Results are presented as n (%) or mean ± SD. n=47. Missing data in the liraglutide group: n=3 for epicardial adipose tissue volume and paracardial adipose tissue volume, n=1 for myocardial TGC. Missing data in placebo group: n=1 for lean body mass (kg and %), n=3 for epicardial adipose tissue volume, n=2 for paracardial adipose tissue volume, and n=1 for myocardial TGC. AT: adipose tissue, TGC: triglyceride content.

Table 3. Clinical parameters, metabolic factors and adipose tissue compartment changes from baseline after 26 weeks of treatment in the per-protocol analysis.

Characteristic	Mean ± SD change from baseline to 26 weeks		Mean [95%CI] changes from baseline (liraglutide *vs* placebo)	*P* value
	Liraglutide (n=20)	Placebo (n=24)		
Clinical parameters				
Body weight (kg)	-4.3 ± 3.4	-0.6 ± 2.2	-4.0 [-5.8, -2.3]	<0.001
BMI (kg/m^2)	-1.6 ± 1.4	-0.2 ± 0.9	-1.5 [-2.2, -0.8]	<0.001
Waist circumference (cm)	-5 ± 4	0 ± 4	-5 [-8, -2)	0.001
Hip circumference (cm)	-4 ± 5	-2 ± 3	-2 [-5, 0]	0.068
Waist-hip ratio	-0.01 ± 0.04	0.02 ± 0.05	-0.01 [-0.04, 0.02]	0.394
Lean body mass (kg)	-2.4 ± 2.4	0.4 ± 3.0	-2.8 [-4.5, -1.1]	0.002
Lean body mass (%)	0.4 ± 1.6	0.8 ± 2.7	-0.4 [-1.8, 1.0]	0.605
Metabolic factors				
HbA1c (mmol/mol)	-10.5 ± 9.1	-6.1 ± 8.8	-6.5 [-11.5, -1.5]	0.011
HbA1c (%)	-1.0 ± 0.8	-0.6 ± 0.8	-0.6 [-1.1, -0.1]	0.011
Total cholesterol (mmol/L)	0.06 ± 0.98	-0.37 ± 0.78	0.28 [-0.26, 0.81]	0.305
HDL-cholesterol (mmol/L)	-0.04 ± 0.12	-0.06 ± 0.11	0.02 [-0.05, 0.10]	0.510
LDL-cholesterol (mmol/L)	0.04 ± 0.66	-0.07 ± 0.68	0.08 [-0.32, 0.48]	0.689
Triglycerides (mmol/L)	0.12 ± 1.13	-0.38 ± 1.32	0.13 [-0.47, 0.74]	0.663
Adipose tissue compartments				
Subcutaneous AT (cm^2)	-26 ± 38	-11 ± 37	-15 [-38, 7]	0.182
Visceral AT (cm^2)	-23 ± 27	-2 ± 17	-17 [-32, -3]	0.020
Epicardial AT (cm^2)	0 ± 2	1 ± 1	-1 [-2, 0]	0.139
Paracardial AT (cm^2)	-1 ± 3	0 ± 3	-1 [-3, 1]	0.467
Hepatic TGC (%)	-1.9 ± 3.6	-3.2 ± 5.5	-0.3 [-2.6, 2.0]	0.807
Myocardial TGC (%)	0.1 ± 0.5	-0.1 ± 0.6	0.2 [-0.1, 0.5]	0.157

Results are presented as n (%) or mean ± SD. n=44. Missing data in the liraglutide group: n=3 for epicardial adipose tissue volume and paracardial adipose tissue volume. Missing data in placebo group: n=1 for lean body mass (kg and %), n=3 for epicardial adipose tissue volume, n=2 for paracardial adipose tissue volume, and n=1 for myocardial triglyceride content. AT: adipose tissue, TGC: triglyceride content.

Effects of liraglutide on body weight and ectopic fat in the intention-to-treat analysis

Results of the intention-to-treat analysis are shown in **Table 2**. Treatment with liraglutide for 26 weeks decreased body weight, while body weight in participants treated with placebo was not affected (-3.9 ± 3.6 kg ***vs*** -0.6 ± 2.2 kg; mean change from baseline (liraglutide ***vs*** placebo): -3.5 kg; 95%CI [-5.3, -1.8]). Part of this weight loss was explained by a decrease in lean body mass that occurred in the liraglutide group but not in the placebo group (-2.3 ± 2.3 kg ***vs*** 0.4 ± 2.9 kg; mean change from baseline (liraglutide ***vs*** placebo): -2.7 kg; 95%CI [-4.3, -1.1]). Notably, waist circumference was decreased by liraglutide, while hip circumference was unaffected. Furthermore, although liraglutide decreased body weight, no effect was present on the investigated separate adipose tissue compartments, with the exception of a tendency to a decreased visceral adipose tissue volume in the liraglutide group compared to the placebo group (-20 ± 29 cm^2 ***vs*** -2 ± 17 cm^2; mean change from baseline (liraglutide ***vs*** placebo): -13 cm^2; 95%CI [-27, 1]).

Effects of liraglutide on HbA1c and lipid levels in the intention-to-treat analysis

In the intention-to-treat analysis HbA1c was decreased in the liraglutide group (-8.5 ± 11.2 mmol/mol; -0.8 ± 1.0%), but also in the placebo group (-6.8 ± 9.3 mmol/mol; -0.6 ± 0.8%), without between group differences (mean change from baseline (liraglutide ***vs*** placebo): -4.0 mmol/mol (-0.4%); 95%CI [-9.7, 1.6 (-0.9, 0.1%)]. To improve glycaemic control metformin was started for 1 participant and sulfonylurea derivatives were started in 3 participants of the placebo group according to clinical guidelines. The mean insulin dose was not significantly changed compared to baseline in the liraglutide and the placebo group (-11 ± 34 units/day ***vs*** 1 ± 23 units/day; mean change from baseline (liraglutide ***vs*** placebo): -12 units/day; 95%CI [-31, 8]). Furthermore, while glycaemic control was improved in both groups, total cholesterol, HDL-cholesterol, LDL-cholesterol and triglyceride were not affected.

Effects of liraglutide on ectopic fat and HbA1c in the per-protocol analysis

Results of the per protocol analysis are shown in **Table 3**. In this analysis, 3 patients who used <80% of the prescribed cumulative dose were excluded from analysis, of whom 2 were randomised to receive liraglutide and 1 to receive placebo. As in the intention-to-treat analysis, treatment with liraglutide decreased body weight and lean body mass. Furthermore, as shown in **Figure 2**, visceral adipose tissue volume was decreased by liraglutide, but not by placebo (-23 ± 27 cm^2 ***vs*** –2 ± 17 cm^2; mean change from baseline (liraglutide ***vs*** placebo): -17 cm^2; 95%CI [-32, -3]). Other adipose tissue compartments were not affected by treatment with liraglutide. HbA1c was decreased in the liraglutide group (-10.5 ± 9.1 mmol/mol; -1.0 ± 0.8%) to a greater extent than in the placebo group (-6.1 ± 8.8 mmol/mol; -0.6 ± 0.8%), with a between group difference (mean change from baseline (liraglutide ***vs*** placebo) of: -6.5 mmol/

mol (-0.6%); 95%CI [-11.5, -1.5 (-1.1, -0.1%)]. Interestingly, an association was present between the decrease of subcutaneous adipose tissue volume and HbA1c after treatment (β: 0.075 mmol/mol (0.007%) per 1 cm^2 decrease of subcutaneous adipose tissue volume; 95%CI [0.004, 0.146 (0.000, 0.013%)]) (**Figure 3A**). A similar but stronger association was present between the decrease of visceral adipose tissue volume and the reduction of HbA1c after treatment (β: 0.165 mmol/mol (0.015%) per 1 cm^2 decrease of visceral adipose tissue volume; 95%CI [0.062, 0.267 (0.006, 0.024%)]) (**Figure 3B**). No association was present between other adipose tissue compartments and HbA1c.

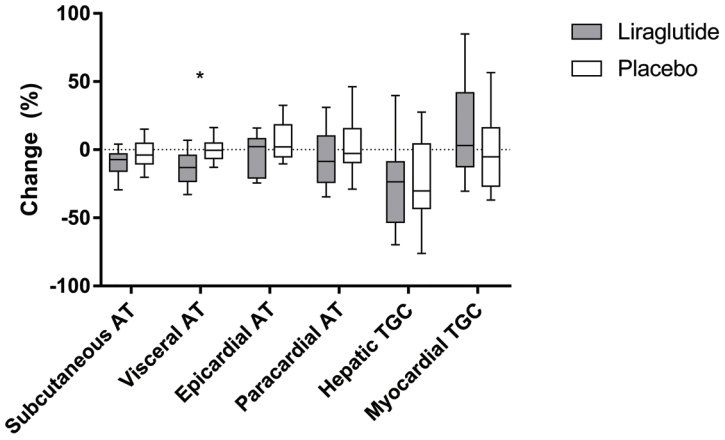

Figure 2. The effect of liraglutide and placebo on different adipose tissue compartments. Percentual changes are depicted after 26 weeks of treatment with liraglutide (n=24) and placebo (n=20) compared to baseline. Box and whiskers show 25th and 75th percentile and 10th and 90th percentile, respectively. Missing data in liraglutide-group: n=3 for epicardial AT and paracardial AT. Missing data in placebo-group: n=3 for epicardial AT, n=2 for paracardial AT and n=1 for Myocardial TGC. AT: adipose tissue, TGC: triglyceride content. * P<0.05.

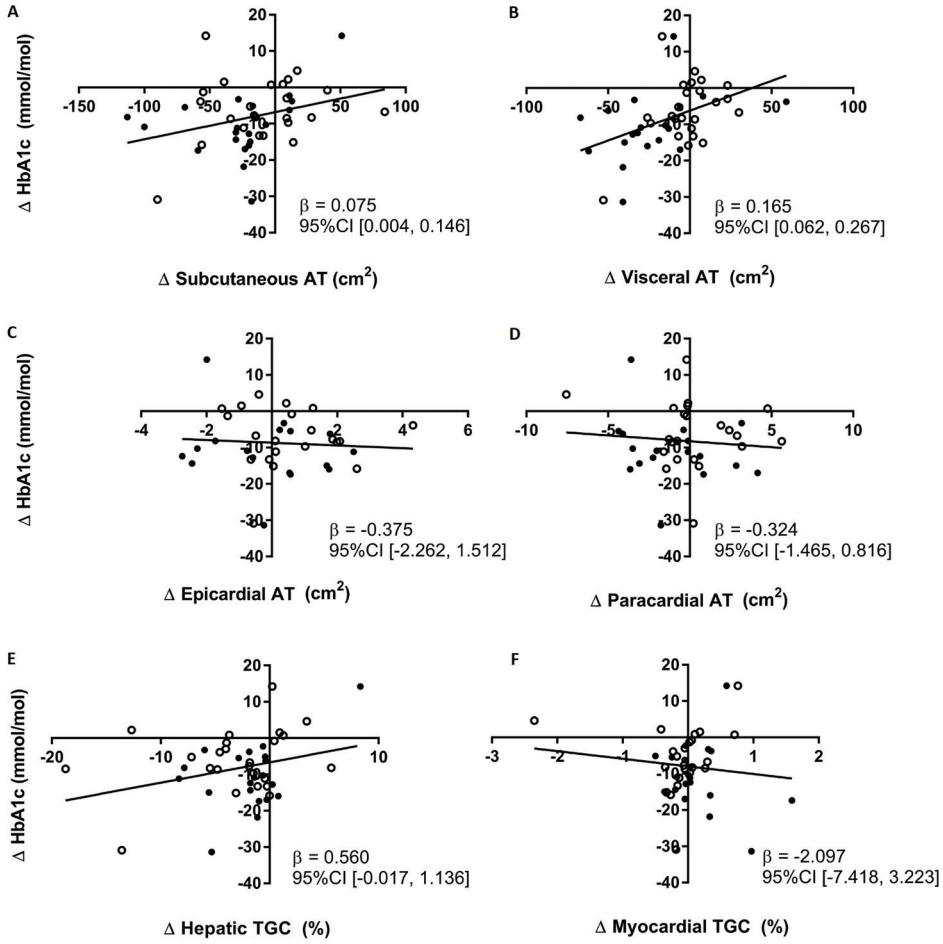

Figure 3. Associations between the change of adipose tissue compartments and HbA1c after treatment. Subcutaneous AT in relation to HbA1c, n=44 (A), Visceral AT in relation to HbA1c, n=44 (B), Epicardial AT in relation to HbA1c, n=38 (C), Paracardial AT in relation to HbA1c, n=39 (D), Hepatic TGC in relation to HbA1c, n=44 (E) and Myocardial TGC in relation to HbA1c, n=43 (F). Regression lines are shown for placebo (open symbol) and liraglutide (closed symbol) combined. AT: adipose tissue, TGC: triglyceride content.

DISCUSSION

In this double-blind, randomised placebo-controlled trial in South Asian patients with type 2 diabetes, we observed that liraglutide decreased body weight. Although this was not accompanied by effects on specific adipose tissue compartments in the intention-to-treat analysis, liraglutide did decrease visceral adipose tissue volume and HbA1c compared to placebo in the per-protocol analysis. In fact, the reduction in visceral adipose tissue was associated with an improved HbA1c. These data imply that GLP-1 analogues such as liraglutide

are an effective treatment option for South Asian patients with type 2 diabetes that might improve glycaemic control by reducing visceral adipose tissue volume.

We are the first to investigate the effects of liraglutide on ectopic fat deposition in a group of South Asians participants. Although the intention-to-treat analysis did not reveal a significant effect of liraglutide on ectopic fat, a trend towards a reduction of visceral adipose tissue volume was observed. This was likely caused by non-adherence of a few participants to the study protocol, as the per-protocol analysis did show that liraglutide decreased visceral adipose tissue. These data are in accordance with results published by Jendle et al. (17), who reported a dose-dependent reduction of visceral adipose tissue and a relatively small reduction of subcutaneous adipose tissue after treatment with 0.6, 1.2 or 1.8 mg liraglutide per day for 26 or 52 weeks in a mixed population. In line, Ishii et al. (20) reported that by treatment of Japanese individuals with liraglutide (0.9 mg/day for 26 weeks) reduced visceral adipose tissue volume without effects on subcutaneous adipose tissue. On the other hand, Suzuki et al. (22) reported that treatment of Japanese individuals with liraglutide (0.9 mg/day for 26 weeks) reduced subcutaneous adipose tissue volume without effects on visceral adipose tissue volume. Furthermore, in a study performed by Morano et al. (18), treatment of patients with type 2 diabetes with liraglutide (1.2 mg/day for 12 weeks) or exenatide, another GLP-1 analogue, resulted in a reduction of epicardial fat volume as assessed by ultrasonography. Iacobellis et al. (21) reported a similar reduction in epicardial fat volume after treatment with liraglutide (up to 1.8 mg/day for 3 and 6 months) and it was recently reported that epicardial adipose tissue expresses the GLP-1 receptor (31). This is of clinical importance, since it was recently shown that inflammatory activity of epicardial adipose tissue volume might induce myocardial remodelling and dysfunction (32). In the current study, a reduction of either epicardial or paracardial adipose tissue volume was not observed after treatment with liraglutide in South Asians as assessed by MRI, which is considered the gold standard for assessment of body fat, including epicardial fat (33). The reason for the discrepancy with previously published results is unclear but may reflect an ethnic-specific response to liraglutide. There are indications for this from a study comparing the effect of very low calorie diet in middle-aged South Asians to Western Europeans. While the very low calorie diet equally reduced body weight in both groups, the diet reduced pericardial adipose tissue, which includes epicardial adipose tissue, in the Western Europeans only (34). Similarly, we did not reproduce the results of Armstrong et al. (19), who reported a histologically assessed reduction of hepatic steatosis in patients with steatohepatitis after treatment with liraglutide (1.8 mg/day for 48 weeks) and of Dutour et al. (35) who reported reduction of hepatic steatosis in obese subjects with type 2 diabetes after treatment with exenatide (20 µg/day for 26 weeks). However, the patients in those studies had considerably higher severity of steatosis comparted to our participants who had a more modest hepatic triglyceride content. These data may indicate that the potency of liraglutide to reduce hepatic steatosis is dependent on hepatic triglyceride content, although an ethnic-specific response to liraglutide cannot be ruled out.

In our trial, in the intention-to-treat analysis, treatment with both liraglutide and placebo resulted in reduction of HbA1c. Importantly, both groups were treated according to current clinical guidelines. Therefore, if necessary, the dose of glucose lowering medication, including insulin, was increased or new medication was started in both groups, which can thus explain the effect of placebo on HbA1c. These results are in line with previously published studies reporting no significant superiority of GLP-analogues over standard treatment (36-38). However, in contrast to the intention-to-treat analysis, in the per-protocol analysis, treatment with liraglutide significantly reduced HbA1c compared to placebo. Interestingly, a previously published meta-analysis showed that the HbA1c-lowering effect of GLP-1 analogues is greater in studies with ≥50% Asian participants than in studies with <50% Asians (39). Therefore, possibly, in South Asian patients with type 2 diabetes treatment with liraglutide exerts more substantial or diverse effects, resulting in a greater reduction of HbA1c. An explanation for this observation could be differences in either insulin sensitivity or beta-cell function between South Asians and other ethnic groups. Importantly, since the change in visceral adipose tissue and the change in HbA1c show a strong association, it is likely that the reduction of visceral adipose tissue contributed to the improved glycaemic control.

Based on our data and current literature, we can speculate on the mechanism behind the liraglutide-induced reduction of visceral adipose tissue in our per-protocol analysis. It has previously been shown that GLP-1 increases the expression of lipolytic markers while reducing expression of lipogenic and adipogenic genes in adipose tissue, with distinct effects on subcutaneous and visceral adipose tissue (40). In another study, expression of brown adipose tissue-related genes was upregulated in subcutaneous adipose tissue of rats after treatment with liraglutide (41). In line, it was recently shown that liraglutide-induced weight reduction resulted in a greater reduction of visceral adipose tissue volume than lifestyle counselling at similar weight reduction (42). Another possible explanation for a specific reduction in visceral adipose tissue may be related to central effects of GLP-1. In rodents, activation of central GLP-1 receptors contributes substantially to improved insulin sensitivity (43) as related to an increase in sympathetic outflow (44). Sympathetic innervation of visceral and subcutaneous adipose tissue, the principal initiator for lipolysis in white adipose tissue, is partially separated (45). Therefore, central action of GLP-1 analogues might induce specific lipolysis in visceral adipose tissue as compared to subcutaneous adipose tissue.

It has previously been proposed that the subcutaneous adipose tissue compartment is less developed in South Asians compared to white people, resulting in a reduced storage capacity of this compartment causing more storage of fat in ectopic sites (46). Furthermore, South Asians have an increased subcutaneous adipose tissue adipocyte size compared to white Caucasians, probably related to limited expansion of this depot, further contributing to overflow of fatty acids to ectopic depots (11). Our results implicate that GLP-1 analogues could be an effective treatment option for South Asian patients with type 2 diabetes, possibly through improving insulin sensitivity via a specific reduction in visceral adipose tissue. If reduction in visceral

adipose tissue is indeed causal for the improvement of HbA1c, GLP-1 analogues are likely to be also beneficial for other patients with high amounts of ectopic fat. All in all, it is clear that liraglutide and other GLP-1 analogues decrease body weight related to a specific decrease in visceral adipose tissue. Further research is warranted to determine treatment effects in different ethnic groups and in subjects with different body compositions.

The main strength of this study is the randomised, double-blind, placebo-controlled trial design. In addition, the study design in which participants were treated according to current clinical guidelines increases the external validity of our results. Moreover, we had no drop-out and study drug compliance was generally high. Furthermore, we performed a per-protocol analysis excluding participants with a low drug adherence or missing data on drug adherence. Limitations are that our study was powered on other outcome measures than the outcomes reported here, and the relatively small group size.

CONCLUSIONS

In summary, in this randomised, placebo-controlled trial, we showed that liraglutide decreases body weight, which is partially caused by a reduction of visceral adipose tissue, and improves HbA1c in South Asian type 2 diabetes patients. Interestingly, the reduction of visceral adipose tissue was associated with a reduction in HbA1c. Collectively, these data indicate that GLP-1 analogues might be useful therapeutic means to improve glycaemic control by reducing visceral adipose tissue volume in South Asian type 2 diabetes patients.

ACKNOWLEDGMENTS

We express our gratitude to all individuals who participated in the MAGNA VICTORIA study. We are grateful to the physicians and nurses of the HMC Westeinde Hospital for inviting eligible participants. We thank N. van Tussenbroek for helping with data analysis, P.J. van den Boogaard for the support in the MRI data acquisition and B. Ladan-Eygenraam for technical assistance during the MAGNA VICTORIA study.

FUNDING

The study was supported financially and by providing trial drugs by Novo Nordisk A/S (Bagsvaerd, Denmark). We also thank Roba Metals B.V. IJsselstein (Utrecht, the Netherlands) for financial support. This project was also funded by the 'Cardio Vascular Imaging Group, LUMC (Leiden, the Netherlands).

REFERENCES

1. International Diabetes Federation. IDF Diabetes Atlas, 8th edn. Brussels, Belgium: International Diabetes Federation, 2017. http://www.diabetesatlas.org.
2. Mukhopadhyay B, Forouhi NG, Fisher BM, Kesson CM, Sattar N. A comparison of glycaemic and metabolic control over time among South Asian and European patients with Type 2 diabetes: results from follow-up in a routine diabetes clinic. Diabet Med 2006;23(1):94-98.
3. Razak F, Anand SS, Shannon H, et al. Defining obesity cut points in a multiethnic population. Circulation 2007;115(16):2111-2118.
4. Bakker LE, Sleddering MA, Schoones JW, Meinders AE, Jazet IM. Pathogenesis of type 2 diabetes in South Asians. Eur J Endocrinol 2013;169(5):R99-R114.
5. Seppala-Lindroos A, Vehkavaara S, Hakkinen AM, et al. Fat accumulation in the liver is associated with defects in insulin suppression of glucose production and serum free fatty acids independent of obesity in normal men. J Clin Endocrinol Metab 2002;87(7):3023-3028.
6. Goodpaster BH, He J, Watkins S, Kelley DE. Skeletal muscle lipid content and insulin resistance: evidence for a paradox in endurance-trained athletes. J Clin Endocrinol Metab 2001;86(12):5755-5761.
7. Despres JP, Lemieux I. Abdominal obesity and metabolic syndrome. Nature 2006;444(7121):881-887.
8. Lear SA, Chockalingam A, Kohli S, Richardson CG, Humphries KH. Elevation in cardiovascular disease risk in South Asians is mediated by differences in visceral adipose tissue. Obesity (Silver Spring) 2012;20(6):1293-1300.
9. Eastwood SV, Tillin T, Wright A, et al. Estimation of CT-derived abdominal visceral and subcutaneous adipose tissue depots from anthropometry in Europeans, South Asians and African Caribbeans. PLoS One 2013;8(9):e75085.
10. Petersen KF, Dufour S, Feng J, et al. Increased prevalence of insulin resistance and nonalcoholic fatty liver disease in Asian-Indian men. Proc Natl Acad Sci U S A 2006;103(48):18273-18277.
11. Anand SS, Tarnopolsky MA, Rashid S, et al. Adipocyte hypertrophy, fatty liver and metabolic risk factors in South Asians: the Molecular Study of Health and Risk in Ethnic Groups (mol-SHARE). PLoS One 2011;6(7):e22112.
12. Snel M, Jonker JT, Schoones J, et al. Ectopic fat and insulin resistance: pathophysiology and effect of diet and lifestyle interventions. Int J Endocrinol 2012;2012:983814.
13. Fox CS, Massaro JM, Hoffmann U, et al. Abdominal visceral and subcutaneous adipose tissue compartments: association with metabolic risk factors in the Framingham Heart Study. Circulation 2007;116(1):39-48.
14. Schlett CL, Lorbeer R, Arndt C, et al. Association between abdominal adiposity and subclinical measures of left-ventricular remodeling in diabetics, prediabetics and normal controls without history of cardiovascular disease as measured by magnetic resonance imaging: results from the KORA-FF4 Study. Cardiovasc Diabetol 2018;17(1):88.
15. Astrup A, Rossner S, Van Gaal L, et al. Effects of liraglutide in the treatment of obesity: a randomised, double-blind, placebo-controlled study. Lancet 2009;374(9701):1606-1616.
16. Drucker DJ, Buse JB, Taylor K, et al. Exenatide once weekly versus twice daily for the treatment of type 2 diabetes: a randomised, open-label, non-inferiority study. Lancet 2008;372(9645):1240-1250.
17. Jendle J, Nauck MA, Matthews DR, et al. Weight loss with liraglutide, a once-daily human glucagon-like peptide-1 analogue for type 2 diabetes treatment as monotherapy or added to metformin, is primarily as a result of a reduction in fat tissue. Diabetes Obes Metab 2009;11(12):1163-1172.
18. Morano S, Romagnoli E, Filardi T, et al. Short-term effects of glucagon-like peptide 1 (GLP-1) receptor agonists on fat distribution in patients with type 2 diabetes mellitus: an ultrasonography study. Acta Diabetol 2015;52(4):727-732.
19. Armstrong MJ, Gaunt P, Aithal GP, et al. Liraglutide safety and efficacy in patients with non-alcoholic steatohepatitis (LEAN): a multicentre, double-blind, randomised, placebo-controlled phase 2 study. Lancet 2016;387(10019):679-690.
20. Ishii S, Nagai Y, Sada Y, et al. Liraglutide Reduces Visceral and Intrahepatic Fat Without Significant Loss of Muscle Mass in Obese Patients With Type 2 Diabetes: A Prospective Case Series. J Clin Med Res 2019;11(3):219-224.
21. Iacobellis G, Mohseni M, Bianco SD, Banga PK. Liraglutide causes large and rapid

epicardial fat reduction. Obesity (Silver Spring) 2017;25(2):311-316.
22. Suzuki D, Toyoda M, Kimura M, et al. Effects of liraglutide, a human glucagon-like peptide-1 analogue, on body weight, body fat area and body fat-related markers in patients with type 2 diabetes mellitus. Intern Med 2013;52(10):1029-1034.
23. Chen P, Hou X, Hu G, et al. Abdominal subcutaneous adipose tissue: a favorable adipose depot for diabetes? Cardiovasc Diabetol 2018;17(1):93.
24. McLaughlin T, Lamendola C, Liu A, Abbasi F. Preferential fat deposition in subcutaneous versus visceral depots is associated with insulin sensitivity. J Clin Endocrinol Metab 2011;96(11):E1756-1760.
25. Lebovitz HE, Banerji MA. Point: visceral adiposity is causally related to insulin resistance. Diabetes Care 2005;28(9):2322-2325.
26. Friedewald WT, Levy RI, Fredrickson DS. Estimation of the concentration of low-density lipoprotein cholesterol in plasma, without use of the preparative ultracentrifuge. Clinical chemistry 1972;18(6):499-502.
27. de Heer P, Bizino MB, Lamb HJ, Webb AG. Parameter optimization for reproducible cardiac (1) H-MR spectroscopy at 3 Tesla. J Magn Reson Imaging 2016;44(5):1151-1158.
28. de Heer P, Bizino MB, Versluis MJ, Webb AG, Lamb HJ. Improved Cardiac Proton Magnetic Resonance Spectroscopy at 3 T Using High Permittivity Pads. Invest Radiol 2016;51(2):134-138.
29. Rial B, Robson MD, Neubauer S, Schneider JE. Rapid quantification of myocardial lipid content in humans using single breath-hold 1H MRS at 3 Tesla. Magn Reson Med 2011;66(3):619-624.
30. Bizino MB, Jazet IM, Westenberg JJM, et al. Effect of liraglutide on cardiac function in patients with type 2 diabetes mellitus: randomized placebo-controlled trial. Cardiovasc Diabetol 2019;18(1):55.
31. Iacobellis G, Camarena V, Sant DW, Wang G. Human Epicardial Fat Expresses Glucagon-Like Peptide 1 and 2 Receptors Genes. Horm Metab Res 2017;49(8):625-630.
32. Cho DH, Joo HJ, Kim MN, Lim DS, Shim WJ, Park SM. Association between epicardial adipose tissue, high-sensitivity C-reactive protein and myocardial dysfunction in middle-aged men with suspected metabolic syndrome. Cardiovasc Diabetol 2018;17(1):95.
33. Ross R, Leger L, Morris D, de Guise J, Guardo R. Quantification of adipose tissue by MRI: relationship with anthropometric variables. J Appl Physiol (1985) 1992;72(2):787-795.
34. Van Schinkel LD, Bakker LE, Jonker JT, et al. Cardiovascular flexibility in middle-aged overweight South Asians vs. white Caucasians: response to short-term caloric restriction. Nutr Metab Cardiovasc Dis 2015;25(4):403-410.
35. Dutour A, Abdesselam I, Ancel P, et al. Exenatide decreases liver fat content and epicardial adipose tissue in patients with obesity and type 2 diabetes: a prospective randomized clinical trial using magnetic resonance imaging and spectroscopy. Diabetes Obes Metab 2016;18(9):882-891.
36. Tang A, Rabasa-Lhoret R, Castel H, et al. Effects of Insulin Glargine and Liraglutide Therapy on Liver Fat as Measured by Magnetic Resonance in Patients With Type 2 Diabetes: A Randomized Trial. Diabetes Care 2015;38(7):1339-1346.
37. Weissman PN, Carr MC, Ye J, et al. HARMONY 4: randomised clinical trial comparing once-weekly albiglutide and insulin glargine in patients with type 2 diabetes inadequately controlled with metformin with or without sulfonylurea. Diabetologia 2014;57(12):2475-2484.
38. D'Alessio D, Haring HU, Charbonnel B, et al. Comparison of insulin glargine and liraglutide added to oral agents in patients with poorly controlled type 2 diabetes. Diabetes Obes Metab 2015;17(2):170-178.
39. Kim YG, Hahn S, Oh TJ, Park KS, Cho YM. Differences in the HbA1c-lowering efficacy of glucagon-like peptide-1 analogues between Asians and non-Asians: a systematic review and meta-analysis. Diabetes Obes Metab 2014;16(10):900-909.
40. El Bekay R, Coin-Araguez L, Fernandez-Garcia D, et al. Effects of glucagon-like peptide-1 on the differentiation and metabolism of human adipocytes. Br J Pharmacol 2016;173(11):1820-1834.
41. Zhao L, Zhu C, Lu M, et al. The key role of a glucagon-like peptide-1 receptor agonist in body fat redistribution. J Endocrinol 2019;240(2):271-286.
42. Santilli F, Simeone PG, Guagnano MT, et al. Effects of Liraglutide on Weight Loss, Fat Distribution, and beta-Cell Function in Obese Subjects With Prediabetes or Early Type 2 Diabetes. Diabetes Care 2017;40(11):1556-1564.
43. Parlevliet ET, de Leeuw van Weenen JE, Romijn JA, Pijl H. GLP-1 treatment reduces endogenous insulin resistance via activation of central GLP-

1 receptors in mice fed a high-fat diet. Am J Physiol Endocrinol Metab 2010;299(2):E318-324.
44. Kooijman S, Wang Y, Parlevliet ET, et al. Central GLP-1 receptor signalling accelerates plasma clearance of triacylglycerol and glucose by activating brown adipose tissue in mice. Diabetologia 2015;58(11):2637-2646.
45. Nguyen NL, Randall J, Banfield BW, Bartness TJ. Central sympathetic innervations to visceral and subcutaneous white adipose tissue. Am J Physiol Regul Integr Comp Physiol 2014;306(6):R375-386.
46. Sniderman AD, Bhopal R, Prabhakaran D, Sarrafzadegan N, Tchernof A. Why might South Asians be so susceptible to central obesity and its atherogenic consequences? The adipose tissue overflow hypothesis. Int J Epidemiol 2007;36(1):220-225.

CHAPTER

5

Effect of liraglutide on cardiovascular function and myocardial tissue characteristics in type 2 diabetes patients of South Asian descent living in the Netherlands: a double-blind randomized placebo-controlled trial

Paiman EHM,* van Eyk HJ,* van Aalst MMA, Bizino MB, van der Geest RJ, Westenberg JJM, Geelhoed-Duijvestijn PH, Kharagjitsingh AV, Rensen PCN, Smit JWA, Jazet IM, Lamb HJ

* shared first author

J Magn Reson Imaging. 2020 Jun;51(6):1679-1688. doi: 10.1002/jmri.27009. Epub 2019 Dec 4.

ABSTRACT

Background

The glucagon-like peptide 1 (GLP-1) receptor agonist liraglutide may be beneficial in the regression of diabetic cardiomyopathy. South Asian ethnic groups in particular are at risk of developing type 2 diabetes. The aim of this study was to assess the effects of liraglutide on left ventricular (LV) diastolic and systolic function in South Asian type 2 diabetes patients.

Methods

Study Type: Prospective, double-blind, randomized, placebo-controlled trial.

Population: Forty-seven type 2 diabetes patients of South Asian ancestry living in the Netherlands, with or without ischemic heart disease, who were randomly assigned to 26-week treatment with liraglutide (1.8 mg/day) or placebo.

Field Strength/Sequence: 3T (balanced steady-state free precession cine MRI, 2D and 4D velocity-encoded MRI, ^{1}H-MRS, T1 mapping).

Assessment: Primary endpoints were changes in LV diastolic function (early deceleration peak [Edec], ratio of early and late peak filling rate [E/A], estimated LV filling pressure [E/Ea]) and LV systolic function (ejection fraction). Secondary endpoints were changes in aortic stiffness (aortic pulse wave velocity [PWV]), myocardial steatosis (myocardial triglyceride content), and diffuse fibrosis (extracellular volume [ECV]).

Statistical Tests: Data were analyzed according to intention-to-treat. Between-group differences were reported as mean (95% confidence interval [CI]) and were assessed using analysis of covariance (ANCOVA).

Results

Liraglutide (n = 22) compared with placebo (n = 25) did not change Edec (+0.2 mL/s^2 × 10^{-3} (–0.3;0.6)), E/A (–0.09 (–0.23;0.05)), E/Ea (+0.1 (–1.2;1.3)) and ejection fraction (0% (–3;2)), but decreased stroke volume (–9 mL (–14;–5)) and increased heart rate (+10 bpm (4;15)). Aortic PWV (+0.5 m/s (–0.6;1.6)), myocardial triglyceride content (+0.21% (–0.09;0.51)), and ECV (–0.2% (–1.4;1.0)) were unaltered.

Conclusion

Liraglutide did not affect LV diastolic and systolic function, aortic stiffness, myocardial triglyceride content, or extracellular volume in Dutch South Asian type 2 diabetes patients with or without coronary artery disease.

INTRODUCTION

Type 2 diabetes is associated with a 2–5-fold increased risk of heart failure (1). Diabetic cardiomyopathy, which is characterized by left ventricular (LV) diastolic dysfunction, may eventually progress to heart failure with preserved ejection fraction (1). A potential antihyperglycemic agent with cardioprotective effects is the glucagon-like peptide 1 (GLP-1) receptor agonist liraglutide (2).

Recently, the LEADER trial demonstrated a reduced total cardiovascular mortality as a result of liraglutide in patients with type 2 diabetes and high cardiovascular risk, presumably because of a lower risk of ischemic events (3). Similar reductions in cardiovascular mortality have been reported in response to treatment with the GLP-1 receptor agonists semaglutide and dulaglutide (4). However, it is largely unknown whether liraglutide in the management of type 2 diabetes is advantageous for heart function in asymptomatic diastolic dysfunction (2). It is conceivable that the favorable metabolic impact of liraglutide on lipid profiles and inflammatory markers (5), in addition to the natriuretic and vasodilatory actions (6,7), has indirect beneficial effects on diastolic function. Liraglutide has been assumed to exert direct actions on the myocardium that may amend myocardial metabolism, although preclinical and clinical studies have not been conclusive (2). The effects of liraglutide on diastolic function may be mediated by regression of type 2 diabetes-related myocardial steatosis, diffuse fibrosis, and aortic stiffening (1,8). Notably, clinical studies have consistently reported an increase in heart rate in individuals using liraglutide (2,5,9). In this regard, the actual effect of liraglutide on heart function, taking into account the wide range of cardiovascular actions, is uncertain.

South Asian ethnic groups in particular are at increased risk of developing type 2 diabetes (10). South Asians appear to have a strong genetic predisposition for insulin resistance, while differences in lifestyle factors seem to have a smaller role in the increased risk of type 2 diabetes as compared with other ethnic groups (11). The impaired insulin sensitivity in South Asians has been related to the relatively high total body fat percentage and high fat storage in the visceral compartments (12). In addition, adipocytes may be dysfunctional, as reflected by the increased release of free fatty acids, adipokines, and proinflammatory cytokines among South Asian individuals (13,14). Previously, it has been demonstrated that hyperglycemia is more detrimental for cardiac function in South Asians than in Europeans (15). As the pathogenesis of type 2 diabetes, but also the impact of type 2 diabetes on cardiac function appears to be different, the cardiometabolic effects of liraglutide in the treatment of type 2 diabetes may be more pronounced in South Asians compared with individuals of other ethnicities.

In this study we aimed to assess the effects of 26-week liraglutide treatment among South Asian type 2 diabetes patients on LV diastolic and systolic function and, secondary, myocardial steatosis and diffuse fibrosis. We used cardiovascular magnetic resonance, as this imaging modality enables the measurement of LV diastolic and systolic function and aortic stiffness (16,17), and also the assessment of myocardial tissue characteristics (18,19).

MATERIALS AND METHODS

Study design and participants

This study was a 26-week double-blind, randomized controlled trial (ClinicalTrials.gov NCT02660047) (20). Written informed consent was obtained prior to inclusion. The study complied with the revised Declaration of Helsinki and was approved by the Institutional Review Board and the Central Committee on Research Involving Human Subjects.

Patients were recruited from the outpatient clinic of the Leiden University Medical Centre (Leiden, the Netherlands), local hospitals, and general practices in Leiden and The Hague, and by advertisements in local newspapers. Individuals aged 18–75 years of South Asian ancestral origin with type 2 diabetes treated with metformin, sulfonylurea derivatives, and/or insulin for at least 3 months in stable dose were eligible for participation. South Asian descent was defined as both biological parents and their ancestors being South Asian (ie, South Asian Surinamese, Indian, Pakistani, Bangladeshi, or Sri Lankan origin). Inclusion criteria were: body mass index (BMI) ≥23 kg/m^2; HbA1c ≥6.5 and <11.0% (≥47.5 and <96.5 mmol/mol); estimated glomerular filtration rate (eGFR) >30 mL/min/1.73 m^2; blood pressure <180/110 mmHg. Main exclusion criteria were: use of GLP-1 receptor agonists; dipeptidyl peptidase-4 inhibitors, or thiazolidinediones within the past 6 months; heart failure, New York Heart Association (NYHA) class III-IV; acute coronary or cerebrovascular accident in the preceding 30 days; pancreatitis or medullary thyroid carcinoma; gastric bypass surgery; pregnant or lactating women; any contraindication for magnetic resonance imaging (MRI). Due to the insufficient number of eligible patients, several criteria were adjusted (initial inclusion criteria: age 18–70 years; HbA1c ≥7.0 and <10.0% (≥53 and <86 mmol/mol); eGFR >60 mL/min/1.73 m^2; blood pressure <150/85 mmHg; no history of cardiovascular disease).

Randomization, blinding, and intervention

Patients were randomized to once-daily subcutaneous injections of liraglutide (Victoza, Novo Nordisk A/S, Bagsvaerd, Denmark) or placebo added to standard care during 26 weeks (randomization with block size 4, with 1:1 stratification for sex and insulin use). A randomization code list was generated by the institutional research pharmacist. If necessary to prevent hypoglycemia, the concomitant glucose-lowering medication was adjusted at study entry. Starting dose of the trial medication was 0.6 mg/day, which was increased every 7 days up to 1.8 mg/day. The dose was reduced upon poor tolerance. Investigators and patients were blinded to treatment allocation. Furthermore, the MRI data were stripped of any information on the participant's identity and measurement date.

Study procedures

Study days at baseline and after 26 weeks consisted of clinical measurements and MRI. Baseline and follow-up measurements were both scheduled either in the morning or evening. Patients

were asked to fast overnight or for 6 hours, when measurements were in the morning or evening, respectively. To prevent hypoglycemia during fasting, the insulin dose was adjusted and other antidiabetic medications were temporarily discontinued. Patients were instructed to adhere to their usual diet and physical activity. During the trial, patients received a weekly telephone call for glycemic control based on their self-monitored blood glucose levels. At week 4 and 12, routine blood tests and clinical measurements were performed. Glycemic control and blood pressure management was according to the current guidelines (21,22). Patients were asked for adverse events once a week. Study drug pens were collected during the trial as a surrogate marker of compliance.

MRI protocol

MRI scans were acquired with a 3T MR scanner (Ingenia, Philips Healthcare, Best, the Netherlands). For contrast-enhanced MRI, 0.15 mmol gadoterate meglumine (0.5 mmol/mL Dotarem; Guerbet, Villepinte, France) per kilogram of body weight was administered intravenously. LV systolic and diastolic function parameters were assessed by short-axis and 4-chamber cine balanced steady-state free precession (bSSFP) and whole-heart gradient-echo 4D velocity-encoded MRI, with retrospective ECG (electrocardiography) gating. To determine aortic stiffness, the aortic pulse wave velocity (PWV) was calculated from a scout view of the aorta and two 2D velocity-encoded scans at the ascending and abdominal aorta. Myocardial steatosis was quantified as the myocardial triglyceride content, examined by proton-magnetic resonance spectroscopy (^{1}H-MRS) in the mid-ventricular septum and expressed as the amplitude of triglyceride methylene divided by the amplitude of unsuppressed water, multiplied by 100%. Myocardial diffuse fibrosis was assessed using native and postcontrast modified Look–Locker inversion (MOLLI) recovery T1 mapping. Native T1 and the extracellular volume (ECV) were measured in the mid-ventricular septum. To identify ischemic scarring, late gadolinium enhancement (LGE) MRI was acquired. If septal delayed enhancement was present, myocardial triglyceride content data were excluded and diffuse fibrosis was measured outside the region with scar. LGE-MRI was assessed visually by a radiologist (H.J.L.) and clinical investigator (E.H.M.P.) with 25 and 4 years of experience in cardiovascular MRI, respectively. A detailed description of the MRI protocol is provided as **Supplementary Material**.

Study endpoints

Primary endpoints were LV diastolic function (peak deceleration slope of the transmitral early peak filling rate [Edec], ratio of transmitral early and late peak filling rate [E/A], early peak diastolic mitral septal tissue velocity [Ea], estimated LV filling pressure [E/Ea]) and LV systolic function (ejection fraction, stroke volume, cardiac output, cardiac index, peak ejection rate). Secondary endpoints included myocardial triglyceride content, ECV, aortic PWV, LV dimensions, and clinical parameters (heart rate, blood pressure, body weight, and HbA1c).

Statistical analysis

Statistical analyses were performed with SPSS v. 23 (IBM, Armonk, NY), according to intention-to-treat. Within-group differences from baseline to 26 weeks are reported as means ± SD. Between-group differences for liraglutide vs. placebo were analyzed using analysis of covariance (ANCOVA) with the baseline values as covariate to reduce within- and between-group variability and are reported as means (95% CI). Statistical tests were 2-sided and $P < 0.05$ was considered significant. The power calculation is described in the **Supplementary Material**.

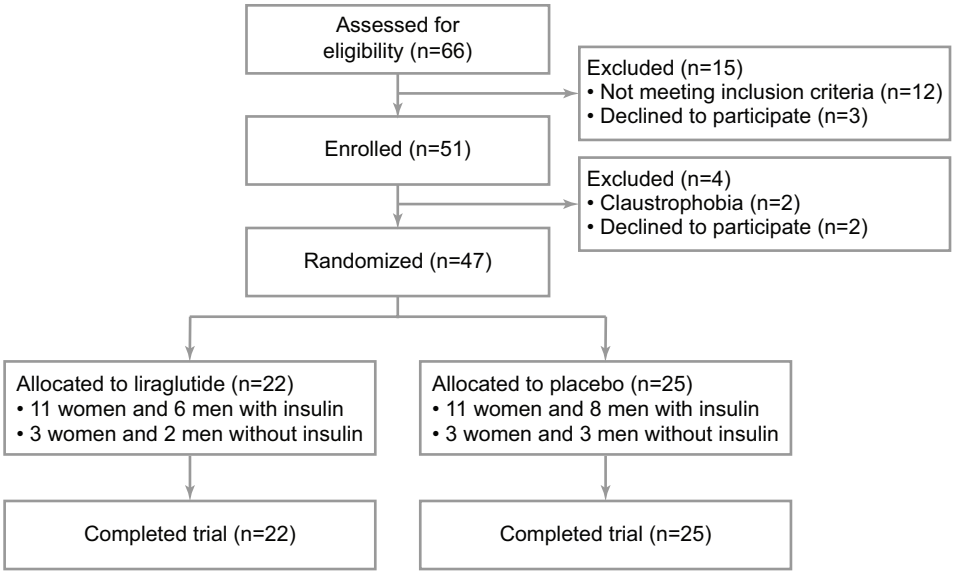

Figure 1. Trial profile.

RESULTS

Baseline characteristics

Patients were recruited between July 16, 2015, and December 6, 2017. A total of 47 patients were randomized to liraglutide (n = 22) or placebo (n = 25) (**Figure 1**). Between October 7, 2015, and March 9, 2018, all participants completed the trial. There were no clinically relevant differences between the treatment groups regarding demographics and clinical, laboratory, and MRI parameters (**Table 1**). The total study population (40% men) had a mean (SD) age of 55 ± 10 years, a diabetes duration of 18 ± 10 years, and HbA1c of 8.4 ± 1.0% (68 ± 11 mmol/mol), while 77% of the patients were using insulin.

Drug compliance and clinical parameters

Study drug compliance was high (95 ± 8% and 99 ± 5% for liraglutide and placebo treatment, respectively) and the dose could be titrated up to 1.8 mg/day in most patients (in 86% and 96% of the patients treated with liraglutide and placebo, respectively). For glycemic control, in some patients in the placebo group concomitant medication was started (metformin [n = 1] or sulfonylurea derivates [n = 3]) or the insulin dose was adjusted (1 ± 23 and –11 ± 34 units/day in the placebo and liraglutide group, respectively). For blood pressure management, in some patients in the placebo and liraglutide group antihypertensive mediation was started or the dose was elevated (n = 5 vs. n = 3) or the dose was reduced (n = 1 vs. n = 2).

In both the liraglutide and placebo group there was a decrease (mean ± SD) after 26 weeks in HbA1c (–0.8 ± 1.0 vs. –0.6 ± 0.8%; –9 ± 11 vs. –7 ± 9 mmol/mol) and systolic blood pressure (–14 ± 18 vs. –7 ± 15 mmHg), but not in diastolic blood pressure (–3 ± 11 vs. –3 ± 9 mmHg). However, between-group differences for liraglutide vs. placebo in HbA1c (–0.4% [95% CI: –0.9 to 0.2]; –4 mmol/mol [95% CI: –10 to 2], $P = 0.16$) and systolic blood pressure (–3 mmHg [95% CI: –9 to 3, $P = 0.36$]) were nonsignificant. Liraglutide compared with placebo decreased body weight (–3.9 ± 3.6 vs. –0.6 ± 2.2 kg; between-group difference: –3.5 kg [95% CI: –5.3 to –1.8, $P < 0.001$]) and increased heart rate (9 ± 11 vs. –2 ± 8 bpm; between-group difference: 10 bpm [95% CI: 4 to 15, $P = 0.001$]).

LV function, aortic stiffness, and myocardial tissue characteristics

LV diastolic function parameters were unaltered by liraglutide. Also, LV systolic function was unaffected upon liraglutide, as the ejection fraction and peak ejection rate were unchanged and, despite the decreased stroke volume, cardiac output and cardiac index were preserved (**Table 2** and **Figure 2**). The decrease in stroke volume was in parallel with the reductions in end-diastolic and end-systolic volume, which persisted when adjusting for body surface area. Whereas liraglutide significantly reduced end-diastolic volume, the decrease in LV mass was not significant. Also, liraglutide did not change aortic stiffness, myocardial triglyceride content, or diffuse fibrosis. A total of six patients had delayed enhancement at baseline, but in only one patient was the ventricular septum involved. In all patients, the extent of delayed enhancement was unchanged at follow-up. Details on missing values are provided as **Supplementary Material**.

Table 1. Baseline characteristics

	Liraglutide (n=22)	Placebo (n=25)
Demographic and clinical characteristics		
Age, years	55 (11)	55 (9)
Men, no.	8 (36%)	11 (44%)
Diabetes duration, years	19 (10)	17 (10)
Diabetes complications, no.	15 (68%)	16 (64%)
Coronary artery disease, no.		
Non-significant coronary artery stenosis	4 (18%)	0 (0%)
Percutaneous coronary intervention	2 (9%)	3 (12%)
Coronary artery bypass grafting	1 (5%)	2 (8%)
Smoking, no.		
Currently	2 (9%)	5 (20%)
Previously	6 (27%)	0 (0%)
Never	14 (64%)	20 (80%)
Medication		
Metformin, no.	22 (100%)	23 (92%)
Sulfonylurea derivatives, no.	3 (14%)	5 (20%)
Insulin, no.	17 (77%)	19 (76%)
Metformin dose, g/day	1.8 (0.7)	1.7 (0.6)
Insulin dose, units/day	77 (34)	67 (30)
Lipid-lowering drugs, no.	17 (77%)	20 (80%)
Anti-hypertensive drugs, no.	16 (73%)	18 (72%)
Beta-blockers, no.	8 (36%)	9 (36%)
Diuretics, no.	9 (41%)	8 (32%)
ACE-inhibitors, no.	6 (27%)	7 (28%)
Angiotensin II receptor-blockers, no.	7 (32%)	9 (36%)
Calcium-antagonists, no.	2 (9%)	5 (20%)
Clinical parameters		
Weight, kg	82 (11)	78 (12)
BMI, kg/m^2	30.4 (3.8)	28.6 (4.0)
Waist circumference, cm	104 (8)	98 (10)
Waist-hip ratio	1.00 (0.07)	0.95 (0.09)
Heart rate, bpm	73 (13)	77 (11)
Systolic blood pressure, mmHg	149 (25)	141 (18)
Diastolic blood pressure, mmHg	85 (11)	85 (10)
Laboratory parameters		
HbA1c, %	8.1 (0.9)	8.6 (1.1)
HbA1c, mmol/mol	65 (10)	70 (12)
Triglycerides, mmol/L	1.6 (0.9)	2.1 (1.8)

Table 1. Baseline characteristics

	Liraglutide (n=22)	Placebo (n=25)
Total cholesterol, mmol/L	4.0 (0.6)	4.5 (1.1)
HDL-cholesterol, mmol/L	1.2 (0.3)	1.2 (0.3)
LDL-cholesterol, mmol/L	2.0 (0.7)	2.2 (1.0)
LV diastolic function		
Edec, mL/s2 x10-3	-2.5 (1.3)	-2.7 (1.2)
E, mL/s	305 (99)	328 (118)
A, mL/s	316 (75)	306 (58)
E/A	0.99 (0.31)	1.11 (0.43)
E, cm/s	34 (9)	37 (9)
Ea, cm/s	5.3 (2.1)	5.7 (1.9)
E/Ea	7.4 (3.9)	7.4 (3.3)
LV systolic function		
Stroke volume, mL	70 (12)	67 (15)
Ejection fraction, %	56 (8)	57 (7)
Cardiac output, L/min	4.7 (0.9)	4.7 (1.1)
Cardiac index, L/min/m2	2.4 (0.4)	2.5 (0.4)
Peak ejection rate, mL/s	338 (82)	345 (84)
LV structure		
End-diastolic volume, mL	128 (25)	120 (36)
End-systolic volume, mL	57 (21)	53 (24)
Mass, g	98 (22)	96 (24)
Aortic stiffness		
Aortic pulse wave velocity, m/s	8.8 (2.4)	8.3 (2.4)
Myocardial tissue characteristics		
Myocardial triglyceride content, %	0.92 (0.43)	1.00 (0.58)
Native T1 relaxation time, ms	1264 (45)	1254 (33)
Extracellular volume, %	25.9 (3.1)	27.0 (2.6)

Data are presented as mean (SD) or number (%). Diabetes complications: retinopathy, neuropathy, nephropathy or macrovascular complications. A: late transmitral peak filling rate; E: early transmitral peak filling rate; Ea: early peak diastolic mitral septal tissue velocity; E/Ea: estimation of LV filling pressure; Edec: early deceleration peak.

Adverse events

There was one serious adverse event in the placebo group (admission for acute coronary syndrome symptoms without requiring further treatment). More patients with treatment with liraglutide compared with placebo had complaints of nausea (73% vs. 40%) and vomiting (27% vs. 8%). There were no cases of severe hypoglycemia.

Table 2. Study endpoints: mean change over 26 weeks

	Mean change (SD) from 0 to 26 weeks		Mean change (95%CI) from 0 to 26 weeks	
	Liraglutide (n=22)	Placebo (n=25)	(liraglutide vs. placebo)	*P* value
Primary				
LV diastolic function				
Edec, mL/s^2 x10^{-3}	0.2 (1.1)	0.1 (0.7)	0.2 (-0.3 to 0.6)	0.46
E, mL/s	-36 (84)	-18 (55)	-24 (-60 to 12)	0.18
A, mL/s	17 (77)	-2 (45)	18 (-21 to 56)	0.35
E/A	-0.11 (0.24)	-0.05 (0.24)	-0.09 (-0.23 to 0.05)	0.21
E, cm/s	-2 (7)	-1 (7)	-2 (-6 to 1)	0.20
Ea, cm/s	-0.1 (1.1)	-0.1 (1.1)	-0.1 (-0.7 to 0.5)	0.73
E/Ea	-0.4 (2.4)	-0.3 (2.6)	0.1 (-1.2 to 1.3)	0.89
LV systolic function				
Ejection fraction, %	0 (5)	0 (3)	0 (-3 to 2)	0.86
Stroke volume, mL	-10 (9)	0 (7)	-9 (-14 to -5)	<0.001
Cardiac output, L/min	-0.2 (0.5)	-0.1 (0.5)	-0.1 (-0.4 to 0.2)	0.44
Cardiac index, L/min/m^2	-0.1 (0.3)	-0.1 (0.3)	0.0 (-0.2 to 0.1)	0.87
Peak ejection rate, mL/s	-9 (60)	-7 (45)	-3 (-34 to 27)	0.83
Secondary				
LV structure				
Mass, g	-4 (9)	0 (7)	-4 (-9 to 0)	0.07
End-diastolic volume, mL	-19 (13)	-1 (11)	-17 (-24 to -10)	<0.001
End-systolic volume, mL	-9 (9)	-1 (7)	-7 (-11 to -3)	0.001
Aortic stiffness				
Aortic pulse wave velocity, m/s	0.2 (2.1)	-0.2 (1.7)	0.5 (-0.6 to 1.6)	0.35
Myocardial tissue characteristics				
Myocardial triglyceride content, %	0.14 (0.47)	-0.09 (0.56)	0.21 (-0.09 to 0.51)	0.16
Native T1 relaxation time, ms	-6 (36)	6 (26)	-7 (-21 to 7)	0.35
Extracellular volume, %	0.5 (2.6)	0.4 (1.3)	-0.2 (-1.4 to 1.0)	0.76

Abbreviations as in Table 1.

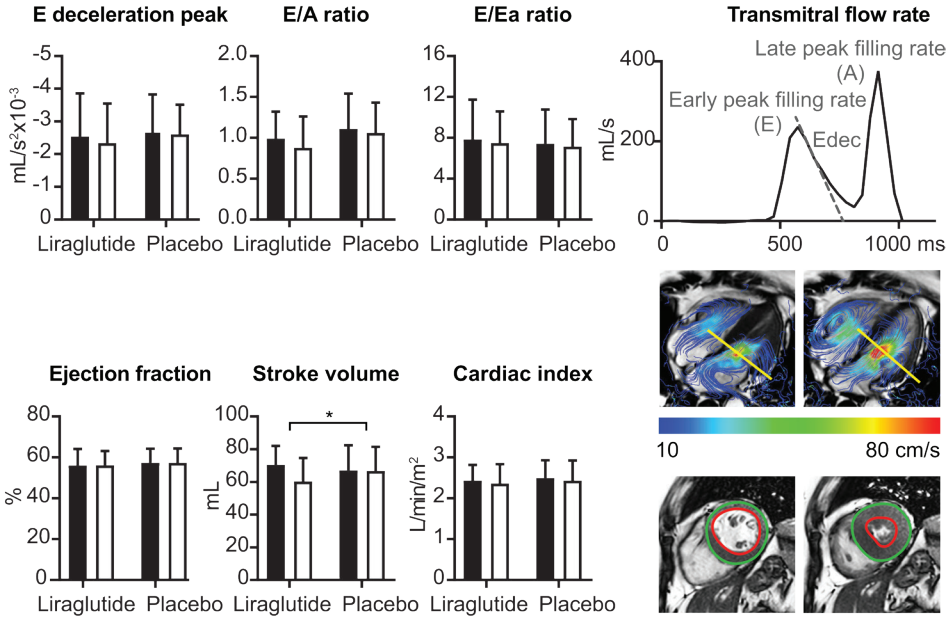

Figure 2. Liraglutide does not alter left ventricular (LV) diastolic and systolic function in South Asian type 2 diabetes patients with or without coronary artery disease and without advanced heart failure. LV diastolic and systolic outcome measures (mean SD) before (black bars) and after (white bars) treatment with liraglutide and placebo are presented. An example of a transmitral flow rate curve, 4D velocity-encoded, and short-axis cine magnetic resonance image is provided for illustration. E/A: ratio of transmitral early and late peak filling rate; E/Ea: estimation of LV filling pressure; Ea: early peak diastolic mitral septal tissue velocity; Edec: early deceleration peak.

DISCUSSION

In this double-blind, randomized controlled trial in type 2 diabetes patients of South Asian descent living in the Netherlands, with or without coronary artery disease, 26-week treatment with 1.8 mg/day liraglutide had no effect on LV diastolic and systolic function, aortic stiffness, myocardial triglyceride content, or extracellular volume as compared with placebo when added to standard care. Our results imply that liraglutide does not amend cardiovascular remodeling in diabetic cardiomyopathy in a Dutch South Asian type 2 diabetes population including patients with preexisting ischemic heart disease, at least not upon a treatment period of 26 weeks.

Mechanisms

Whether liraglutide exerts direct actions on the ventricles, such as enhancement of coronary blood flow and myocardial glucose uptake, has been debated (2). The GLP-1 receptor has been demonstrated to be present on the sinoatrial node and atrial cardiomyocytes (23), but its function as well as its presence on ventricular cardiomyocytes and blood vessels in humans is still uncertain. Furthermore, it has been suggested that the cardioprotective effects of native GLP-1 as described in earlier studies may be related to actions of degradation products of GLP-1, which are not produced by GLP-1 analogs (2). We hypothesized that liraglutide may reverse diabetic cardiomyopathy, partly as a result of its indirect cardiovascular actions (5-7). However, based on our findings, at least large immediate effects on LV function in South Asian type 2 diabetes patients can be excluded.

The reductions in LV end-diastolic volume and stroke volume in our study were not explained by liraglutide-induced body weight loss. It is conceivable that the decreased end-diastolic volume and stroke volume were related to the increased heart rate and consequent reduced ventricular filling time. Notably, the elevation in heart rate in our study was relatively large compared with other trials with the same dose and of similar duration (2,5,9). Proposed mechanisms for the heart rate acceleration upon treatment with GLP-1 receptor agonists include enhancement of the sympathetic activity (24) and inhibition of the cardiac vagal neurons (25) as well as direct sinoatrial node stimulation (9). Our study population included patients with prevalent coronary artery disease. It has been suggested that individuals with preexisting cardiac disease may be more susceptible to heart rate acceleration upon GLP-1 receptor agonists (2). Furthermore, South Asians may have an altered balance in the autonomic nervous system (26), which may have contributed to the profound heart rate elevation by liraglutide treatment in our study population.

Previous studies

Only a few previous studies, including two open-label randomized controlled trials (27,28) and one small double-blind randomized controlled trial (29), assessed the effect of liraglutide on diastolic function in type 2 diabetes, during an intervention period of 4–6 months. One study demonstrated an improvement in myocardial relaxation in response to liraglutide, with amelioration of aortic stiffening (28), whereas others reported no improvement of diastolic function (27,29). Large trials on the impact of liraglutide on systolic function have been previously performed in heart failure with reduced ejection fraction, where no effect was reported (30,31). Regarding the impact of GLP-1 receptor agonists on myocardial tissue characteristics, most research has been limited to preclinical studies. In animal models of type 2 diabetes, liraglutide has been shown to reduce cardiac fibrosis (32), possibly by inhibition of the endoplasmic reticulum (ER) stress pathway via activation of the AMP-activated protein kinase (AMPK) system (33,34). Activation of AMPK, which acts as a regulator of cellular energy status, has also been proposed as the underlying mechanism for improved cardiac function

in type 2 diabetes after liraglutide, as observed in preclinical research (33). Furthermore, GLP-1 receptor agonists have been shown to relieve the intramyocardial lipid deposition in diabetic mice, in association with ameliorated levels of plasma cholesterol (35). However, attenuation of myocardial steatosis by treatment with GLP-1 receptor agonists in type 2 diabetes has not been confirmed in human studies (36).

In a recent double-blind randomized controlled trial on the effect of liraglutide on cardiac function in European type 2 diabetes patients (37), liraglutide decreased the LV filling pressure, presumably through natriuresis and vasorelaxation, whereas myocardial relaxation was unaltered. Apart from ethnicity, the present South Asian cohort was distinct from this European study group regarding sex (40% vs. 59% men), diabetes duration (18 ± 10 vs. 11 ± 7 years), insulin use (77% vs. 65%), and ischemic heart disease (17% vs. 0%). As there have been no large-scale clinical studies, it remains unknown whether certain patient characteristics have a modifying role in the cardiovascular actions of liraglutide.

Strengths and limitations

The most important strengths of the present study are related to its double-blind, randomized controlled design, the absence of dropouts, and high study drug compliance. Liraglutide was added to standard care, mimicking the real-world setting. There are some limitations that need to be addressed. This trial comprised South Asian individuals living in a high-income country and included predominantly South Asian Surinamese, who originate from the northern part of India. Extrapolation of our results to other South Asian ethnic groups should be performed with caution. Furthermore, we did not use echocardiography, which is the routine clinical approach for evaluating diastolic function. Nonetheless, MRI is widely used in clinical studies for the assessment of diastolic function and, importantly, it has been validated with echocardiography (38). It has to be noted that in individuals with high heart rate (>100 bpm), early and late diastolic filling cannot be separated. As a consequence, two participants in the liraglutide group had missing data for diastolic function at follow-up, which might have introduced bias. The LV diastolic function parameters in our study population, as well as aortic pulse wave velocity, were approximately one standard deviation from the mean in healthy individuals (39). However, in contrast to the clear impairments in LV diastolic function, the myocardial triglyceride content was 0.92–1.00% in this type 2 diabetes cohort, whereas the values in healthy controls are ~0.58% and 0.84% among Europeans and South Asians, respectively (39). The type 2 diabetes patients in the present study did not demonstrate abnormalities in myocardial extracellular volume, possibly as a result of angiotensin-converting enzyme (ACE) inhibitors, which may relieve fibrotic remodeling (39). Hence, we cannot exclude a beneficial effect of liraglutide on extracellular volume in type 2 diabetes patients with marked cardiac fibrosis. Also, we cannot preclude cardiovascular benefits after prolonged (>26 weeks) therapy with liraglutide. Nevertheless, in animal studies, improved myocardial function has been reported already after brief (1 week) treatment with liraglutide (33).

Implications

In our study, liraglutide did not enhance heart function and may therefore have no specific role in the prevention of heart failure with preserved ejection fraction in South Asian type 2 diabetes patients. In contrast, recent studies have indicated that the sodium-glucose cotransporter 2 (SGLT2) inhibitors empagliflozin, canagliflozin, and dapagliflozin have a benefit on the incidence of heart failure (4), potentially because of direct improvement of myocardial relaxation in addition to diuretic effects (40). Conversely, the previously reported reduced cardiovascular mortality rate in response to liraglutide among patients with type 2 diabetes and high cardiovascular risk is probably primarily related to slowed progression of atherosclerosis (3,41). Following the results from recent cardiovascular outcome trials (3,4), SGLT2 inhibitors have been recommended as part of type 2 diabetes management among individuals with coexisting heart failure or at risk of heart failure, and either GLP-1 receptor agonists or SGLT2 inhibitors should be considered in type 2 diabetes patients with established atherosclerotic disease and no specific concerns of heart failure (22). Our study did not demonstrate regression of LV diastolic dysfunction in response to liraglutide. Nonetheless, because of its presumed antiatherosclerotic actions, GLP-1 receptor agonists remain worth considering, especially in South Asian type 2 diabetes patients, given their disadvantageous cardiometabolic profile and high risk of ischemic heart disease (10).

CONCLUSION

In this 26-week double-blind randomized placebo-controlled trial in Dutch South Asian type 2 diabetes patients with or without coronary artery disease, liraglutide had no effect on LV diastolic and systolic function, nor on aortic stiffness, myocardial triglyceride content, or extracellular volume. A previous study reported a reduced LV filling pressure after liraglutide therapy in a European cohort of type 2 diabetes patients without ischemic heart disease, who were predominantly men, with a shorter diabetes duration, and less use of insulin as compared with the South Asian type 2 diabetes patients in the present study (37). Further research should reveal whether the cardiovascular impact of liraglutide might be dependent on patient characteristics such as sex, ethnicity, diabetes duration, comedication, or history of ischemic heart disease.

ACKNOWLEDGEMENTS

We are grateful to all participating patients. We thank all physicians and nurses from Haaglanden Medical Centre (The Hague, the Netherlands) for inviting eligible patients, P.J. van den Boogaard for the support in the MRI acquisition and B. Ladan-Eygenraam for the assistance in the clinical data collection.

FUNDING

This work was supported by the 'Cardio Vascular Imaging Group (CVIG)', Leiden University Medical Centre (Leiden, the Netherlands), Roba Metals B.V. IJsselstein (Utrecht, the Netherlands) and Novo Nordisk A/S (Bagsvaerd, Denmark), which also provided the trial medication. Novo Nordisk had no role in the trial design, data collection and analysis or reporting of results.

REFERENCES

1. Marwick TH, Ritchie R, Shaw JE, Kaye D. Implications of Underlying Mechanisms for the Recognition and Management of Diabetic Cardiomyopathy. J Am Coll Cardiol 2018;71(3):339-351.
2. Drucker DJ. The Cardiovascular Biology of Glucagon-like Peptide-1. Cell Metab 2016;24(1):15-30.
3. Marso SP, Daniels GH, Brown-Frandsen K, et al. Liraglutide and Cardiovascular Outcomes in Type 2 Diabetes. N Engl J Med 2016;375(4):311-322.
4. Zelniker TA, Wiviott SD, Raz I, et al. Comparison of the Effects of Glucagon-Like Peptide Receptor Agonists and Sodium-Glucose Cotransporter 2 Inhibitors for Prevention of Major Adverse Cardiovascular and Renal Outcomes in Type 2 Diabetes Mellitus. Circulation 2019;139(17):2022-2031.
5. Dalsgaard NB, Vilsboll T, Knop FK. Effects of glucagon-like peptide-1 receptor agonists on cardiovascular risk factors: A narrative review of head-to-head comparisons. Diabetes Obes Metab 2018;20(3):508-519.
6. Lovshin JA, Barnie A, DeAlmeida A, Logan A, Zinman B, Drucker DJ. Liraglutide promotes natriuresis but does not increase circulating levels of atrial natriuretic peptide in hypertensive subjects with type 2 diabetes. Diabetes Care 2015;38(1):132-139.
7. Koska J, Sands M, Burciu C, et al. Exenatide Protects Against Glucose- and Lipid-Induced Endothelial Dysfunction: Evidence for Direct Vasodilation Effect of GLP-1 Receptor Agonists in Humans. Diabetes 2015;64(7):2624-2635.
8. Gulsin GS, Swarbrick DJ, Hunt WH, et al. Relation of Aortic Stiffness to Left Ventricular Remodeling in Younger Adults With Type 2 Diabetes. Diabetes 2018;67(7):1395-1400.
9. Nakatani Y, Kawabe A, Matsumura M, et al. Effects of GLP-1 Receptor Agonists on Heart Rate and the Autonomic Nervous System Using Holter Electrocardiography and Power Spectrum Analysis of Heart Rate Variability. Diabetes Care 2016;39(2):e22-23.
10. Tillin T, Hughes AD, Mayet J, et al. The relationship between metabolic risk factors and incident cardiovascular disease in Europeans, South Asians, and African Caribbeans: SABRE (Southall and Brent Revisited) -- a prospective population-based study. J Am Coll Cardiol 2013;61(17):1777-1786.
11. Bakker LE, Sleddering MA, Schoones JW, Meinders AE, Jazet IM. Pathogenesis of type 2 diabetes in South Asians. Eur J Endocrinol 2013;169(5):R99-R114.
12. Banerji MA, Faridi N, Atluri R, Chaiken RL, Lebovitz HE. Body composition, visceral fat, leptin, and insulin resistance in Asian Indian men. J Clin Endocrinol Metab 1999;84(1):137-144.
13. Abate N, Chandalia M, Snell PG, Grundy SM. Adipose tissue metabolites and insulin resistance in nondiabetic Asian Indian men. J Clin Endocrinol Metab 2004;89(6):2750-2755.
14. Forouhi NG, Sattar N, McKeigue PM. Relation of C-reactive protein to body fat distribution and features of the metabolic syndrome in Europeans and South Asians. Int J Obes Relat Metab Disord 2001;25(9):1327-1331.
15. Park CM, Tillin T, March K, et al. Hyperglycemia has a greater impact on left ventricle function in South Asians than in Europeans. Diabetes Care 2014;37(4):1124-1131.
16. Brandts A, Bertini M, van Dijk EJ, et al. Left ventricular diastolic function assessment from three-dimensional three-directional velocity-encoded MRI with retrospective valve tracking. J Magn Reson Imaging 2011;33(2):312-319.
17. Grotenhuis HB, Westenberg JJ, Steendijk P, et al. Validation and reproducibility of aortic pulse wave velocity as assessed with velocity-encoded MRI. J Magn Reson Imaging 2009;30(3):521-526.
18. van der Meer RW, Doornbos J, Kozerke S, et al. Metabolic imaging of myocardial triglyceride content: reproducibility of 1H MR spectroscopy with respiratory navigator gating in volunteers. Radiology 2007;245(1):251-257.
19. Diao KY, Yang ZG, Xu HY, et al. Histologic validation of myocardial fibrosis measured by T1 mapping: a systematic review and meta-analysis. J Cardiovasc Magn Reson 2016;18(1):92.
20. van Eyk HJ, Paiman EHM, Bizino MB, et al. A double-blind, placebo-controlled, randomised trial to assess the effect of liraglutide on ectopic fat accumulation in South Asian type 2 diabetes patients. Cardiovasc Diabetol 2019;18(1):87.
21. American Diabetes A. 6. Glycemic Targets: Standards of Medical Care in Diabetes-2019. Diabetes Care 2019;42(Suppl 1):S61-S70.
22. American Diabetes A. 10. Cardiovascular Disease and Risk Management: Standards of

Medical Care in Diabetes-2019. Diabetes Care 2019;42(Suppl 1):S103-S123.
23. Baggio LL, Yusta B, Mulvihill EE, et al. GLP-1 Receptor Expression Within the Human Heart. Endocrinology 2018;159(4):1570-1584.
24. Yamamoto H, Lee CE, Marcus JN, et al. Glucagon-like peptide-1 receptor stimulation increases blood pressure and heart rate and activates autonomic regulatory neurons. J Clin Invest 2002;110(1):43-52.
25. Griffioen KJ, Wan R, Okun E, et al. GLP-1 receptor stimulation depresses heart rate variability and inhibits neurotransmission to cardiac vagal neurons. Cardiovasc Res 2011;89(1):72-78.
26. Bathula R, Francis DP, Hughes A, Chaturvedi N. Ethnic differences in heart rate: can these be explained by conventional cardiovascular risk factors? Clin Auton Res 2008;18(2):90-95.
27. Nystrom T, Padro Santos I, Hedberg F, et al. Effects on Subclinical Heart Failure in Type 2 Diabetic Subjects on Liraglutide Treatment vs. Glimepiride Both in Combination with Metformin: A Randomized Open Parallel-Group Study. Front Endocrinol (Lausanne) 2017;8:325.
28. Lambadiari V, Pavlidis G, Kousathana F, et al. Effects of 6-month treatment with the glucagon like peptide-1 analogue liraglutide on arterial stiffness, left ventricular myocardial deformation and oxidative stress in subjects with newly diagnosed type 2 diabetes. Cardiovasc Diabetol 2018;17(1):8.
29. Jorgensen PG, Jensen MT, Mensberg P, et al. Effect of exercise combined with glucagon-like peptide-1 receptor agonist treatment on cardiac function: A randomized double-blind placebo-controlled clinical trial. Diabetes Obes Metab 2017;19(7):1040-1044.
30. Jorsal A, Kistorp C, Holmager P, et al. Effect of liraglutide, a glucagon-like peptide-1 analogue, on left ventricular function in stable chronic heart failure patients with and without diabetes (LIVE)-a multicentre, double-blind, randomised, placebo-controlled trial. Eur J Heart Fail 2017;19(1):69-77.
31. Margulies KB, Hernandez AF, Redfield MM, et al. Effects of Liraglutide on Clinical Stability Among Patients With Advanced Heart Failure and Reduced Ejection Fraction: A Randomized Clinical Trial. JAMA 2016;316(5):500-508.
32. Zhao T, Chen H, Xu F, et al. Liraglutide alleviates cardiac fibrosis through inhibiting P4halpha-1 expression in STZ-induced diabetic cardiomyopathy. Acta Biochim Biophys Sin (Shanghai) 2019;51(3):293-300.
33. Noyan-Ashraf MH, Shikatani EA, Schuiki I, et al. A glucagon-like peptide-1 analog reverses the molecular pathology and cardiac dysfunction of a mouse model of obesity. Circulation 2013;127(1):74-85.
34. Ji Y, Zhao Z, Cai T, Yang P, Cheng M. Liraglutide alleviates diabetic cardiomyopathy by blocking CHOP-triggered apoptosis via the inhibition of the IRE-alpha pathway. Mol Med Rep 2014;9(4):1254-1258.
35. Monji A, Mitsui T, Bando YK, Aoyama M, Shigeta T, Murohara T. Glucagon-like peptide-1 receptor activation reverses cardiac remodeling via normalizing cardiac steatosis and oxidative stress in type 2 diabetes. Am J Physiol Heart Circ Physiol 2013;305(3):H295-304.
36. Dutour A, Abdesselam I, Ancel P, et al. Exenatide decreases liver fat content and epicardial adipose tissue in patients with obesity and type 2 diabetes: a prospective randomized clinical trial using magnetic resonance imaging and spectroscopy. Diabetes Obes Metab 2016;18(9):882-891.
37. Bizino MB, Jazet IM, Westenberg JJM, et al. Effect of liraglutide on cardiac function in patients with type 2 diabetes mellitus: randomized placebo-controlled trial. Cardiovasc Diabetol 2019;18(1):55.
38. Buss SJ, Krautz B, Schnackenburg B, et al. Classification of diastolic function with phase-contrast cardiac magnetic resonance imaging: validation with echocardiography and age-related reference values. Clin Res Cardiol 2014;103(6):441-450.
39. Paiman EHM, van Eyk HJ, Bizino MB, et al. Phenotyping diabetic cardiomyopathy in Europeans and South Asians. Cardiovasc Diabetol 2019;18(1):133.
40. Pabel S, Wagner S, Bollenberg H, et al. Empagliflozin directly improves diastolic function in human heart failure. Eur J Heart Fail 2018;20(12):1690-1700.
41. Rakipovski G, Rolin B, Nohr J, et al. The GLP-1 Analogs Liraglutide and Semaglutide Reduce Atherosclerosis in ApoE(-/-) and LDLr(-/-) Mice by a Mechanism That Includes Inflammatory Pathways. JACC Basic Transl Sci 2018;3(6):844-857. mized clinical trial using magnetic resonance imaging and spectroscopy. Diabetes Obes Metab 2016;18(9):882-891.

SUPPLEMENTARY MATERIAL

MRI acquisition and analysis

LV systolic and diastolic function

MRI scans were acquired on a 3 Tesla magnetic resonance scanner (Ingenia, Philips Healthcare, Best, the Netherlands), using a dStream Torso anterior coil and a FlexCoverage posterior coil in the table top, resulting in up to 32 coil elements for signal reception. LV dimensions and systolic and diastolic function were quantified by standard short-axis and 4-chamber long-axis cine balanced steady-state free precession (bSSFP) and free-breathing whole-heart gradient-echo 4D velocity-encoded MR, with retrospective electrocardiography (ECG) gating. Typical imaging parameters of the bSSFP cines were: echo/repetition time (TE/TR) 1.5/3.0 ms, flip angle (FA) 45°, field-of-view (FOV) 350x350 mm^2 (4-chamber) and 400x352 mm^2 (short-axis), acquired voxel size 2.0x1.6 mm^2 (4-chamber) and 1.5x1.5 mm^2 (short-axis), slice thickness 8 mm, number of phases 30 (4-chamber) and 35 (short-axis). For short-axis bSSFP cine, the complete LV was imaged using 14-16 slices. 4D velocity-encoded (venc 150 cm/s) MR was acquired in parallel with the 4-chamber view, with typical imaging parameters: TE/TR 4.6/9.0 ms, FA 10°, FOV 360x360 mm^2, acquired voxel size 3.0x3.0 mm^2, slice thickness 3 mm, number of slices 41, number of phases 30, sensitivity encoding (SENSE) factor 2.

LV function and dimensions were assessed with MASS version 2015-EXP (Leiden University Medical Center, Leiden, the Netherlands). For LV diastolic function, the flow rate curves over the mitral valve were derived from the 4D velocity-encoded scans by retrospective mitral valve tracking, perpendicular to the streamlines of inflow across the mitral valve, at the location of peak flow velocity (1,2). Subsequently, the ratio of the transmitral early (E) and late (A) peak filling rate (E/A ratio), the peak deceleration slope of the E wave (Edec) and the transmitral early peak velocity were calculated. The transmitral filling rate curves were corrected for the through-plane background velocity of the LV myocardial wall. The early peak diastolic mitral septal tissue velocity (Ea) was measured on 4-chamber cines. The mitral septal tissue velocity curves were calculated from the displacement of the semi-automatically tracked mitral valve, at the insertion to the LV septum, relative to the LV apex, throughout the cardiac cycle. The estimated LV filling pressure was defined as the ratio of the transmitral early peak velocity and Ea (3). For LV dimensions and systolic function, LV endocardial and epicardial contours were semi-automatically drawn in the short-axis cines in the end-diastolic and end-systolic phase, to quantify the end-diastolic LV mass, LV end-diastolic and end-systolic volumes and subsequently LV stroke volume, ejection fraction, cardiac output and cardiac index. The peak ejection rate was derived from the systolic flow rate curves over the aortic valve after retrospective valve tracking (4).

Aortic stiffness

For aortic PWV a double-oblique sagittal scout view of the aorta and free-breathing through-plane 2D velocity-encoded MR scans were obtained (one transecting the proximal ascending aorta, with venc 200 cm/s, and one transecting the abdominal aorta above the bifurcation, with venc 150 cm/s). Typical imaging parameters were: TE/TR 2.5/4.4 ms, FA 20°, FOV 350x282 mm^2, slice thickness 8 mm, acquired voxel size 2.8x2.8 mm^2, temporal resolution 10 ms. Aortic PWV analyses were performed as previously described, using MASS version 2015-EXP (Leiden University Medical Center, Leiden, the Netherlands) and custom-made software for further analysis of the aorta velocity-time curves (5). Aortic PWV was calculated by dividing the distance between ascending and abdominal aorta by the transit time of the onset of the systolic wave front.

Myocardial tissue characteristics

Myocardial triglyceride content was measured by proton-magnetic resonance spectroscopy (^{1}H-MRS), in a voxel of 40x15x25 mm^3 in the mid-ventricular septum, with ECG-triggering, using a respiratory navigator. Typical parameters were: TE 35 ms, TR 3.5 or 9 seconds (water-suppressed and non-water suppressed acquisition, respectively), acquired samples 2048 (spectral resolution 0.73 Hz/sample), number of signal averages 64 or 6 (water-suppressed and non-water suppressed acquisition, respectively). The signal-to-noise ratio was increased by a high permittivity pad on the thorax (6). The myocardial triglyceride content was quantified using in-house developed software to assess the individual 64 water-suppressed and 6 non-water suppressed signals and the Java-based MR user interface (jMRUI v5.0; MRUI Consortium) to fit the averaged signal (7,8). Prior knowledge for the fit included the following starting values: triglyceride methyl (CH_3) 0.9 ppm, triglyceride methylene $(CH_2)^n$ 1.3 ppm, COO-CH_2 2.05 ppm, creatine 3.05 ppm, trimethylamines (TMA) 3.25 ppm. Myocardial lipid-to-water ratios were calculated as the signal of triglyceride methylene divided by the unsuppressed water signal, multiplied by 100% (9).

The extracellular volume (ECV) as a measure of myocardial diffuse fibrosis was determined using native and post-contrast T1 mapping (5s(3s)3s and 4s(1s)3s(1s)2s modified Look-Locker inversion recovery (MOLLI) scheme, respectively), obtained in short-axis orientation at the mid-ventricular level. Post-contrast T1 mapping was acquired 20-25 minutes after contrast administration. Typical imaging parameters were: TE/TR 1.1/2.3 ms, FA 20°, FOV 350x300 mm^2, slice thickness 8 mm, acquired voxel size 2.1x2.1 mm^2, SENSE factor 2. ECV and T1 relaxation times were obtained using Medis Suite 3.0 Qmap 2.2.18 (Medis medical imaging systems, Leiden, the Netherlands), in the mid-ventricular septum, after manual correction for motion of the T1 images.

Late gadolinium enhanced (LGE) MRI was acquired 15-20 minutes after contrast administration, with an ECG-triggered 3D whole-heart gradient-echo phase-sensitive inversion recovery sequence, with respiratory navigating, as previously described (10). LGE MRI was assessed visually by an experienced radiologist and a clinical investigator.

Power calculation

The power calculation for LV diastolic and systolic function, based on previous data on MRI-derived LV function in type 2 diabetes (11), showed that a total of 25 patients in each group would be needed to detect a change upon liraglutide of approximately 15-20% and 10-20% in diastolic and systolic function parameters, respectively, with at least 90% power (α=0.05) and estimated drop-out rate of 10%. Post-hoc power calculation for the secondary endpoints demonstrated a power of at least 90% (α=0.05) to detect an absolute change upon liraglutide of 0.40% in myocardial triglyceride content, 2.5% in ECV and 2.5 m/s in aortic PWV.

Missing data

At baseline, the number of missing values in the liraglutide group was: n=1 for LV diastolic function, and in the placebo group: n=1 for LV diastolic function and myocardial tissue characteristics. For the assessment of the difference between baseline and follow-up, the number of missing values in the liraglutide group was: n=3 for E, A, E/A ratio, Ea and LV filling pressure (n=1 excluded because of mitral valve stenosis, n=2 missing due to a heart rate of ≥100 bpm with fusion of the E/A peak at follow-up), n=4 for Edec peak (n=1 missing due to a heart rate of 96 bpm with partial fusion of the E/A peak at follow-up), n=1 for myocardial triglyceride content (excluded due to insufficient quality), and in the placebo group: n=1 for LV diastolic function (excluded because of mitral valve stenosis) and peak ejection rate (missing due to imaging time constraints), n=1 for myocardial triglyceride content (excluded due to ischemic scarring of the septum) and native T1 (excluded due to insufficient quality), n=2 for post-contrast T1 and extracellular volume (missing due to imaging time constraints). In both the liraglutide and placebo group n=1 was missing for study drug compliance.

REFERENCES

1. Westenberg JJ, Roes SD, Ajmone Marsan N, et al. Mitral valve and tricuspid valve blood flow: accurate quantification with 3D velocity-encoded MR imaging with retrospective valve tracking. Radiology 2008;249(3):792-800.
2. Brandts A, Bertini M, van Dijk EJ, et al. Left ventricular diastolic function assessment from three-dimensional three-directional velocity-encoded MRI with retrospective valve tracking. J Magn Reson Imaging 2011;33(2):312-319.
3. Paelinck BP, de Roos A, Bax JJ, et al. Feasibility of tissue magnetic resonance imaging: a pilot study in comparison with tissue Doppler imaging and invasive measurement. J Am Coll Cardiol 2005;45(7):1109-1116.
4. Roes SD, Hammer S, van der Geest RJ, et al. Flow assessment through four heart valves simultaneously using 3-dimensional 3-directional velocity-encoded magnetic resonance imaging with retrospective valve tracking in healthy volunteers and patients with valvular regurgitation. Invest Radiol 2009;44(10):669-675.
5. Grotenhuis HB, Westenberg JJ, Steendijk P, et al. Validation and reproducibility of aortic pulse wave velocity as assessed with velocity-encoded MRI. J Magn Reson Imaging 2009;30(3):521-526.
6. de Heer PM, Bizino MBMD, Versluis MJP, Webb AGP, Lamb HJMDP. Improved Cardiac Proton Magnetic Resonance Spectroscopy at 3 T Using High Permittivity Pads. Investigative Radiology 2016;51(2):134-138.
7. Naressi A, Couturier C, Devos JM, et al. Java-based graphical user interface for the MRUI quantitation package. MAGMA 2001;12(2-3):141-152.
8. Naressi A, Couturier C, Castang I, de Beer R, Graveron-Demilly D. Java-based graphical user interface for MRUI, a software package for quantitation of in vivo/medical magnetic resonance spectroscopy signals. Comput Biol Med 2001;31(4):269-286.
9. Rial B, Robson MD, Neubauer S, Schneider JE. Rapid quantification of myocardial lipid content in humans using single breath-hold 1H MRS at 3 Tesla. Magn Reson Med 2011;66(3):619-624.
10. Bizino MB, Tao Q, Amersfoort J, et al. High spatial resolution free-breathing 3D late gadolinium enhancement cardiac magnetic resonance imaging in ischaemic and non-ischaemic cardiomyopathy: quantitative assessment of scar mass and image quality. Eur Radiol 2018;28(9):4027-4035.
11. van der Meer RW, Rijzewijk LJ, de Jong HW, et al. Pioglitazone improves cardiac function and alters myocardial substrate metabolism without affecting cardiac triglyceride accumulation and high-energy phosphate metabolism in patients with well-controlled type 2 diabetes mellitus. Circulation 2009;119(15):2069-2077.

CHAPTER

Late effects of pediatric hematopoietic stem cell transplantation on left ventricular function, aortic stiffness and myocardial tissue characteristics

Paiman EHM, Louwerens M, Bresters D, Westenberg JJM, Tao Q, van der Geest RJ, Lankester AC, Roest AAW,* Lamb HJ*

* shared last author

J Cardiovasc Magn Reson. 2019 Jan 17;21(1):6. doi: 10.1186/s12968-018-0513-4

ABSTRACT

Background

Pediatric hematopoietic stem cell transplantation (HSCT) recipients are at increased risk of cardiovascular disease later in life. As HSCT survival has significantly improved, with a growing number of HSCT indications, tailored screening strategies for HSCT-related late effects are warranted. Little is known regarding the value of cardiovascular magnetic resonance (CMR) for early identification of high-risk patients after HSCT, before symptomatic cardiovascular disease manifests. This study aimed to assess CMR-derived left ventricular (LV) systolic and diastolic function, aortic stiffness and myocardial tissue characteristics in young adults who received HSCT during childhood.

Methods

A total of 16 patients (age 22.1±1.5 years), who were treated with HSCT during childhood, and 16 healthy controls (age 22.1±1.8 years) underwent 3T CMR. LV systolic and diastolic function were measured as LV ejection fraction (LVEF), the ratio of transmitral early and late peak filling rate (E/A), the estimated LV filling pressure (E/Ea) and global longitudinal and circumferential systolic strain and diastolic strain rates, using balanced steady-state free precession cine MR and 2D velocity-encoded MR over the mitral valve. Aortic stiffness, myocardial fibrosis and steatosis were assessed with 2D velocity-encoded MR, native T1 mapping and proton magnetic resonance spectroscopy (^{1}H-MRS), respectively.

Results

In the patient compared to the control group, E/Ea (9.92±3.42 vs. 7.24±2.29, ***P***=0.004) was higher, LVEF (54±6% vs. 58±5%, ***P***=0.055) and global longitudinal strain (GLS) (-20.7±3.5% vs. -22.9±3.0%, ***P***=0.063) tended to be lower, while aortic pulse wave velocity (4.40±0.26 vs. 4.29±0.29 m/s, ***P***=0.288), native T1 (1211±36 vs. 1227±28 ms, ***P***=0.158) and myocardial triglyceride content (0.47±0.18 vs. 0.50±0.13%, ***P***=0.202) were comparable. There were no differences between patients and controls in E/A (2.76±0.92 vs. 2.97±0.91, ***P***=0.599) and diastolic strain rates.

Conclusion

In young adults who received HSCT during childhood, LV diastolic function was decreased (higher estimated LV filling pressure) and LV systolic function (LVEF and GLS) tended to be reduced as compared to healthy controls, whereas no concomitant differences were found in aortic stiffness and myocardial tissue characteristics. When using CMR, assessment of LV diastolic function in particular is important for early detection of patients at risk of HSCT-related cardiovascular disease, which may warrant closer surveillance.

INTRODUCTION

Hematopoietic stem cell transplantation (HSCT) recipients are exposed to several pre-transplant and/or HSCT-related therapies which may increase the risk of cardiovascular disease (1,2). As HSCT survival has significantly improved over the last decades (3,4), with an increasing number of HSCT indications for both malignant and non-malignant disease (5), targeted follow-up strategies for the HSCT population are needed (6). Recently, several international working groups have been established aimed at a greater understanding of the late effects including arterial disease and cardiac dysfunction (7,8). Most of the available studies on late effects involve HSCT in adults. Adequate screening in young HSCT recipients is even more challenging (9).

According to current guidelines (10), pediatric HSCT recipients who have an increased susceptibility to complications later in life, based on pre-existing comorbidities, pre-transplant exposures, the HSCT preparative regimen, post-transplant complications such as graft-versus-host-disease, or relapse of the primary disease, are selected for patient-specific follow-up programs. Identification of imaging markers which indicate subclinical disease would be supportive in the detection of high-risk patient groups for closer monitoring or targeted therapy (6). In general, clinical follow-up after cardiotoxic exposures comprises echocardiography for left ventricular (LV) systolic and diastolic function. Less is known regarding the value of cardiovascular magnetic resonance (CMR) for screening of late effects (11). CMR may be suited for comprehensive evaluation of subclinical deteriorations within the cardiovascular system after HSCT, that may be present before overt LV functional abnormalities arise.

Pre-transplant or HSCT-related cardiotoxic exposures may cause endothelial damage leading to increased aortic stiffness and myocyte cell death with reactive interstitial fibrosis (1,2). In addition, the immunosuppressive therapies in allogeneic HSCT increase the susceptibility to developing the metabolic syndrome at young age (12). Aortic stiffening is known to occur in relation to normal, physiological ageing (13), but will be more progressive in response to hypertension, dyslipidemia or hyperglycemia (14) and possibly due to iron overload (15). Increased aortic stiffness induces LV concentric remodeling and is recognized as an independent predictor for cardiovascular events (16). Myocardial diffuse fibrosis in different types of cardiomyopathies is considered to reflect subclinical disease before cardiac dysfunction becomes manifest (17). The metabolic derangements among allogeneic HSCT recipients may predispose to myocardial steatosis. In individuals with the metabolic syndrome, myocardial steatosis has been associated with LV remodeling (18).

We hypothesize that, when using CMR, subclinical deteriorations in LV function, aortic stiffness and/or myocardial tissue characteristics can be detected in young adults who received HSCT during childhood. Therefore, CMR may be suitable for early identification of patients at increased risk of developing HSCT-related cardiovascular disease. Accordingly, the aim of this study is to assess CMR-derived LV systolic and diastolic function, aortic stiffness and myocardial

fibrosis and steatosis in young adults who have received pediatric HSCT and to compare these measures with those in healthy controls in the same age range.

METHODS

Study population

The patient group consisted of young adults (age range 18 to 25 years old), who received HSCT for malignant or non-malignant disease during childhood. Patients were recruited from the outpatient clinic for screening and treatment of late effects of childhood cancer and/or HSCT of the Internal Medicine Department (Leiden University Medical Centre, the Netherlands). Healthy controls were recruited by local advertising in Leiden University, the Netherlands. The control group was in the same age range as the patients and was sex-matched. Laboratory measures in the patient group were performed based on clinical indication and were typically measured within one year prior or after CMR examination. No blood samples were drawn in the healthy control group.

CMR acquisition

The study participants underwent 3T CMR (Ingenia, Philips Healthcare, Best, the Netherlands), with a dStream Torso anterior coil and a FlexCoverage posterior coil in the table top, resulting in up to 32 coil elements for signal reception. The protocol consisted of standard electrocardiographic (ECG)-triggered two-, three- and four-chamber and short-axis cine balanced steady-state free precession (bSSFP) MR and ECG-gated gradient-echo 2D velocity-encoded MR over the mitral valve to quantify LV structure, systolic and diastolic function; 2D velocity-encoded MR transecting the aortic arch and abdominal aorta to derive aortic stiffness; cardiac native T1 mapping to assess diffuse fibrosis and ^{1}H-MRS to measure the myocardial triglyceride content. For standardization of the measurement of myocardial triglyceride content, all participants were asked to fast for 6 hours and the CMR examinations were scheduled at fixed times (evenings). No MR contrast material was used.

For the bSSFP cines, typical field-of-view (FOV) was 350x350 mm^2 (long-axis) and 400x352 mm^2 (short-axis), acquired voxel size 2.0x1.6 mm^2 (long-axis) and 1.5x1.5 mm^2 (short-axis), slice thickness 8 mm, echo/repetition time (TE/TR) 1.5/3.0 ms, flip angle 45°, number of phases 30 (long-aixs) and 35 (short-axis). For short-axis bSSFP cine, the complete LV was imaged, using 14-16 slices, depending on the size of the LV, with 2 slices per breath-hold. Free-breathing through-plane 2D velocity-encoded (venc 100 cm/s) MR was acquired perpendicular to the mitral valve, with FOV 350x350 mm^2, acquired voxel size: 2.5x2.5mm^2, slice thickness 8 mm, flip angle 10°, TE/TR 2.9/4.6 ms, number of phases 40.

Aortic pulse wave velocity (PWV) was quantified as a measure of aortic stiffness. For aortic PWV, first, a double-oblique sagittal scout view of the aorta was obtained. Then, two free-

breathing through-plane 2D velocity-encoded MR scans were acquired, one transecting the ascending aorta (venc 150 cm/s) and one transecting the abdominal aorta, above the aortic bifurcation (venc 100 cm/s). Typical imaging parameters were: FOV 350x282 mm^2, slice thickness 8 mm, acquired voxel 2.8x2.8 mm^2, flip angle 20°, TE/TR 2.5/4.4 ms, temporal resolution 10 ms.

Native T1 mapping was acquired in the mid-ventricular short-axis slice, with breath-holding, using the 5s(3s)3s modified Look-Locker inversion recovery (MOLLI) scheme. Typical imaging parameters were: FOV 350x300 mm^2, slice thickness 8 mm, acquired voxel size: 2.1x2.1 mm^2, flip angle 20°, TE/TR 1.1/2.3 ms, SENSitivity Encoding (SENSE) factor 2. ^{1}H-MRS was performed as described previously (19). In summary, a voxel of 40x15x25 mm^3 was placed in the interventricular septum. For the acquisition with and without water suppression, 48 and 6 signal averages were obtained, respectively. ECG-triggering was used to acquire ^{1}H-MRS at 200 ms after the R-wave, and a respiratory navigator, tracking the lung-liver interface, for acquisition at end-expiration. A high permittivity pad was placed on the chest for improved signal-to-noise ratio.

Image analysis

MR data were analyzed using MASS Research Software V2016-EXP (Leiden University Medical Center, the Netherlands) for LV structure and function and aortic PWV, custom-made software for further analysis of the aorta velocity-time curves (20), Medis Suite 3.0 (Medis medical imaging systems, Leiden, the Netherlands) for LV systolic and diastolic strain (QStrain 2.0) and native T1 (QMap 2.2.18), and the Java-based magnetic resonance user interface (jMRUI v5.0; MRUI Consortium) for ^{1}H-MRS. The image analysis was blinded to patient or healthy control status.

For LV mass and volumes, the endocardial and epicardial LV borders were manually outlined in the end-diastolic and end-systolic phase, with exclusion of the LV papillary muscles. For the feature tracking based strain calculations, the manually annotated endocardial LV borders were automatically tracked throughout the cardiac cycle. Global longitudinal strain (GLS), and longitudinal peak systolic strain rate (GLSR-S) and early peak diastolic strain rate (GLSR-E) were calculated based on the two-, three- and four-chamber cine images. Global circumferential strain (GCS) and circumferential peak systolic strain rate (GCSR-S) and early peak diastolic strain rate (GCSR-E) were extracted from the mid-ventricular short-axis cine slice (**Figure 1**). The ratio of the transmitral early and late peak filling rate (E/A ratio) and the transmitral early peak maximum velocity were derived from the 2D velocity-encoded scans (**Figure 1**), as described previously (21). The transmitral filling rate was measured after correction for the through-plane background velocity of the LV myocardial wall. Furthermore, the early diastolic mitral septal tissue velocity (Ea) was extracted from the four-chamber cine images. Subsequently, the estimated LV filling pressure (ratio of transmitral early peak maximum velocity without through-plane myocardial motion correction and early diastolic mitral septal tissue velocity) was calculated (E/Ea ratio).

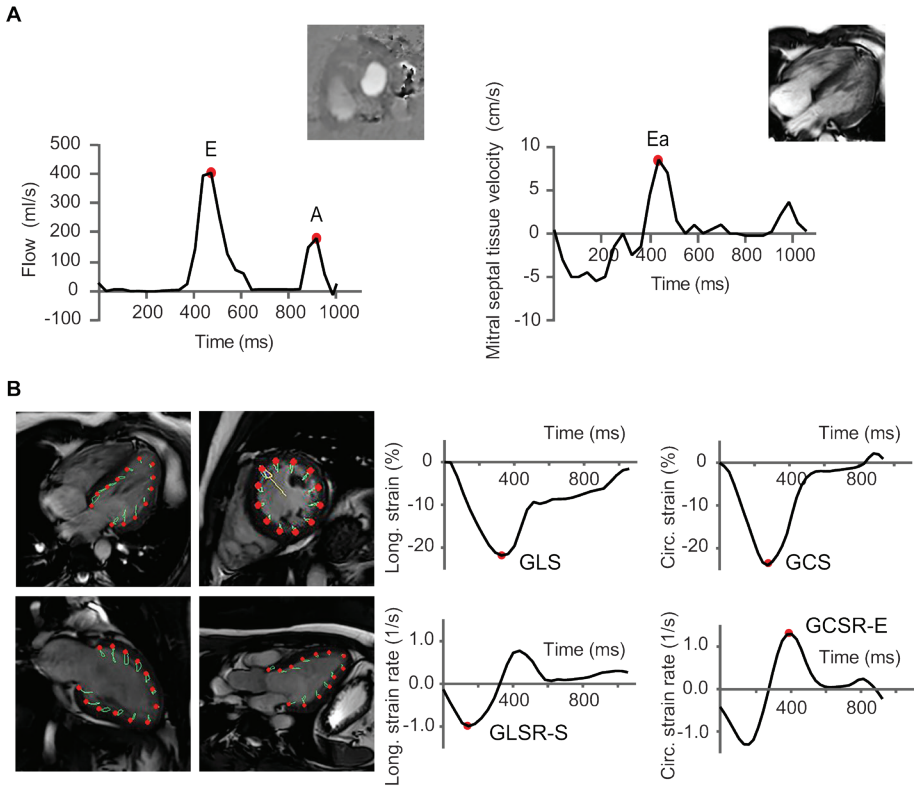

Figure 1. Example of a 22-year-old man, who was transplanted for a non-malignant bone marrow failure disorder at the age of 8 years. (**A**) the E/A ratio (early peak filling rate/late peak filling rate) was measured using 2D velocity-encoded MR (***left panel***) and the early peak diastolic mitral septal tissue velocity (Ea) was derived from the 4 chamber long-axis relaxation ***(right panel)***. LV filling pressure was estimated by the ratio of the transmitral early peak maximum velocity and the early peak diastolic mitral septal tissue velocity. (**B**) From two, three- and four-chamber and mid-ventricular short-axis cine CMR (***left panel***), the longitudinal and circumferential strain and strain rate curves were extracted (***right panel***). The myocardial features at the endocardial borders (red dots), which were automatically tracked throughout the cardiac cycle (green lines), were manually annotated in the end-diastolic and end-systolic phase. GLS: global longitudinal strain; GCS: global circumferential strain; GLSR-S: global longitudinal peak systolic strain rate; GCSR-E: global circumferential early peak diastolic strain rate.

Aortic PWV was calculated by dividing the distance between ascending and abdominal aorta by the transit time of the onset of the systolic velocity wave front (**Figure 2**), as described previously (20). In short, the aortic path length was measured manually along the aortic centerline on the double-oblique sagittal aorta scout scan. The onset of the systolic wave front was automatically determined from the resulting velocity graph by the intersection point of the constant horizontal diastolic velocity and upslope of the systolic wave front, modeled by linear regression (using the velocity values between 20% and 80% of the total range) along

the upslope. T1 maps were constructed after manual in-plane motion correction of the T1 images, using a pixel-wise, mono-exponential three-parameter fit for the T1 relaxation curve. For the measurement of native T1, a region-of-interest in the mid-ventricular septum was drawn (**Figure 2**). Myocardial triglyceride content was expressed as the percentage of triglyceride methyl (at 0.9 ppm) and triglyceride methylene (at 1.3 ppm) relative to the sum of the triglyceride signal and the unsuppressed water signal (at 4.7 ppm) (**Figure 2**) (22).

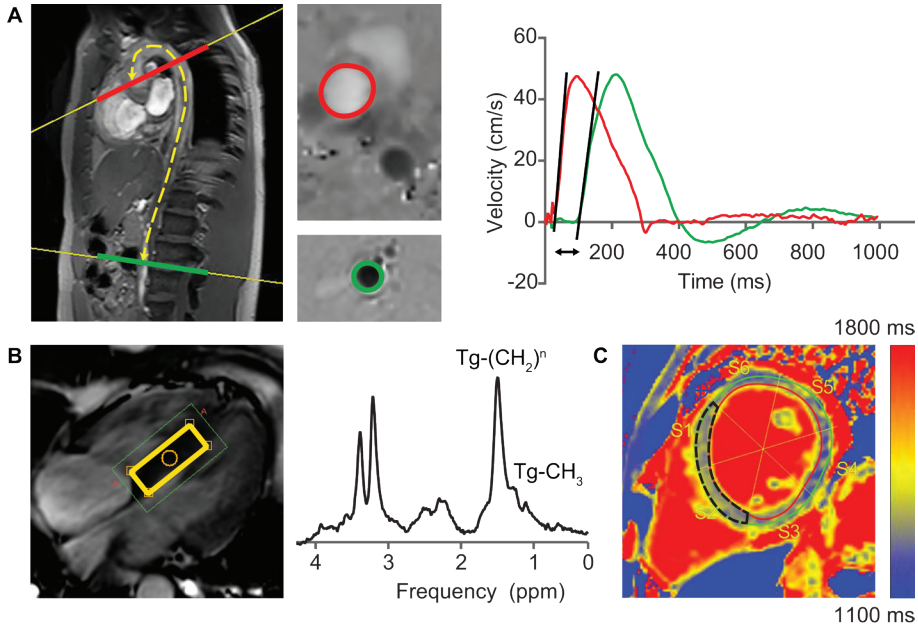

Figure 2. The same patient as in Figure 1 is presented. (**A**) Aortic pulse wave velocity was calculated from through-plane 2D velocity-encoded MR transecting the ascending aorta (red) and the abdominal aorta, above the aortic bifurcation (green) (***left panel***), according to: aortic pulse wave velocity = $\Delta x/\Delta t$, with Δx: the distance between the ascending and abdominal aorta (yellow dotted line) and Δt: transit time of the onset of the systolic velocity wave front (black arrow) (***right panel***). (**B**) Proton-magnetic resonance spectroscopy (^{1}H-MRS) was used to measure the myocardial triglyceride content. The voxel of interest was placed in the mid-ventricular septum (yellow box) (***left panel***). Myocardial triglyceride content was calculated as Tg-$(CH_2)^n$ and Tg-CH_3 relative to the sum of the triglyceride and the unsuppressed water signal (not shown). Triglycerides were measured using the water-suppressed spectrum (***right panel***). (**C**) Native T1 was measured in the mid-ventricular septal segments in short-axis view (black, dotted region of interest).

Statistics

Statistical analyses were performed in SPSS 23 (IBM Corp, New York, United States). Normal distribution was checked using the Shapiro-Wilk test. Differences between groups were tested for statistical significance using the Student's t-test or the Mann-Whitney U test for normally and non-normally distributed variables, respectively. Patients with prior HSCT vs. controls were compared and additional analyses were performed for patients with HSCT for malignancies vs. controls. Levels for statistical significance were set at $P<0.05$ and all tests were two-sided. Additionally, we performed a post-hoc power analysis (alfa 0.05, two-sided).

RESULTS

In total, sixteen patients (22.1 ± 1.5 years, 11/16 (69%) men) and sixteen healthy controls (22.1 ± 1.8 years, 11/16 (69%) men) were included and analyzed. In one patient, ^{1}H-MRS data were not analyzed due to insufficient quality. Also, in one patient 2D velocity-encoded MR over the mitral valve was not acquired due to imaging time constraints. Height and body surface area (BSA) in the patient group were lower compared to the healthy control group. The anthropometric characteristics are presented in **Table 1**.

Table 1. Demographic and anthropometric characteristics

	Pediatric HSCT recipients (n=16)	**Healthy controls (n=16)**	***P* value**
Men, n (%)	11 (69%)	11 (69%)	1.000
Age, y	22.1 ± 1.5	22.1 ± 1.8	1.000
Length, cm	173 ± 7	179 ± 8	0.017*
Weight, kg	66.6 ± 10.9	72.1 ± 6.9	0.095
Body mass index (BMI), kg/m^2	22.4 ± 3.6	22.5 ± 2.7	0.929
Body surface area (BSA), m^2	1.78 ± 0.16	1.89 ± 0.11	0.029*

Values are presented as numbers (percentages) or means ± standard deviations. *$P<0.05$. BSA based on the Mosteller formula.

In ten patients, HSCT was indicated for a malignant disorder. Seven patients were treated with anthracyclines prior to HSCT, eight received total body irradiation (typically unfractionated 7.5 Gy or 2x6 Gy) and fourteen were given high-dose cyclophosphamide (>1 g/m^2) for HSCT conditioning. Five patients had a ferritin level above 250 µmol/L. In two of them, cardiac T2* was assessed upon clinical indication. In both, the T2* values were not suggestive of myocardial iron deposition. Clinical and biochemical patients characteristics are presented in **Table 2 and 3**.

Table 2. Clinical patient characteristics

	Pediatric HSCT recipients (n=16)
Transplant-related characteristics	
Age at time of HSCT, years	7.2 ± 5.3
Time after HSCT, years	14.8 ± 5.0
Malignant disorder, n (%)	10 (62.5%)
ALL or AML	8
MDS or CML	2
Non-malignant disorder, n (%)	6 (37.5%)
Hematological disease	4
Other	2
Anthracycline therapy, n (%)	7 (43.8%)
< 300 mg/m^2	5
≥ 300 mg/m^2	2
Radiotherapy, n (%)	8 (50.0%)
Total body irradiation	7
Chest irradiation	1
Cyclophosphamide therapy, n (%)	14 (87.6%)
< 1 g/m^2	1
≥ 1 g/m^2	13
Allogeneic HSCT, n (%)	15 (94%)
HLA-identical sibling	6
Other related or unrelated donor	9
Graft versus host disease, n (%)	5 (31.3%)
Acute	2
Chronic	3
Clinical parameters	
Systolic blood pressure, mmHg	121 ± 12
Diastolic blood pressure, mmHg	76 ± 9
Pulse, beats per minute	75 ± 12

Values are presented as numbers (percentages) or means ± standard deviations. HSCT: hematopoietic stem cell transplantation, ALL: acute lymphatic leukemia, AML: acute myeloid leukemia, MDS: myelodysplastic syndrome, CML: chronic myeloid leukemia.

Table 3. Biochemical patient characteristics

	Pediatric HSCT recipients (n=16)	Normal values
Fasting glucose, mmol/L	5.1 ± 0.8	3.1-6.4
Total cholesterol, mmol/L	4.90 ± 1.20	3.90-7.30
HDL-cholesterol, mmol/L	1.30 ± 0.32	0.80-2.30
LDL-cholesterol, mmol/L	2.69 ± 0.87	0.00-3.37
Triglycerides, mmol/L	1.87 ± 1.29	0.80-2.30
Alanine aminotransferase (ALT), U/L	Men: 32 ± 17	0-45
	Women: 15 ± 4	0-34
Aspartate aminotransferase (AST), U/L	Men: 31 ± 16	0-35
	Women: 21 ± 2	0-31
Gamma-glutamyl transpeptidase (GGT), U/L	Men: 40 ± 24	0-55
	Women: 19 ±10	0-38
Free thyroxin (FT4), pmol/L	15.9 ± 2.6	12.0-22.0
Thyroid-stimulating hormone (TSH), mU/L	2.695 ± 1.472	0.300-4.800
eGFR (CKD-EPI) > 60 mL/min/1.73m^2, n (%)	16 (100%)	NA
Ferritin, µmol/L	Men: 187, 183 (61, 910)	35-260
	Women: 31, 437 (8, 792)	10-150
Ferritin > 250 µmol/L, n (%)	5 (31.3%)	NA
Hemoglobin, mmol/L	Men: 9.0 ± 0.7	8.5-11.0
	Women: 8.4 ± 0.9	7.5-10.0

Values are presented as numbers (percentages), mean ± standard deviation or median, interquartile range (minimum, maximum), if the distribution was skewed. Separate values are reported for men (n=11) and women (n=5), if applicable. HSCT: hematopoietic stem cell transplantation.

Patients as compared to the healthy controls had a higher E/Ea ratio (9.92 ± 3.42 vs. 7.24 ± 2.29, ***P***=0.004), while the E/A ratio (2.76 ± 0.92 vs. 2.97 ± 0.91, ***P***=0.599) and diastolic strain rates were comparable. There was a trend towards a lower LV ejection fraction (LVEF) (54 ± 6 vs. 58 ± 5%, ***P***=0.055) and lower GLS (-20.7 ± 3.5 vs. -22.9 ± 3.0%, ***P***=0.063), whereas GCS was preserved (-23.2 ± 3.6 vs. -23.9 ± 3.5%, ***P***=0.587). Stroke volume (83 ± 15 vs. 101 ± 17 mL, ***P***=0.003) but also cardiac output (5.2 ± 1.0 vs. 6.5 ± 1.0 L, ***P***=0.001) and cardiac index (2.9 ± 0.6 vs. 3.4 ± 0.5 L/m^2, ***P***=0.021) were lower. In contrast, aortic PWV (4.40 ± 0.26 vs.4.29 ± 0.29 m/s, ***P***=0.288), LV concentricity (0.62 ± 0.10 vs.0.61 ± 0.08 g/mL, ***P***=0.867), native T1 (1211 ± 36 vs.1227 ± 28 ms, ***P***=0.158) and myocardial triglyceride content (0.47 ± 0.18 vs.0.50 ± 0.13%, ***P***=0.202) were comparable. CMR results are presented in **Table 4** and **Figure 3**.

When comparing the subgroup with HSCT for malignancies with controls, the higher E/Ea persisted (10.33 ± 3.55 vs. 7.24 ± 2.29, *P*=0.013). Additionally, LVEF (52 ± 4 vs. 58 ± 5%, *P*=0.008), GLS (-19.8 ± 3.3 vs. -22.9 ± 3.0%, *P*=0.022) and GCSR-S (-1.13 ± 0.15 vs. -1.32 ± 0.26 1/s, *P*=0.047) were lower. For the HSCT recipients treated for malignancies, aortic PWV was: 4.39 ± 0.18 m/s (*P*=0.360 vs. controls), LV concentricity: 0.63 ± 0.10 g/mL (*P*=0.733), native T1: 1208 ± 36 ms (*P*=0.138) and myocardial triglyceride content: 0.53 ± 0.21 (*P*=0.693).

Table 4. CMR parameters

	Pediatric HSCT recipients (n=16)	Healthy controls (n=16)	*P* value
LV mass and dimensions			
Mass, g	95 ± 18	108 ± 23	0.078
Mass/BSA, g/m^2	53 ± 9	57 ± 10	0.328
End-diastolic volume, mL	155 ± 29	176 ± 30	0.052
End-diastolic volume/BSA, mL/m^2	87 ± 14	93 ± 13	0.238
Mass/end-diastolic volume, g/mL	0.62 ± 0.10	0.61 ± 0.08	0.867
LV systolic function			
Stroke volume, mL	83 ± 15	101 ± 17	0.003*
Cardiac output, L	5.2 ± 1.0	6.5 ± 1.0	0.001*
Cardiac index, L/m^2	2.9 ± 0.6	3.4 ± 0.5	0.021*
Ejection fraction, %	54 ± 6	58 ± 5	0.055
Global longitudinal strain, %	-20.7 ± 3.5	-22.9 ± 3.0	0.063
Global circumferential strain, %	-23.2 ± 3.6	-23.9 ± 3.5	0.587
Longitudinal peak systolic strain rate, 1/s	-0.95 ± 0.20	-1.06 ± 0.21	0.137
Circumferential peak systolic strain rate, 1/s	-1.21 ± 0.22	-1.32 ± 0.36	0.216
LV diastolic function			
E/A ratio	2.76 ± 0.92	2.97 ± 0.91	0.599‡
Estimated LV filling pressure	9.92 ± 3.42	7.24 ± 2.29	0.004‡
Longitudinal early diastolic strain rate, 1/s	1.01 ± 0.26	1.15 ± 0.35	0.224
Circumferential early diastolic strain rate, 1/s	1.28 ± 0.29	1.38 ± 0.35	0.396
LV myocardial tissue characteristics			
Myocardial triglyceride content, %	0.47 ± 0.18	0.50 ± 0.13	0.202‡
Native T1 relaxation time, ms	1211 ± 36	1227 ± 28	0.158
Aortic stiffness			
Aortic pulse wave velocity, m/s	4.40 ± 0.26	4.29 ± 0.29	0.288

Values are presented as means ± standard deviations. *P<0.05. ‡P value not based on the Student's t-test but on the Mann-Whitney U test. HSCT: hematopoietic stem cell transplantation. LV: left ventricle. BSA: body surface area. E/A ratio: ratio of early and late peak filling rate. Estimated LV filling pressure: ratio of transmitral early peak velocity and early diastolic mitral septal tissue velocity (E/Ea).

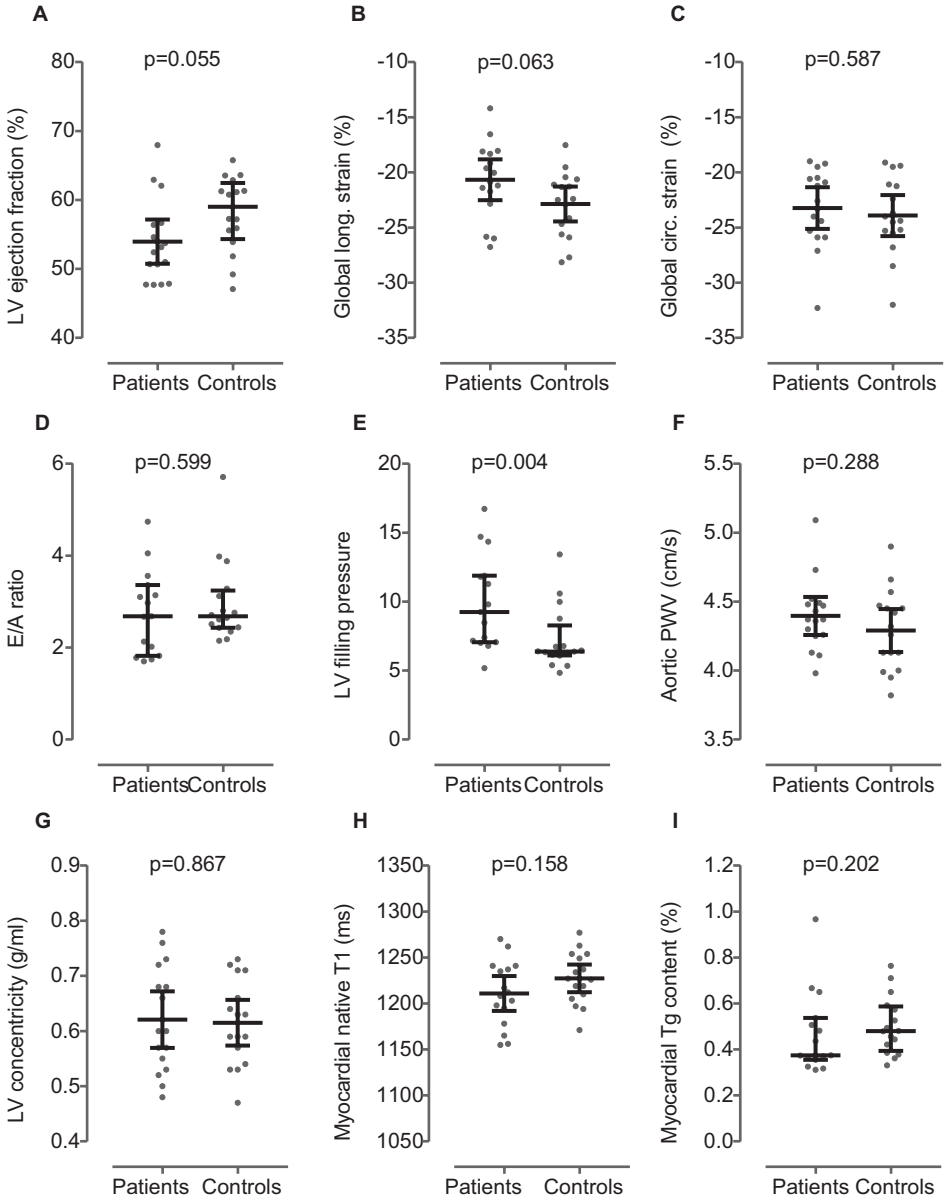

Figure 3. CMR measurements with means and 95% confidence intervals and median and interquartile ranges for normally and non-normally distributed data, respectively. Despite a non-significantly lower left ventricular (LV) systolic function (**A-C**) and lower LV diastolic function (**D-E**) as indicated by the increased estimated LV filling pressure, the CMR parameters for aortic stiffness (**F**) and LV structure (**G**) and myocardial tissue characteristics (**H-I**) were comparable for the patients who received HSCT and the healthy controls. Abbreviations as in Table 4.

Post-hoc power analysis

We had 0.90 power to detect a statistically significant difference if the HSCT population would have had an aortic PWV of 4.64 m/s or higher (+0.33 m/s higher as compared to the healthy controls), myocardial triglyceride content of 0.69% or higher (+0.19%) and native T1 of 1268 ms or higher (+39 ms). These differences in aortic PWV, myocardial triglyceride content and native T1 are comparable to approximately 3, 20 and 35 years of normal aging, respectively (23-25).

DISCUSSION

Our study showed that young adults with a history of pediatric HSCT, as compared to healthy controls in the same age range, have subclinical impairments in LV diastolic function and tend to have a lower LV systolic function, whereas aortic stiffness and myocardial tissue characteristics are comparable. Our results indicate that CMR-derived LV diastolic parameters, rather than aortic PWV, cardiac native T1 or myocardial triglyceride content, are early markers of cardiovascular deterioration after HSCT.

LV function

The estimated LV filling pressure was found to be increased after childhood HSCT, which is indicative of reduced LV diastolic function. When LV myocardial relaxation progressively deteriorates, LV filling pressure becomes increased to compensate for the impaired LV diastolic filling (26). Accordingly, in the patients who received HSCT during childhood, the E/A ratio was comparable as in the controls, whereas LV filling pressure was higher. In contrast to the impairments in LV diastolic function, the decrease in LV systolic function in the HSCT group compared to the control group was non-significant. This observation is in keeping with prior longitudinal studies using echocardiography, which showed that diastolic dysfunction precedes systolic dysfunction in response to cardiotoxic exposures (27,28). Anthracycline-related cardiomyopathy is considered to result from free radical formation, the consequent mitochondrial dysfunction and myofibrillar disarray, and eventual myocyte necrosis; in turn, with the ongoing remodeling of the injured heart, functional impairments may progressively develop (2). Furthermore, irradiation may cause microcirculatory damage, leading to myocardial ischemia and cell death (2). However, despite the reduced LV diastolic function, there was no interstitial fibrosis based on native T1 mapping. Furthermore, aortic stiffening or myocardial steatosis did not appear contributing factors to the abnormalities in LV diastolic function. Hence, when using CMR, LV diastolic parameters in particular may be important in the monitoring of HSCT-related cardiovascular deteriorations.

In our study, the non-significantly lower LVEF and significantly lower cardiac index in the pediatric HSCT recipients compared to the controls seemed to be related to impairments in GLS rather than GCS. GLS and GCS, respectively, can be interpreted as measures of the

contractility of the cardiomyocytes in oblique orientation in the subendocardium and those in circumferential arrangement in the mesomyocardium (29,30). Accordingly, our results may suggest that the HSCT-related therapies predominately affect the subendocardial myocardium, and not the midwall. In the subgroup with a history of a malignant disorder, longitudinal and circumferential systolic strain-derived parameters were lower as compared to healthy controls; this is consistent with previous studies which assessed LV systolic strain parameters in patients receiving anthracyclines (31,32).

We hypothesized that aortic stiffening or altered myocardial tissue characteristics would be early markers of cardiovascular disturbances after HSCT, preceding manifest LV dysfunction. Of interest, as chemotherapy is considered to disrupt mitochondrial function and irradiation has been demonstrated to induce microcirculatory damage (2), several other CMR-derived parameters may have potential for the early detection of cardiac effects of HSCT, for example phosphorus MRS (^{31}P-MRS) for the assessment of myocardial energetics and perfusion imaging (33).

Aortic stiffness

No differences were observed in aortic stiffness between the HSCT study population and the healthy controls. Based on previous studies, we expected to find a significantly higher aortic stiffness, at least in the patients with HSCT for a malignant disorder, because of the pre-transplant cardiotoxic exposures. Anthracycline and/or chest irradiation in the treatment of the primary cancer may cause endothelial damage due to the generation of reactive oxygen species (34,35). Also, the conditioning in allogeneic HSCT, including total body irradiation and/or chemotherapy, is considered to initiate disruption of the endothelium (36). Subsequently, the structural changes in the vascular matrix and the disturbed endothelial function may increase the vascular tone of the arterial wall (2). In addition, metabolic disturbances caused by the immune dysregulation and iron overload are well recognized adverse effects of HSCT (12,37). There is extensive evidence for an elevated aortic stiffness due to hypertension, dyslipidemia and hyperglycemia in the general population (14). The role of iron overload in endothelial dysfunction is less evident, although iron chelation in coronary artery disease has been shown to improve endothelium-dependent vasodilation (38).

Previous longitudinal studies in patients with breast cancer, lymphoma or leukemia showed that aortic PWV increases by approximately 1.5 to 2–fold upon anthracyclines in the first 4 to 6 months, also for low or moderate dosages, compared to the pre-treatment measurements (39,40). Another study measured a higher carotid artery stiffness in children who had received allogeneic HSCT, for malignant or non-malignant disease, even though this study population showed only minor, subclinical metabolic derangements, and no other cardiovascular impairments were detected (41). However, the increased aortic stiffness due to cardiotoxic exposures may decrease after the cardiotoxic therapy has been discontinued, as was shown in breast cancer patients who were followed before and 1, 4 and 14 months after anthracycline or

trastuzumab chemotherapy (42). We measured aortic PWV after a mean time of 14.8 ± 5.0 years after HSCT. Possibly, there may have been changes in aortic PWV acutely after pediatric HSCT, which may have normalized after several years.

Myocardial tissue characteristics

There were no differences in myocardial tissue characteristics and LV concentricity between the HSCT study population and the healthy controls, which otherwise would have been indicative of LV remodeling. To our knowledge, this is the first study in which native T1, as a measure of interstitial fibrosis, and myocardial triglyceride content, as a measure of metabolic remodeling, have been assessed in young adults with prior HSCT. It should be noted that diffuse fibrosis can be estimated based on calculating native T1 or the extracellular volume fraction (ECV) the latter requires MR contrast administration (17). Recent CMR studies have demonstrated that both native T1 and ECV are increased in middle-aged patients with prior anthracycline therapy (43,44). Other studies in adolescents exposed to anthracyclines, however, reported native T1 and/or ECV values within the normal range (45,46); nonetheless, a correlation was found between the cumulative anthracycline dose and native T1 and ECV (46). In contrast to these observations suggestive of diffuse fibrosis, focal fibrosis, visualized with late gadolinium enhancement CMR, is uncommon after anthracycline exposure, even when systolic function is subnormal (44-47). In our HSCT study population as compared to the controls, we did not find a higher native T1, even though a lower LVEF was measured. Also, when analyzing the patients who received HSCT for a malignant indication separately, no difference with the control group was found. Therefore, in contrast to middle-aged patients with prior anthracycline therapy as described in other studies, we may conclude that there is no myocardial fibrosis, at least not substantial, in young adults with a history of childhood HSCT as compared to healthy controls.

From previous studies it is known that the metabolic syndrome, presumably due to changes in myocardial fatty acid uptake and/or oxidation, is associated with myocardial steatosis (18,48). Although allografting increases the risk of early development of the metabolic syndrome (12), our HSCT study population aged 18-25 years had on average no obesity, impaired fasting glucose or hypertriglyceridemia. Possibly, myocardial steatosis may arise after HSCT at middle-age, when metabolic disorders may have developed, while myocardial triglyceride content remains within the normal ranges at younger age. Based on our findings, we may conclude that myocardial triglyceride content does not represent an early marker of cardiometabolic disease after pediatric HSCT in the young adult population.

Strengths

Strength of this study is the comprehensive CMR evaluation, including measures of both LV systolic and diastolic function, vascular function and myocardial tissue characteristics. CMR rather than ultrasound is the most accurate non-invasive modality to quantify aortic stiffness (49). Diffuse fibrosis was measured using native T1 mapping, which is a non-contrast technique;

contrast-enhanced CMR can be considered less suitable for screening programs. Cardiac ^{1}H-MRS is the gold standard for non-invasive assessment of myocardial steatosis (48). In clinical practice, echocardiography is commonly used for follow-up after cardiotoxic therapies (11). Compared to echocardiography, little is known regarding the value of CMR for cardiovascular screening after HSCT.

Limitations

Our study did not comprise CMR before and shortly after HSCT, but had a cross-sectional design because of ethical considerations. Therefore, we cannot exclude temporary deteriorations in, for example, aortic stiffness. Our study population was too small to evaluate the patient group with HSCT for non-malignant disease separately. The observed abnormalities in LV diastolic function and the non-significantly lower LV systolic function seemed to be driven by the patients who had received HSCT for a malignant disease. However, based on our study we cannot rule out late LV functional impairment after HSCT for non-malignant disease. Also, we were not able to assess the correlations between the different HSCT conditioning regimens, graft-versus-host-disease or iron overload and cardiovascular measures. However, this study was aimed at identifying CMR parameters which may show deteriorations before overt cardiovascular disease develops, and not to identify HSCT-related factors which may be helpful in late cardiovascular disease risk stratification. Echocardiography was not applied in the present study, which would have allowed for comparison of CMR with echocardiography for the early detection of cardiac effects of HSCT.

As a measure of interstitial fibrosis, ECV may be preferable. The native T1 value may be affected by several processes other than edema or increased myocardial collagen in the extracellular compartment (17). Hence, based on the native T1 measurements, we may not be able to exclude the presence of diffuse fibrosis in post-HSCT patients. However, as all patients were clinically monitored for cardiac iron deposition and as myocardial steatosis was ruled out based on the ^{1}H-MRS measurements, it is unlikely that fibrosis related increases in native T1 might have been cancelled out by myocardial iron or fat related native T1 decreases.

CONCLUSION

In young adults who received HSCT during childhood, LV diastolic function was decreased (higher estimated LV filling pressure) and LV systolic function (LVEF and GLS) tended to be reduced as compared to healthy controls, whereas no concomitant differences were found in aortic stiffness (aortic PWV) and myocardial tissue characteristics (native T1 and myocardial triglyceride content). Therefore, when using CMR, the assessment of LV diastolic function in particular is important for early detection of patients at risk of HSCT-related cardiovascular disease. Further research, including longitudinal CMR measurements, is needed to show the

predictive value of subclinical LV functional abnormalities for the development of symptomatic cardiovascular disease after HSCT. Also, comparative studies of imaging modalities should reveal whether CMR-derived LV function has additive value for screening programs when performed next to the current echocardiography-based follow-up of the cardiovascular late effects of HSCT. For example, CMR may be used for the selection of patients who require frequent follow-up by standard echocardiography.

REFERENCES

1. Uderzo C, Pillon M, Corti P, et al. Impact of cumulative anthracycline dose, preparative regimen and chronic graft-versus-host disease on pulmonary and cardiac function in children 5 years after allogeneic hematopoietic stem cell transplantation: a prospective evaluation on behalf of the EBMT Pediatric Diseases and Late Effects Working Parties. Bone Marrow Transplant 2007;39(11):667-675.
2. Lipshultz SE, Adams MJ, Colan SD, et al. Long-term cardiovascular toxicity in children, adolescents, and young adults who receive cancer therapy: pathophysiology, course, monitoring, management, prevention, and research directions: a scientific statement from the American Heart Association. Circulation 2013;128(17):1927-1995.
3. Pulte D, Gondos A, Brenner H. Trends in 5- and 10-year survival after diagnosis with childhood hematologic malignancies in the United States, 1990-2004. J Natl Cancer Inst 2008;100(18):1301-1309.
4. Chima RS, Daniels RC, Kim MO, et al. Improved outcomes for stem cell transplant recipients requiring pediatric intensive care. Pediatr Crit Care Med 2012;13(6):e336-342.
5. Niederwieser D, Baldomero H, Szer J, et al. Hematopoietic stem cell transplantation activity worldwide in 2012 and a SWOT analysis of the Worldwide Network for Blood and Marrow Transplantation Group including the global survey. Bone Marrow Transplant 2016;51(6):778-785.
6. Battiwalla M, Tichelli A, Majhail NS. Long-Term Survivorship after Hematopoietic Cell Transplantation: Roadmap for Research and Care. Biol Blood Marrow Transplant 2017;23(2):184-192.
7. Battiwalla M, Hashmi S, Majhail N, Pavletic S, Savani BN, Shelburne N. National Institutes of Health Hematopoietic Cell Transplantation Late Effects Initiative: Developing Recommendations to Improve Survivorship and Long-Term Outcomes. Biol Blood Marrow Transplant 2017;23(1):6-9.
8. Armenian SH, Chemaitilly W, Chen M, et al. National Institutes of Health Hematopoietic Cell Transplantation Late Effects Initiative: The Cardiovascular Disease and Associated Risk Factors Working Group Report. Biol Blood Marrow Transplant 2017;23(2):201-210.
9. Pulsipher MA, Skinner R, McDonald GB, et al. National Cancer Institute, National Heart, Lung and Blood Institute/Pediatric Blood and Marrow Transplantation Consortium First International Consensus Conference on late effects after pediatric hematopoietic cell transplantation: the need for pediatric-specific long-term follow-up guidelines. Biol Blood Marrow Transplant 2012;18(3):334-347.
10. Chow EJ, Anderson L, Baker KS, et al. Late Effects Surveillance Recommendations among Survivors of Childhood Hematopoietic Cell Transplantation: A Children's Oncology Group Report. Biol Blood Marrow Transplant 2016;22(5):782-795.
11. Shankar SM, Marina N, Hudson MM, et al. Monitoring for cardiovascular disease in survivors of childhood cancer: report from the Cardiovascular Disease Task Force of the Children's Oncology Group. Pediatrics 2008;121(2):e387-396.
12. Taskinen M, Saarinen-Pihkala UM, Hovi L, Lipsanen-Nyman M. Impaired glucose tolerance and dyslipidaemia as late effects after bone-marrow transplantation in childhood. Lancet 2000;356(9234):993-997.
13. McEniery CM, Yasmin, Hall IR, et al. Normal vascular aging: differential effects on wave reflection and aortic pulse wave velocity: the Anglo-Cardiff Collaborative Trial (ACCT). J Am Coll Cardiol 2005;46(9):1753-1760.
14. Terentes-Printzios D, Vlachopoulos C, Xaplanteris P, et al. Cardiovascular Risk Factors Accelerate Progression of Vascular Aging in the General Population: Results From the CRAVE Study (Cardiovascular Risk Factors Affecting Vascular Age). Hypertension 2017;70(5):1057-1064.
15. Cheung YF, Chan GC, Ha SY. Arterial stiffness and endothelial function in patients with beta-thalassemia major. Circulation 2002;106(20):2561-2566.
16. Ben-Shlomo Y, Spears M, Boustred C, et al. Aortic pulse wave velocity improves cardiovascular event prediction: an individual participant meta-analysis of prospective observational data from 17,635 subjects. J Am Coll Cardiol 2014;63(7):636-646.
17. Puntmann VO, Peker E, Chandrashekhar Y, Nagel E. T1 Mapping in Characterizing Myocardial Disease: A Comprehensive Review. Circ Res 2016;119(2):277-299.
18. Rayner JJ, Banerjee R, Holloway CJ, et al.

The relative contribution of metabolic and structural abnormalities to diastolic dysfunction in obesity. Int J Obes (Lond) 2017.
19. de Heer P, Bizino MB, Versluis MJ, Webb AG, Lamb HJ. Improved Cardiac Proton Magnetic Resonance Spectroscopy at 3 T Using High Permittivity Pads. Invest Radiol 2016;51(2):134-138.
20. Grotenhuis HB, Westenberg JJ, Steendijk P, et al. Validation and reproducibility of aortic pulse wave velocity as assessed with velocity-encoded MRI. J Magn Reson Imaging 2009;30(3):521-526.
21. Brandts A, Bertini M, van Dijk EJ, et al. Left ventricular diastolic function assessment from three-dimensional three-directional velocity-encoded MRI with retrospective valve tracking. J Magn Reson Imaging 2011;33(2):312-319.
22. de Heer P, Bizino MB, Lamb HJ, Webb AG. Parameter optimization for reproducible cardiac (1) H-MR spectroscopy at 3 Tesla. J Magn Reson Imaging 2016;44(5):1151-1158.
23. Ohyama Y, Teixido-Tura G, Ambale-Venkatesh B, et al. Ten-year longitudinal change in aortic stiffness assessed by cardiac MRI in the second half of the human lifespan: the multi-ethnic study of atherosclerosis. Eur Heart J Cardiovasc Imaging 2016;17(9):1044-1053.
24. van der Meer RW, Rijzewijk LJ, Diamant M, et al. The ageing male heart: myocardial triglyceride content as independent predictor of diastolic function. Eur Heart J 2008;29(12):1516-1522.
25. Roy C, Slimani A, de Meester C, et al. Age and sex corrected normal reference values of T1, T2 T2* and ECV in healthy subjects at 3T CMR. J Cardiovasc Magn Reson 2017;19(1):72.
26. Zile MR, Baicu CF, Gaasch WH. Diastolic heart failure--abnormalities in active relaxation and passive stiffness of the left ventricle. N Engl J Med 2004;350(19):1953-1959.
27. Tassan-Mangina S, Codorean D, Metivier M, et al. Tissue Doppler imaging and conventional echocardiography after anthracycline treatment in adults: early and late alterations of left ventricular function during a prospective study. Eur J Echocardiogr 2006;7(2):141-146.
28. Nagy AC, Cserep Z, Tolnay E, Nagykalnai T, Forster T. Early diagnosis of chemotherapy-induced cardiomyopathy: a prospective tissue Doppler imaging study. Pathol Oncol Res 2008;14(1):69-77.
29. Ingels NB, Jr. Myocardial fiber architecture and left ventricular function. Technol Health Care 1997;5(1-2):45-52.
30. Dorri F, Niederer PF, Lunkenheimer PP, Anderson RH. The architecture of the left ventricular myocytes relative to left ventricular systolic function. Eur J Cardiothorac Surg 2010;37(2):384-392.
31. Ong G, Brezden-Masley C, Dhir V, et al. Myocardial strain imaging by cardiac magnetic resonance for detection of subclinical myocardial dysfunction in breast cancer patients receiving trastuzumab and chemotherapy. Int J Cardiol 2018.
32. Lunning MA, Kutty S, Rome ET, et al. Cardiac magnetic resonance imaging for the assessment of the myocardium after doxorubicin-based chemotherapy. Am J Clin Oncol 2015;38(4):377-381.
33. Hudsmith LE, Neubauer S. Magnetic resonance spectroscopy in myocardial disease. JACC Cardiovasc Imaging 2009;2(1):87-96.
34. Keltai K, Cervenak L, Mako V, Doleschall Z, Zsary A, Karadi I. Doxorubicin selectively suppresses mRNA expression and production of endothelin-1 in endothelial cells. Vascul Pharmacol 2010;53(5-6):209-214.
35. Soucy KG, Attarzadeh DO, Ramachandran R, et al. Single exposure to radiation produces early anti-angiogenic effects in mouse aorta. Radiat Environ Biophys 2010;49(3):397-404.
36. Woywodt A, Scheer J, Hambach L, et al. Circulating endothelial cells as a marker of endothelial damage in allogeneic hematopoietic stem cell transplantation. Blood 2004;103(9):3603-3605.
37. de Witte T. The role of iron in patients after bone marrow transplantation. Blood Rev 2008;22 Suppl 2:S22-28.
38. Duffy SJ, Biegelsen ES, Holbrook M, et al. Iron chelation improves endothelial function in patients with coronary artery disease. Circulation 2001;103(23):2799-2804.
39. Chaosuwannakit N, D'Agostino R, Jr., Hamilton CA, et al. Aortic stiffness increases upon receipt of anthracycline chemotherapy. J Clin Oncol 2010;28(1):166-172.
40. Drafts BC, Twomley KM, D'Agostino R, Jr., et al. Low to moderate dose anthracycline-based chemotherapy is associated with early noninvasive imaging evidence of subclinical cardiovascular disease. JACC Cardiovasc Imaging 2013;6(8):877-885.
41. Turanlahti MI, Taskinen M, Saarinen-Pihkala U, Jokinen EV. Time-related arterial changes after allogeneic hematopoietic stem cell transplantation in children. Pediatr Res 2013;73(6):777-782.
42. Grover S, Lou PW, Bradbrook C, et al. Early

and late changes in markers of aortic stiffness with breast cancer therapy. Intern Med J 2015;45(2):140-147.
43. Jordan JH, Vasu S, Morgan TM, et al. Anthracycline-Associated T1 Mapping Characteristics Are Elevated Independent of the Presence of Cardiovascular Comorbidities in Cancer Survivors. Circ Cardiovasc Imaging 2016;9(8).
44. Neilan TG, Coelho-Filho OR, Shah RV, et al. Myocardial extracellular volume by cardiac magnetic resonance imaging in patients treated with anthracycline-based chemotherapy. Am J Cardiol 2013;111(5):717-722.
45. Toro-Salazar OH, Gillan E, O'Loughlin MT, et al. Occult cardiotoxicity in childhood cancer survivors exposed to anthracycline therapy. Circ Cardiovasc Imaging 2013;6(6):873-880.
46. Tham EB, Haykowsky MJ, Chow K, et al. Diffuse myocardial fibrosis by T1-mapping in children with subclinical anthracycline cardiotoxicity: relationship to exercise capacity, cumulative dose and remodeling. J Cardiovasc Magn Reson 2013;15:48.
47. Ylanen K, Poutanen T, Savikurki-Heikkila P, Rinta-Kiikka I, Eerola A, Vettenranta K. Cardiac magnetic resonance imaging in the evaluation of the late effects of anthracyclines among long-term survivors of childhood cancer. J Am Coll Cardiol 2013;61(14):1539-1547.
48. van der Meer RW, Lamb HJ, Smit JW, de Roos A. MR imaging evaluation of cardiovascular risk in metabolic syndrome. Radiology 2012;264(1):21-37.
49. Cavalcante JL, Lima JA, Redheuil A, Al-Mallah MH. Aortic stiffness: current understanding and future directions. J Am Coll Cardiol 2011;57(14):1511-1522.

CHAPTER

When should we use contrast material in cardiac MRI?

Paiman EHM, Lamb HJ

J Magn Reson Imaging. 2017 Dec;46(6):1551-1572. doi: 10.1002/jmri.25754.
Epub 2017 May 8. Review.

ABSTRACT

At present, most of the cardiac magnetic resonance imaging (MRI) examinations rely on contrast-enhanced protocols, but noncontrast alternatives are emerging. Late gadolinium enhancement (LGE) imaging for the detection of myocardial scar can be considered the main cause for the embedding of cardiac MRI into the clinical routine. The novel noncontrast technique of native T1 mapping shows promise for tissue characterization in ischemic and nonischemic cardiomyopathy and may provide additional information over conventional LGE imaging. Technical issues, including measurements variability, still need to be resolved to facilitate a wide clinical application. Ischemia detection can be performed with contrast-based stress perfusion and contrast-free stress wall motion imaging. For coronary magnetic resonance angiography (MRA), protocols with and without contrast material have been developed. Research on coronary atherosclerotic plaque characterization has introduced new applications of contrast material. For MRA of the aorta, which traditionally relied on contrast administration, several noncontrast protocols have become available. This review provides an overview of when to use contrast material in cardiac and cardiac-related vascular MRI, summarizes the major imaging building blocks, and describes the diagnostic value of the available contrast-enhanced and noncontrast techniques. Contrast material in cardiac MRI should be used for LGE imaging for tissue characterization in ischemic or nonischemic cardiomyopathy and may be used for stress perfusion imaging for the detection of ischemia. In cardiac-related vascular MRI, use of contrast material should be avoided, unless high-quality angiography is required that cannot be obtained with noncontrast protocols.

Cardiac magnetic resonance imaging (MRI) has taken an important role in the work-up of cardiovascular disease. Compared to general radiology, MR contrast material is used in a high number of examinations (92%) (1). In this review, we aim to provide an overview of contrast-enhanced and noncontrast cardiac and cardiac-related vascular MRI protocols (**Table 1**). First, the considerations of when to use contrast material in cardiac MRI are discussed. Second, the major imaging building blocks are described, including cine and flow imaging, late gadolinium enhancement (LGE), stress and rest first-pass perfusion and wall motion imaging, native T1 and extracellular volume (ECV) mapping, and magnetic resonance angiography (MRA) of the coronary arteries and large vessels with and without contrast material. Third, most common clinical indications are listed, including myocardial infarction and ischemia, nonischemic cardiomyopathy, cardiac mass, and visualization of the coronary arteries and large vessels, with an overview of the diagnostic value of the available contrast-enhanced and noncontrast techniques.

CONTRAST MATERIAL IN CARDIAC MRI

Safety

REGULATION. The decision whether gadolinium-based contrast agents can be safely used in cardiac MRI is dependent on the individual patient characteristics, similar to general radiology. In patients with previous severe hypersensitivity reactions, contrast material should be avoided. For contrast administration in patients with impaired renal function, pregnancy or lactation, institutional, regional, or national guidelines should be followed (2-5). If noncontrast techniques with comparable diagnostic performance are available, those should be preferred over contrast-enhanced techniques. If contrast administration is indicated, the administered dosage should be as low as possible.

It should be noted that administration of gadolinium-based contrast material in cardiac and cardiac-related vascular MRI is not regulatory-approved (6). The decision to use gadolinium chelates in cardiac MRI should be based on strong evidence in the literature and the prescribing clinician is responsible for maintaining records of the contrast agent's use and effects (7). The decision whether or not to discuss the off-label status of a product with the patient is rather an ethical than a legal issue, and should be based on professional judgment (8). In our center, similar to any other medical intervention, we inform the patient in advance that there is a risk of adverse events and tailor more detailed information to the individual patient. Given the widely accepted use of gadolinium-based contrast material in cardiac MRI, we do not specifically address the off-label status. Up-to-date figures regarding informed consent procedures among centers are not available.

Table 1. Clinical protocols for contrast-enhanced and noncontrast cardiac and cardiac-related vascular MRI.

Indication	MRI protocol with contrast material	MRI protocol without contrast material
Myocardial infarction (viability assessment, postreperfusion therapy)	LGE imaging ECV mapping	Native T1 mapping
Myocardial ischemia (viability assessment, postreperfusion therapy)	Stress perfusion imaging	Stress wall motion imaging
Nonischemic cardiomyopathy (including arrhythmia and myocarditis)	LGE imaging ECV mapping Early gadolinium enhancement (for myocarditis)	Native T1 mapping T2-weighted black and bright blood imaging (not discussed) T2 and T2* mapping (not discussed)
Cardiac mass	First pass imaging Post contrast T1-weighted imaging LGE imaging	T1-and T2-weighted imaging (with and without fat suppression) Native T1 and T2 mapping
Coronary artery anomalies/ patency	Contrast-enhanced T1-weighted MRA	Time-of-flight imaging Balanced SSFP imaging
Large vessels (including congenital disease and pulmonary vein evaluation pre- and postablation)	Contrast-enhanced T1-weighted MRA (also for pulmonary vein evaluation)	Balanced SSFP imaging (thoracic aorta) Partial-Fourier FSE imaging (peripheral arteries) Time-of-flight imaging Phase-contrast imaging Quiescent-interval slice selective (QISS) imaging

For details regarding standardized protocols and contrast dosing, see the standardized cardiac MR protocols of the Society for Cardiovascular Magnetic Resonance (SCMR) (24). LGE: late gadolinium enhancement; ECV: extracellular volume; MRA: magnetic resonance angiography; SSFP: steady-state free precession; FSE: fast spin echo.

HYPERSENSITIVITY REACTIONS. Based on the reported numbers in routine cardiac MRI, use of gadolinium chelates in a clinical cardiac MRI setting can be considered safe in terms of frequency and severity of adverse reactions. Retrospective analysis, based on 158,796 MR exams in the United States, showed an event rate of 0.055% for cardiac MRI, compared to 0.059% for overall MRI (9). The EuroCMR Registry, including 37,788 patients in 57 European centers, reports a number of 0.12%, with most of the adverse events being mild (eg, rashes and hives, nausea, or flushes) (10). No deaths due to contrast administration in cardiac MRI were reported. The above number is comparable to data on adverse events in general radiology, ranging from 0.059% to 0.3% in recent reports (9,11,12).

NEPHROGENIC SYSTEMIC FIBROSIS. The first report on nephrogenic systemic fibrosis (NSF), observed in patients with endstage chronic kidney disease, was published in 2000 (13). As studies found an association between high dosage of gadolinium chelates (0.2–0.3 mmol/kg) and increased incidence of NSF, double or triple dosing is no longer common practice (14,15). Although the association between NSF and gadolinium chelates in patients with renal failure is well recognized, the mechanism and the relation to the different compounds is still controversial. Prevailing hypothesis explaining the differences in the number of reported cases is the difference in gadolinium chelate stability. Several reviews are available regarding the association between gadolinium chelates and NSF (14-16).

GADOLINIUM DEPOSITION IN THE BRAIN. In 2014 the first report was published that showed that serial injection of gadolinium-based contrast material correlated with a signal intensity increase in the dentate nucleus and the globus pallidus on T1-weighted MRI, also in patients with normal renal function (17). Subsequent studies found evidence of gadolinium deposition in the brain of deceased patients and a correlation between the cumulative intravenous dose and the total amount of gadolinium stored in the tissue (18,19). Comparable to NSF, it is hypothesized that the potential of gadolinium-based contrast agents to cause hyperintensities or gadolinium deposition in the brain is related to stability. In the last 2 years, multiple retrospective patient studies and prospective animal studies have been performed, as summarized in the review of Radbruch (20). Up until now, the clinical relevance of the gadolinium brain deposition is unknown. It has not been associated with neurologic or biological adverse effects. A definite conclusion has not been formed yet and multiple research groups are currently working on this topic.

SPECIFIC POPULATIONS. As impaired renal function increases the risk of NSF, use of gadolinium chelates in patients with renal dysfunction should be avoided unless the diagnostic information is absolutely required and cannot be obtained with noncontrast MRI or other modalities. The risk of NSF is highest in patients with chronic severe kidney disease (glomerular filtration rate [GFR] <30 ml/min/1.73 m^2) or acute kidney injury (21). For all patients at risk of chronically reduced renal function (including age >60 years, hypertension, or diabetes), GFR should be estimated through laboratory sampling. Relatively unstable, high-risk gadolinium-based contrast agents (ie, gadopentetate dimeglumine, gadodiamide, and gadoversetamide) should be avoided. The remaining gadolinium-based contrast agents should be used with caution. In patients with endstage renal disease, contrast administration should be followed by dialysis (2-5,22). There are limited studies on the safety of contrast administration in pregnant or nursing women. Only if the potential benefits justify the potential risk, gadolinium-based contrast material may be used (2-5,22). Several gadolinium chelates are approved for pediatric use (2–18 years) (2).

Dosage

Approved clinical doses range from 0.1 and 0.3 mmol/kg body weight, although for most labeled indications the recommended dose is 0.1 mmol/kg. Contrast dose as used in cardiac MRI practice is in general higher than the recommended label dose. A meta-analysis on the administered dose of gadolinium-based contrast material in cardiac MRI trials found a median total dose per exam (LGE imaging and/or perfusion testing) of 0.2 mmol/kg (23). The document on standardized cardiac MR protocols of the Society for Cardiovascular Magnetic Resonance (SCMR) provides a practical overview of the recommended contrast and chasing bolus doses and injections rates (0.05–0.1 mmol/kg for perfusion imaging and 0.1–0.2 mmol/kg for LGE imaging) (24).

There is limited evidence on the efficacy of infarct detection by LGE in relation to dosage. To date, there is one multicenter, double-blinded, randomized trial, which studied the diagnostic performance of LGE in patients with acute and chronic myocardial infarction, for varying gadoversetamide doses. Sensitivity and specificity for detection of myocardial infarction increased with increasing doses of 0.1, 0.2, and 0.3 mmol/kg (for acute infarction 84, 95, 99%, respectively, and for chronic infarction 83, 87, 94%, respectively) (25). For perfusion cardiac MRI, there are two dose ranging multicenter trials that used gadopentetate dimeglumine.26,27 For a dosage of 0.05, 0.10, or 0.15 mmol/kg for rest and stress perfusion imaging (total dose per exam 0.1, 0.2, and 0.3 mmol/kg), Wolff et al (26) reported an area under the receiver-operating curve (AUC) of 0.90, 0.72, and 0.83, respectively, for the detection of obstructive coronary artery disease, compared to quantitative coronary angiography. Giang et al (27) reported an AUC of 0.53, 0.91, and 0.86, respectively. Although higher doses were shown to result in increased myocardial enhancement, higher doses did not result in improved diagnostic performance, as susceptibility artifacts may have led to false-positive findings.

Types of contrast agents

CHEMICAL STABILITY. The chemical structure of gadolinium chelates can be categorized as ionic versus nonionic and linear versus macrocyclic compounds. Gadolinium chelates need to be highly stable, to prevent release of free Gd^{3+} and guarantee safety. Stability is defined by the thermodynamic and kinetic stability constants and the chelates metal selectivity for Gd^{3+} over another metal species. Thermodynamic stability refers to the energy difference between the Gd^{3+} ligand complex before and after chelation and can be explained as "how tightly the ligand binds with Gd^{3+}." Kinetic stability is a measure of the activation energy needed to change the state of the Gd^{3+} complex and can be interpreted as "how easily Gd^{3+} is released from the chelate" (28). In general, ionic (negatively charged) chelates have higher stability compared to nonionic (uncharged) chelates, and a macrocyclic is favorable in terms of stability compared to a linear structure (29).

RELAXIVITY. Most gadolinium chelates have comparable T1 and T2 relaxivity (relaxation rate as a function of contrast agent concentration), except for gadofosveset trisodium, gadoxetate disodium, gadobenate dimeglumine, and gadobutrol, which have increased relaxivity compared to other agents. As gadobutrol is available in high concentration (1.0 mol/L), in combination with its high relaxivity, gadobutrol provides the largest T1 shortening effects per volume (30). In LGE imaging, gadobutrol results in superior contrast between infarct and blood, but generates similar contrast between infarct and normal tissue, compared to gadobenate dimeglumine (31).

NONBLOOD POOL VERSUS BLOOD POOL. All gadolinium chelates are extracellular (nonblood pool) agents, except for gadofosveset trisodium. Gadofosveset is an albumin-binding (blood pool) agent with longer plasma half-lives. For aorta MRA, when using gadofosveset, smaller total amounts are required and the imaging window is prolonged for up to 30–60 minutes after contrast administration (32). Improved image quality was shown for coronary MRA when using gadofosveset compared to gadobenate dimeglumine (33). However, as intravascular contrast agents do not allow for LGE imaging, gadofosveset cannot be used in a comprehensive protocol for the evaluation of both coronary artery patency and scar tissue. Currently, gadofosveset is commercially not available.

FERUMOXYTOL. Ferumoxytol has been proposed as an alternative to gadolinium-based contrast material. Ferumoxytol is an ultrasmall superparamagnetic iron oxide particle (USPIO), approved for the treatment of iron-deficiency anemia in patients with chronic kidney disease (34). In some institutions, it is used in standard clinical examinations including aorta, coronary, and peripheral vascular imaging (35). In contrast to MRA, the experience with ferumoxytol for myocardial tissue imaging is limited.

Ferumoxytol can be prescribed in patients with reduced renal function. Another advantage is its prolonged intravascular half-life of more than 15 hours. Timing of acquisition relative to contrast administration is not needed and prolonged or repeated imaging is possible (36). One concern, however, is the rare, but serious, hypersensitivity reactions that are observed in the context of the therapeutic use of ferumoxytol in dialysis centers (37). For imaging applications, in contrast, ferumoxytol is used at a much lower dose. To date, there are few studies on the safety of ferumoxytol as a contrast agent in MRI (38).

MAJOR BUILDING BLOCKS OF CARDIAC MRI

Cine imaging

Each clinical cardiac MR examination starts with cine long-axis (2-chamber, 4-chamber, and 3-chamber view) and short-axis images for the assessment of left ventricular (LV) function and structure. Recommended method is balanced steady-state free precession (SSFP) (24). Balanced SSFP employs the high T2/ T1 ratio of blood compared to myocardium to generate a high signal-to-noise ratio (SNR) and high contrast to noise ratio (CNR), without the need of contrast administration (39).

Flow imaging

Velocity of flow across valves or in vessels can be quantified using phase-contrast techniques. Conventionally, a motion-encoded gradient in one direction is applied to quantify through-plane flow (2D flow) (24). For more detailed flow information, velocity-encoding in three directions is possible (4D flow) (40). Flow imaging does not require contrast administration.

Late gadolinium enhancement

LGE imaging for the visualization of myocardial infarction has been an important and pioneering development in cardiac MRI. As explained by Kim et al (41), in myocardial infarction the functional capillary density is diminished, as a result of microvascular damage in combination with an increased distribution volume caused by, for example, edema and necrosis (acute stages) and replacement scar tissue (chronic infarction). A decrease in functional capillary density causes prolonged wash-in/wash-out time constants of the contrast agent, because of the decrease in capillary surface area available for solute transport and the increase in diffusion distance in the interstitium to fill the extracellular space. As the T1 relaxation time increases with the wash-out of contrast agent, healthy myocardium appears relatively hypoenhanced, compared to the delayed hyperenhancement in infarcted myocardium.

The technique of LGE for myocardium infarct imaging has been improved since the introduction of phase-sensitive inversion recovery (PSIR) imaging, compared to the conventional magnitude-reconstructed technique (42,43). Whereas in magnitude reconstruction, the rendered image intensity relies on the magnitude of the net magnetization, in phase-sensitive techniques, it depends on the polarity additionally. The PSIR technique prevents diminished contrast when the inversion time (TI) is earlier than the null time for healthy tissue, with therefore less variation in apparent infarct size (44). Other advances include free-breathing techniques; for example, respiratory navigator gated high-resolution whole-heart 3D LGE (**Figure 1**) (45). High-resolution whole-heart LGE facilitates scar detection for the complete LV, with precise scar delineation. Another free-breathing approach is automatic, nonrigid registration for motion correction. This approach enables robust LGE imaging, with high image quality and diagnostic performance, without the patient needing to perform breath-holds (46).

Since the introduction of modified Look-Locker inversion recovery (MOLLI)-based T1 mapping, not only fast and reliable pixel-wise T1 mapping became possible, but also synthetic inversion recovery (IR) images could be generated. Synthetic IR images can be calculated retrospectively at any TI, based on the myocardial T1 values generated with a MOLLI acquisition. Conventional LGE acquisition could then be eliminated, if T1 mapping is already in the clinical protocol (47).

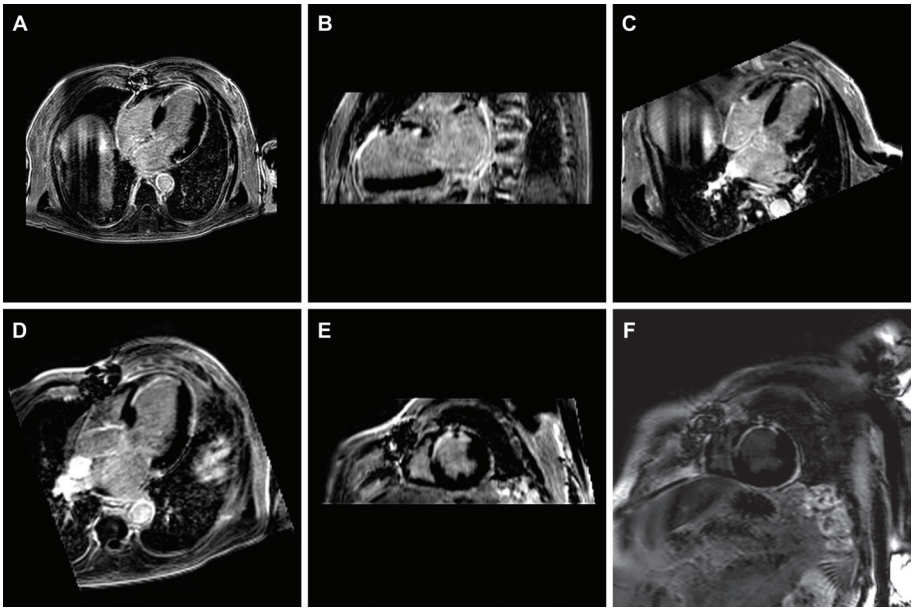

Figure 1. Example of respiratory navigator gated high-resolution whole-heart 3D late gadolinium enhancement (LGE) imaging: a 77-year-old man, with a history of anteroseptal myocardial infarction, multiple coronary artery bypass grafts, and percutaneous coronary intervention. (**A**) Transverse stack covering the complete left ventricle. Given the high spatial resolution, multiplanar reformatting can be performed with high in-plane resolution: reformatted 2-chamber (**B**), 4-chamber (**C**) 3-chamber (**D**), and short-axis (**E**) view. (**F**) For comparison, the conventional 2D LGE short-axis image is provided.

Stress perfusion and stress wall motion imaging

Stress and rest first-pass perfusion provides insight into both reversible and irreversible myocardial ischemia, and can be used to test for viability in chronic ischemic heart disease or to verify successful revascularization. At rest, a lesion is flow-limiting not until a luminal narrowing of >85% (48), since stenotic coronary arteries can restore flow by vasodilation. During pharmacological stress, however, stenotic coronary arteries cannot increase flow to meet the increasing myocardial demands. Based on relative perfusion deficits, stress perfusion is able to detect a stenosis of >50% (49).

First-pass perfusion imaging measures the first pass of a contrast bolus through the ventricular cavity and myocardial tissue, based on T1-weighted dynamic imaging (**Figure 2**)

(50). The signal intensity correlates with the amount of contrast material, which allows both qualitative and (semi)quantitative analysis of perfusion and hypoperfusion. The initial part of the signal intensity curve can be quantitatively analyzed, avoiding fast redistribution of contrast material into the extracellular space (51).

A contrast-free alternative to stress perfusion cardiac MRI is stress wall motion imaging, which allows detection of ischemia by qualitative evaluation of regional wall motion during infusion of increasing doses of pharmacological stress agents (52). In general, adenosine (a vasodilator) is used for the detection of stress-inducible perfusion deficits, and dobutamine (a positive inotropic and positive chronotropic) for wall motion abnormalities (53).

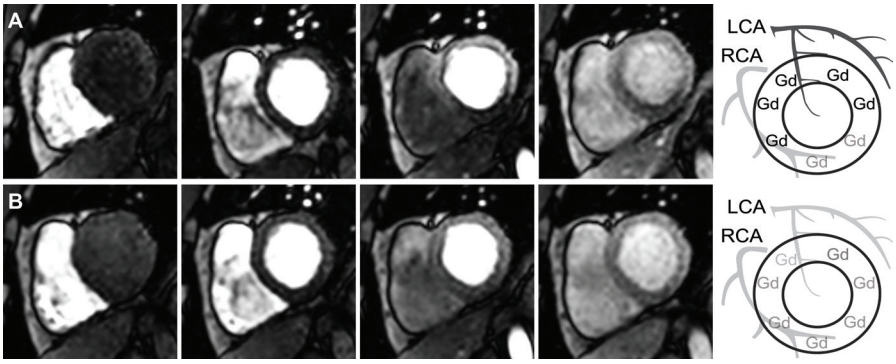

Figure 2. Example of first-pass adenosine stress and rest perfusion cardiac MRI: a 57-year-old man with a significant perfusion deficit in the inferior segments. (**A**) Dynamic adenosine stress perfusion MR images (dosage of gadoterate meglumine [Dotarem]: 0.1 mmol/kg). In contrast to the left coronary artery (LCA), the stenotic right coronary artery (RCA) cannot further dilate in response to stress, which results in pronounced hypoenhancement of the inferior segments. (**B**) Dynamic rest perfusion MR images (dosage of gadoterate meglu-mine [Dotarem]: 0.1 mmol/kg). The differences in perfusion between the inferior segments and the other segments are less pronounced. The impaired blood flow in the stenotic RCA during stress is largely restored by vasodilation in rest.

Native T1 and extracellular volume mapping

Advances in cardiac MRI have rendered it feasible to not merely obtain cardiac T1-weighted images, but to estimate the T1 relaxation times quantitatively, and display them pixel-wise. The concept of T1 mapping is sampling the recovery of magnetization after saturation or inversion and fitting a T1 recovery curve. T1 maps can be acquired solely without contrast material (native T1), or both prior and after contrast agent administration (postcontrast T1), which enables calculation of ECV maps (**Figures 3 and 4**).

With the technique of ECV mapping, the myocardium is dichotomized into an intracellular compartment (myocytes) and extracellular compartment (extracellular matrix and vessels) (54). The difference in T1 relaxation rate (1/T1) of blood between pre-and postcontrast imaging

is converted with the hematocrit value into a reference for plasma T1. Based on T1 changes in myocardial tissue, the ratio of extracellular to myocardial volume can be calculated. Whereas native T1 values are a reflection of both intra-and extracellular characteristics, ECV can be seen as an estimate of the extracellular space, which is affected by edema, fibrosis, or amyloid, etc.

A drawback of ECV mapping is the dependence on several measurements, including native and postcontrast T1 images, blood T1, and hematocrit. All need to be measured correctly to avoid an accumulation of errors. To facilitate implementation of ECV mapping, there have been methods suggested for ECV estimation without blood sampling to determine the hematocrit level (55). The relationship between hematocrit and the T1 relaxation rate of blood can be calibrated, which is used to generate a synthetic ECV. Treibel et al (55) found a linear relationship between the native T1 relaxation rate of blood and hematocrit. Synthetic ECV values based on this relationship correlated well with conventional ECV and histology.

There are several limitations that hamper translation of native T1 mapping and ECV mapping from research to clinical setting. Measured T1 values vary with vendor and field strength (higher at 3T compared to 1.5T), type of pulse sequence (most applied is the MOLLI sequence), and across the myocardium (higher in septal than lateral wall) (56). The ECV mapping technique, in which systematic differences are cancelled out, may be more comparable across MR field strengths, acquisition protocols, and imaging centers. For clinical application, T1 mapping should be highly reproducible to avoid misclassification of patients (insufficient precision, more than inaccuracy, is a major limitation for clinical use) (57). Certain technical development is needed to reduce measurement variability, to enable the detection of differences between disease groups, diagnosis in the individual patient, or monitoring of therapy effect (58).

In the SCMR expert consensus document on T1 and ECV mapping, recommendations regarding site preparation, scan protocols, and quality control are listed (59). Tight control of the scan protocol is required, as it is not fully known to what extent changes in software updates or imaging parameters affect T1 mapping. New T1 mapping sequences should be validated in phantoms with T1 values in the range of the expected values and with simulation of a range of heart rates. Ideally, for each particular setting, normal values should be acquired in a healthy control group. In multicenter studies, stratified analysis is recommended, to account for variations among centers. Recently, the first steps towards multicenter-based reference values have been made, registries are in progress (SCMR Registry, HCM Registry, UK Biobank), quality control systems are explored, and commercial sequences are available.

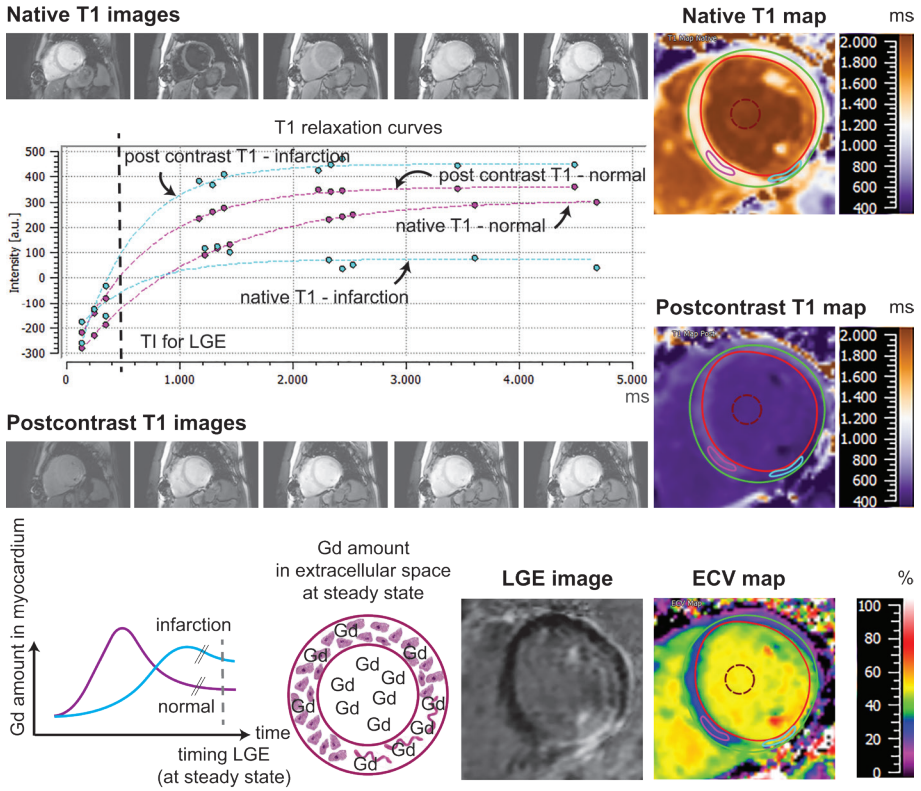

Figure 3. Concept of native and postcontrast T1 mapping and late gadolinium enhancement (LGE) imaging. A 54-year-old man, with an inferolateral myocardial infarction and prior sternotomy. (***Upper panel***) T1 mapping is performed before and after contrast adminis-tration. Presented T1 relaxation curves represent the areas with normal (purple) and infarcted (blue) myocardium. T1 mapping is based on the 3(3)3(3)5 modified Look-Locker (MOLLI) sequence. The T1 relaxation curve is sampled after three 1808 inversion pulses, with a rest period of 3 heart beats (respectively 3, 3, and 5 images at diastole are obtained). Based on the 11 images, the T1 relaxation curve can be fitted pixel-wise. (***Lower panel***) 10–15 minutes after contrast administration, a dynamic steady state in gadolinium (Gd) concen-tration between myocardium and blood pool is established. Given the increased extracellular volume (ECV) of infarcted myocardium, due to necrosis and/or replacement fibrosis, the amount of Gd is higher in infarcted compared to normal myocardium at steady state, which results in increased T1 shortening. In late gadolinium enhancement (LGE) imaging, the inversion time (TI) nulls normal myocar-dium. Based on native and postcontrast T1 maps, the ECV map can be calculated. Note: T1 relaxation times vary with vendor, field strength, and pulse sequence. (Image analysis in Medis Suite 2.1.)

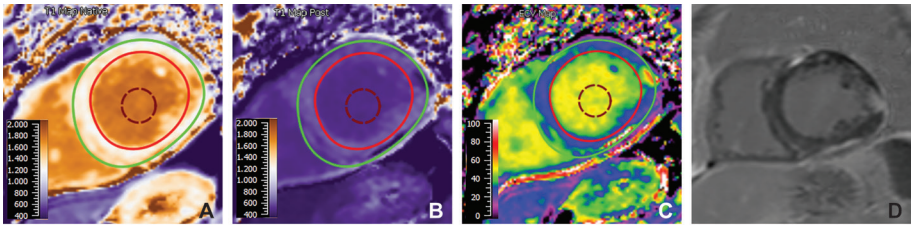

Figure 4. Example of native T1 mapping (**A**), postcontrast T1 mapping (**B**), extracellular volume (ECV) mapping (**C**), and LGE imaging (**D**): a 65-year-old man, scheduled for reablation of atrial fibrillation. The patchy areas of increased ECV correspond to the areas of LGE. Cardiac MRI findings are suggestive of nonischemic cardiomyopathy, myocarditis, sarcoidosis, or storage disease. (Image analysis in Medis Suite 2.1.)

Coronary MRA with and without contrast material

In contrast-based coronary MRA, contrast between blood and surrounding tissue is the result of the T1 shortening effect of contrast material. In general, extracellular gadolinium chelates are used that extravasate in about 10 to 15 minutes after administration. Hence, contrast-enhanced coronary MRA is limited by the fast redistribution of the contrast agent, which reduces the SNR for the coronary arteries and increases the signal in the coronary veins. Proposed techniques to obtain a prolonged blood signal enhancement time is slow infusion (0.3 ml/s) of contrast media (61,62), or using albumin-binding contrast agents with longer plasma half-lives (63).

A commonly used technique for coronary MRA without contrast material is balanced SSFP (64). At 3T, balanced SSFP is more challenging, due to the sensitivity to magnetic field inhomogeneities and increased energy deposition with increasing field strength. Therefore, 3T coronary MRA generally relies on gradient echo (GRE) sequences, in which contrast is generated using time-of-flight techniques (61). Noncontrast coronary MRA can be combined with T2 preparation for suppression of myocardium and deoxygenized venous blood and fat saturation for nulling of epicardial fat. An alternative technique for improved contrast between coronary vessels and myocardium is magnetization transfer (65). The magnetization transfer pulse saturates myocardium via transfer of magnetization between water and macromolecular protons. Magnetization transfer has potential for the visualization of the coronary veins, as the magnetization transfer pulse leaves venous blood unaffected, which is an advantage as compared to T2 preparation. A recently introduced contrast-free technique for coronary MRA is Dixon-based (**Figures 5 and 6**), which has more consistent and reliable fat suppression as compared to fat-saturated balanced SSFP (66).

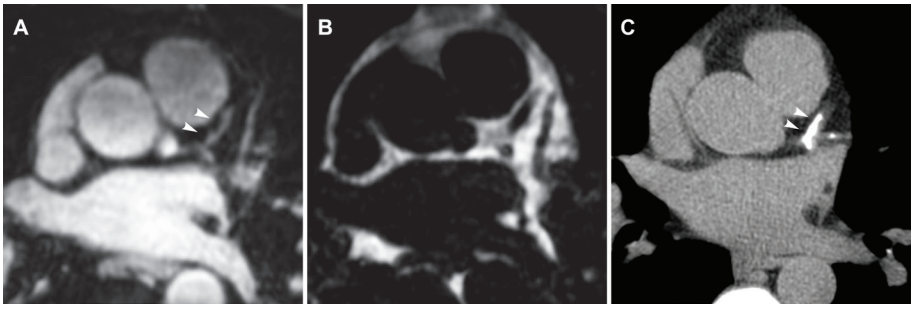

Figure 5. Example of respiratory navigator-gated 3D whole-heart coronary dual-echo Dixon gradient echo (GRE) imaging with water-fat separation: a 57-year-old man with familial hypercholesterolemia and a positive family history for coronary artery disease. (**A**) Transverse Dixon water-image. (**B**) Transverse Dixon fat-image. (**C**) CT image for calcium scoring. Note the severe calcification (arrows) in the left main (LM) coronary artery and proximal left anterior descending (LAD) and left circumflex coronary artery, corresponding to the dark areas on the water-fat resolved Dixon coronary MRA images (arrows).

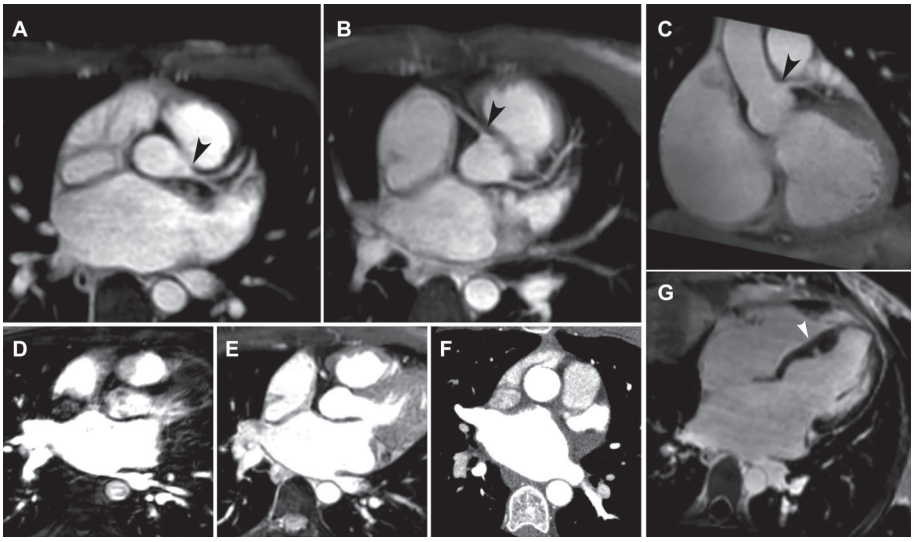

Figure 6. Example of a comprehensive cardiac MR examination prior to catheter ablation for atrial fibrillation: a 38-year-old woman, scheduled for reablation. (**A–C**) Reformatted transverse (A,B) and coronal (C) Dixon water-images for the identification of the left main (LM) coronary artery, which serves as an anatomic landmark for the integration of the MR images with the electro-anatomical maps. Note the origo of the left and right coronary arteries (black arrows). (**D**) Contrast-enhanced MRA of the pulmonary veins for the evaluation for anatomic variants. In this patient, the left upper and lower lobe pulmonary veins have one common ostium into the left atrium, while the right pulmonary veins drain into separate ostia. The presented image shows the left common ostium and the right upper ostium. (**E**) Noncontrast-enhanced Dixon water-image of the ostia of the pulmonary veins. (**F**) For comparison, the contrast-enhanced CT image of the ostia of the pulmonary veins is provided. (**G**) Reformatted 4-chamber late gadolinium enhancement (LGE) for the evaluation of myocardial scar. Note the midventricular septal hypertrophy with a deep myocardial crypt (white arrow).

Coronary vessel wall imaging and plaque characterization

In the research setting, more advanced coronary MRA techniques are explored, including techniques for coronary vessel wall imaging and plaque characterization. The coronary vessel wall can be visualized using nonenhanced, black-blood techniques. Double-IR nulls the signal of flowing blood, rendering a bright vessel wall; the addition of fat suppression improves contrast between outer vessel wall and epicardium (67,68). Measurement of the thickness of the coronary vessel wall may have potential for the detection of subclinical atherosclerosis (69,70).

Vessel wall remodeling and inflammation may be visualized with use of contrast-enhanced techniques. In the carotid arteries, the rate of contrast enhancement on dynamic MRI highly correlates with histological evidence of plaque angiogenesis and macrophage content (71). Also, as confirmed by histologic studies, gadolinium enhancement can discriminate the fibrous cap from the lipid-rich necrotic core, which lacks vasculature and matrix (72). In the coronary arteries, likewise, it has been observed that some plaques express gadolinium uptake, while others do not (73), which may be associated with an expansion of the extracellular volume of the coronary wall as a result of edema or fibrosis, with increased neovascularization and vascular permeability or with endothelial dysfunction. Another study showed that coronary segments with strong delayed gadolinium enhancement resemble the segments with severe atherosclerosis on computed tomography (CT) (74). Others found evidence of increased wall enhancement, probably as a result of inflammatory activity in coronary atherosclerosis, in the acute stage of the acute coronary syndrome, compared to a drop in signal intensity and in extent several months postmyocardial infarction (75). Furthermore, tissue-specific contrast agents have been introduced for detecting disease activity; for instance, USPIO, which is taken up by macrophages within the atherosclerotic plaque (76), fibrin-specific contrast agents for thrombi labeling (77), or elastin-specific contrast agents that detect the increased expression of elastin during plaque development (78).

There are several contrast-free MRI techniques for plaque characterization. Plaque regions can be characterized as fibrocellular, lipid-rich, or calcified, on the basis of biochemical and biophysical parameters, such as chemical composition or molecular motion and diffusion, by using different contrast-weighted techniques (T1-or T2-weighted, proton density, time-of-flight techniques) (79). For instance, coronary thrombus and intraplaque hemorrhage can be identified on noncontrast-enhanced T1-weighted MRI, based on the hyperintense signals as a result of the short T1 relaxation time (80,81).

MRA of the aorta with contrast material

Contrast-enhanced MRA techniques were introduced in the 1990s by Prince (82), to overcome the limitations related to the flow-dependency of noncontrast MRA at that time. The first pass of the contrast bolus through the large arteries is visualized by using a T1-weighted GRE sequence. The short repetition times selectively saturate the surrounding tissue. In contrast, because of the short T1 relaxation time of gadolinium, the blood pool remains unsaturated. The short echo times minimize flow-induced intravoxel dephasing, for example due to turbulent flow in stenosis. A major advantage of contrast-enhanced over noncontrast MRA is the robustness, also when inflow is limited (including slow, retrograde, or turbulent flow), and the short acquisition time, which minimizes motion artifacts and enables breath-holding. Since contrast agent rapidly redistributes into the tissue, additional bolus injections are not that useful. Therefore, an important limitation for spatial coverage and resolution is the short duration of the arterial phase. A pitfall is the timing of the acquisition relative to the timing of the contrast bolus, to ensure a perfect arterial phase without venous enhancement (83). Several methods are recommended for optimized timing: measurement of the time to peak enhancement following injection of a test bolus, based on transaxial images at the level of the distal abdominal aorta; an automated bolus triggering technique; or rapid multi-phase 3D acquisitions without timing (24).

MRA of the aorta without contrast material

Noncontrast MRA sequences can be categorized as inflow-based, flow-encoding, cardiac phase-dependent, or relaxation-based techniques (84-86). First, MRA protocols in the 1980s were noncontrast time-of-fight sequences (inflow-based techniques) (87). Whereas repeated excitation saturates stationary spins, inflowing blood spins with fresh longitudinal magnetization generate high signal intensity. In contrast to vessels with continuous laminar flow, in vessels with slow, retrograde, or turbulent flow blood, spins within the slice become partially saturated. Contamination by high signal of inflowing venous blood can be minimized by presaturation of the upstream venous region. Whereas time-of-flight techniques are still widely used in intracranial angiography, it is less suitable for peripheral arteries (the transverse instead of craniocaudal acquisition prolongs the acquisition time) and thoracic aorta (the complex anatomy makes it prone to in-plane signal loss).

An inflow-based alternative developed in the 1980s is phase-contrast MRA (88). Flowing blood, in contrast to stationary tissue, acquires a substantial phase change as the result of bipolar velocity-encoding gradients. As the signal intensity is proportional to the velocity of flowing blood, phase-contrast MRA can be used to extract additional hemodynamic information (89). Compared to the time-of-flight method, phase-contrast MRA results in superior background suppression. Its clinical use for MRA of the aorta, however, is limited by the relatively long acquisition time and the reduced signal intensity in relation to pulsatile blood flow.

Figure 7. Example of noncontrast-enhanced MRA of the aorta: a 34-year-old man, diagnosed with Marfan's disease. (**A,B**) Reformatted sagittal Dixon fat-image (A) and water-image (B) along the thoracic aorta. (**C**) 3D visualization based on Dixon-water MRA of the aorta. (**D,E**) Conventional black-blood MRA of the aorta. Note the flow artifacts, due to inadequate suppression of in-plane flow (arrows). (**F,G**) Conventional cine balanced steady-state free precession (SSFP) for measurement of the aortic root dimensions.

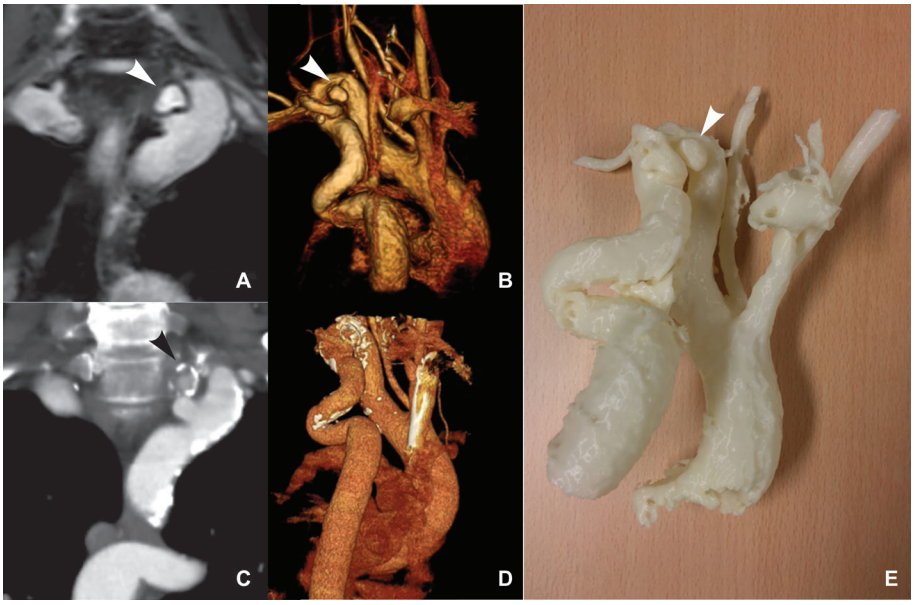

Figure 8. Example of noncontrast-enhanced water-fat resolved Dixon MRA of the thoracic aorta: a 66-year-old man, known with a cervical aortic arch (type C: left cervical arch with right-sided looping descending aorta). (**A,B**) Dixon water-image: (A) enlarged coronal view of the cervical aortic arch and (B) posterior view of the 3D visualization of the aorta. Note the aneurysm at the cervical loop (white arrows) (**C,D**). For comparison, contrast-enhanced CT images are provided: (C) enlarged coronal view. Note the calcified wall of the aneurysm (black arrow); (D) posterior view of the 3D visualization. (**E**) Posterior view of the 3D print, based on Dixon MRA of the aorta.

A novel inflow-based technique is quiescent-interval slice-selective (QISS) MRA, which is a 2D ECG-gated single-or two-shot balanced SSFP acquisition with slice-selective IR preparation for suppression of background tissue (90). Saturation of the image slice is timed at the beginning of the systole, followed by a quiescent inflow period in the systolic phase, with the balanced SSFP acquisition during diastole. Given the relatively long inflow period and the timing during systole, the refreshment effect in QISS is high compared to the conventional time-of-flight technique. As QISS acquires a complete slice per cardiac cycle, QISS has a relatively short acquisition time. The inflow effect is less dependent on blood flow velocity, flow patterns, and heart rate. A drawback of QISS is the dependency on magnetic field homogeneity, as it is a balanced SSFP-based acquisition. A cardiac-phase-dependent technique is ECG-gated 3D partial-Fourier fast spin echo (FSE) (91). Imaging is based on the physiological difference in systolic and diastolic blood flow velocity. Spins are repeatedly refocused during the echo train. Fast-flowing blood in the arterial phase results in loss of signal, whereas slow flow in the diastole causes high signal intensity. Bright-blood MRA is generated by subtraction of the systolic and diastolic acquisition. To reduce the total scan time, commonly one or two shots per slice are

used. T2 blurring is minimized by shortening of the echo train length using a partial-Fourier echo train. ECG-gated 3D partial-Fourier FSE is extensively applied, given the large craniocaudal coverage and the insensitivity to magnetic field inhomogeneities. A drawback for thoracic aortic MRA is the susceptibility to artifacts caused by the multidirectional flow patterns.

Balanced SSFP is a relaxation-based technique. Image contrast relies on the difference in T2/T1 relaxation times between blood and surrounding tissue. Typically, 3D balanced SSFP is combined with an IR preparation pulse. With an appropriate TI, background tissue is nulled, and inflowing blood from outside the IR-prepared volume is visualized with high signal intensity. Balanced SSFP has little dependence on blood flow, which makes it less prone to artifacts. Furthermore, respiratory navigator-gated 3D dual-echo Dixon GRE with water–fat separation, which has been reported in the literature for coronary artery imaging, can be used for the visualization of the aorta as well (**Figures 7 and 8**) (66).

New promising techniques

MYOCARDIAL ARTERIAL SPIN LABELING. Myocardial arterial spin labeling (ASL) has been studied as a contrast-free alternative to first-pass perfusion imaging (92). Arterial spins are magnetically labeled, thereby creating an endogenous tracer. Subtraction of the images with and without prior labeling of inflowing blood results in signal intensities that are proportional to myocardial blood flow. Contrary to first-pass perfusion imaging, which visualizes relative signal intensities across the ventricle, ASL enables absolute quantification of myocardial blood flow. ASL is still challenging and limited to the research domain. Only relatively small signal changes can be achieved with the labeling. Given the pulsatile blood flow, the labeling pulse and image acquisition need to be synchronized to the cardiac cycle. Also, interfering effects of cardiac motion and the multidirectional blood flow complicate adequate selection of the labeling volume.

Myocardial ASL can be performed using flow-sensitive alternating inversion recovery (FAIR), in which labeling and imaging is timed at mid-diastole in consecutive heartbeats, or with the more recent steady-pulsed ASL (spASL) technique, in which the timing is in end-systole and mid-diastole, respectively. Although spASL is more efficient, a drawback is its sensitivity to errors in ECG triggering and variability in heart rate. Recently, the first steps have been made towards clinical utility. Zun et al (93) performed myocardial rest and stress ASL in patients with and without ischemia based on first-pass perfusion MRI and X-ray coronary angiography. In patients without ischemia, myocardial ASL was capable of detecting clinically significant increases in myocardial blood flow after adenosine stress compared to rest. In the ischemic patients, myocardial perfusion reserve was found to be decreased in the most remote ischemic segments compared to healthy myocardium. For diagnosis of ischemia in the individual patient, however, several complex technical issues remain to be resolved, including the insufficient SNR at rest when myocardial blood flow is low.

DIFFUSION MRI. Cardiac diffusion tensor imaging (DTI) is a contrast-free technique that allows assessment of myocardial fiber structure in healthy and infarcted myocardium (94). Commonly, cardiac DTI is performed with up to 16 diffusion-encoding direction. To increase SNR, several acquisitions are averaged after spatiotemporal registration. The helix angle is used as a measure of myocardial fiber organization, which is defined as the inclination of the myocardial fibers out of the local radial plane. Whereas in the normal heart, the fiber architecture is highly coherent, infarction results in severe fiber disarrangement with high anisotropy. Chronic infarction is characterized by substantial loss of myocardial fibers in the infarct zone and a network of residual fibers propagating from border to core zone. In contrast to DTI of the brain, DTI of the heart is still limited to the research setting, due to technical challenges (including cardiac and respiratory motion, short myocardial T2, and magnetic field inhomogeneity) and long acquisition times (free-breathing whole-heart DTI is in the range of 15 minutes) (95).

CLINICAL INDICATIONS

Myocardial infarction

LATE GADOLINIUM ENHANCEMENT. LGE can be used to identify the location and the extent of irreversible injury of both acute and chronic myocardial infarction, with high accuracy and reproducibility (25). There is a close link in spatial delineation by LGE on cardiac MRI and myocardial necrosis or collagenous scar on histology, confirmed at various timepoints after infarction. LGE is capable of the detection of small subendocardial infarcts, given the high spatial resolution, which, in contrast to transmural infarcts, are systematically missed by single photon emission computed tomography (SPECT) (96,97). In patients with myocardial infarction, the extent of scarring as identified by LGE is a strong predictor for all-cause mortality and cardiac death (98). Likewise, in patients with known or suspected coronary artery disease, but without known prior myocardial infarction, the presence of LGE is a strong predictor of major adverse cardiovascular endpoints, even when taking into account the traditional clinical, angiographic, and functional variables, including the LV ejection fraction (99). Furthermore, studies confirmed an inverse relation between LGE transmurality and contractile response to pharmacological stress (100). In general, segments with less than 50% transmurality can be considered viable, and more than 10 viable segments indicate a high likelihood of recovery of cardiac function after revascularization (101). A reduction in the extent of LGE early after infarction can be interpreted as an early restoration of blood flow and is associated with functional improvement (102). In contrast, LGE in the infarct zone shortly after revascularization is an independent predictor of impaired LV systolic thickening and remodeling (103).

When performing LGE imaging after reperfusion therapy, there may be areas with lack of contrast within the hyperenhanced areas ("no-reflow" phenomenon) (**Figure 9**). This

observation has been explained as microvascular obstruction. Due to strong, prolonged impairment of myocardial perfusion as a result of microthrombi and swelling of ischemic tissue, contrast wash-in becomes severely impaired (104). More recently, however, evidence has been found that the hypoenhanced areas within the infarct core are not related to microvascular obstruction, but to severe microvascular injury and intramyocardial hemorrhage. Histologic assessment of an in vivo porcine model of reperfused ST-segment-elevation myocardial infarction (STEMI) showed in the hypointense areas severe disruption of the endothelial cells with extravasated erythrocytes, whereas the areas surrounding the infarct core showed an intact microvasculature with microthrombi (the true anatomical location of microvascular obstruction) (105). In view of above findings, studies have been performed on the prognostic value of intramyocardial hemorrhage, as assessed on T2 and T2* maps, in reperfused STEMI. Intramyocardial hemorrhage showed a closer association with adverse outcome, compared to microvascular obstruction, as assessed on LGE images (106).

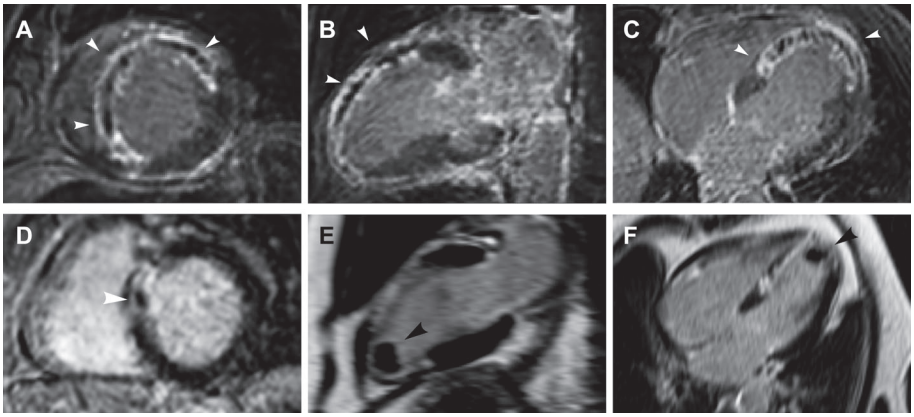

Figure 9. Example of 2D late gadolinium enhancement (LGE) images showing hypoenhanced areas in acute myocardial infarction after reperfusion therapy (white arrows). (**A–C**) an 81-year-old man, with a recent anteroseptal myocardial infarction and stenting of the left anterior descending (LAD) coronary artery. (**D–F**) a 65-year-old man, with a recent anteroseptal infarction and balloon dilating of the LAD. Note the thrombus formation in left ventricular apex (black arrows).

In the research setting, several other LGE-based variables have been studied that may have potential for clinical use. For instance, core and border zone characteristics may have potential for risk stratification for mortality in postinfarction patients (107). Border zone (peri-infarct zone) refers to areas with "intermediate" LGE intensity. Those regions consist of a mixture of healthy and diseased myocytes, which may represent a substrate for ventricular arrhythmia (108). Several definitions exist; for instance, the regions with an LGE intensity level between 2 to 3 standard deviations above the reference remote myocardial region or those with a signal intensity between 35–50% of the maximum in the infarct core. Another more advanced application, requiring high expert knowledge, is scar identification in the right ventricle (RV) and in the thin walls of the atria. Furthermore, recent work shows promise for early gadolinium enhancement for the detection of the areas at risk, marking both the reversibly and irreversibly injured myocardium based on an increase in extracellular volume (109). In contrast, conventional LGE provides information on the extent of infarcted myocardium, but does not provide information on the characteristics of viable myocardium; for instance, how well it will adapt to the increased work load and whether it is at risk for additional scarring.

NATIVE T1 MAPPING AND EXTRACELLULAR VOLUME MAPPING. Native T1 mapping may provide comparative information as the established LGE technique (110). Both acute and chronic myocardial infarcts may be identified on native T1 maps, as a result of edema and replacement fibrosis, respectively, with infarcts having higher native T1 relaxation times. Furthermore, when using native and postcontrast T1 mapping, acute and chronic infarcts may be differentiated on the basis of different patterns of contrast-induced T1 shortening. Possibly, this is due to a significant increase in distribution volume in acute necrosis and a smaller expansion of extracellular space in the chronic stage with scarring (111). ECV mapping has been shown to be significantly different in infarct tissue (51 ± 8%) compared to normal myocardium (27 ± 3%). A potential advantage, compared to conventional LGE images, is the additional information, beyond the binary information provided by LGE. ECV mapping has been shown to have potential for tracing subclinical abnormalities in non-LGE myocardium remote from infarcted areas (112).

A drawback is that native T1 and ECV mapping for ischemic cardiomyopathy is not that robust and artifact-free yet, as compared to LGE, and it seems difficult to determine the threshold values for abnormal and normal native T1 and ECV. Also, T1 mapping needs to be performed with sufficient spatial resolution to determine the infarct's transmurality.

Myocardial ischemia

STRESS PERFUSION AND STRESS WALL MOTION IMAGING. Current guidelines consider ischemia testing by cardiac MRI appropriate in patients with an intermediate likelihood of obstructive coronary artery disease, in patients with resting ECG abnormalities,

an uninterpretable ECG, or those incapable of exercise for stress ECG. High-risk patients should undergo invasive angiography directly (101). Cardiac MR stress perfusion imaging shows superior results compared to SPECT for the diagnosis of ischemia (113,114) and for the prediction of major adverse cardiac events (115). A meta-analysis on the diagnostic value of cardiac MR stress perfusion imaging for coronary artery disease showed, per-patient level, a sensitivity and specificity of 91% and 81%, respectively (116). A meta-analysis of dobutamine-stress wall motion cardiac MRI showed a sensitivity of 83% and specificity of 86% for the detection of coronary artery disease on a per-patient level (116). Also, dobutamine-stress wall motion in patients with resting akinetic wall segments can identify those who will improve in systolic function after revascularization (117,118). Regarding the prognostic value of abnormal adenosine-stress perfusion and dobutamine/atropine-stress wall motion, a 3-year event-free survival of 83.5% was reported, compared to 99.2% in patients with known or suspected coronary artery disease but with normal stress perfusion and stress wall motion imaging (119).

There is one study comparing both adenosine-stress perfusion and dobutamine/atropine wall motion imaging to invasive coronary angiography. Dobutamine-stress wall motion was superior to adenosine-stress perfusion, based on superior specificity (80% compared to 62%) (as it detects only patients with high-grade perfusion deficits) and comparable sensitivity (89% compared to 91%) (120). Most of the evidence regarding the diagnostic accuracy of stress perfusion and stress wall motion imaging is in individual studies, with various combinations in the studied image modality and stress agent, in different patient populations. Whether stress wall motion or stress perfusion imaging is preferable in under debate, and it is recommended that the method be used in which there is local expertise (53). Since stress imaging myocardium is typically combined with a LGE module, the patient will receive contrast material during the MR examination, even if stress wall motion imaging is chosen over stress perfusion imaging. If contrast material has already been administered for perfusion imaging (for example, 0.05 mmol/lg for stress and rest perfusion), an additional dose is given, to come to a total dose of 0.1–0.2 mmol/kg for LGE imaging (24).

NATIVE T1 MAPPING. Recently, there have been studies that may suggest that ischemia detection may be possible without contrast administration. Liu et al (121) showed that native T1 remains unchanged in infarcted tissue in response to adenosine stress, while there is an increase in native T1 in healthy tissue because of vasodilation (**Figure 10**). The principle lies in native T1 as a measure of myocardial blood volume and myocardial water content. The authors were able to distinguish normal, infarcted, ischemic, and remote myocardium, based on T1 mapping during adenosine vasodilatory stress and rest.

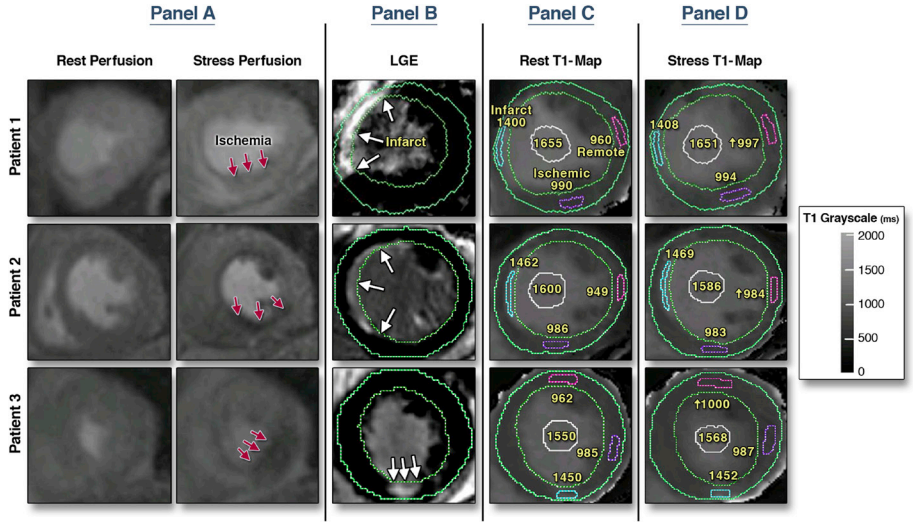

Figure 10. Example of noncontrast-enhanced myocardial perfusion based on native T1 measurements at rest and during adeno-sine stress. Ischemic areas can be identified on stress T1 mapping based on nonsignificant T1 reactivity, related to the absence of increased myocardial blood volume. Reprinted from Liu et al (121) under the terms of the Creative Commons Licence.

Nonischemic cardiomyopathy

LATE GADOLINIUM ENHANCEMENT. Although LGE is primarily performed in the context of ischemic heart disease, it is of significant clinical value in nonischemic cardiomyopathy as well. The different types of cardiomyopathy show typically different LGE patterns (**Figure 11**) (122). Ischemic cardiomyopathy is characterized by subendocardial and/or transmural LGE, whereas isolated midwall or subepicardial enhancement, not corresponding to any known coronary perfusion territory, is suggestive of nonischemic cardiomyopathy (123). For hypertrophic cardiomyopathy (HCM), LGE is seen at the junctions of the septum and RV free wall and in severely hypertrophic areas (124), most likely related to disorganized myocardial tissue and/or demand ischemia. For dilated cardiomyopathy (DCM), a typical finding is LGE midwall enhancement (125). Comparable to ischemic heart disease, the presence of LGE in HCM (126) and DCM (127) has strong predictive value for adverse cardiac events. Furthermore, amyloidosis (128) and sarcoidosis (129) can be identified based on diffuse subendocardial enhancement and more focal enhancement, respectively. In myocarditis, LGE can be observed in the lateral free wall (midwall and subepicardal enhancement) (130). LGE in the RV is typical for arrhythmogenic RV cardiomyopathy (ARVC) (131) and in Chagas disease (132).

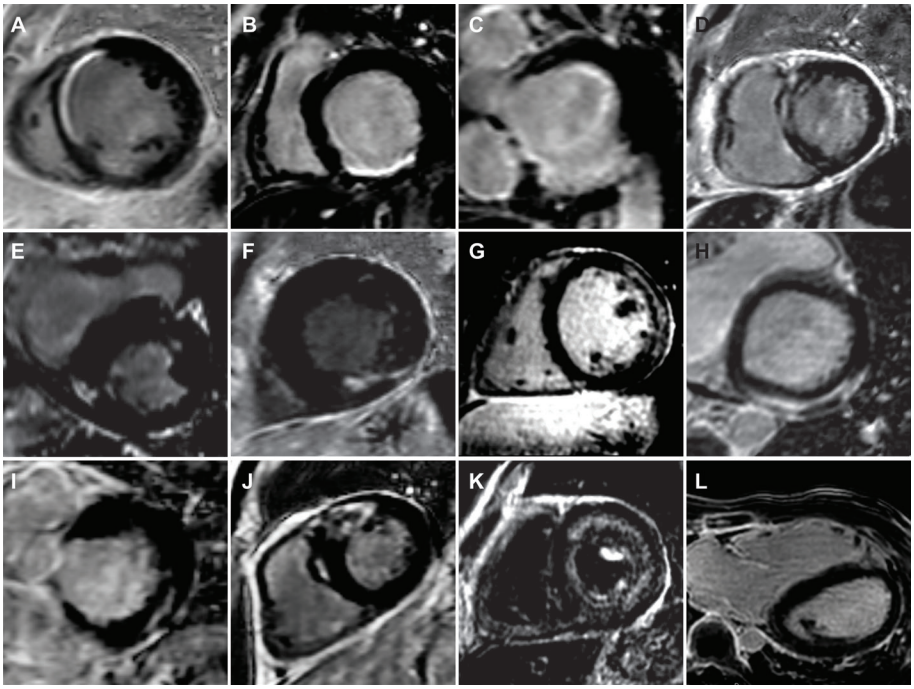

Figure 11. Examples of typical patterns of late gadolinium enhancement (LGE) in ischemic and nonischemic cardiomyopathy (A– K: 2D short-axis LGE images; L: 2D transverse LGE image). (**A**) Chronic subendocardial anteroseptal infarction, related to occlusion of the left anterior descending (LAD) coronary artery. (**B**) Chronic subendocardial inferior infarction, due to an occluded right coro-nary artery (RCA). (**C**) Transmural inferior infarction. (**D**) Dilated cardiomyopathy (DCM) with midwall LGE. (**E,F**) Hypertrophic car-diomyopathy (HCM) with typical LGE at the insertion points of the right ventricle (E) or in the hypertrophic areas (F). (**G,H**) Myocarditis with midwall (G) or subendocardial (H) LGE in the lateral free wall. (**I,J**) Sarcoidosis with typical focal LGE. (**K**) Amyloidosis with typical diffuse subendocardial LGE. (**L**) Arrhythmogenic right ventricular cardiomyopathy (ARVC), with typical LGE in the right ventricle.

NATIVE T1 MAPPING AND EXTRACELLULAR VOLUME MAPPING. Native T1 values have been shown to be increased in diffuse myocardial fibrosis in various nonischemic cardiomyopathies and amyloidosis, and reduced by lipid infiltration (Anderson-Fabry disease) or iron overload compared to normal myocardium (133). Interesting proof of native T1 mapping as an alternative to conventional contrast-based imaging protocols is the evaluation of acute myocarditis. While the standard criteria for diagnosis include early and late gadolinium enhancement criteria, Luetkens et al (134) showed that native T1 mapping even has superior diagnostic performance. Based on cellular edema, myocyte necrosis, and increased extracellular space, the T1 relaxation time is significantly prolonged in acute myocarditis.

A unique feature of ECV mapping, contrary to LGE, is the ability to detect diffuse changes in myocardial tissue. The technique is not dependent on spatial variation in fibrosis across the myocardium and does not need normal tissue as an internal reference. Edema, fibrosis, or amyloid, etc., result in an increase in ECV values. Several studies showed a correlation between ECV measured by cardiac MRI and histology (135). ECV has been associated with adverse outcome, in some cohorts even outperforming LV ejection fraction (136), and can therefore be regarded as an intrinsic myocardial characteristic.

Cardiac masses (including thrombus)

Using cardiac MRI, location, functional characteristics, and tissue composition of a cardiac mass can be evaluated, to dis-criminate benign and malignant tumors and to differentiate cardiac tumor from intracardiac thrombus (137). A typical MR examination for cardiac mass consists of T1-weighted FSE images for assessment of location and size, a T2-weighted FSE sequence with fat suppression for evaluation of edema and fibrosis within the cardiac mass, followed by first-pass perfusion imaging, postcontrast T1-weighted FSE with fat suppression, and LGE imaging (24). Based on the absence of contrast uptake, nonvascularized thrombus can be differentiated from tumor. Postcontrast serial imaging will help to differentiate a hypoperfused necrotic core from thrombus.

Lipoma can be recognized by low signal intensity on T2-weighted images, a dropout in signal intensity on T1-weighted images when using fat saturation, and no delayed enhancement. Myxoma and fibroma can be distinguished by high versus low T2-weighted signal and heterogeneous versus intense delayed enhancement, respectively. In general, malignant tumors have an irregular and invasive border and are of considerable size. Location in the right atrial wall or presence of pericardial effusion is suspicious for malignancy. Myxomas and fibromas may contain small calcifications, whereas large calcified foci are typical for osteosarcoma (137). A recent study showed the potential of T1 and T2 mapping to provide discriminative diagnostic information as an alternative to conventional T1-and T2-weighted images combined with LGE imaging (for example, for the diagnosis of papillary fibroelastomas) (138).

Coronary arteries

Coronary MRA (with or without contrast material) is considered appropriate for identifying coronary artery anomalies and aneurysm and for determining coronary artery patency, but is not appropriate for the detection of single-vessel disease (101). The first multicenter study on the diagnostic performance of coronary MRA for coronary artery disease was published by Kim et al in 2001 (139). The authors showed high specificity for the detection of left main coronary or three-vessel disease (100%), but insufficient sensitivity (85%) for ruling out coronary artery disease. They used a contrast-free GRE sequence, with a target volume approach consisting of repeated acquisitions of 3D double-oblique 3 cm volumes along the coronary arteries, with an

average scanning time of 70 minutes. Despite technical improvements in coronary MRA since then (140), and despite the insusceptibility to calcification in contrast to the blooming artifacts on CTA (141), the limited spatial resolution and long acquisition time render MR still inferior to CT for the assessment of coronary stenosis (142).

There are few studies comparing the diagnostic performance of coronary MRA with and without contrast material. A comparison between 3T GRE coronary MRA with slow infusion of contrast material and 1.5T noncontrast balanced SSFP coronary MRA in healthy volunteers resulted in higher CNR and superior visualization of the coronary segments for the contrast-enhanced compared to the noncontrast approach (143). Several studies compared image quality when using an extracellular or intravascular gadolinium chelate for coronary MRA. The intravascular agent gadofosveset trisodium shows slightly better or comparable performance (33,63,144).

Large vessels

Studies showed agreement in measured aortic diameter between contrast-enhanced MRA and unenhanced 3D balanced SSFP and equal sensitivity and specificity for the diagnosis of thoracic aorta pathologies (145). 3D balanced SSFP shows even better visualization of the aortic root and higher SNR and CNR for all segments (146). For peripheral MRA, contrast-enhanced MRA, compared to ECG-gated 3D partial-Fourier FSE, is superior in terms of robustness (fewer artifacts) and diagnostic accuracy for detection of stenosis (147,148).

For the evaluation of pulmonary veins pre-and postablation for atrial fibrillation (**Figure 6**), both contrast-enhanced MRA and noncontrast balanced SSFP have been proven to be accurate regarding detection of anatomic variants and measurement of pulmonary vein diameters (149). As signal void artifacts may occur due to off-resonance effects in non-contrast pulmonary vein imaging (150) and because the clinical MRI exam pre-and postablation typically includes LGE imaging for the evaluation of myocardial scar, in general, contrast-enhanced pulmonary vein MRA is used in clinical practice (24).

CONCLUSION

Contrast material in cardiac MRI should be used for tissue characterization in ischemic and nonischemic cardiomyopathy and may be used for stress perfusion imaging for the detection of ischemia. In cardiac-related vascular MRI, use of contrast material should be avoided, unless high-quality angiography is required that cannot be obtained with non-contrast protocols.

In general, noncontrast protocols should be preferred over contrast-enhanced techniques if the diagnostic performance is comparable. In all patients, dosage should be as low as possible. Differences between the available contrast agents in terms of chemical stability, relaxivity, and intravascular residence time may guide the choice of contrast agent. Gadolinium-

based contrast material in cardiac MRI should be avoided in patients with previous severe hypersensitivity reactions. Specific guidelines are available for the use of contrast material in patients with reduced renal function, in pregnant or lactating women, and in children. In patients at risk of impaired renal function, renal function should always be tested.

Cardiac structure and function is assessed by balanced SSFP cine imaging. Balanced SSFP generates an intrinsic high contrast between blood and myocardium based on the differences in the T2/T1 ratio. Velocity of flow across the valves can be measured using phase-contrast techniques. LGE imaging for myocardial scar visualization has been thoroughly validated in histological studies and the prognostic value of LGE has been confirmed in a variety of patient groups, in both acute and chronic stages of myocardial infarction and in nonischemic cardiomyopathy. Stress testing for ischemia can be performed with contrast-based first-pass imaging or contrast-free wall motion imaging. The choice of technique should depend on the local expertise available. Contrast-free native T1 mapping and contrast-based ECV mapping show promise for the evaluation of ischemic and nonischemic cardiomyopathy and may even provide additional information over conventional LGE imaging. However, prospective studies, against the standard of care, are needed to show whether these techniques represent alternatives to the current cardiac MR protocols in clinical routine. Contrast-enhanced and noncontrast MRA protocols are avail-able for the visualization of the coronary arteries and large vessels. For atherosclerotic plaque characterization in a research setting, contrast material can be of additive value.

In conclusion, the majority of cardiac MRI examinations rely on gadolinium-based contrast material, but a range of exciting noncontrast alternatives with high potential for clinical application are under development.

REFERENCES

1. Bruder O, Wagner A, Lombardi M, et al. European Cardiovascular Magnetic Resonance (EuroCMR) registry--multinational results from 57 centers in 15 countries. J Cardiovasc Magn Reson 2013;15:9.
2. American College of Radiology. ACR Manual on Contrast Media version 10.2 2016; https://www.acr.org/Quality-Safety/Resources/Contrast-Manual. Last accessed April 3, 2017.
3. European Society of Urogenital Radiology. ESUR Guidelines on Contrast Media 2012; http://www.esur.org/guidelines. Last accessed April 3, 2017.
4. U.S. Food and Drug Administration. Information for Healthcare Professionals: Gadolinium-Based Contrast Agents for Magnetic Resonance Imaging 2007; https://www.fda.gov/Drugs/DrugSafety/PostmarketDrugSafetyInformationforPatientsandProviders/ucm142884.htm. Last accessed April 3, 2017.
5. European Medicines Agency. Assessment report for Gadolinium-containing contrast agents 2010; http://www.ema.europa.eu/docs/en_GB/document_library/ Referrals_document/gadolinium_31/WC500099538.pdf. Last accessed April 3, 2017.
6. Reimer P, Vosshenrich R. Off-label use of contrast agents. Eur Radiol 2008;18:1096–1101.
7. U.S. Food and Drug Administration. "Off-label" and investigational use of marketed drugs, biologics and medical devices 2016; http://www.fda.gov/Regulatory Information/Guidances/ucm126486.htm. Last accessed December 1, 2016.
8. Wittich CM, Burkle CM, Lanier WL. Ten common questions (and their answers) about off-label drug use. Mayo Clin Proc 2012;87:982–990.
9. Prince MR, Zhang H, Zou Z, Staron RB, Brill PW. Incidence of Immediate Gadolinium Contrast Media Reactions. Am J Roentgenol 2011;196:W138–W143.
10. Bruder O, Schneider S, Pilz G, et al. 2015 Update on Acute Adverse Reactions to Gadolinium based Contrast Agents in Cardiovascular MR. Large Multi-National and Multi-Ethnical Population Experience With 37788 Patients From the EuroCMR Registry. J Cardiovasc Magn Reson 2015;17:58.
11. Jung J-W, Kang H-R, Kim M-H, et al. Immediate Hypersensitivity Reaction to Gadolinium-based MR Contrast Media. Radiology 2012;264:414–422.
12. Granata V, Cascella M, Fusco R, et al. Immediate Adverse Reactions to Gadolinium-Based MR Contrast Media: A Retrospective Analysis on 10,608 Examinations. Biomed Res Int 2016;2016:1–6.
13. Cowper SE, Robin HS, Steinberg SM, Su LD, Gupta S, LeBoit PE. Scleromyxoedema-like cutaneous diseases in renal-dialysis patients. Lancet 2000;356:1000–1001.
14. Todd DJ, Kay J. Gadolinium-Induced Fibrosis. Annu Rev Med 2016;67:273–291.
15. Prince MR, Zhang HL, Prowda JC, Grossman ME, Silvers DN. Nephrogenic systemic fibrosis and its impact on abdominal imaging. Radiographics 2009;29:1565–1574.
16. Reiter T, Ritter O, Prince MR, et al. Minimizing Risk of Nephrogenic systemic fibrosis in Cardiovascular Magnetic Resonance. J Cardiovasc Magn Reson 2012;14:31.
17. Kanda T, Ishii K, Kawaguchi H, Kitajima K, Takenaka D. High signal intensity in the dentate nucleus and globus pallidus on unenhanced T1-weighted MR images: relationship with increasing cumulative dose of a gadolinium-based contrast material. Radiology 2014;270:834–841.
18. Kanda T, Fukusato T, Matsuda M, et al. Gadolinium-based Contrast Agent Accumulates in the Brain Even in Subjects without Severe Renal Dysfunction: Evaluation of Autopsy Brain Specimens with Inductively Coupled Plasma Mass Spectroscopy. Radiology 2015;276:228–232.
19. McDonald RJ, McDonald JS, Kallmes DF, et al. Intracranial Gadolinium Deposition after Contrast-enhanced MR Imaging. Radiology 2015;275:772–782.
20. Radbruch A. Are some agents less likely to deposit gadolinium in the brain? Magn Reson Imaging 2016;34:1351–1354.
21. U.S. Food and Drug Administration. FDA Drug Safety Communication: New warnings for using gadolinium-based contrast agents in patients with kidney dysfunction 2010; https://www.fda.gov/Drugs/DrugSafety/ucm223966.htm. Last accessed April 3, 2017.
22. Fraum TJ, Ludwig DR, Bashir MR, Fowler KJ. Gadolinium-based contrast agents: A comprehensive risk assessment. J Magn Reson Imaging 2017;
23. Nacif MS, Arai AE, Lima JAC, Bluemke D. Gadolinium-enhanced cardiovascular

magnetic resonance: administered dose in relationship to United States Food and Drug Administration (FDA) guidelines. J Cardiovasc Magn Reson 2012;14:18.
24. Kramer CM, Barkhausen J, Flamm SD, Kim RJ, Nagel E. Standardized cardiovascular magnetic resonance (CMR) protocols 2013 update. J Cardiovasc Magn Reson 2013;15:91.
25. Kim RJ, Albert TSE, Wible JH, et al. Performance of Delayed-Enhancement Magnetic Resonance Imaging With Gadoversetamide Contrast for the Detection and Assessment of Myocardial Infarction: An International, Multicenter, Double-Blinded, Randomized Trial. Circulation 2008;117:629–637.
26. Wolff SD, Schwitter J, Coulden R, et al. Myocardial first-pass perfusion magnetic resonance imaging: a multicenter dose-ranging study. Circulation 2004;110:732–737.
27. Giang TH, Nanz D, Coulden R, et al. Detection of coronary artery disease by magnetic resonance myocardial perfusion imaging with various contrast medium doses: First european multi-centre experience. Eur Heart J 2004;25:1657–1665.
28. Gibby WA. MRI contrast agents. Zimmerman RA, Gibby WA, Carmody RF, editors. In: Neuroimaging: Clinical and Physical Principles. New York: Springer; 2000. p 313–364.
29. Port M, Idée J-M, Medina C, Robic C, Sabatou M, Corot C. Efficiency, thermodynamic and kinetic stability of marketed gadolinium chelates and their possible clinical consequences: a critical review. BioMetals 2008;21:469–490.
30. Lohrke J, Frenzel T, Endrikat J, et al. 25 Years of Contrast-Enhanced MRI: Developments, Current Challenges and Future Perspectives. Adv Ther 2016;33:1–28.
31. Wildgruber M, Stadlbauer T, Rasper M, et al. Single-Dose Gadobutrol in Comparison With Single-Dose Gadobenate Dimeglumine for Magnetic Resonance Imaging of Chronic Myocardial Infarction at 3 T. Invest Radiol 2014;49:728–734.
32. Hartmann M, Wiethoff AJ, Hentrich H-R, Rohrer M. Initial imaging recommendations for Vasovist angiography. Eur Radiol 2006;16 Suppl 2:B15-23.
33. Raman FS, Nacif MS, Cater G, et al. 3.0-T whole-heart coronary magnetic resonance angiography: comparison of gadobenate dimeglumine and gadofosveset trisodium. Int J Cardiovasc Imaging 2013;29:1085–1094.
34. Li W, Tutton S, Vu AT, et al. First-pass contrast-enhanced magnetic resonance angiography in humans using ferumoxytol, a novel ultrasmall superparamagnetic iron oxide (USPIO)-based blood pool agent. J Magn Reson Imaging 2005;21:46–52.
35. Hope MD, Hope TA, Zhu C, et al. Vascular Imaging With Ferumoxytol as a Contrast Agent. Am J Roentgenol 2015;205:W366–W373.
36. Finn JP, Nguyen K-L, Han F, et al. Cardiovascular MRI with ferumoxytol. Clin Radiol 2016;71:796–806.
37. Schiller B, Bhat P, Sharma A. Safety and Effectiveness of Ferumoxytol in Hemodialysis Patients at 3 Dialysis Chains in the United States Over a 12-Month Period. Clin Ther 2014;36:70–83.
38. Nguyen K-L, Yoshida T, Han F, et al. MRI with ferumoxytol: A single center experience of safety across the age spectrum. J Magn Reson Imaging 2017;45:804–812.
39. Thiele H, Nagel E, Paetsch I, et al. Functional cardiac MR imaging with steady-state free precession (SSFP) significantly improves endocardial border delineation without contrast agents. J Magn Reson Imaging 2001;14:362–367.
40. Dyverfeldt P, Bissell M, Barker AJ, et al. 4D flow cardiovascular magnetic resonance consensus statement. J Cardiovasc Magn Reson 2015;17:72.
41. Kim RJ, Chen E-L, Lima JAC, Judd RM. Myocardial Gd-DTPA Kinetics Determine MRI Contrast Enhancement and Reflect the Extent and Severity of Myocardial Injury After Acute Reperfused Infarction. Circulation 1996;94:3318–3326.
42. Young IR, Bailes DR, Bydder GM. Apparent changes of appearance of inversion-recovery images. Magn Reson Med 1985;2:81–85.
43. Noll DC, Nishimura DG, Macovski A. Homodyne detection in magnetic resonance imaging. IEEE Trans Med Imaging 1991;10:154–163.
44. Kellman P, Arai AE, McVeigh ER, Aletras AH. Phase-sensitive inversion recovery for detecting myocardial infarction using gadolinium-delayed hyperenhancement. Magn Reson Med 2002;47:372–383.
45. Bizino M, Amersfoort J, Tao Q, van der Geest RJ, Lamb HJ. Free-breathing 3D phase-sensitive inversion recovery late gadolinium enhancement at 3.0 Tesla: reliability and image quality in ischemic and non-ischemic cardiomyopathy in comparison with multiple breath-hold 3D imaging. J Cardiovasc Magn Reson 2015;17:P97.
46. Piehler KM, Wong TC, Puntil KS, et al. Free-

Breathing, Motion-Corrected Late Gadolinium Enhancement Is Robust and Extends Risk Stratification to Vulnerable Patients. Circ Cardiovasc Imaging 2013;6:423–432.
47. Varga-Szemes A, van der Geest RJ, Spottiswoode BS, et al. Myocardial Late Gadolinium Enhancement: Accuracy of T1 Mapping–based Synthetic Inversion-Recovery Imaging. Radiology 2016;278:374–382.
48. Gould KL, Lipscomb K. Effects of coronary stenoses on coronary flow reserve and resistance. Am J Cardiol 1974;34:48–55.
49. Rieber J. Cardiac magnetic resonance perfusion imaging for the functional assessment of coronary artery disease: a comparison with coronary angiography and fractional flow reserve. Eur Heart J 2005;27:1465–1471.
50. Al-Saadi N, Nagel E, Gross M, et al. Noninvasive Detection of Myocardial Ischemia From Perfusion Reserve Based on Cardiovascular Magnetic Resonance. Circulation 2000;101:1379–1383.
51. Schaefer S, Tyen R Van, Saloner D. Evaluation of myocardial perfusion abnormalities with gadolinium-enhanced snapshot MR imaging in humans. Work in progress. Radiology 1992;185:795.
52. Baer FM, Voth E, Theissen P, Schicha H, Sechtem U. Gradient-echo magnetic resonance imaging during incremental dobutamine infusion for the localization of coronary artery stenoses. Eur Heart J 1994;15:218–225.
53. Nagel E. Moving Toward the Optimal Test for the Assessment of Myocardial Ischemia. J Am Heart Assoc 2016;5:e003266.
54. Taylor AJ, Salerno M, Dharmakumar R, Jerosch-Herold M. T1 Mapping. JACC Cardiovasc Imaging 2016;9:67–81.
55. Treibel TA, Fontana M, Maestrini V, et al. Automatic Measurement of the Myocardial Interstitium. JACC Cardiovasc Imaging 2016;9:54–63.
56. Kawel N, Nacif M, Zavodni A, et al. T1 mapping of the myocardium: Intra-individual assessment of the effect of field strength, cardiac cycle and variation by myocardial region. J Cardiovasc Magn Reson 2012;14:27.
57. Higgins DM, Moon JC. Review of T1 Mapping Methods: Comparative Effectiveness Including Reproducibility Issues. Curr Cardiovasc Imaging Rep 2014;7:9252.
58. Captur G, Manisty C, Moon JC. Cardiac MRI evaluation of myocardial disease. Heart 2016;102:1429–1435.
59. Moon JC, Messroghli DR, Kellman P, et al. Myocardial T1 mapping and extracellular volume quantification: a Society for Cardiovascular Magnetic Resonance (SCMR) and CMR Working Group of the European Society of Cardiology consensus statement. J Cardiovasc Magn Reson 2013;15:92.
60. Dabir D, Child N, Kalra A, et al. Reference values for healthy human myocardium using a T1 mapping methodology: results from the International T1 Multicenter cardiovascular magnetic resonance study. J Cardiovasc Magn Reson 2014;16:69.
61. Bi X, Carr JC, Li D. Whole-heart coronary magnetic resonance angiography at 3 Tesla in 5 minutes with slow infusion of Gd-BOPTA, a high-relaxivity clinical contrast agent. Magn Reson Med 2007;58:1–7.
62. Yang Q, Li K, Liu X, et al. Contrast-Enhanced Whole-Heart Coronary Magnetic Resonance Angiography at 3.0-T. A Comparative Study With X-Ray Angiography in a Single Center. J Am Coll Cardiol 2009;54:69–76.
63. Wagner M, Rösler R, Lembcke A, et al. Whole-Heart Coronary Magnetic Resonance Angiography at 1.5 Tesla: does a blood-pool contrast agent improve diagnostic accuracy? Invest Radiol 2011;46:152–159.
64. Maintz D, Aepfelbacher FC, Kissinger K V., et al. Coronary MR Angiography: Comparison of Quantitative and Qualitative Data from Four Techniques. Am J Roentgenol 2004;182:515–521.
65. Li D, Paschal CB, Haacke EM, Adler LP. Coronary arteries: three-dimensional MR imaging with fat saturation and magnetization transfer contrast. Radiology 1993;187:401–406.
66. Börnert P, Koken P, Nehrke K, Eggers H, Ostendorf P. Water/fat-resolved whole-heart Dixon coronary MRA: An initial comparison. Magn Reson Med 2014;71:156–163.
67. Fayad ZA, Fuster V, Fallon JT, et al. Noninvasive In Vivo Human Coronary Artery Lumen and Wall Imaging Using Black-Blood Magnetic Resonance Imaging. Circulation 2000;102:506–510.
68. Botnar RM, Kim WY, Börnert P, Stuber M, Spuentrup E, Manning WJ. 3D coronary vessel wall imaging utilizing a local inversion technique with spiral image acquisition. Magn Reson Med 2001;46:848–854.
69. Macedo R, Chen S, Lai S, et al. MRI detects increased coronary wall thickness in asymptomatic individuals: The multi-ethnic study of atherosclerosis (MESA). J Magn Reson Imaging 2008;28:1108–1115.

70. Kim WY, Stuber M, Börnert P, Kissinger K V, Manning WJ, Botnar RM. Three-dimensional black-blood cardiac magnetic resonance coronary vessel wall imaging detects positive arterial remodeling in patients with nonsignificant coronary artery disease. Circulation 2002;106:296–299.
71. Kerwin WS, O'Brien KD, Ferguson MS, Polissar N, Hatsukami TS, Yuan C. Inflammation in carotid atherosclerotic plaque: a dynamic contrast-enhanced MR imaging study. Radiology 2006;241:459–468.
72. Wasserman BA, Smith WI, Trout HH, Cannon RO, Balaban RS, Arai AE. Carotid artery atherosclerosis: in vivo morphologic characterization with gadolinium-enhanced double-oblique MR imaging initial results. Radiology 2002;223:566–573.
73. Maintz D, Ozgun M, Hoffmeier A, et al. Selective coronary artery plaque visualization and differentiation by contrast-enhanced inversion prepared MRI. Eur Heart J 2006;27:1732–1736.
74. Yeon SB, Sabir A, Clouse M, et al. Delayed-Enhancement Cardiovascular Magnetic Resonance Coronary Artery Wall Imaging. J Am Coll Cardiol 2007;50:441–447.
75. Ibrahim T, Makowski MR, Jankauskas A, et al. Serial Contrast-Enhanced Cardiac Magnetic Resonance Imaging Demonstrates Regression of Hyperenhancement Within the Coronary Artery Wall in Patients After Acute Myocardial Infarction. JACC Cardiovasc Imaging 2009;2:580–588.
76. Kooi ME, Cappendijk VC, Cleutjens KBJM, et al. Accumulation of ultrasmall superparamagnetic particles of iron oxide in human atherosclerotic plaques can be detected by in vivo magnetic resonance imaging. Circulation 2003;107:2453–2458.
77. Botnar RM, Buecker A, Wiethoff AJ, et al. In vivo magnetic resonance imaging of coronary thrombosis using a fibrin-binding molecular magnetic resonance contrast agent. Circulation 2004;110:1463–1466.
78. Makowski MR, Wiethoff AJ, Blume U, et al. Assessment of atherosclerotic plaque burden with an elastin-specific magnetic resonance contrast agent. Nat Med 2011;17:383–388.
79. Fayad ZA. MR imaging for the noninvasive assessment of atherothrombotic plaques. Magn Reson Imaging Clin N Am 2003;11:101–113.
80. Kawasaki T, Koga S, Koga N, et al. Characterization of Hyperintense Plaque With Noncontrast T1-Weighted Cardiac Magnetic Resonance Coronary Plaque Imaging. Comparison With Multislice Computed Tomography and Intravascular Ultrasound. JACC Cardiovasc Imaging 2009;2:720–728.
81. Noguchi T, Kawasaki T, Tanaka A, et al. High-Intensity Signals in Coronary Plaques on Noncontrast T1-Weighted Magnetic Resonance Imaging as a Novel Determinant of Coronary Events. J Am Coll Cardiol 2014;63:989–999.
82. Prince MR. Gadolinium-enhanced MR aortography. Radiology 1994;191:155–164.
83. Lohan DG, Saleh R, Nael K, Krishnam M, Finn JP. Contrast-enhanced MRA versus nonenhanced MRA: Pros and cons. Appl Radiol 2007;36:3–15.
84. Wheaton AJ, Miyazaki M. Non-contrast enhanced MR angiography: Physical principles. J Magn Reson Imaging 2012;36:286–304.
85. Miyazaki M, Lee VS. Nonenhanced MR Angiography. Radiology 2008;248:20–43.
86. Hartung MP, Grist TM, François CJ. Magnetic resonance angiography: current status and future directions. J Cardiovasc Magn Reson 2011;13:19.
87. Wedeen VJ, Meuli R a, Edelman RR, et al. Projective imaging of pulsatile flow with magnetic resonance. Science 1985;230:946–948.
88. Dumoulin CL, Souza SP, Walker MF, Wagle W. Three-dimensional phase contrast angiography. Magn Reson Med 1989;9:139–149.
89. Ståhlberg F, Søndergaard L, Thomsen C, Henriksen O. Quantification of complex flow using MR phase imaging—A study of parameters influencing the phase/velocity relation. Magn Reson Imaging 1992;10:13–23.
90. Edelman RR, Sheehan JJ, Dunkle E, Schindler N, Carr J, Koktzoglou I. Quiescent-interval single-shot unenhanced magnetic resonance angiography of peripheral vascular disease: Technical considerations and clinical feasibility. Magn Reson Med 2010;63:951–958.
91. Miyazaki M, Sugiura S, Tateishi F, Wada H, Kassai Y, Abe H. Non-contrast-enhanced MR angiography using 3D ECG-synchronized half-Fourier fast spin echo. J Magn Reson Imaging 2000;12:776–783.
92. Kober F, Jao T, Troalen T, Nayak KS. Myocardial arterial spin labeling. J Cardiovasc Magn Reson 2016;18:22.
93. Zun Z, Varadarajan P, Pai RG, Wong EC, Nayak KS. Arterial Spin Labeled CMR Detects Clinically Relevant Increase in Myocardial Blood Flow With Vasodilation. JACC Cardiovasc Imaging 2011;4:1253–1261.

94. Mekkaoui C, Reese TG, Jackowski MP, Bhat H, Sosnovik DE. Diffusion MRI in the heart. NMR Biomed 2017;30:e3426.
95. Mekkaoui C, Reese TG, Jackowski MP, et al. Diffusion Tractography of the Entire Left Ventricle by Using Free-breathing Accelerated Simultaneous Multisection Imaging. Radiology 2017;282:850–856.
96. Wagner A, Mahrholdt H, Holly TA, et al. Contrast-enhanced MRI and routine single photon emission computed tomography (SPECT) perfusion imaging for detection of subendocardial myocardial infarcts: an imaging study. Lancet 2003;361:374–379.
97. Ibrahim T, Bülow HP, Hackl T, et al. Diagnostic Value of Contrast-Enhanced Magnetic Resonance Imaging and Single-Photon Emission Computed Tomography for Detection of Myocardial Necrosis Early After Acute Myocardial Infarction. J Am Coll Cardiol 2007;49:208–216.
98. Lee S-A, Yoon YE, Kim J-E, et al. Long-Term Prognostic Value of Late Gadolinium-Enhanced Magnetic Resonance Imaging in Patients With and Without Left Ventricular Dysfunction Undergoing Coronary Artery Bypass Grafting. Am J Cardiol 2016;118:1647–1654.
99. Kwong RY. Impact of Unrecognized Myocardial Scar Detected by Cardiac Magnetic Resonance Imaging on Event-Free Survival in Patients Presenting With Signs or Symptoms of Coronary Artery Disease. Circulation 2006;113:2733–2743.
100. Gerber BL, Rochitte CE, Bluemke D a, et al. Relation Between Gd-DTPA Contrast Enhancement and Regional Inotropic Response in the Periphery and Center of Myocardial Infarction. Circulation 2001;104:998–1004.
101. Hundley WG, Bluemke DA, Finn JP, et al. ACCF/ACR/AHA/NASCI/SCMR 2010 expert consensus document on cardiovascular magnetic resonance: A report of the american college of cardiology foundation task force on expert consensus documents. Circulation 2010;121:2462–2508.
102. Hillenbrand HB, Kim RJ, Parker M a, Fieno DS, Judd RM. Early assessment of myocardial salvage by contrast-enhanced magnetic resonance imaging. Circulation 2000;102:1678–1683.
103. Baks T, van Geuns R-J, Biagini E, et al. Effects of primary angioplasty for acute myocardial infarction on early and late infarct size and left ventricular wall characteristics. J Am Coll Cardiol 2006;47:40–44.
104. van Kranenburg M, Magro M, Thiele H, et al. Prognostic Value of Microvascular Obstruction and Infarct Size, as Measured by CMR in STEMI Patients. JACC Cardiovasc Imaging 2014;7:930–939.
105. Robbers LFHJ, Eerenberg ES, Teunissen PFA, et al. Magnetic resonance imaging-defined areas of microvascular obstruction after acute myocardial infarction represent microvascular destruction and haemorrhage. Eur Heart J 2013;34:2346–2353.
106. Carrick D, Haig C, Ahmed N, et al. Myocardial Hemorrhage After Acute Reperfused ST-Segment-Elevation Myocardial Infarction: Relation to Microvascular Obstruction and Prognostic Significance. Circ Cardiovasc Imaging 2016;9:e004148.
107. Yan AT. Characterization of the Peri-Infarct Zone by Contrast-Enhanced Cardiac Magnetic Resonance Imaging Is a Powerful Predictor of Post-Myocardial Infarction Mortality. Circulation 2006;114:32–39.
108. Schmidt A, Azevedo CF, Cheng A, et al. Infarct Tissue Heterogeneity by Magnetic Resonance Imaging Identifies Enhanced Cardiac Arrhythmia Susceptibility in Patients With Left Ventricular Dysfunction. Circulation 2007;115:2006–2014.
109. Hammer-Hansen S, Leung SW, Hsu L-Y, et al. Early Gadolinium Enhancement for Determination of Area at Risk. JACC Cardiovasc Imaging 2017;10:130–139.
110. Nagel E, Puntmann VO. Is Myocardial Native T1 the One Answer for All? JACC Cardiovasc Imaging 2016;9:37–39.
111. Messroghli DR, Walters K, Plein S, et al. Myocardial T1 mapping: Application to patients with acute and chronic myocardial infarction. Magn Reson Med 2007;58:34–40.
112. Ugander M, Oki AJ, Hsu L-Y, et al. Extracellular volume imaging by magnetic resonance imaging provides insights into overt and sub-clinical myocardial pathology. Eur Heart J 2012;33:1268–1278.
113. Greenwood JP, Maredia N, Younger JF, et al. Cardiovascular magnetic resonance and single-photon emission computed tomography for diagnosis of coronary heart disease (CE-MARC): A prospective trial. Lancet 2012;379:453–460.
114. Schwitter J, Wacker CM, van Rossum AC, et al. MR-IMPACT: comparison of perfusion-cardiac magnetic resonance with single-photon emission computed tomography for the detection of coronary artery disease in a multicentre, multivendor, randomized trial. Eur

Heart J 2008;29:480–489.
115. Greenwood JP, Herzog BA, Brown JM, et al. Prognostic value of cardiovascular magnetic resonance and single-photon emission computed tomography in suspected coronary heart disease: Long-term follow-up of a prospective, diagnostic accuracy cohort study. Ann Intern Med 2016;165:1–9.
116. Nandalur KR, Dwamena BA, Choudhri AF, Nandalur MR, Carlos RC. Diagnostic Performance of Stress Cardiac Magnetic Resonance Imaging in the Detection of Coronary Artery Disease. J Am Coll Cardiol 2007;50:1343–1353.
117. Baer FM, Theissen P, Schneider CA, et al. Dobutamine Magnetic Resonance Imaging Predicts Contractile Recovery of Chronically Dysfunctional Myocardium After Successful Revascularization. J Am Coll Cardiol 1998;31:1040–1048.
118. Sayad DE, Willett DL, Hundley WG, Grayburn PA, Peshock RM. Dobutamine magnetic resonance imaging with myocardial tagging quantitatively predicts improvement in regional function after revascularization. Am J Cardiol 1998;82:1149–1151.
119. Jahnke C, Nagel E, Gebker R, et al. Prognostic value of cardiac magnetic resonance stress tests: Adenosine stress perfusion and dobutamine stress wall motion imaging. Circulation 2007;115:1769–1776.
120. Paetsch I, Jahnke C, Wahl A, et al. Comparison of dobutamine stress magnetic resonance, adenosine stress magnetic resonance, and adenosine stress magnetic resonance perfusion. Circulation 2004;110:835–842.
121. Liu A, Wijesurendra RS, Francis JM, et al. Adenosine Stress and Rest T1 Mapping Can Differentiate Between Ischemic, Infarcted, Remote, and Normal Myocardium Without the Need for Gadolinium Contrast Agents. JACC Cardiovasc Imaging 2016;9:27–36.
122. Cummings KW, Bhalla S, Javidan-Nejad C, Bierhals AJ, Gutierrez FR, Woodard PK. A pattern-based approach to assessment of delayed enhancement in nonischemic cardiomyopathy at MR imaging. Radiographics 2009;29:89–103.
123. Mahrholdt H, Wagner A, Judd RM, Sechtem U, Kim RJ. Delayed enhancement cardiovascular magnetic resonance assessment of non-ischaemic cardiomyopathies. Eur Heart J 2005;26:1461–1474.
124. Choudhury L, Mahrholdt H, Wagner A, et al. Myocardial scarring in asymptomatic or mildly symptomatic patients with hypertrophic cardiomyopathy. J Am Coll Cardiol 2002;40:2156–2164.
125. McCrohon JA, Moon JCC, Prasad SK, et al. Differentiation of heart failure related to dilated cardiomyopathy and coronary artery disease using gadolinium-enhanced cardiovascular magnetic resonance. Circulation 2003;108:54–59.
126. Chan RH, Maron BJ, Olivotto I, et al. Prognostic value of quantitative contrast-enhanced cardiovascular magnetic resonance for the evaluation of sudden death risk in patients with hypertrophic cardiomyopathy. Circulation 2014;130:484–495.
127. Assomull RG, Prasad SK, Lyne J, et al. Cardiovascular Magnetic Resonance, Fibrosis, and Prognosis in Dilated Cardiomyopathy. J Am Coll Cardiol 2006;48:1977–1985.
128. Maceira AM, Joshi J, Prasad SK, et al. Cardiovascular magnetic resonance in cardiac amyloidosis. Circulation 2005;111:186–193.
129. Smedema J-P, Snoep G, van Kroonenburgh MPG, et al. Evaluation of the accuracy of gadolinium-enhanced cardiovascular magnetic resonance in the diagnosis of cardiac sarcoidosis. J Am Coll Cardiol 2005;45:1683–1690.
130. Mahrholdt H. Cardiovascular Magnetic Resonance Assessment of Human Myocarditis: A Comparison to Histology and Molecular Pathology. Circulation 2004;109:1250–1258.
131. Tandri H, Saranathan M, Rodriguez ER, et al. Noninvasive detection of myocardial fibrosis in arrhythmogenic right ventricular cardiomyopathy using delayed-enhancement magnetic resonance imaging. J Am Coll Cardiol 2005;45:98–103.
132. Patel R, DiMarco J, Akar J, Voros S, Kramer C. Chagas Myocarditis and Syncope. J Cardiovasc Magn Reson 2005;7:685–688.
133. Puntmann VO, Peker E, Chandrashekhar Y, Nagel E. T1 Mapping in Characterizing Myocardial Disease. Circ Res 2016;119:277–299.
134. Luetkens JA, Homsi R, Sprinkart AM, et al. Incremental value of quantitative CMR including parametric mapping for the diagnosis of acute myocarditis. Eur Hear J – Cardiovasc Imaging 2016;17:154–161.
135. de Meester de Ravenstein C, Bouzin C, Lazam S, et al. Histological Validation of measurement of diffuse interstitial myocardial fibrosis by myocardial extravascular volume fraction from Modified Look-Locker imaging (MOLLI) T1 mapping at 3 T. J Cardiovasc Magn Reson

2015;17:48.
136. Schelbert EB, Piehler KM, Zareba KM, et al. Myocardial Fibrosis Quantified by Extracellular Volume Is Associated With Subsequent Hospitalization for Heart Failure, Death, or Both Across the Spectrum of Ejection Fraction and Heart Failure Stage. J Am Heart Assoc 2015;4:e002613.
137. O'Donnell DH, Abbara S, Chaithiraphan V, et al. Cardiac Tumors: Optimal Cardiac MR Sequences and Spectrum of Imaging Appearances. Am J Roentgenol 2009;193:377–387.
138. Caspar T, El Ghannudi S, Ohana M, et al. Magnetic resonance evaluation of cardiac thrombi and masses by T1 and T2 mapping: an observational study. Int J Cardiovasc Imaging 2016;
139. Kim WY, Danias PG, Stuber M, et al. Coronary magnetic resonance angiography for the detection of coronary stenoses. N Engl J Med 2001;345:1863–1869.
140. Yonezawa M, Nagata M, Kitagawa K, et al. Quantitative Analysis of 1.5-T Whole-Heart Coronary MR Angiograms Obtained with 32-Channel Cardiac Coils: A Comparison with Conventional Quantitative Coronary Angiography. Radiology 2014;271:356–364.
141. Liu X, Zhao X, Huang J, et al. Comparison of 3D Free-Breathing Coronary MR Angiography and 64-MDCT Angiography for Detection of Coronary Stenosis in Patients with High Calcium Scores. Am J Roentgenol 2007;189:1326–1332.
142. Schuetz GM, Zacharopoulou NM, Schlattmann P, Dewey M. Meta-analysis: Noninvasive Coronary Angiography Using Computed Tomography Versus Magnetic Resonance Imaging. Ann Intern Med 2010;125:167–177.
143. Liu X, Bi X, Huang J, Jerecic R, Carr J, Li D. Contrast-Enhanced Whole-Heart Coronary Magnetic Resonance Angiography at 3.0 T. Invest Radiol 2008;43:663–668.
144. Camren GP, Wilson GJ, Bamra VR, Nguyen KQ, Hippe DS, Maki JH. A Comparison between Gadofosveset Trisodium and Gadobenate Dimeglumine for Steady State MRA of the Thoracic Vasculature. Biomed Res Int 2014;2014:1–6.
145. François CJ, Tuite D, Deshpande V, Jerecic R, Weale P, Carr JC. Unenhanced MR angiography of the thoracic aorta: initial clinical evaluation. AJR Am J Roentgenol 2008;190:902–906.
146. Krishnam MS, Tomasian A, Malik S, Desphande V, Laub G, Ruehm SG. Image quality and diagnostic accuracy of unenhanced SSFP MR angiography compared with conventional contrast-enhanced MR angiography for the assessment of thoracic aortic diseases. Eur Radiol 2010;20:1311–1320.
147. Lim RP, Hecht EM, Xu J, et al. 3D nongadolinium-enhanced ECG-gated MRA of the distal lower extremities: Preliminary clinical experience. J Magn Reson Imaging 2008;28:181–189.
148. Haneder S, Attenberger UI, Riffel P, Henzler T, Schoenberg SO, Michaely HJ. Magnetic resonance angiography (MRA) of the calf station at 3.0 T: intraindividual comparison of non-enhanced ECG-gated flow-dependent MRA, continuous table movement MRA and time-resolved MRA. Eur Radiol 2011;21:1452–1461.
149. François CJ, Tuite D, Deshpande V, Jerecic R, Weale P, Carr JC. Pulmonary Vein Imaging with Unenhanced Three-dimensional Balanced Steady-State Free Precession MR Angiography: Initial Clinical Evaluation. Radiology 2009;250:932–939.
150. Hu P, Stoeck CT, Smink J, et al. Noncontrast SSFP pulmonary vein magnetic resonance angiography: Impact of off-resonance and flow. J Magn Reson Imaging 2010;32:1255–1261.

CHAPTER

Association of cardiovascular magnetic resonance-derived circumferential strain parameters with the risk of ventricular arrhythmia and all-cause mortality in patients with prior myocardial infarction and primary prevention implantable cardioverter defibrillator

Paiman EHM, Androulakis AFA, Shahzad R, Tao Q, Zeppenfeld K, Lamb HJ, van der Geest RJ

J Cardiovasc Magn Reson. 2019 May 16;21(1):28. doi: 10.1186/s12968-019-0536-5127

ABSTRACT

Background

Impaired left ventricular (LV) contraction and relaxation may further promote adverse remodeling and may increase the risk of ventricular arrhythmia (VA) in ischemic cardiomyopathy. We aimed to examine the association of CMR-derived circumferential strain parameters for LV regional systolic function, LV diastolic function and mechanical dispersion with the risk of VA in patients with prior myocardial infarction and primary prevention implantable cardioverter defibrillator (ICD).

Methods

Patients with ischemic cardiomyopathy and primary prevention ICD, who underwent CMR prior to ICD implantation, were retrospectively included. LV segmental circumferential strain curves were extracted from short-axis cine CMR. For LV regional strain analysis, the extent of moderately and severely impaired strain (percentage of LV segments with strain between -10% and -5% and >-5%, respectively) were calculated. LV diastolic function was quantified by the early and late diastolic strain rate. Mechanical dispersion was defined as the standard deviation in delay time between each strain curve and the patient-specific reference curve. Cox proportional hazard ratios (HR) (95%CI) were calculated to assess the association between LV strain parameters and appropriate ICD therapy.

Results

A total of 121 patients (102 (85%) men, age: 63±11 years, LV ejection fraction (LVEF) 27±9%) were included. During a median (interquartile range) follow-up of 47 (27;69) months, 30 (25%) patients received appropriate ICD therapy. The late diastolic strain rate (HR 1.1 (1.0;1.2) per -0.25 1/s, ***P***=0.043) and the extent of moderately impaired strain (HR 1.5 (1.0;2.2) per +10%, ***P***=0.048) but not the extent of severely impaired strain (HR 0.9 (0.6;1.4) per +10%, ***P***=0.685) were associated with appropriate ICD therapy, independent of LVEF, late gadolinium enhancement (LGE) scar border size and acute revascularization. Mechanical dispersion was not related to appropriate ICD therapy (HR 1.1 (0.8;1.6) per +25 ms, ***P***=0.464).

Conclusion

The extent of moderately impaired strain and late diastolic strain rate were associated with the risk of appropriate ICD therapy, independent of LVEF, scar border size and acute revascularization. These findings suggest that disturbed LV contraction and relaxation may contribute to an increased risk of VA after myocardial infarction.

INTRODUCTION

Ventricular arrhythmia (VA) risk stratification in patients with ischemic cardiomyopathy remains challenging. Left ventricular ejection fraction (LVEF) is the major determinant in the selection of post-infarct patients for implantable cardioverter defibrillator (ICD) therapy for the primary prevention of sudden death (1); however, appropriate ICD therapy is documented in only 35% of the patients (2).

Adverse post-infarct LV remodeling is known to further increase the risk of VA (3,4). Disturbances in LV mechanics are recognized as important contributors to progressive ischemic remodeling (5-7). LV strain is considered a more sensitive measure of contractile function as compared to LVEF (8). Both circumferential strain and longitudinal strain have been found to be predictive of LV remodeling after myocardial infarction (9,10). In particular global circumferential strain may be related to ischemic remodeling, as LV circumferential function helps to maintain LV structure after severe impairment of LV longitudinal function (10,11). Also, the LV sphericity index, as a marker of adverse LV remodeling, may be associated with the risk of VA (12,13). In recent years, several echocardiography studies have shown the potential of LV strain parameters for the prediction of VA (14-17). However, none of these echocardiography studies have assessed the predictive value of LV strain parameters in comparison with infarct tissue characteristics. Of interest, with the introduction of feature tracking it has become feasible to semi-automatically quantify myocardial circumferential strain based on balanced steady-state free precession (bSSFP) short-axis cine CMR (18,19). LV mechanical parameters indicative of adverse remodeling can be derived from standard CMR examinations, in addition to late gadolinium enhancement (LGE) scar characteristics.

Notably, pathologic LV remodeling after myocardial infarction may predispose to VA but also to progressive heart failure (10). In patients with ischemic cardiomyopathy and primary prevention ICD, non-sudden death due to severe heart failure has been demonstrated to be an important competing risk of sudden death (20). Previously, a large number of LV segments with systolic dysfunction soon after myocardial infarction has been shown to be an independent predictor of adverse outcome (21,22). Possibly, patients with a high extent of severely impaired strain may be at risk of death due to progressive heart failure, whereas those with a high extent of moderately impaired strain may be at specific risk of arrhythmia related death. In this regard, the assessment of LV regional systolic strain may help to distinguish patients with ischemic cardiomyopathy at risk of sudden death in particular and may add to the identification of individuals who may benefit from ICD therapy.

As well as disturbed LV contractility, impaired LV diastolic function is related to LV remodeling (23). Recently, an echocardiography study has provided the first evidence that LV diastolic dysfunction, in particular impairment of the late diastolic tissue velocity, is predictive of VA (16). Furthermore, as global strain reflects the amplitude but not the timing of the contraction, new indices have been proposed, for example mechanical dispersion (24). In

previous echocardiography studies, mechanical dispersion has been shown to be associated with VA (14,15,25). Prior studies have demonstrated that LV segmental strain (26), but also LV diastolic function (27) and mechanical dispersion (28) can be extracted from bSSFP cine CMR.

The aim of this hypothesis generating study was to assess the association of LV circumferential strain parameters for LV regional systolic function (i.e. extent of moderately and severely impaired strain), LV diastolic function (i.e. early and late diastolic strain rate) and mechanical dispersion, derived from short-axis cine CMR, with appropriate ICD therapy in patients with prior myocardial infarction and primary prevention ICD, independent of LVEF and LGE scar border size. Additionally, the relation of LV strain parameters with the competing risk of all-cause mortality without appropriate ICD therapy was examined.

METHODS

Study population

The study was performed at the Leiden University Medical Center (The Netherlands). Consecutive patients with myocardial infarction and ICD implantation for primary prevention of VA between May 2003 and May 2012 were retrospectively included if CMR was performed prior to ICD implantation. Part of this population has been previously described (29). Patients who underwent surgical LV reconstruction within one year after CMR were excluded. For those with late LV repair, follow-up data after surgery were censored. Patients received a dual or single chamber ICD or an ICD combined with cardiac resynchronization therapy (CRT-ICD), according to the guidelines of the European Society of Cardiology (ESC) valid at the time of implantation (30-32). The assessment of LV function to determine the patient's eligibility for primary prevention ICD implantation was based on CMR or echocardiography (at another time point). The Dutch Central Committee on Human-related Research (CCMO) allows use of anonymous data without prior approval of an institutional review board provided that the data is acquired for patient care and that the data contains no identifiers that could be traced back to the individual patient. All data used for this study was acquired for clinical treatment, and was stripped of any identifying information. For the present retrospective study, informed consent was waived by the institutional medical research ethics committee.

Clinical parameters

Clinical baseline characteristics were retrieved from the patients' medical records. A creatinine serum level ≥1.4 mg/dL was considered to indicate renal failure. Presence of a significant stenosis in ≥2 coronary arteries was regarded as multi-vessel disease. Patients with a single myocardial infarction and reperfusion therapy within 24 hours from onset of symptoms were categorized as having received acute revascularization.

CMR data acquisition

Patients were scanned on a 1.5T Gyoscan ACS-NT/Intera magnetic resonance scanner (Philips, Best, The Netherlands) using a 5-element cardiac coil. After obtaining scout views, a stack of short-axis slices comprising the complete LV was acquired, using an electrocardiographic triggered bSSFP sequence. Typical imaging parameters were: field of view 400x320 mm^2, matrix 256x206, voxel size 1.56x1.56 mm^2, number of slices 12-18, slice thickness 10 mm, slice gap 0 mm, flip angle 35º, echo/repetition time 1.7/3.6 ms, number of phases 30-40. Additionally, LGE imaging in short-axis view, covering the complete LV, was performed approximately 15 minutes after administration of gadolinium diethylenetriamine penta-acetic acid (Magnevist, Schering/Berlin, Germany; 0.15 mmol/kg), using an inversion-recovery 3D turbo-field echo sequence with imaging parameters as previously described (29).

CMR data analysis

MASS Research Software V2016-EXP (Leiden University Medical Centre, The Netherlands) was used for the extraction of the LV circumferential strain curves and the quantification of the LGE scar size. The LV circumferential strain-derived parameters were calculated using MATLAB R2015a (MathWorks, Massachusetts, United States). Based on a spatiotemporal feature tracking approach, the manually outlined endocardial contours at end-diastole were automatically traced over the entire cardiac cycle (33,34). Group-wise image registration was performed to calculate the deformation field, which was used to track the endocardial contours. Basal slices with intersection of the aorta outflow and the lower two apical slices were excluded. Endocardial strain curves were calculated for twelve segments per slice.

LV circumferential strain parameters for global function were global strain, the peak systolic strain rate and the early and late peak diastolic strain rate. Global strain and peak strain rates were defined as the average of peak systolic strain and peak strain rate, respectively, of all segments. Peak systolic strain rate was defined as the minimum strain rate between end-diastole and maximum peak systolic strain. The early and late diastolic strain rate were measured as the maximum strain rate between maximum peak systolic strain and mid-diastole and between mid- and end-diastole, respectively. A comparable approach has previously been applied in tagged and strain-encoded CMR (35). For curves with peak systolic strain of >-5% and oscillating curves, the assigned peak systolic, early and late diastolic strain rate was defined as zero, as those segments were assumed to have lost the physiological strain patterns.

To assess LV regional systolic function, the LV was characterized according to the extent of different categories of impaired strain (severely, moderately and mildly impaired strain). Reported normal values for feature tracking-based global circumferential strain are -23% (-24.3 to -21.7%) (36). As feature tracking-based strain calculation has been recently introduced, no reference values for segmental circumferential strain are available. We presumed that the discriminative ability in segmental peak systolic strain would be at best around 5% based on the acquisition, image analysis and patient population. Therefore, each category of segmental

peak systolic strain was spanning a range of 5%. The first category ranging from -20% to -15% was regarded as relatively preserved strain, whereas the other categories were assumed to include segments with impaired strain. Accordingly, the following cut-off values were applied: >-5% (severely impaired strain), -10% to -5% (moderately impaired strain) and -15% to -10% (mildly impaired strain).

To derive mechanical dispersion, the strain curves were clustered according to the similarity of the motion patterns to constitute a patient-specific reference curve, after exclusion of the curves with peak systolic strain of >-5% and the oscillating curves. Delay time between the curve of each segment and the reference curve was calculated by cross correlation. Mechanical dispersion was defined as the standard deviation in delay time between each strain curve and the reference curve, as previously proposed (37).

LGE scar size was measured according to a previously described semi-automatic scar identification method (29). The LGE total and border scar zone were defined as myocardium with a signal intensity (SI) >35% of the maximum SI and with SI ≥35% but <50% of the maximum SI, respectively. The scar size was quantified in gram, with an estimated myocardial density of 1.05 g/mL. LV sphericity was calculated as the ratio of the LV end-diastolic volume (derived from the short-axis images) to the volume of a sphere with a diameter equal to the LV end-diastolic 4-chamber length, as described previously (12). The investigators (EHMP, QT and RJvdG) were blinded to the clinical baseline characteristics and events during the CMR data analysis.

Follow-up and events

ICD device interrogation was scheduled two months after implantation and every six months thereafter. ICD devices were typically programmed to include three zones: monitor zone (150-188 beats per minute; antitachycardia pacing (ATP) if indicated), fast ventricular tachycardia (VT) zone (188-210 beats per minute; ATP and shock), and ventricular fibrillation (VF) zone (>210 beats per minute; if available ATP during charging, and shock). Appropriate ICD therapy was defined as ATP or shock subsequent to monomorphic VT or VF. All-cause mortality without appropriate ICD therapy was defined as death without documented appropriate ICD discharge. In case of incomplete follow-up for ICD therapy until death, data were censored after the last ICD device interrogation. The investigator who collected the clinical patient data (AFAA) was blinded to the CMR data.

Statistical analysis

Statistical analyses were performed using STATA 14.1 (StataCorp LLC, Texas, United States). The independent-samples Student's t-test or Fisher exact test was used to assess the differences in baseline characteristics. Cox proportional hazards regression models were constructed to examine the association of the baseline variables with appropriate ICD therapy and all-cause mortality without appropriate ICD therapy. The Harrell's C-statistic was calculated to

assess the discriminative performance of each baseline variable for appropriate ICD therapy. The proportional hazards assumption was satisfied for all CMR parameters based on the assessment of the Schoenfeld residuals and the time interaction terms. In addition, Kaplan-Meier curves were constructed for the extent of severely and moderately impaired strain, early and late diastolic strain rate and mechanical dispersion. The difference between patients with values below vs. above the observed median in the population in the cumulative incidence of appropriate ICD therapy was assessed using the log-rank test.

Nested Cox regression modeling was performed to test whether the CMR parameters for LV regional strain, LV diastolic function and mechanical function improved the fit of the model for appropriate ICD therapy; first, in comparison to a null model containing LVEF and scar border size; second, in comparison to a null model comprising LVEF, scar border size and the clinical parameter with the best discriminative ability based on the C-statistic in univariable Cox regression analysis. Only one clinical parameter was added to the reference model, as the number of covariables in the model is limited by the number of events in the population. The differences between the extended and the null models were assessed for statistical significance using the $\chi 2$ likelihood ratio (LR) test. Multi-collinearity was ruled out by calculation of the correlation matrix of the coefficients in the Cox regression model (all correlation coefficients were below 0.75). Additionally, we performed a sensitivity analysis. According to guidelines, LV function to determine the patient's eligibility for primary prevention ICD implantation should be assessed at least 40 days post myocardial infarction or at least 3 months after revascularization (38). Therefore, we calculated the Cox hazard ratio for the patients with CMR in the acute/subacute phase and for those with CMR in the chronic stage of myocardial infarction (CMR < or >40 days after myocardial infarction and < or >3 months following revascularization, respectively). Intra-observer agreement was evaluated by the intra-class correlation coefficient (ICC) for absolute agreement using a two-way random model based on a random sample of 20 patients from the total population. All statistical tests were two-sided and a ***P*** value below 0.05 was considered statistically significant.

RESULTS

Baseline characteristics

A total of 149 patients with previous myocardial infarction and CMR prior to ICD implantation for primary prevention were identified. Eleven patients were excluded due to insufficient image quality (n=3 for short-axis cine and n=18 for LGE CMR) and 17 because of surgical LV reconstruction. In total, 121 patients (102 (84%) men, age: 63 ± 11 years) were included. In 77 (64%) and the remaining 44 (36%) patients, ICD indication was based on the 2003 ESC guidelines update (IIa recommendation if LVEF <30%) and the 2008 ESC guidelines (Ia recommendation if LVEF ≤35% and New York Heart Association (NYHA) Functional Classification ≥II despite optimal medical therapy), respectively (30,31).

During a median (interquartile range (IQR)) follow-up of 47 (27, 69) months, 30 (25%) received appropriate ICD therapy and 23 (19%) died without having received appropriate ICD therapy. Three patients who died without documented ICD therapy had no complete ICD follow-up until death (last ICD device interrogation was 6-12 months before death). Median (IQR) duration was 22 (0, 168) days between myocardial infarction and CMR acquisition and 34 (9, 125) days between CMR and ICD implantation.

Clinical parameters

Among patients with as compared to those without appropriate ICD therapy the percentage of acute revascularization was lower. Patients who died without appropriate ICD therapy as compared to those who survived or received appropriate ICD therapy had more often multivessel disease, NYHA class III-IV or IV, diabetes mellitus, and used more frequently angiotensin-converting-enzyme (ACE) inhibitors. The clinical baseline characteristics are presented according to appropriate ICD therapy and all-cause mortality without appropriate ICD therapy (**Table 1**).

CMR parameters

LVEF (mean ± SD) was 27 ± 9%, total scar size: 49 ± 27 g, scar core size: 30 ± 21 g, scar border size: 20 ± 10 g, global strain: -13.3 ± 3.9%, peak systolic strain rate: -0.79 ± 0.27 1/s, extent of severely impaired strain: 16 ± 12%, extent of moderately impaired strain: 25 ± 10%, extent of mildly impaired strain: 23 ± 8%, early diastolic strain rate: 0.76 ± 0.29 1/s, late diastolic strain rate: 0.50 ± 0.23 1/s, mechanical dispersion: 83 ± 24 ms and LV sphericity index: 0.55 ± 0.14. Patients with as compared to those without appropriate ICD therapy had a lower LVEF, higher extent of scar border size, lower global strain, lower peak systolic strain rate, higher extent of severely and moderately impaired strain and a lower early and late diastolic strain rate. In patients who died without appropriate ICD therapy as compared to those who survived or received appropriate ICD therapy, total scar size and scar core size were larger, peak systolic strain rate was lower, the extent of severely impaired strain was larger, late diastolic strain rate was lower and mechanical dispersion was larger. The CMR results are summarized according to appropriate ICD therapy and all-cause mortality without appropriate ICD therapy (**Table 2**).

All circumferential strain-derived measures were highly reproducible. The ICC (95%CI) was 0.96 (0.90, 0.98) for severely impaired strain, 0.93 (0.84, 0.97) for moderately impaired strain, 0.98 (0.95, 0.99) for early diastolic strain rate, 0.97 (0.93, 0.99) for late diastolic strain rate, and 0.96 (0.90, 0.98) for mechanical dispersion.

Table 1. Baseline clinical variables

	No appropriate ICD therapy (n=91)	Appropriate ICD therapy (n=30)	Survived or appropriate ICD therapy (n=98)	Deceased without appropriate ICD therapy (n=23)
Age, years	64 ± 10	63 ± 13	63 ± 11	66 ± 8
Men	74/91 (81%)	28/30 (93%)	81/98 (83%)	21/23 (91%)
Smoking	48/89 (54%)	15/27 (56%)	50/94 (53%)	13/22 (59%)
Hypertension	40/85 (47%)	10/29 (34%)	41/92 (45%)	9/22 (41%)
Hypercholesterolemia	46/76 (61%)	14/24 (58%)	48/80 (60%)	12/20 (60%)
Diabetes mellitus	23/91 (26%)	3/30 (10%)	17/98 (17%)*	9/23 (39%)
Renal failure	16/91 (18%)	10/30 (33%)	18/98 (18%)	8/23 (35%)
Atrial fibrillation	18/91 (20%)	7/30 (23%)	19/98 (19%)	6/23 (26%)
Left bundle branch block	29/91 (32%)	11/30 (37%)	33/98 (34%)	7/23 (30%)
QRS>120 ms	26/91 (29%)	11/30 (37%)	26/98 (27%)	11/23 (48%)
CRT device	67/91 (74%)	23/30 (77%)	72/98 (73%)	18/23 (78%)
NYHA III-IV	32/91 (35%)	14/30 (47%)	32/98 (33%)†	14/23 (61%)
NYHA IV	4/91 (4%)	1/30 (3%)	1/98 (1%)†	4/23 (17%)
Multi-vessel disease	60/90 (67%)	24/29 (83%)	62/96 (65%)†	22/23 (96%)
Acute revascularization	53/91 (58%)†	8/27 (27%)	51/98 (52%)	10/23 (43%)
Prior CABG	33/91 (36%)	12/30 (40%)	34/98 (35%)	11/23 (48%)
Medication				
Statins	76/90 (84%)	24/30 (80%)	79/98 (81%)	21/22 (95%)
ACE inhibitor	65/90 (72%)	16/30 (53%)	62/98 (63%)*	19/22 (86%)
Aldosterone antagonist	29/90 (32%)	9/30 (30%)	32/98 (33%)	6/22 (27%)
Amiodarone	8/90 (9%)	4/30 (13%)	12/98 (12%)	0/22 (0%)
ARB	15/90 (17%)	6/30 (20%)	19/98 (19%)	2/22 (9%)
Beta blocker	76/90 (84%)	26/30 (87%)	84/98 (86%)	18/22 (82%)
Calcium channel blocker	5/90 (6%)	3/30 (10%)	8/98 (8%)	0/22 (0%)
Any diuretic	54/90 (60%)	21/30 (70%)	61/98 (62%)	14/22 (64%)

Continuous data are expressed as means ± standard deviation and categorical data as numbers (percentages). The presented percentages may not be equal to the percentages of the total number of patients due to missing values. *P<0.05, †P<0.01, ‡P <0.001 vs. appropriate ICD therapy or all-cause mortality without appropriate ICD therapy. ACE inhibitor: angiotensin-converting-enzyme inhibitor. ARB: angiotensin receptor blocker. CABG: coronary artery bypass graft. CRT: cardiac resynchronization therapy. NYHA: New York Heart Association Functional Classification.

Table 2. Baseline CMR variables

	No appropriate ICD therapy (n=91)	Appropriate ICD therapy (n=30)	Survived or appropriate ICD therapy (n=98)	Deceased without appropriate ICD therapy (n=23)
LVEF, %	29 ± 9†	23 ± 10	28 ± 9	25 ± 10
Total scar size, g	48 ± 28	55 ± 25	47 ± 24*	60 ± 38
Scar core size, g	29 ± 22	33 ± 19	28 ± 17*	39 ± 31
Scar border size, g	19 ± 9*	23 ± 11	19 ± 10	21 ± 10
LV mass, g	151 ± 35	160 ± 42	152 ± 37	160 ± 35
LV end-diastolic volume, mL	291 ± 104	319 ± 96	290 ± 95	333 ± 128
Global strain, %	-14 ± 4†	-11 ± 3	-14 ± 4	-12 ± 4
Peak systolic strain rate, 1/s	-0.83 ± 0.27†	-0.66 ± 0.20	-0.81 ± 0.27*	-0.68 ± 0.24
Extent of impaired strain, %				
Severely (<-5%)	15 ± 11*	20 ± 14	15 ± 11*	21 ± 14
Moderately (-5, -10%)	23 ± 10‡	30 ± 10	24 ± 11	26 ± 9
Mildly (-10, -15%)	23 ± 8	22 ± 7	23 ± 8	22 ± 7
Early diastolic strain rate, 1/s	0.79 ± 0.30*	0.64 ± 0.25	0.78 ± 0.29	0.68 ± 0.26
Late diastolic strain rate, 1/s	0.52 ± 0.24*	0.42 ± 0.20	0.52 ± 0.23*	0.40 ± 0.23
Sphericity index	0.54 ± 0.13	0.57 ± 0.17	0.54 ± 0.14	0.58 ± 0.17
Mechanical dispersion, ms	82 ± 24	83 ± 25	80 ± 24*	92 ± 21

Means ± standard deviations. *P<0.05, †P<0.01, ‡P<0.001 vs. appropriate ICD therapy or all-cause mortality without appropriate ICD therapy. Missing values for sphericity index: n=2 (no appropriate ICD therapy); n=1 (appropriate ICD therapy); n=2 survived or appropriate ICD therapy; n=1 deceased without appropriate ICD therapy. LV: left ventricle. LVEF: left ventricular ejection fraction. Extent of impaired strain: percentage of LV segments with strain >-15%.

Appropriate ICD therapy

The risk of appropriate ICD therapy was higher for patients without acute revascularization, for those with multi-vessel disease, renal failure, a relatively lower LVEF, larger total scar size, larger scar border size, lower global strain, lower peak systolic strain rate, a higher extent of severely and moderately impaired strain, a lower early and late diastolic strain rate. In contrast, mechanical dispersion and the LV sphericity index were not associated with the risk of appropriate ICD therapy (**Table 3 and 4**). Furthermore, the incidence of appropriate ICD therapy was significantly higher for patients with a relatively high extent of moderately impaired strain or a relatively low early and late diastolic strain rate (log-rank test P=0.004, P=0.01 and P=0.01, respectively) (**Figure 1**). In contrast, no differences in the cumulative incidence curves of appropriate ICD therapy were observed for the extent of severely impaired strain or mechanical dispersion (log-rank test P=0.215 and P=0.813, respectively).

Table 3. Unadjusted Cox hazard ratio for the clinical parameters

	Appropriate ICD therapy (30/121)			All-cause mortality without appropriate ICD therapy (23/121)		
	Cox HR (95%CI)	***P* value**	**Harrell's C-statistic**	**Cox HR (95%CI)**	***P* value**	**Harrell's C-statistic**
Age, per +1 year	1.0 (1.0, 1.0)	0.785	0.49	1.0 (1.0, 1.1)	0.353	0.50
Men	3.5 (0.8, 15)	0.086	0.57	2.8 (0.7, 12)	0.164	0.57
Smoking	1.1 (0.5, 2.3)	0.882	0.51	1.4 (0.6, 3.4)	0.449	0.55
Hypertension	0.6 (0.3, 1.3)	0.193	0.54	0.7 (0.3, 1.8)	0.543	0.53
Hypercholesterolemia	1.0 (0.4, 2.2)	0.958	0.50	1.0 (0.4, 2.5)	0.941	0.50
Diabetes mellitus	0.4 (0.1, 1.4)	0.154	0.56	2.2 (1.0, 5.2)	0.062	0.59
Renal failure	2.3 (1.1, 5.0)	0.028	0.58	2.5 (1.1, 6.0)	0.038	0.59
Atrial fibrillation	1.2 (0.5, 2.9)	0.636	0.53	1.5 (0.6, 3.7)	0.426	0.53
Left bundle branch block	1.1 (0.5, 2.3)	0.789	0.52	0.8 (0.3, 2.0)	0.689	0.52
QRS>120 ms	1.5 (0.7, 3.3)	0.249	0.56	2.3 (1.0, 5.2)	0.051	0.58
CRT device	1.1 (0.5, 2.6)	0.825	0.51	1.3 (0.5, 3.3)	0.661	0.49
NYHA III-IV	1.8 (0.9, 3.7)	0.113	0.58	3.0 (1.3, 6.9)	0.012	0.62
NYHA IV	1.3 (0.2, 9.7)	0.785	0.51	5.6 (1.7, 18)	0.004	0.56
Acute revascularization	0.3 (0.1, 0.7)	0.003	0.65	0.6 (0.2, 1.3)	0.185	0.54
Multi-vessel disease	2.8 (1.0, 7.2)	0.040	0.61	12 (1.7, 92)	0.014	0.65
Prior CABG	1.2 (0.6, 2.5)	0.628	0.53	1.6 (0.7, 3.7)	0.251	0.53
Medication						
Statins	0.8 (0.3, 2.0)	0.621	0.62	4.1 (0.5, 30)	0.170	0.56
ACE inhibitor	0.6 (0.3, 1.2)	0.116	0.57	2.9 (0.9, 10)	0.081	0.59
Aldosterone antagonist	0.9 (0.4, 1.9)	0.729	0.50	0.8 (0.3, 2.1)	0.678	0.55
Amiodarone	1.3 (0.4, 3.6)	0.666	0.52	-		
ARB	1.1 (0.4, 2.6)	0.867	0.50	0.5 (0.1, 2.0)	0.308	0.54
Beta blocker	1.1 (0.4, 3.1)	0.903	0.49	0.7 (0.2, 2.1)	0.552	0.52
Calcium channel blocker	1.5 (0.5, 5.1)	0.476	0.52	-		0.53
Any diuretic	1.3 (0.6, 2.9)	0.456	0.53	1.1 (0.4, 2.6)	0.882	0.47

Abbreviations as in Table 1. The discriminative performance of each parameter for appropriate ICD therapy or all-cause mortality without appropriate ICD therapy is indicated the Harrell's C-statistic (no, good, excellent and perfect discriminative ability is indicated by a C-statistic of 0.5, >0.7, >0.8 and 1, respectively). Note: none of the patients who died during follow-up without having received appropriate ICD therapy used amiodarone or calcium channel blockers.

Table 4. Unadjusted Cox hazard ratio for the CMR parameters

	Appropriate ICD therapy (30/121)			All-cause mortality without appropriate ICD therapy (23/121)		
	Cox HR (95%CI)	*P* value	Harrell's C-statistic	Cox HR (95%CI)	*P* value	Harrell's C-statistic
LVEF, per -10%	2.1 (1.4, 3.2)	0.001	0.70	1.5 (0.9, 2.4)	0.084	0.60
Total scar size, per 10 g	1.1 (1.0, 1.3)	0.030	0.65	1.2 (1.0, 1.3)	0.009	0.63
Scar core size, per 10 g	1.1 (1.0, 1.3)	0.115	0.60	1.2 (1.1, 1.4)	0.007	0.61
Scar border size, per 10 g	1.6 (1.2, 2.1)	0.009	0.65	1.4 (0.9, 2.0)	0.122	0.62
Global strain, per +5%	2.9 (1.6, 5.2)	<0.001	0.69	2.1 (1.1, 4.0)	0.020	0.64
Peak systolic strain rate, per +0.25 1/s	2.3 (1.4, 3.7)	0.001	0.68	2.0 (1.2, 3.3)	0.011	0.66
Extent of impaired strain, %						
Severely (<-5%)	1.5 (1.1, 1.9)	0.005	0.64	1.5 (1.1, 2.1)	0.005	0.66
Moderately (-5, -10%)	1.9 (1.4, 2.5)	<0.001	0.71	1.4 (0.9, 2.0)	0.099	0.63
Mildly (-10, -15%)	0.7 (0.4, 1.2)	0.203	0.59	0.8 (0.4, 1.4)	0.359	0.55
Early diastolic strain rate, per -0.25 1/s	1.1 (1.0, 1.2)	0.005	0.66	1.1 (1.0, 1.1)	0.066	0.61
Late diastolic strain rate, per -0.25 1/s	1.1 (1.0, 1.2)	0.008	0.66	1.1 (1.0, 1.3)	0.008	0.71
Mechanical dispersion, per +25 ms	1.1 (0.8, 1.6)	0.464	0.55	1.6 (1.1, 2.3)	0.014	0.66
Sphericity index, per +0.1	1.2 (0.9, 1.5)	0.271	0.53	1.2 (0.9, 1.6)	0.296	0.58

Abbreviations as in Table 2.

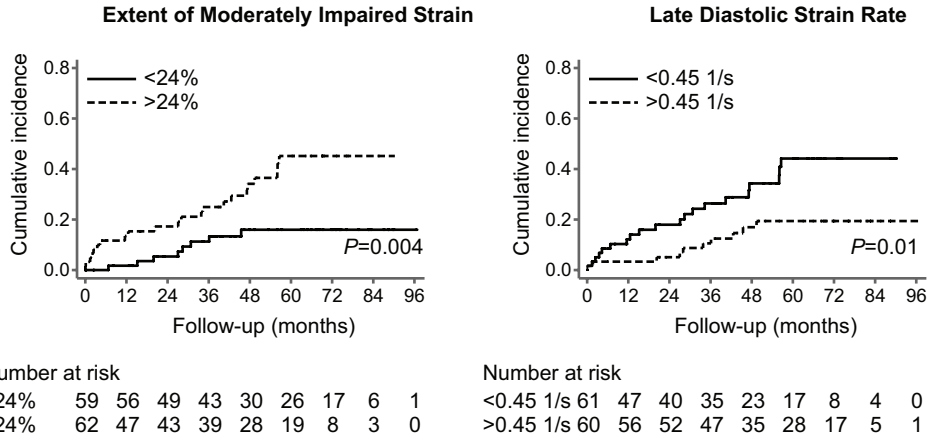

Figure 1. Kaplan-Meier curves for the cumulative incidence of appropriate implantable cardioverter defibrillator (ICD) therapy, with the observed median as the cut-off. *P* values for the log-rank test are shown.

On multivariable analysis, the extent of moderately impaired strain and late diastolic strain rate were associated with the risk of appropriate ICD therapy, independent of LVEF, scar border size and acute revascularization, and both parameters significantly improved the fit of the model for the risk of appropriate ICD therapy as compared LVEF and scar border zone (C-statistic increased from 0.71 to 0.73 (LR test ***P***=0.041) and 0.73 (LR test ***P***=0.034), respectively) (**Table 5**). When acute revascularization was additionally included in the reference model for the risk of appropriate ICD therapy, late diastolic strain rate remained to add incremental benefit (C-statistic increased from 0.73 to 0.75, LR test ***P***=0.033), whereas the extent of moderately impaired strain tended to have additive value for the fit of the model (C-statistic increased from 0.73 to 0.76, LR test ***P***=0.056) (**Table 5**). An example of a patient with appropriate ICD therapy with a relatively large extent of moderately impaired strain and relatively low late diastolic strain rate is provided (**Figure 2**).

Table 5. Multivariable Cox regression model for appropriate ICD therapy

	Cox HR (95%CI)	***P* value**	**Harrell's C-statistic**	**LR test χ2**	***P* value**
LVEF, scar border size			**0.71**	**13.12**	**Reference**
Added to null model:					
Extent of impaired strain, per +10%					
Severely (<-5%)	1.0 (0.6, 1.5)	0.844	0.71	13.16	0.844
Moderately (-5, -10%)	1.5 (1.0, 2.2)	0.034	0.73	17.30	0.041
Mildly (-10, -15%)	0.8 (0.5, 1.4)	0.487	0.71	13.62	0.482
Early diastolic strain rate, per -0.25 1/s	1.1 (1.0, 1.1)	0.179	0.71	15.06	0.164
Late diastolic strain rate, per -0.25 1/s	1.1 (1.0, 1.2)	0.044	0.73	17.64	0.034
Mechanical dispersion, per +25 ms	1.0 (0.7, 1.5)	0.815	0.71	13.18	0.812
LVEF, scar border size, acute revascularization			**0.73**	**17.65**	**Reference**
Added to null model:					
Extent of impaired strain, per +10%					
Severely (<-5%)	0.9 (0.6, 1.4)	0.685	0.73	17.82	0.685
Moderately (-5, -10%)	1.5 (1.0, 2.2)	0.048	0.76	21.30	0.056
Mildly (-10, -15%)	0.8 (0.5, 1.3)	0.403	0.74	18.38	0.394
Early diastolic strain rate, per -0.25 1/s	1.0 (1.0, 1.1)	0.355	0.73	18.54	0.345
Late diastolic strain rate, per -0.25 1/s	1.1(1.0, 1.2)	0.043	0.75	22.19	0.033
Mechanical dispersion, per +25 ms	1.1 (0.8, 1.7)	0.490	0.74	18.12	0.495

Abbreviations as in Table 2. The incremental value of each LV strain parameter for the fit of the Cox regression model for the risk of appropriate ICD therapy as compared to the null model was assessed using the likelihood ratio (LR) chi-square statistic (χ2).

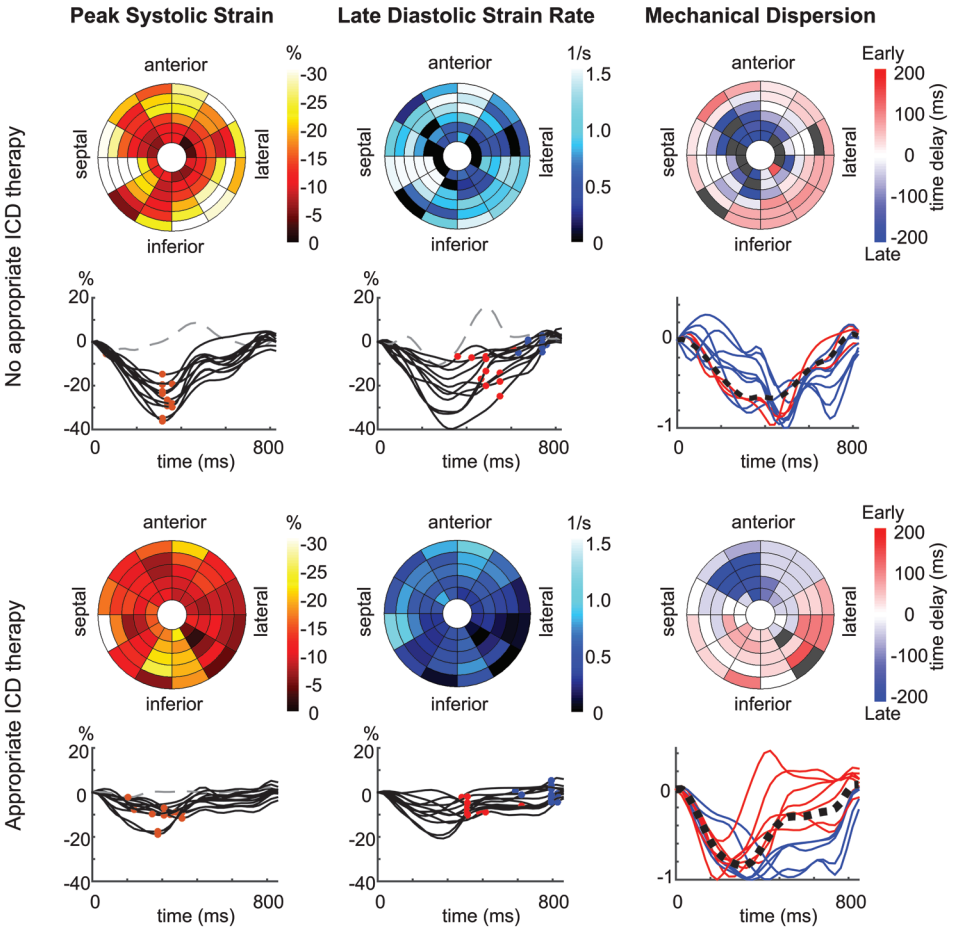

Figure 2. Example of LV circumferential strain in a patient without and with appropriate ICD therapy. LV bullseye representation of peak systolic strain, late diastolic strain rate and mechanical dispersion and LV segmental strain curves per slice with LV segmental peak systolic strain (orange dots), early diastolic strain rate (red dots), late diastolic strain rate (blue dots) and normalized curves with the patient-specific reference curve (black dotted lines). In the LV bullseye for mechanical dispersion, LV segments with early and late contraction patterns are shown in red and blue, respectively. (***Upper panel***) 71-year-old woman without appropriate ICD therapy (LVEF 30%). (***Lower panel***) 71-year-old man with appropriate ICD therapy at 40 months after ICD implantation (LVEF 26%). In the presented patient with appropriate ICD therapy, the extent of moderately impaired strain (percentage of LV segments with peak systolic strain between -5% and -10%) is relatively large, the early and late diastolic strain rate are low, whereas mechanical dispersion is comparable in the presented cases.

All-cause mortality without appropriate ICD therapy

The clinical parameters multi-vessel disease, NYHA class III-IV or IV and renal failure were associated with an increased risk of death without having received appropriate ICD therapy. Regarding the CMR parameters, a larger total scar size, larger scar core size, lower global strain, lower peak systolic strain rate, higher extent of severely impaired strain, lower late diastolic strain rate and higher mechanical dispersion were related to an increased risk of all-cause mortality without appropriate ICD therapy (**Table 3 and 4**). The LV sphericity index was not associated with the risk of all-cause mortality without having received appropriate ICD therapy.

Sensitivity analysis

CMR was acquired in the acute/subacute phase vs. chronic stage in 72 and 49 patients, respectively. In the acute/subacute and chronic subgroup, respectively, 18/72 (25%) and 12/49 (24%) received appropriate ICD therapy and 9/72 (13%) and 14/49 (29%) died without having received appropriate ICD therapy. In the acute/subacute vs. the chronic subgroup, the risk of appropriate ICD therapy was comparable in relation to the scar border size (HR 1.6 (0.9, 2.6) and 1.6 (1.0, 2.5) per +10 g, respectively), the extent of moderately impaired strain (HR 1.9 (1.3, 2.7) and 1.8 (1.1, 3.1) per +10%, respectively) and late diastolic strain rate (HR 1.1 (1.0, 1.2) and 1.1 (1.0, 1.3) per -0.25 1/s, respectively). In contrast, the risk of appropriate ICD therapy in relation to LVEF was lower in the acute/subacute compared to the chronic subgroup (HR 1.9 (1.1, 3.4) per -10% vs. 3.1 (1.4, 6.8) per -10%) (**Supplemental Table 1**).

DISCUSSION

CMR-derived circumferential strain analysis showed that the extent of moderately impaired strain and late diastolic strain rate were associated with the risk of appropriate ICD therapy, independent of LVEF, LGE scar border size and acute revascularization, in patients with prior myocardial infarction and primary prevention ICD. In contrast, there was no relation between mechanical dispersion and the risk of appropriate ICD therapy.

LV segmental strain

Of interest, the extent of moderately impaired strain was specifically related to an increased risk of VA, whereas the extent of severely impaired strain was associated with both the risk of appropriate ICD therapy and the risk of all-cause mortality without appropriate ICD therapy. Therefore, the assessment of the extent of moderately impaired strain in particular may be helpful for sudden death risk stratification. Circumferential contractile performance is considered essential for maintaining LV shape and restraining LV dilation (10). In this regard, the extent of impaired strain may be associated with appropriate ICD therapy, as it may be indicative of an increased susceptibility to ongoing adverse remodeling after myocardial infarction which

has been shown to correlate with electrical instability and an increased risk of sudden death (4). Previously, LV sphericity has been proposed as a marker of adverse LV remodeling and has been shown to be associated with appropriate ICD therapy in patients with ischemic and non-ischemic cardiomyopathy (12,13). Notably, in our study population selectively including patients with prior myocardial infarction, LV mechanical parameters and scar characteristics rather than LV structural indices such as LV sphericity were related to the risk of VA.

Several echocardiography studies have previously addressed LV regional function in relation to adverse outcome in ischemic cardiomyopathy. The regional extent of systolic dysfunction after myocardial infarction has been shown to be independently associated with heart failure and mortality (22,39). Also, an independent relation between impaired regional strain in the scar border zone and appropriate ICD therapy has been demonstrated (40). Most research on CMR-derived LV regional strain has been limited to studies on the predictive value of LV segmental strain for persistent contractile dysfunction shortly after myocardial infarction (41,42). To our knowledge, this is the first CMR study in which the association between LV segmental strain and the risk of VA in ischemic cardiomyopathy has been examined.

LV diastolic function

Late but not early diastolic function was independently associated with appropriate ICD therapy and late but not early diastolic function was associated with all-cause mortality without appropriate ICD therapy. As well as systolic abnormalities, diastolic dysfunction, due to the resulting elevated LV filling pressure and the progressive LV enlargement, may contribute to an increased risk of sudden and non-sudden death (23,43). It has to be pointed out that early and late diastolic function reflect different relaxation processes. Whereas early diastolic function is an active, energy requiring process, which is therefore highly susceptible to ischemia, the late diastolic function parameters are predominantly dependent on the passive LV stiffness and left atrial function (44). Late diastolic function parameters are considered to deteriorate when left atrial function fails to compensate for the progressive increase in the passive LV stiffness (16). In this regard, in a population with severely depressed LVEF late diastolic function in particular may be indicative of adverse LV remodeling, which may further increase the risk of sudden and non-sudden death.

Our observations are consistent with previous echocardiography studies, in which late but not early diastolic function was associated with adverse cardiac outcome including VA, cardiac mortality and/or heart failure (16,45). Our study adds to the current, limited evidence that LV diastolic function may have potential for VA risk stratification in patients with myocardial infarction and reduced LVEF.

LV mechanical dispersion

In our study population with relatively depressed LVEF, mechanical dispersion was not associated with appropriate ICD therapy. Some echocardiography studies have shown a strong and independent relation between mechanical dispersion and VA (14,15,25), whereas others did not find such association (16,17). The observed association between mechanical dispersion and death without appropriate ICD therapy is in keeping with other studies, which reported a relation of mechanical dispersion with heart failure and mortality (28,46). We speculate that, depending on the cohort characteristics, mechanical dispersion may be a risk stratifier for either sudden or non-sudden death.

LGE scar

In the present study, the extent of moderately impaired strain and late diastolic strain rate provided incremental benefit for VA risk stratification above LVEF and LGE scar border size. It remains debated which LGE scar characteristics are most predictive of sudden death. Although several studies have demonstrated that LGE scar border size in particular is indicative of an increased VA susceptibility (29,47), others observed no association between the border size and the risk of VA (48,49) or reported a comparable association for border and total scar size (50). In this regard, CMR-derived LV circumferential strain parameters may or may not have additive value above LGE scar for VA risk stratification, if other approaches for the quantification of infarct tissue heterogeneity would have been applied.

Limitations

Because of the retrospective design, no conclusions on causality can be drawn. We used CMR as this enabled the assessment of the incremental value of LV strain parameters above LGE scar characteristics for VA risk stratification. Whereas the high number of extracted strain curves in CMR is a plus, disadvantage of CMR as compared to echocardiography is the inferior temporal resolution when analyzing LV diastolic function and mechanical dispersion. Also, our study was limited by the arbitrary definition of the strain categorization of the LV segments and prospective studies are required for validation. Furthermore, the sample size was not sufficient for more detailed subgroup analyses, for example according to the type of arrhythmic event, although our study population was relatively large for a single center cohort.

In our retrospective study the CMR examinations were acquired in the chronic stage as well as in the acute/subacute phase of myocardial infarction. Importantly, the associations of the scar border size, the extent of moderately impaired strain and late diastolic strain rate with the risk of appropriate ICD therapy were comparable for the subgroups with CMR in the acute/subacute phase and in the chronic stage of myocardial infarction. In contrast, our results suggested that the predictive value of LVEF for appropriate ICD therapy was substantially higher when LVEF was assessed in patients with chronic compared to acute/subacute myocardial infarction. Therefore, prospective studies with CMR at 40 days after myocardial infarction or 3 months

after revascularization are needed to confirm the additive value of the extent of moderately impaired strain and late diastolic strain rate for VA risk stratification beyond LVEF.

Implications

Our findings suggest that both disturbed LV contraction and relaxation increase the risk of VA, which may contribute to a better understanding of the complex pathophysiology of VA in ischemic cardiomyopathy. The extent of impaired LV segmental strain has previously been assessed in relation to adverse outcome including heart failure and mortality (21,22,39). In this study, we showed that LV regional strain is also related to the risk of appropriate ICD therapy. Furthermore, our results confirm previous findings that LV diastolic function can be helpful in VA risk stratification and add to the existing evidence that LV diastolic function provides incremental benefit above LGE scar (16).

Patients with appropriate ICD therapy were slightly better identified after assessment of the extent of moderately impaired strain or late diastolic strain rate in addition to LV global function and LGE scar. Our findings indicate that VA risk stratification in ischemic cardiomyopathy can be improved by the evaluation of additional imaging parameters derived from standard clinical CMR examinations. For clinical implementation, our model including LVEF, the scar border size, regional strain and diastolic function, might be extended by other imaging parameters, for example novel scar characteristics, which together may further increase the discriminative performance for appropriate ICD therapy.

CONCLUSION

In patients with prior myocardial infarction and primary prevention ICD, the extent of moderately impaired strain and late diastolic strain rate were associated with appropriate ICD therapy, independent of LVEF, LGE scar border size and acute revascularization. In contrast, mechanical dispersion showed no relation with appropriate ICD therapy. Notably, the extent of moderately impaired strain was specifically associated with appropriate ICD therapy, whereas the extent of severely impaired strain was also related to death without having received appropriate ICD therapy. Furthermore, deterioration of late diastolic function in particular may be indicative of adverse LV remodeling in patients with severe LV dysfunction, which may explain the observed association of late rather than early diastolic function with an increased risk of appropriate ICD therapy. This work can be seen as a hypothesis generating study, which may help to elucidate which mechanical parameters are predictive of an increased risk of VA in addition to established functional and scar-related imaging markers. In this study, no longitudinal imaging data was available, which would have provided more insight into the role LV remodeling in LV arrhythmogenesis. Therefore, whether the increased VA vulnerability in association with disturbed LV contraction and relaxation is related to late adverse remodeling needs to be assessed in further research.

FUNDING

The Department of Cardiology (Leiden University Medical Center, The Netherlands) receives unrestricted research grants from Edwards Lifesciences, Medtronic, Biotronik and Boston Scientific. This work was funded by NWO Domain Applied and Engineering Sciences [grant number 12899].

REFERENCES

1. Brignole M, Auricchio A, Baron-Esquivias G, et al. 2013 ESC Guidelines on cardiac pacing and cardiac resynchronization therapy: the Task Force on cardiac pacing and resynchronization therapy of the European Society of Cardiology (ESC). Developed in collaboration with the European Heart Rhythm Association (EHRA). Eur Heart J 2013;34(29):2281-2329.
2. Moss AJ, Greenberg H, Case RB, et al. Long-term clinical course of patients after termination of ventricular tachyarrhythmia by an implanted defibrillator. Circulation 2004;110(25):3760-3765.
3. St John Sutton M, Lee D, Rouleau JL, et al. Left ventricular remodeling and ventricular arrhythmias after myocardial infarction. Circulation 2003;107(20):2577-2582.
4. Gaudron P, Kugler I, Hu K, Bauer W, Eilles C, Ertl G. Time course of cardiac structural, functional and electrical changes in asymptomatic patients after myocardial infarction: their interrelation and prognostic impact. J Am Coll Cardiol 2001;38(1):33-40.
5. D'Elia N, D'Hooge J, Marwick TH. Association Between Myocardial Mechanics and Ischemic LV Remodeling. JACC Cardiovasc Imaging 2015;8(12):1430-1443.
6. Mollema SA, Liem SS, Suffoletto MS, et al. Left ventricular dyssynchrony acutely after myocardial infarction predicts left ventricular remodeling. J Am Coll Cardiol 2007;50(16):1532-1540.
7. Carluccio E, Biagioli P, Alunni G, et al. Patients with hibernating myocardium show altered left ventricular volumes and shape, which revert after revascularization: evidence that dyssynergy might directly induce cardiac remodeling. J Am Coll Cardiol 2006;47(5):969-977.
8. Mordi I, Bezerra H, Carrick D, Tzemos N. The Combined Incremental Prognostic Value of LVEF, Late Gadolinium Enhancement, and Global Circumferential Strain Assessed by CMR. JACC Cardiovasc Imaging 2015;8(5):540-549.
9. Joyce E, Hoogslag GE, Leong DP, et al. Association between left ventricular global longitudinal strain and adverse left ventricular dilatation after ST-segment-elevation myocardial infarction. Circ Cardiovasc Imaging 2014;7(1):74-81.
10. Hung CL, Verma A, Uno H, et al. Longitudinal and circumferential strain rate, left ventricular remodeling, and prognosis after myocardial infarction. J Am Coll Cardiol 2010;56(22):1812-1822.
11. Wang J, Khoury DS, Yue Y, Torre-Amione G, Nagueh SF. Preserved left ventricular twist and circumferential deformation, but depressed longitudinal and radial deformation in patients with diastolic heart failure. Eur Heart J 2008;29(10):1283-1289.
12. Nakamori S, Ismail H, Ngo LH, Manning WJ, Nezafat R. Left ventricular geometry predicts ventricular tachyarrhythmia in patients with left ventricular systolic dysfunction: a comprehensive cardiovascular magnetic resonance study. J Cardiovasc Magn Reson 2017;19(1):79.
13. Levine YC, Matos J, Rosenberg MA, Manning WJ, Josephson ME, Buxton AE. Left ventricular sphericity independently predicts appropriate implantable cardioverter-defibrillator therapy. Heart Rhythm 2016;13(2):490-497.
14. Ersboll M, Valeur N, Andersen MJ, et al. Early echocardiographic deformation analysis for the prediction of sudden cardiac death and life-threatening arrhythmias after myocardial infarction. JACC Cardiovasc Imaging 2013;6(8):851-860.
15. Haugaa KH, Grenne BL, Eek CH, et al. Strain echocardiography improves risk prediction of ventricular arrhythmias after myocardial infarction. JACC Cardiovasc Imaging 2013;6(8):841-850.
16. Biering-Sorensen T, Olsen FJ, Storm K, et al. Prognostic value of tissue Doppler imaging for predicting ventricular arrhythmias and cardiovascular mortality in ischaemic cardiomyopathy. Eur Heart J Cardiovasc Imaging 2016;17(7):722-731.
17. Biering-Sorensen T, Knappe D, Pouleur AC, et al. Regional Longitudinal Deformation Improves Prediction of Ventricular Tachyarrhythmias in Patients With Heart Failure With Reduced Ejection Fraction: A MADIT-CRT Substudy (Multicenter Automatic Defibrillator Implantation Trial-Cardiac Resynchronization Therapy). Circ Cardiovasc Imaging 2017;10(1).
18. Schuster A, Hor KN, Kowallick JT, Beerbaum P, Kutty S. Cardiovascular Magnetic Resonance Myocardial Feature Tracking: Concepts and Clinical Applications. Circ Cardiovasc Imaging 2016;9(4):e004077.
19. Hor KN, Baumann R, Pedrizzetti G, et al.

Magnetic resonance derived myocardial strain assessment using feature tracking. J Vis Exp 2011(48).
20. Friedman DJ, Al-Khatib SM, Zeitler EP, et al. New York Heart Association class and the survival benefit from primary prevention implantable cardioverter defibrillators: A pooled analysis of 4 randomized controlled trials. Am Heart J 2017;191:21-29.
21. Bodi V, Sanchis J, Nunez J, et al. Prognostic value of a comprehensive cardiac magnetic resonance assessment soon after a first ST-segment elevation myocardial infarction. JACC Cardiovasc Imaging 2009;2(7):835-842.
22. Wang N, Hung CL, Shin SH, et al. Regional cardiac dysfunction and outcome in patients with left ventricular dysfunction, heart failure, or both after myocardial infarction. Eur Heart J 2016;37(5):466-472.
23. Temporelli PL, Giannuzzi P, Nicolosi GL, et al. Doppler-derived mitral deceleration time as a strong prognostic marker of left ventricular remodeling and survival after acute myocardial infarction: results of the GISSI-3 echo substudy. J Am Coll Cardiol 2004;43(9):1646-1653.
24. Haugaa KH, Amlie JP, Berge KE, Leren TP, Smiseth OA, Edvardsen T. Transmural differences in myocardial contraction in long-QT syndrome: mechanical consequences of ion channel dysfunction. Circulation 2010;122(14):1355-1363.
25. Matsuzoe H, Tanaka H, Matsumoto K, et al. Left ventricular dyssynergy and dispersion as determinant factors of fatal ventricular arrhythmias in patients with mildly reduced ejection fraction. Eur Heart J Cardiovasc Imaging 2016;17(3):334-342.
26. Khan JN, Singh A, Nazir SA, Kanagala P, Gershlick AH, McCann GP. Comparison of cardiovascular magnetic resonance feature tracking and tagging for the assessment of left ventricular systolic strain in acute myocardial infarction. Eur J Radiol 2015;84(5):840-848.
27. Moody WE, Taylor RJ, Edwards NC, et al. Comparison of magnetic resonance feature tracking for systolic and diastolic strain and strain rate calculation with spatial modulation of magnetization imaging analysis. J Magn Reson Imaging 2015;41(4):1000-1012.
28. Muser D, Tioni C, Shah R, Selvanayagam JB, Nucifora G. Prevalence, Correlates, and Prognostic Relevance of Myocardial Mechanical Dispersion as Assessed by Feature-Tracking Cardiac Magnetic Resonance After a First ST-Segment Elevation Myocardial Infarction. Am J Cardiol 2017;120(4):527-533.
29. Roes SD, Borleffs CJ, van der Geest RJ, et al. Infarct tissue heterogeneity assessed with contrast-enhanced MRI predicts spontaneous ventricular arrhythmia in patients with ischemic cardiomyopathy and implantable cardioverter-defibrillator. Circ Cardiovasc Imaging 2009;2(3):183-190.
30. Priori SG, Aliot E, Blomstrom-Lundqvist C, et al. Update of the guidelines on sudden cardiac death of the European Society of Cardiology. Eur Heart J 2003;24(1):13-15.
31. Dickstein K, Cohen-Solal A, Filippatos G, et al. ESC guidelines for the diagnosis and treatment of acute and chronic heart failure 2008: the Task Force for the diagnosis and treatment of acute and chronic heart failure 2008 of the European Society of Cardiology. Developed in collaboration with the Heart Failure Association of the ESC (HFA) and endorsed by the European Society of Intensive Care Medicine (ESICM). Eur J Heart Fail 2008;10(10):933-989.
32. Dickstein K, Vardas PE, Auricchio A, et al. 2010 Focused Update of ESC Guidelines on device therapy in heart failure: an update of the 2008 ESC Guidelines for the diagnosis and treatment of acute and chronic heart failure and the 2007 ESC guidelines for cardiac and resynchronization therapy. Developed with the special contribution of the Heart Failure Association and the European Heart Rhythm Association. Eur Heart J 2010;31(21):2677-2687.
33. Metz CT, Klein S, Schaap M, van Walsum T, Niessen WJ. Nonrigid registration of dynamic medical imaging data using nD + t B-splines and a groupwise optimization approach. Med Image Anal 2011;15(2):238-249.
34. Tsadok Y, Friedman Z, Haluska BA, Hoffmann R, Adam D. Myocardial strain assessment by cine cardiac magnetic resonance imaging using non-rigid registration. Magn Reson Imaging 2016;34(4):381-390.
35. Neizel M, Lossnitzer D, Korosoglou G, et al. Strain-encoded (SENC) magnetic resonance imaging to evaluate regional heterogeneity of myocardial strain in healthy volunteers: Comparison with conventional tagging. J Magn Reson Imaging 2009;29(1):99-105.
36. Vo HQ, Marwick TH, Negishi K. MRI-Derived Myocardial Strain Measures in Normal Subjects. JACC Cardiovasc Imaging 2017.
37. Suever JD, Fornwalt BK, Neuman LR, Delfino JG, Lloyd MS, Oshinski JN. Method to create regional mechanical dyssynchrony maps from short-axis cine steady-state free-precession

images. J Magn Reson Imaging 2014;39(4):958-965.
38. Al-Khatib SM, Stevenson WG, Ackerman MJ, et al. 2017 AHA/ACC/HRS Guideline for Management of Patients With Ventricular Arrhythmias and the Prevention of Sudden Cardiac Death: A Report of the American College of Cardiology/American Heart Association Task Force on Clinical Practice Guidelines and the Heart Rhythm Society. J Am Coll Cardiol 2017.
39. Ersboll M, Valeur N, Mogensen UM, et al. Relationship between left ventricular longitudinal deformation and clinical heart failure during admission for acute myocardial infarction: a two-dimensional speckle-tracking study. J Am Soc Echocardiogr 2012;25(12):1280-1289.
40. Ng AC, Bertini M, Borleffs CJ, et al. Predictors of death and occurrence of appropriate implantable defibrillator therapies in patients with ischemic cardiomyopathy. Am J Cardiol 2010;106(11):1566-1573.
41. Buss SJ, Krautz B, Hofmann N, et al. Prediction of functional recovery by cardiac magnetic resonance feature tracking imaging in first time ST-elevation myocardial infarction. Comparison to infarct size and transmurality by late gadolinium enhancement. Int J Cardiol 2015;183:162-170.
42. Khan JN, Nazir SA, Singh A, et al. Relationship of Myocardial Strain and Markers of Myocardial Injury to Predict Segmental Recovery After Acute ST-Segment-Elevation Myocardial Infarction. Circ Cardiovasc Imaging 2016;9(6).
43. Gaudron P, Kugler L, Hu K, et al. Effect of quinapril initiated during progressive remodeling in asymptomatic patients with healed myocardial infarction. Am J Cardiol 2000;86(2):139-144.
44. Zile MR, Baicu CF, Gaasch WH. Diastolic heart failure--abnormalities in active relaxation and passive stiffness of the left ventricle. N Engl J Med 2004;350(19):1953-1959.
45. Mogelvang R, Biering-Sorensen T, Jensen JS. Tissue Doppler echocardiography predicts acute myocardial infarction, heart failure, and cardiovascular death in the general population. Eur Heart J Cardiovasc Imaging 2015;16(12):1331-1337.
46. Shin SH, Hung CL, Uno H, et al. Mechanical dyssynchrony after myocardial infarction in patients with left ventricular dysfunction, heart failure, or both. Circulation 2010;121(9):1096-1103.
47. Schmidt A, Azevedo CF, Cheng A, et al. Infarct tissue heterogeneity by magnetic resonance imaging identifies enhanced cardiac arrhythmia susceptibility in patients with left ventricular dysfunction. Circulation 2007;115(15):2006-2014.
48. Gao P, Yee R, Gula L, et al. Prediction of arrhythmic events in ischemic and dilated cardiomyopathy patients referred for implantable cardiac defibrillator: evaluation of multiple scar quantification measures for late gadolinium enhancement magnetic resonance imaging. Circ Cardiovasc Imaging 2012;5(4):448-456.
49. Klem I, Weinsaft JW, Bahnson TD, et al. Assessment of myocardial scarring improves risk stratification in patients evaluated for cardiac defibrillator implantation. J Am Coll Cardiol 2012;60(5):408-420.
50. de Haan S, Meijers TA, Knaapen P, Beek AM, van Rossum AC, Allaart CP. Scar size and characteristics assessed by CMR predict ventricular arrhythmias in ischaemic cardiomyopathy: comparison of previously validated models. Heart 2011;97(23):1951-1956.

SUPPLEMENTARY MATERIAL

Supplemental Table 1. Unadjusted Cox hazard ratio for the CMR parameters in the acute/subacute phase vs. the chronic stage

	Appropriate ICD therapy					
	Acute/subacute subgroup (18/72)			Chronic subgroup (12/49)		
	Cox HR (95%CI)	*P* value	Harrell's C-statistic	Cox HR (95%CI)	*P* value	Harrell's C-statistic
LVEF, per -10%	1.9 (1.1, 3.4)	0.022	0.67	3.1 (1.4, 6.8)	0.005	0.75
Total scar size, per 10 g	1.1 (0.9, 1.3)	0.369	0.58	1.2 (1.0, 1.4)	0.036	0.73
Scar core size, per 10 g	1.1 (0.8, 1.4)	0.712	0.54	1.2 (1.0, 1.4)	0.069	0.67
Scar border size, per 10 g	1.6 (0.9, 2.6)	0.093	0.59	1.6 (1.0, 2.5)	0.044	0.70
Global strain, per +5%	2.8 (1.3, 5.9)	0.007	0.68	3.3 (1.2, 8.7)	0.017	0.69
Peak systolic strain rate, per +0.25 1/s	2.1 (1.2, 3.7)	0.011	0.68	3.1 (1.3, 7.6)	0.014	0.70
Extent of impaired strain, %						
Severely (<-5%)	1.6 (1.0, 2.3)	0.033	0.63	1.5 (1.0, 2.2)	0.051	0.64
Moderately (-5, -10%)	1.9 (1.3, 2.7)	0.002	0.72	1.8 (1.1, 3.1)	0.025	0.69
Mildly (-10, -15%)	0.8 (0.4, 1.5)	0.476	0.56	0.6 (0.3, 1.4)	0.259	0.62
Early diastolic strain rate, per -0.25 1/s	1.1 (1.0, 1.1)	0.137	0.59	1.3 (1.1, 1.5)	0.001	0.79
Late diastolic strain rate, per -0.25 1/s	1.1 (1.0, 1.2)	0.052	0.64	1.1 (1.0, 1.3)	0.076	0.66
Mechanical dispersion, per +25 ms	1.5 (0.9, 2.3)	0.113	0.59	0.8 (0.5, 1.6)	0.601	0.50
Sphericity index, per +0.1	1.0 (0.7, 1.6)	0.843	0.51	1.3 (0.9, 1.8)	0.218	0.55

LV: left ventricle. LVEF: left ventricular ejection fraction. Extent of impaired strain: percentage of LV segments with strain >-15%. Acute/subacute subgroup: CMR <40 days post myocardial infarction or <3 months following revascularization. Chronic subgroup: CMR >40 days post myocardial infarction or >3 months following revascularization.

CHAPTER

General discussion and future perspectives

GENERAL DISCUSSION AND FUTURE PERSPECTIVES

Current magnetic resonance methods enable detailed phenotyping of the left ventricle and accurate characterization of body fat distribution, by assessment of cardiac morphology and function, myocardial triglyceride content, diffuse fibrosis, and visceral and subcutaneous adipose tissue. The objective of this thesis was to characterize cardiovascular remodeling associated with metabolic disturbances, using several magnetic resonance techniques.

Cardiovascular Remodeling in Type 2 Diabetes

In Chapter 2, we examined the relationship of insulin resistance, an important predictor of type 2 diabetes, to cardiovascular imaging parameters in a middle-aged population-based cohort. Previous large-scale studies have shown that abnormalities in glucose metabolism are associated with impairments in diastolic function, independently of body mass index (BMI) (1,2). However, the cardiovascular effects of insulin resistance and body fat, in particular visceral fat, might not be fully separated by adjustment for BMI. In our population-based study, we confirmed that the relation of insulin resistance to a lower diastolic function is independent of body fat.

In this thesis, we evaluated the role of insulin resistance in obesity-related impairments in diastolic function. However, several other factors such as increased inflammatory cytokines, high levels of circulating fatty acids, microvascular dysfunction and autonomic neuropathy have been implicated in the pathogenesis of HFpEF in obesity and type 2 diabetes (3-5). Accordingly, in our population-based study, insulin resistance was associated with impaired diastolic function, but the associations between adipose tissue and reduced diastolic function were not completely mediated by insulin resistance. Up till now, heart failure treatment options are limited, and the efficacy of therapies developed for HFrEF (such as angiotensin-converting enzyme inhibitors and beta blockers) has been uncertain in patients with HFpEF (6-9). Therefore, hopefully, future research on the contributing factors to diastolic dysfunction in obesity and type 2 diabetes may help to guide the development of new treatment strategies through a better understanding of the pathogenesis of diabetic heart failure.

Furthermore, our population-based results showed that visceral and total body fat are associated with lower and higher left ventricular end-diastolic volumes, respectively, which suggests that the body fat distribution phenotype may influence the cardiac phenotype in obesity. These findings are in keeping with the disparity in the cardiac remodeling types in relation to visceral and subcutaneous fat as reported in previous population-based studies (10-13). Importantly, left ventricular hypertrophy and concentric remodeling, independent of cardiovascular risk factors, have been associated with a higher risk of heart failure events (14). To date, routine use of imaging in type 2 diabetes patients to detect early abnormalities in cardiac function has not been recommended, although functional capacity and natriuretic peptides may be potential markers to identify high-risk patients who may benefit from cardiac screening

(15,16). Interestingly, distinct imaging-based cardiac phenotypes in type 2 diabetes patients have been associated with distinct cardiovascular risks; for example, high cardiac mass and dimensions and low systolic function, despite similar clinical characteristics, have been related to a higher cardiovascular risk (17). Therefore, risk stratification in type 2 diabetes patients based on the cardiometabolic phenotype using imaging techniques may merit further investigation.

Diabetic Cardiomyopathy Phenotype

In Chapter 3, we explored the differences in diabetic cardiomyopathy characteristics between Dutch South Asians and Dutch Europeans. Both the South Asian and the European type 2 diabetes patients demonstrated abnormalities in diastolic function, but the results regarding myocardial tissue characteristics were different between the two study groups. Based on the results of this thesis and previous studies (18,19), we speculate that myocardial lipotoxicity and altered substrate metabolism may be significant contributors to diabetic cardiomyopathy in European populations, whereas increased cardiac mass may be a predominant factor in South Asian ethnic groups. Likewise, findings of previous studies suggest that the etiology of diabetic heart failure may be different in South Asian compared with European ethnicities (20,21). Prospective studies are warranted to confirm the differential impact of type 2 diabetes on myocardial remodeling across ethnic groups. Although several large-scale studies, particularly in the United States (22) and in the United Kingdom (23), have investigated the ethnic disparities in the risk of cardiometabolic disease, the separate effects of genetic and behavioral conditions remain to be elucidated (24).

Cardiometabolic Effects of Type 2 Diabetes Medication

In our study on the effect of liraglutide on ectopic fat in type 2 diabetes patients of South Asian origin residing in the Netherlands, we reported a liraglutide-related reduction in visceral adipose tissue, which was associated with improved glycemic control (Chapter 4). Liraglutide has consistently been documented to reduce body weight, with approximately three to four kilograms (25); however, some studies have described a reduction in visceral fat, while others have reported a decrease in subcutaneous fat (26-28). Interestingly, it has been documented that the glucose-lowering effects of liraglutide are pronounced in South Asian type 2 diabetes patients (29). Our study was the first that assessed the effects of liraglutide on specific fat compartments in type 2 diabetes patients of South Asian ethnicity. The results of this thesis show that liraglutide can be used for glucose regulation in South Asians, and that glucose control might be improved by reduction of visceral adipose tissue.

In contrast to the liraglutide-related improvement of glucose levels and reduction of visceral adipose tissue, liraglutide had no effect on diastolic function and myocardial tissue characteristics in Dutch South Asian type 2 diabetes patients (Chapter 5). Similarly, the liraglutide-placebo controlled trial in Dutch European type 2 diabetes patients did not reveal an improvement of myocardial relaxation parameters in response to liraglutide, although liraglutide was found

to reduce the left ventricular end-diastolic filling pressure (presumably due to vasodilation or diuretic effects) (30). Recent cardiovascular outcome trials have demonstrated that glucagon-like peptide 1 (GLP-1) receptor agonists have no benefit on the incidence of heart failure, in contrast to sodium-glucose cotransporter 2 (SGLT-2) inhibitors which have been shown to reduce hospitalization for heart failure (31,32). In our study, we did not observe amelioration of diastolic function, neither a reduction of the myocardial triglyceride content and myocardial extracellular volume, which are more sensitive cardiac measures than heart failure incidence. Therefore, from our results, together with those of other single-center studies (33,34), we may conclude that liraglutide does not reverse diabetic cardiomyopathy.

Since recently, guidelines have recommended GLP-1 receptor agonists and SGLT-2 inhibitors as part of type 2 diabetes management in patients with overt atherosclerotic disease, whereas in type 2 diabetes patients with manifest heart failure, SGLT-2 inhibitors may be considered (35). Although liraglutide has no beneficial effect on heart failure incidence, liraglutide remains worth considering in South Asian type 2 diabetes patients because of the unfavorable cardiometabolic profile and high risk of atherosclerotic disease within this group, as well as the efficacy of liraglutide for glycemic control and the reduction of visceral adiposity in South Asians, as demonstrated in this thesis. Interestingly, it has been speculated that a combination treatment of GLP-1 receptor agonists and SGLT-2 inhibitors might have synergistic benefits on atherosclerotic and non-atherosclerotic cardiovascular morbidity in type 2 diabetes, which might be investigated in future studies (36).

In our studies we explored the diabetic cardiomyopathy phenotype and assessed the effects of the antidiabetic agent liraglutide. However, lifestyle modifications in type 2 diabetes patients for the regression of diabetic cardiomyopathy have not been addressed in this thesis, although dietary and behavioral therapies may be more efficient for the prevention of type 2 diabetes and the reduction of cardiovascular risk factors (37). In a recent trial, intensive lifestyle intervention did not decrease the rate of cardiovascular events compared with standard type 2 diabetes support and education, but several other positive effects such as less use of cardiovascular medication and improved quality of life were reported in the lifestyle intervention group (38). There is a limited number of studies on the effects of health behavior on the incidence of cardiometabolic disease among different ethnic groups (39,40). Therefore, multi-ethnic studies on the efficacy of lifestyle modification in individuals at risk of type 2 diabetes and diabetic cardiomyopathy seem warranted.

Imaging-based Cardiovascular Risk Stratification after Pediatric Hematopoietic Stem Cell Transplantation

Currently, pediatric hematopoietic stem cell transplantation recipients are selected for patient-specific follow-up programs according to the risk of late complications, based on pre-existing comorbidities, pre-transplant exposures, the transplant-preparative regimen, post-transplant complications such as graft-versus-host-disease, or relapse of the primary

disease (41). There has been limited research on the value of imaging-based cardiovascular risk stratifiers after hematopoietic stem cell transplantation. The results in this thesis suggest that diastolic function parameters, rather than systolic strain, aortic pulse wave velocity, myocardial triglyceride content or native T1, may represent early markers of cardiovascular disease after pediatric hematopoietic stem cell transplantation (Chapter 6). Future longitudinal studies are needed to confirm the predictive value of diastolic function for the development of manifest cardiovascular disease. Also, comparative studies are required to assess the effectiveness of magnetic resonance for the selection of patients who may require frequent follow-up by standard echocardiography.

Imaging-based Cardiovascular Risk Stratification in Ischemic Cardiomyopathy

Patients with prior myocardial infarction are at risk of life-threatening ventricular arrhythmia. Currently, selection for primary prevention implantable cardioverter defibrillator (ICD) therapy is based on left ventricular ejection fraction, but in only 35% patients, ICD therapy is appropriate (42). Most studies have investigated the role of late gadolinium enhancement (LGE) scar characteristics in ventricular arrhythmia risk stratification, whereas in this thesis, we examined the association of cardiac function abnormalities with ventricular arrhythmia. Our results suggest that the extent of impaired systolic strain and the late diastolic strain rate may play a role in the pathogenesis of ventricular arrhythmia, possibly by promoting adverse cardiac remodeling (Chapter 8). This work was a hypothesis-generating study and longitudinal research is needed to demonstrate causality of the relation between functional parameters, adverse remodeling and subsequent ventricular arrhythmia in patients with prior myocardial infarction. Thus far, studies have not demonstrated additional prognostic value of novel imaging markers above left ventricular ejection fraction; yet, advanced imaging markers have not been adopted in current risk stratification guidelines. The complex pathogenesis of ventricular arrhythmia remains uncertain, and further research is required.

Future Role of Magnetic Resonance in Characterizing Cardiometabolic Disease

To date, heart failure in type 2 diabetes patients without coronary artery disease remains overlooked. Although reduced diastolic function in type 2 diabetes patients may be predictive of diabetic heart failure, it is also a characteristic of normal aging and it is related to other conditions than type 2 diabetes as well, such as hypertension. To facilitate the early recognition of diabetic heart failure, researchers should continue to search for markers that are specific for diabetic cardiomyopathy. Possibly, magnetic resonance methods may contribute not only to the mechanistic understanding of diabetic heart failure, but also to the establishment of improved diagnostic criteria for diabetic cardiomyopathy.

In recent cardiovascular outcome trials, the effects of new antidiabetic agents have been evaluated by assessment of the incidence of non-fatal myocardial infarction, stroke, cardiovascular-specific death and heart failure hospitalization. The approval of GLP-1 receptor

agonists and SGLT-2 inhibitors to reduce the risk of cardiovascular events in type 2 diabetes with established atherosclerotic disease has been unique in the history of type 2 diabetes management. Although cardiovascular outcome trials provide essential information on the long-term cardiovascular safety of novel antidiabetic drugs, imaging-based studies will remain important to elucidate the biological actions of glucose-lowering medication on the cardiovascular system.

Cardiac magnetic resonance methods continue to be improved. In our center as well, techniques for the assessment of diastolic function using 4D flow imaging and for myocardial tissue characterization including cardiac T1 mapping and proton-magnetic resonance spectroscopy (^{1}H-MRS) have been optimized over the past years. The ongoing advances in cardiac magnetic resonance may increase the potential of imaging-based risk stratification in cardiometabolic disease, and perhaps in the near future, magnetic resonance parameters may prove to provide additional value above current clinical measures in selected patient groups.

Interestingly, a growing number of population-based studies such as the UK Biobank, but also earlier studies such as MESA, contain a wide variety of detailed imaging-based phenotypic characteristics (22,43). As such, in the coming years, magnetic resonance methods seem to be increasingly exploited in large-scale research on human biology and, hopefully, this will add to the development of efficient personalized strategies for the prevention, but also the treatment of diabetic heart failure and other cardiometabolic diseases.

CONCLUSION

The results of this thesis demonstrate that reduced diastolic function is a common characteristic of myocardial remodeling in cardiometabolic diseases (Chapter 2, 3, 5 and 6) and a potential marker for the detection of patients at increased cardiovascular risk (Chapter 6 and 8). Our findings show that the evaluation of visceral adiposity and myocardial triglyceride content may help to identify distinct cardiometabolic phenotypes in obesity and type 2 diabetes (Chapter 2 and 3), and to better understand the cardiometabolic actions of antidiabetic agents (Chapter 4 and 5). Interestingly, in our study, the GLP-1 receptor agonist liraglutide reduced visceral adipose tissue in South Asian type 2 diabetes patients, but did not improve cardiac function. With the emergence of non-contrast cardiovascular protocols (Chapter 7), magnetic resonance techniques may be increasingly used for cardiometabolic phenotyping in population-based cohorts as well as clinical studies.

REFERENCES

1. Capaldo B, Di Bonito P, Iaccarino M, et al. Cardiovascular characteristics in subjects with increasing levels of abnormal glucose regulation: the Strong Heart Study. Diabetes Care 2013;36(4):992-997.
2. Skali H, Shah A, Gupta DK, et al. Cardiac structure and function across the glycemic spectrum in elderly men and women free of prevalent heart disease: the Atherosclerosis Risk In the Community study. Circ Heart Fail 2015;8(3):448-454.
3. Paulus WJ, Tschope C. A novel paradigm for heart failure with preserved ejection fraction: comorbidities drive myocardial dysfunction and remodeling through coronary microvascular endothelial inflammation. J Am Coll Cardiol 2013;62(4):263-271.
4. Bugger H, Abel ED. Molecular mechanisms of diabetic cardiomyopathy. Diabetologia 2014;57(4):660-671.
5. Boudina S, Abel ED. Diabetic cardiomyopathy revisited. Circulation 2007;115(25):3213-3223.
6. Borlaug BA, Redfield MM. Diastolic and systolic heart failure are distinct phenotypes within the heart failure spectrum. Circulation 2011;123(18):2006-2013; discussion 2014.
7. Seferovic PM, Paulus WJ. Clinical diabetic cardiomyopathy: a two-faced disease with restrictive and dilated phenotypes. Eur Heart J 2015;36(27):1718-1727, 1727a-1727c.
8. Pfeffer MA, Shah AM, Borlaug BA. Heart Failure With Preserved Ejection Fraction In Perspective. Circ Res 2019;124(11):1598-1617.
9. Parikh KS, Sharma K, Fiuzat M, et al. Heart Failure With Preserved Ejection Fraction Expert Panel Report: Current Controversies and Implications for Clinical Trials. JACC Heart Fail 2018;6(8):619-632.
10. Neeland IJ, Gupta S, Ayers CR, et al. Relation of regional fat distribution to left ventricular structure and function. Circ Cardiovasc Imaging 2013;6(5):800-807.
11. van Hout MJP, Dekkers IA, Westenberg JJM, Schalij MJ, Scholte A, Lamb HJ. The impact of visceral and general obesity on vascular and left ventricular function and geometry: a cross-sectional magnetic resonance imaging study of the UK Biobank. Eur Heart J Cardiovasc Imaging 2019.
12. Abbasi SA, Hundley WG, Bluemke DA, et al. Visceral adiposity and left ventricular remodeling: The Multi-Ethnic Study of Atherosclerosis. Nutr Metab Cardiovasc Dis 2015;25(7):667-676.
13. Shah RV, Abbasi SA, Heydari B, et al. Insulin resistance, subclinical left ventricular remodeling, and the obesity paradox: MESA (Multi-Ethnic Study of Atherosclerosis). J Am Coll Cardiol 2013;61(16):1698-1706.
14. Zile MR, Gottdiener JS, Hetzel SJ, et al. Prevalence and significance of alterations in cardiac structure and function in patients with heart failure and a preserved ejection fraction. Circulation 2011;124(23):2491-2501.
15. Marwick TH, Ritchie R, Shaw JE, Kaye D. Implications of Underlying Mechanisms for the Recognition and Management of Diabetic Cardiomyopathy. J Am Coll Cardiol 2018;71(3):339-351.
16. Yancy CW, Jessup M, Bozkurt B, et al. 2017 ACC/AHA/HFSA Focused Update of the 2013 ACCF/AHA Guideline for the Management of Heart Failure: A Report of the American College of Cardiology/American Heart Association Task Force on Clinical Practice Guidelines and the Heart Failure Society of America. J Am Coll Cardiol 2017;70(6):776-803.
17. Ernande L, Audureau E, Jellis CL, et al. Clinical Implications of Echocardiographic Phenotypes of Patients With Diabetes Mellitus. J Am Coll Cardiol 2017;70(14):1704-1716.
18. Rijzewijk LJ, van der Meer RW, Smit JW, et al. Myocardial steatosis is an independent predictor of diastolic dysfunction in type 2 diabetes mellitus. J Am Coll Cardiol 2008;52(22):1793-1799.
19. Rijzewijk LJ, van der Meer RW, Lamb HJ, et al. Altered myocardial substrate metabolism and decreased diastolic function in nonischemic human diabetic cardiomyopathy: studies with cardiac positron emission tomography and magnetic resonance imaging. J Am Coll Cardiol 2009;54(16):1524-1532.
20. Park CM, Tillin T, March K, et al. Hyperglycemia has a greater impact on left ventricle function in South Asians than in Europeans. Diabetes Care 2014;37(4):1124-1131.
21. Bank IEM, Gijsberts CM, Teng TK, et al. Prevalence and Clinical Significance of Diabetes in Asian Versus White Patients With Heart Failure. JACC Heart Fail 2017;5(1):14-24.
22. Bild DE, Bluemke DA, Burke GL, et al. Multi-Ethnic Study of Atherosclerosis: objectives and design. Am J Epidemiol 2002;156(9):871-881.

23. Tillin T, Forouhi NG, McKeigue PM, Chaturvedi N, Group SS. Southall And Brent REvisited: Cohort profile of SABRE, a UK population-based comparison of cardiovascular disease and diabetes in people of European, Indian Asian and African Caribbean origins. Int J Epidemiol 2012;41(1):33-42.
24. Stronks K, Snijder MB, Peters RJ, Prins M, Schene AH, Zwinderman AH. Unravelling the impact of ethnicity on health in Europe: the HELIUS study. BMC Public Health 2013;13:402.
25. Davies MJ, Bergenstal R, Bode B, et al. Efficacy of Liraglutide for Weight Loss Among Patients With Type 2 Diabetes: The SCALE Diabetes Randomized Clinical Trial. JAMA 2015;314(7):687-699.
26. Jendle J, Nauck MA, Matthews DR, et al. Weight loss with liraglutide, a once-daily human glucagon-like peptide-1 analogue for type 2 diabetes treatment as monotherapy or added to metformin, is primarily as a result of a reduction in fat tissue. Diabetes Obes Metab 2009;11(12):1163-1172.
27. Suzuki D, Toyoda M, Kimura M, et al. Effects of liraglutide, a human glucagon-like peptide-1 analogue, on body weight, body fat area and body fat-related markers in patients with type 2 diabetes mellitus. Intern Med 2013;52(10):1029-1034.
28. Bizino MB, Jazet IM, de Heer P, et al. Placebo-controlled randomised trial with liraglutide on magnetic resonance endpoints in individuals with type 2 diabetes: a pre-specified secondary study on ectopic fat accumulation. Diabetologia 2020;63(1):65-74.
29. Kim YG, Hahn S, Oh TJ, Park KS, Cho YM. Differences in the HbA1c-lowering efficacy of glucagon-like peptide-1 analogues between Asians and non-Asians: a systematic review and meta-analysis. Diabetes Obes Metab 2014;16(10):900-909.
30. Bizino MB, Jazet IM, Westenberg JJM, et al. Effect of liraglutide on cardiac function in patients with type 2 diabetes mellitus: randomized placebo-controlled trial. Cardiovasc Diabetol 2019;18(1):55.
31. Marso SP, Daniels GH, Brown-Frandsen K, et al. Liraglutide and Cardiovascular Outcomes in Type 2 Diabetes. N Engl J Med 2016;375(4):311-322.
32. Zelniker TA, Wiviott SD, Raz I, et al. Comparison of the Effects of Glucagon-Like Peptide Receptor Agonists and Sodium-Glucose Cotransporter 2 Inhibitors for Prevention of Major Adverse Cardiovascular and Renal Outcomes in Type 2 Diabetes Mellitus. Circulation 2019;139(17):2022-2031.
33. Nystrom T, Santos-Pardo I, Hedberg F, et al. Effects on Subclinical Heart Failure in Type 2 Diabetic Subjects on Liraglutide Treatment vs. Glimepiride Both in Combination with Metformin: A Randomized Open Parallel-Group Study. Front Endocrinol (Lausanne) 2017;8:325.
34. Lambadiari V, Pavlidis G, Kousathana F, et al. Effects of 6-month treatment with the glucagon like peptide-1 analogue liraglutide on arterial stiffness, left ventricular myocardial deformation and oxidative stress in subjects with newly diagnosed type 2 diabetes. Cardiovasc Diabetol 2018;17(1):8.
35. American Diabetes A. 10. Cardiovascular Disease and Risk Management: Standards of Medical Care in Diabetes-2020. Diabetes Care 2020;43(Suppl 1):S111-S134.
36. Hupfeld C, Mudaliar S. Navigating the "MACE" in Cardiovascular Outcomes Trials and decoding the relevance of Atherosclerotic Cardiovascular Disease benefits versus Heart Failure benefits. Diabetes Obes Metab 2019;21(8):1780-1789.
37. Diabetes Prevention Program Research G. Long-term effects of lifestyle intervention or metformin on diabetes development and microvascular complications over 15-year follow-up: the Diabetes Prevention Program Outcomes Study. Lancet Diabetes Endocrinol 2015;3(11):866-875.
38. Look Ahead Research Group, Wing RR, Bolin P, et al. Cardiovascular effects of intensive lifestyle intervention in type 2 diabetes. N Engl J Med 2013;369(2):145-154.
39. Admiraal WM, van Valkengoed IG, JS LdM, Stronks K, Hoekstra JB, Holleman F. The association of physical inactivity with Type 2 diabetes among different ethnic groups. Diabet Med 2011;28(6):668-672.
40. Eriksen A, Tillin T, O'Connor L, et al. The impact of health behaviours on incident cardiovascular disease in Europeans and South Asians--a prospective analysis in the UK SABRE study. PLoS One 2015;10(3):e0117364.
41. Chow EJ, Anderson L, Baker KS, et al. Late Effects Surveillance Recommendations among Survivors of Childhood Hematopoietic Cell Transplantation: A Children's Oncology Group Report. Biol Blood Marrow Transplant 2016;22(5):782-795.
42. Moss AJ, Greenberg H, Case RB, et al. Long-term clinical course of patients after termination of ventricular tachyarrhythmia by an implanted defibrillator. Circulation 2004;110(25):3760-

3765.
43. Bycroft C, Freeman C, Petkova D, et al. The UK Biobank resource with deep phenotyping and genomic data. Nature 2018;562(7726):203-209.

CHAPTER

10

Summary | List of publications | Curriculum vitae |
Nederlandse samenvatting | Dankwoord

SUMMARY

In the studies in this thesis, cardiovascular remodeling was characterized in individuals with type 2 diabetes of Dutch South Asian ethnicity, in young adults who received hematopoietic stem cell transplantation in childhood and in patients with ischemic heart disease, by using several cardiovascular magnetic resonance methods, including 2D and 4D flow imaging, feature tracking cine imaging, T1 mapping and proton-magnetic resonance spectroscopy (^{1}H-MRS).

Part I Type 2 Diabetes

Abnormalities in glucose regulation have been associated with reduced diastolic function, separately from excess body weight, but the relation of insulin resistance to cardiovascular remodeling, independent of excess adipose tissue, remained to be examined. Therefore, in **Chapter 2** we investigated the role of insulin resistance in the association of visceral, abdominal subcutaneous and total body fat with cardiovascular function. In this cross-sectional analysis of the prospective population-based Netherlands Epidemiology of Obesity (NEO) study, 914 middle-aged men and women were included. Several magnetic resonance methods were used, including standard cine imaging for the assessment of cardiac structure and systolic function, 2D velocity-encoded imaging to evaluate the transmitral diastolic flow rates and aortic pulse wave velocity and 2-point Dixon to quantify visceral and abdominal subcutaneous fat areas, whereas total body fat was assessed by bio-impedance analysis. In this study, insulin resistance was related to reduced diastolic function, separately from visceral and total body fat, and partly mediated the relations of the adipose tissue compartments to a lower diastolic function, suggesting that insulin resistance is involved in the pathogenesis of adiposity-related reduced diastolic function.

Little is known regarding the putative differences in diabetic cardiomyopathy among ethnicities. **Chapter 3** reports the results of a prospective cross-sectional case-control study in 131 individuals including type 2 diabetes patients and healthy controls of Dutch European and Dutch South Asian ethnicity. In addition to the magnetic resonance methods as used in Chapter 2, we performed 4D velocity-encoded imaging to examine diastolic function, and cardiac T1 mapping and ^{1}H-MRS to investigate myocardial tissue characteristics. Reduced diastolic function was a characteristic of diabetic cardiomyopathy in both South Asians and Europeans. However, we observed an increased cardiac mass solely in South Asian type 2 diabetes patients, while there we only differences in myocardial triglyceride content between type 2 diabetes patients and controls in the European study population. The findings of this study suggest that the impact of type 2 diabetes on cardiac remodeling may differ between subsets of type 2 diabetes patients, for example across ethnicities.

The glucagon-like peptide 1 (GLP-1) receptor agonist liraglutide is an antidiabetic drug with potential cardiometabolic benefits. In **Chapter 4 and 5**, we evaluated the effects of liraglutide on ectopic fat (including visceral, abdominal subcutaneous and total body fat, pericardial fat, and myocardial and hepatic triglyceride content) and cardiovascular function, in a 26-week randomized controlled trial in 47 Dutch South Asian type 2 diabetes patients. Liraglutide diminished the visceral fat volume, which was related to improved blood glucose levels. In contrast, liraglutide did not affect diastolic and systolic function, aortic stiffness, myocardial triglyceride content or myocardial extracellular volume. These results suggest that liraglutide has no effect on intrinsic myocardial function, in contrast to the reported benefits of liraglutide on cardiometabolic risk factors in type 2 diabetes patients.

Part II Pediatric Hematopoietic Stem Cell Transplantation

Imaging-based markers may help to identify individuals at increased risk of cardiovascular disease after hematopoietic stem cell transplantation in childhood. In **Chapter 6**, we evaluated cardiovascular function and myocardial tissue characteristics in 16 young adults who received pediatric hematopoietic stem cell transplantation and in 16 healthy controls. In the post-transplantation group, left ventricular end-diastolic filling pressure was increased and left ventricular ejection fraction and global longitudinal strain tended to be lower than in the controls, but there were no concomitant abnormalities in aortic stiffness, myocardial triglyceride content or native T1 relaxation times. These findings suggest that reduced diastolic function might be an early marker of transplant-related cardiovascular disease.

Part III Ischemic Heart Disease

Cardiac magnetic resonance has important clinical value, as late gadolinium enhancement (LGE) imaging enables the assessment of myocardial scar in patients with ischemic heart disease. However, LGE imaging relies on the administration of gadolinium-based contrast material. Interestingly, non-contrast techniques for myocardial tissue characterization are evolving, and, possibly, native T1 mapping might substitute LGE imaging. In **Chapter 7**, we provided an overview of the indications for contrast-enhanced and non-contrast cardiac and cardiac-related vascular magnetic resonance. In this review, we concluded that contrast material remains to be used in LGE imaging in ischemic (and non-ischemic) cardiomyopathy; however, the use of contrast material should be avoided in cardiac-related vascular magnetic resonance.

Most previous studies on risk stratification for ventricular arrhythmia after myocardial infarction have assessed the predictive value of myocardial scar characteristics, derived from LGE imaging. In contrast, in **Chapter 8**, we explored the association of cardiac function parameters,

derived from non-contrast magnetic resonance scans, with the risk of appropriate implantable cardioverter defibrillator (ICD) therapy, as surrogate marker of ventricular arrhythmia. In this retrospective analysis including 121 patients, the extent of moderately impaired strain and late diastolic strain rate were related to the risk of appropriate ICD therapy. These findings may suggest that disturbed myocardial contraction and relaxation might be involved in the pathogenesis of ventricular arrhythmia.

LIST OF PUBLICATIONS

Paiman EHM, de Mutsert R, Widya RL, Rosendaal FR, Jukema JW, Lamb HJ. The role of insulin resistance in the relation of visceral, abdominal subcutaneous and total body fat to cardiovascular function. ***Nutr Metab Cardiovasc Dis.*** 2020; in press. doi: 10.1016/j.numecd.2020.07.011.

van Eyk HJ, Paiman EHM, Bizino MB, IJzermans SJ, Kleiburg F, Boers TGW, Rappel EJ, Burakiewicz J, Kan HE, Smit JWA, Lamb HJ, Jazet IM, Rensen PR. Liraglutide decreases energy expenditure and does not affect the fat fraction of supraclavicular brown adipose tissue in patients with type 2 diabetes. ***Nutr Metab Cardiovasc Dis.*** 2020 Apr 12;30(4):616-624. doi: 10.1016/j.numecd.2019.12.005. Epub 2019 Dec 13.

Paiman EHM, van Eyk HJ, van Aalst MMA, Bizino MB, van der Geest RJ, Westenberg JJM, Geelhoed-Duijvestijn PH, Kharagjitsingh AV, Rensen PCN, Smit JWA, Jazet IM, Lamb HJ. Effect of liraglutide on cardiovascular function and myocardial tissue characteristics in type 2 diabetes patients of South Asian descent living in the Netherlands: a double-blind, randomized, placebo-controlled trial. ***J Magn Reson Imaging***. 2020 Jun;51(6):1679-1688. doi: 10.1002/jmri.27009. Epub 2019 Dec 4.

Bizino MB, Jazet IM, de Heer P, van Eyk HJ, Dekkers IA, Rensen PCN, Paiman EHM, Lamb HJ, Smit JW. Placebo-controlled randomised trial with liraglutide on magnetic resonance endpoints in individuals with type 2 diabetes: a pre-specified secondary study on ectopic fat accumulation. ***Diabetologia***. 2020 Jan;63(1):65-74. doi: 10.1007/s00125-019-05021-6. Epub 2019 Nov 5.

Paiman EHM, van Eyk HJ, Bizino MB, Dekkers IA, de Heer P, Smit JWA, Jazet IM, Lamb HJ. Phenotyping diabetic cardiomyopathy in Europeans and South Asians. ***Cardiovasc Diabetol***. 2019 Oct 11;18(1):133. doi: 10.1186/s12933-019-0940-z.

van Eyk HJ, Paiman EHM, Bizino MB, de Heer P, Geelhoed-Duijvestijn PH, Kharagjitsingh AV, Smit JWA, Lamb HJ, Rensen PCN, Jazet IM. A double-blind, placebo-controlled, randomised trial to assess the effect of liraglutide on ectopic fat accumulation in South Asian type 2 diabetes patients. ***Cardiovasc Diabetol***. 2019 Jul 9;18(1):87. doi: 10.1186/s12933-019-0890-5.

Paiman EHM, Androulakis AFA, Shahzad R, Tao Q, Zeppenfeld K, Lamb HJ, van der Geest RJ. Association of cardiovascular magnetic resonance-derived circumferential strain parameters with the risk of ventricular arrhythmia and all-cause mortality in patients with prior myocardial infarction and primary prevention implantable cardioverter defibrillator. ***J Cardiovasc Magn Reson***. 2019 May 16;21(1):28. doi: 10.1186/s12968-019-0536-5.

Bizino MB, Jazet IM, Westenberg JJM, van Eyk HJ, Paiman EHM, Smit JWA, Lamb HJ. Effect of liraglutide on cardiac function in patients with type 2 diabetes mellitus: randomized placebo-controlled trial. ***Cardiovasc Diabetol***. 2019 Apr 30;18(1):55. doi: 10.1186/s12933-019-0857-6. Erratum in: Cardiovasc Diabetol. 2019 Aug 9;18(1):101.

Androulakis AFA, Zeppenfeld K, Paiman EHM, Piers SRD, Wijnmaalen AP, Siebelink HJ, Sramko M, Lamb HJ, van der Geest RJ, de Riva M, Tao Q. Entropy as a novel measure of myocardial tissue heterogeneity for prediction of ventricular arrhythmias and mortality in post-infarct patients. ***JACC Clin Electrophysiol***. 2019 Apr;5(4):480-489. doi: 10.1016/j.jacep.2018.12.005. Epub 2019 Feb 27.

Paiman EHM, Louwerens M, Bresters D, Westenberg JJM, Tao Q, van der Geest RJ, Lankester AC, Roest AAW, Lamb HJ. Late effects of pediatric hematopoietic stem cell transplantation on left ventricular function, aortic stiffness and myocardial tissue characteristics. ***J Cardiovasc Magn Reson***. 2019 Jan 17;21(1):6. doi: 10.1186/s12968-018-0513-4.

Tao Q, Yan W, Wang Y, Paiman EHM, Shamonin DP, Garg P, Plein S, Huang L, Xia L, Sramko M, Tintera J, de Roos A, Lamb HJ, van der Geest RJ. Deep learning-based method for fully automatic quantification of left ventricle function from cine MR images: a multivendor, multicenter study. ***Radiology***. 2019 Jan;290(1):81-88. doi: 10.1148/radiol.2018180513. Epub 2018 Oct 9.

Dekkers IA, Paiman EHM, de Vries APJ, Lamb HJ. Reproducibility of native T1 mapping for renal tissue characterization at 3T. ***J Magn Reson Imaging***. 2019 Feb;49(2):588-596. doi: 10.1002/jmri.26207. Epub 2018 Sep 1.

Tao Q, van der Tol P, Berendsen FF, Paiman EHM, Lamb HJ, van der Geest RJ. Robust motion correction for myocardial T1 and extracellular volume mapping by principle component analysis-based groupwise image registration. ***J Magn Reson Imaging***. 2018 May;47(5):1397-1405. doi: 10.1002/jmri.25863. Epub 2017 Sep 27.

Paiman EHM, Lamb HJ. When should we use contrast material in cardiac MRI? ***J Magn Reson Imaging***. 2017 Dec;46(6):1551-1572. doi: 10.1002/jmri.25754. Epub 2017 May 8. Review.

van de Weijer T, Paiman EHM, Lamb HJ. Cardiac metabolic imaging: current imaging modalities and future perspectives. ***J Appl Physiol (1985)***. 2018 Jan 1;124(1):168-181. doi: 10.1152/japplphysiol.01051.2016. Epub 2017 May 4. Review.

van Nijnatten TJA, Schipper RJ, Lobbes MBI, van Roozendaal LM, Vöö S, Moossdorff M, Paiman ML, de Vries B, Keymeulen KBMI, Wildberger JE, Smidt ML, Beets-Tan RGH. Diagnostic performance of gadofosveset-enhanced axillary MRI for nodal (re)staging in breast cancer patients: results of a validation study. ***Clin Radiol***. 2018 Feb;73(2):168-175. doi: 10.1016/j.crad.2017.09.005. Epub 2017 Oct 10.

van Everdingen WM, Paiman ML, van Deursen CJ, Cramer MJ, Vernooy K, Delhaas T, Prinzen FW. Comparison of septal strain patterns in dyssynchronous heart failure between speckle tracking echocardiography vendor systems. ***J Electrocardiol***. 2015 Jul-Aug;48(4):609-16. doi: 10.1016/j.jelectrocard.2014.12.021. Epub 2014 Dec 31.

Schipper RJ, Paiman ML, Beets-Tan RG, Nelemans PJ, de Vries B, Heuts EM, van de Vijver KK, Keymeulen KB, Brans B, Smidt ML, Lobbes MB. Diagnostic performance of dedicated axillary T2- and diffusion-weighted MR imaging for nodal staging in breast cancer. ***Radiology***. 2015 May;275(2):345-55. doi: 10.1148/radiol.14141167. Epub 2014 Dec 15.

CURRICULUM VITAE

Before starting her PhD research at the department of Radiology at the Leiden University Medical Center (September 2014–August 2018), Marie-Louise Paiman (born in Leiderdorp, January 1988), studied Technical Medicine at Twente University (BSc degree cum laude, August 2009) and attended the master's program Physician-Clinical Investigator at Maastricht University (MD/MSc degree cum laude, August 2014). During her final master's internship at the department of Radiology and Surgery (Maastricht University Medical Center), she assisted in a clinical study on the diagnostic value of axillary magnetic resonance imaging in the work-up of breast cancer. Furthermore, she fulfilled an extracurricular medical internship at the department of Surgery in Suriname (Academic Hospital Paramaribo). During her PhD period, she presented the results of her studies at the annual Scientific Sessions of the Society of Cardiovascular Magnetic Resonance (SCMR) and the European Congress of Radiology (ECR).

NEDERLANDSE SAMENVATTING

In de afgelopen decennia is het aantal mensen met type 2 diabetes wereldwijd aanzienlijk toegenomen, wat hoofdzakelijk te verklaren is door de toename van overgewicht. Type 2 diabetes is gerelateerd aan verschillende aandoeningen, waaronder hartfalen en ischemische hartziekte. Ondanks grote verbeteringen op het gebied van cardiovasculaire preventie en behandeling blijft hartziekte een belangrijke oorzaak van sterfte en gezondheidsverlies.

Het doel van de studies in dit proefschrift 'Phenotyping Cardiometabolic Disease with magnetic resonance techniques' (Nederlandse titel: 'Fenotypering van Cardiometabole Ziekte met Magnetische Resonantie') was om meer inzicht te krijgen in de gevolgen van type 2 diabetes voor de functie, geometrie en weefselkarakteristieken van het hart, en meer te weten te komen over de cardiometabole effecten van de GLP-1 ('glucagon-like peptide 1') receptor agonist liraglutide (Deel I). Daarnaast was het doel om bij te dragen aan verbetering van de risicostratificatie voor cardiovasculaire ziekte na hematopoëtische stamceltransplantatie (Deel II) en voor ventriculaire aritmie gerelateerd aan ischemische hartziekte (Deel III).

Fenotypering van cardiometabole ziekte

In het begin van de twintigste eeuw werd het concept 'fenotype' geïntroduceerd, waarmee verwezen werd naar de uiterlijke verschijning van een organisme. Inmiddels wordt deze term gebruikt om alle waarneembare karakteristieken te beschrijven, waaronder de morfologie en fysiologie van inwendige organen tot op celniveau, maar ook gedragskenmerken en de manifestatie van ziekte. De term 'fenotypering' wordt ook steeds meer toegepast in het kader van epidemiologische studies. Door informatie over het fenotype te combineren met gegevens over het genotype en de omgevingsfactoren kan er inzicht verkregen worden in de mechanismen van het ontstaan van ziekte. In dit proefschrift hebben we radiologische fenotypering van het hart en de vetverdeling in het lichaam ingezet om meer te weten te komen over de karakteristieken van cardiometabole ziekten in verschillende patiëntgroepen.

In deze thesis verwijst de term 'cardiometabool' naar de relatie tussen stofwisseling en het hart en vaatstelsel. Type 2 diabetes is een belangrijke metabole oorzaak voor cardiovasculaire ziekte. Bij type 2 diabetes is niet alleen het risico op het ontwikkelen van een hartinfarct als gevolg van atherosclerose verhoogd, maar ook het risico op hartfalen door de directe effecten van type 2 diabetes. De veranderingen in het hart rechtstreeks door type 2 diabetes worden ook wel aangeduid met 'diabetische cardiomyopathie'. Ook medische behandelingen, bijvoorbeeld hematopoëtische stamceltransplantatie voor bloedziekte, kunnen oorzaak zijn voor metabole verstoringen, met hierdoor een hoger risico op cardiovasculaire ziekte. In deze thesis is diabetische cardiomyopathie bekeken bij mensen van Europees-Nederlandse en Hindostaans-Nederlandse afkomst. Ook zijn de fenotypische veranderingen van het hart onderzocht bij jongeren die hematopoëtische stamceltransplantatie hebben ontvangen op kinderleeftijd en bij patiënten met ischemische hartziekte.

Toegepaste magnetische resonantie technieken

Veelgebruikte beeldvormende technieken in de geneeskunde zijn CT ('computer tomography') en MRI ('magnetic resonance imaging'). Terwijl CT gebruik maakt van röntgenstraling, is MRI gebaseerd op het doen resoneren van waterstofatomen in het lichaam door radiofrequente golven, in een sterk magnetisch veld. Gezien de moleculaire samenstelling van weefsels in het lichaam van elkaar verschilt, relaxeren de waterstofatomen na de excitatie door een radiofrequente puls met verschillende snelheden terug naar de rusttoestand. Hierdoor ontvangt de scanner van elk weefsel andere signaalintensiteiten. In deze thesis hebben we niet alleen beeldvormende protocollen gebruikt, maar ook magnetische resonantie spectroscopie en kwantitatieve technieken. Door middel van spectroscopie kan de moleculaire samenstelling van weefsels bepaald worden. In de studies in deze thesis hebben we gekeken naar de hoeveelheid vet in organen op moleculair niveau, niet alleen in de lever maar ook in de hartspier. Ook door middel van kwantitatieve metingen van de relaxatietijden kan meer informatie verkregen worden over de samenstelling van het weefsel.

De volgende magnetische resonantie technieken zijn gebruikt in deze thesis: 'velocity-encoding' (2D en 4D 'flow imaging') en 'feature tracking cine imaging' voor het meten van de diastolische functie (relaxatie) en systolische functie (contractie) van het linker ventrikel van het hart, en cardiale 'T1 mapping' en 'proton-magnetic rensance spectroscopy' (^{1}H-MRS) voor het beoordelen van respectievelijk diffuse fibrose van het hart (diffuse verlittekening van de hartspier) en myocardiale steatose (vetstapeling in de hartspier).

Doelstellingen

Het overkoepelende doel van de studies in dit proefschrift was het karakteriseren van cardiovasculaire remodelering gerelateerd aan metabole verstoringen, door gebruik te maken van magnetische resonantie technieken. De hypothese van deze thesis was dat fenotypering op basis van beeldvorming kan bijdragen aan meer inzicht in de relatie tussen metabole factoren en de weefselkarakteristieken, geometrie en functie van het hart, en aan verbetering van de cardiovasculaire risicostratificatie van specifieke patiëntgroepen. In deze thesis hebben we het cardiovasculaire fenotype onderzocht in relatie tot type 2 diabetes en na behandeling met liraglutide (Deel I), na hematopoëtische stamceltransplantatie (Deel II) en bij ischemische hartziekte (Deel III).

Deel I Diabetes mellitus type 2

In Deel I van de thesis zijn radiologische technieken ingezet om meer te weten te komen over de kenmerken van hartziekte door type 2 diabetes, en om de effecten van het antidiabeticum liraglutide op de hartfunctie en de vetverdeling in het lichaam bij mensen met type 2 diabetes te onderzoeken.

Insulineresistentie is een belangrijke voorspeller voor type 2 diabetes. Eerdere populatieonderzoeken hebben laten zien dat voorstadia van type 2 diabetes gerelateerd zijn

aan verminderde diastolische functie, onafhankelijk van een te hoog lichaamsgewicht. De relatie tussen insulineresistentie en cardiovasculaire veranderingen, los van lichaamsvet, is echter onvoldoende onderzocht. In **Hoofdstuk 2** hebben we door middel van retrospectief populatieonderzoek in 914 mannen en vrouwen aangetoond dat insulineresistentie geassocieerd is met een verminderde diastolische functie, onafhankelijk van visceraal vet en totaal lichaamsvet. Ook hebben we laten zien dat insulineresistentie de relaties tussen de verschillende vetdepots en een verminderde diastolische functie deels medieert. Deze resultaten duiden erop dat insulineresistentie waarschijnlijk betrokken is bij het ontstaan van diastolische dysfunctie bij mensen met overgewicht.

Er is nog weinig onderzoek gedaan naar de eventuele verschillen in diabetische cardiomyopathie tussen etnische groepen, terwijl bekend is dat mensen van Hindostaanse afkomst over het algemeen een hoger risico hebben op cardiometabole ziekte. In **Hoofdstuk 3** worden de resultaten van prospectief patiënt-controle onderzoek beschreven, waaraan 131 mensen deelnamen. In deze studie was verminderde diastolische functie een karakteristiek van diabetische cardiomyopathie, zowel in Europees-Nederlandse als Hindostaans-Nederlandse patiënten. Er werd echter alleen een verschil in myocardiale vetstapeling tussen de type 2 diabetes groep en de controlegroep gezien in de Europees-Nederlandse populatie, terwijl er alleen een verhoogde massa van het linker ventrikel werd gemeten in de Hindostaans-Nederlandse type 2 diabetes groep. Deze bevindingen suggereren dat het effect van type 2 diabetes op cardiale remodelering mogelijk niet gelijk is voor alle subgroepen, en er bijvoorbeeld etnische verschillen bestaan.

Liraglutide is een bloedglucoseverlagend middel voor de behandeling van type 2 diabetes, met mogelijk een beschermend effect op het hart en de bloedvaten. In **Hoofdstuk 4 en 5** hebben we de effecten van liraglutide op de vetstapeling in het lichaam (waaronder visceraal, abdominaal subcutaan en totaal lichaamsvet, pericardiaal vet, en myocardiale en hepatische triglyceridegehaltes) en cardiovasculaire functie onderzocht, in een 26-weken durende gerandomiseerde placebo-gecontroleerde studie in 47 mensen van Hindostaans-Nederlandse afkomst met type 2 diabetes. Liraglutide verminderde het viscerale vet, en deze afname was geassocieerd met een verbeterde glucoseregulatie. Liraglutide had echter geen invloed op diastolische en systolische functie, aortastijfheid, myocardiale steatose en diffuse fibrose. Deze resultaten wijzen erop dat liraglutide geen effect heeft op de intrinsieke hartfunctie in type 2 diabetes patiënten, in tegenstelling tot de eerder beschreven voordelen van liraglutide op cardiometabole risicofactoren zoals hypertensie en lipidespiegels.

Deel II Hematopoëtische stamceltransplantatie op kinderleeftijd

In Deel II is radiologische beeldvorming gebruikt om markers te vinden die wijzen op een verhoogd cardiovasculair risico.

In **Hoofdstuk 6** hebben we in prospectief patiënt-controle onderzoek de cardiovasculaire functie en myocardiale weefselkarakteristieken onderzocht in 16 jongeren die op kinderleeftijd

hematopoëtische stamceltransplantatie hebben ontvangen voor een goedaardige of kwaadaardige bloedziekte en, ter vergelijking, in 16 gezonde controles. In de patiëntgroep was de linker ventrikel eind-diastolische druk hoger en de ejectiefractie en globale longitudinale strain niet-significant lager dan in de controlegroep, maar er waren geen bijkomende verschillen in aortastijfheid, myocardiaal triglyceridegehalte of natieve T1 relaxatietijden. Deze resultaten laten zien dat verminderde diastolische functie mogelijk een vroege aanwijzing is van cardiovasculaire ziekte na hematopoëtische stamceltransplantatie.

Deel III Ischemische hartziekte

Ook in Deel III is gekeken naar de mogelijkheden van beeldvorming voor de risicostratificatie voor cardiovasculaire ziekte.

In **Hoofdstuk 7** hebben we een overzicht gegeven van de verschillende indicaties voor cardiale en vasculaire magnetische resonantie met en zonder gebruik van contrastmiddel. 'Native T1 mapping' is een relatief nieuwe techniek en zou op termijn wellicht een alternatief kunnen vormen voor 'late gadolinium enhancement' (LGE) imaging, wat een veelgebruikte techniek in de kliniek is om littekenweefsel af te beelden na een hartinfarct. Conclusie van ons review was dat contrastmiddel nog steeds gebruikt dient te worden voor LGE imaging bij patiënten met ischemische (en niet-ischemische) cardiomyopathie, maar dat er geschikte niet-contrast alternatieven zijn voor vasculaire magnetische resonantie.

In **Hoofdstuk 8** hebben we gekeken naar de associatie tussen hartfunctie en het risico op ventriculaire aritmie in een retrospectieve analyse van 121 patiënten met ischemische hartziekte. In tegenstelling tot eerdere onderzoeken waarin littekenkarakteristieken op contrast-versterkte (LGE) magnetische resonantie werden bekeken, hebben we in deze studie gebruik gemaakt van parameters gebaseerd op magnetische resonantie technieken zonder contrast. In ons onderzoek waren zowel de uitgebreidheid van matige verslechtering in systolische strain als de late diastolische strain gerelateerd aan het risico op ventriculaire aritmie. Deze bevindingen suggereren dat een verstoorde myocardiale contractie en relaxatie mogelijk betrokken zijn in de pathogenese van ventriculaire aritmie na een hartinfarct.

Conclusies

De bevindingen in deze thesis laten zien dat verminderde diastolische functie een generieke verandering is bij type 2 diabetes en overgewicht, maar ook een potentiële marker voor de detectie van patiënten met een verhoogd risico op cardiovasculaire ziekte na hematopoëtische stamceltransplantatie en een mogelijke factor in het ontstaan van ventriculaire aritmie bij ischemische hartziekte. Verder blijkt dat de GLP-1 receptor agonist liraglutide bij mensen met type 2 diabetes van Hindostaans-Nederlandse afkomst, een hoogrisicogroep voor cardiometabole ziekte, weliswaar het viscerale vet doet verminderen, maar dat liraglutide geen verbetering geeft in hartfunctie. Tegelijkertijd volgt uit deze thesis dat zowel visceraal vet als vetstapeling in de hartspier ongunstig is voor het risico op cardiale ziekte. Nader onderzoek

met magnetische resonantie naar hartfunctie en ectopische vetstapeling is daarmee niet alleen waardevol voor het verkrijgen van inzicht in de cardiometabole effecten van antidiabetica, maar het zou tevens kunnen bijdragen aan de differentiatie van de verschillende cardiometabole fenotypen bij type 2 diabetes en overgewicht.

Vooralsnog blijft de herkenning en behandeling van hartfalen door de directe effecten van type 2 diabetes een uitdaging. Diastolische dysfunctie bij type 2 diabetes is een voorspeller voor hartfalen, maar vermindering van diastolische functie vindt ook plaats bij normale veroudering en is tevens gerelateerd aan andere cardiovasculaire risicofactoren zoals hypertensie. Voor vroegtijdige herkenning van hartfalen door type 2 diabetes zijn daarom nieuwe markers nodig die specifiek zijn voor diabetische cardiomyopathie. Mogelijk kan magnetische resonantie, bijvoorbeeld via weefselkarakterisatie van het hart, in de toekomst niet alleen bijdragen aan meer inzicht in het ontstaan van niet-ischemisch hartfalen bij type 2 diabetes, maar ook aan verbeterde diagnostiek van diabetische cardiomyopathie.

Voor de toepassing van nieuwe geneesmiddelen in de behandeling van type 2 diabetes zijn cardiovasculaire uitkomststudies essentieel. Uit recente trials volgde dat GLP-1 receptor agonisten en SGLT-2 ('sodium-glucose cotransporter 2') remmers voordelen leken te hebben bij patiënten met een verhoogd cardiovasculair risico, wat een unieke bevinding is, en inmiddels zijn deze geneesmiddelgroepen opgenomen in de richtlijnen van de American Diabetes Association (ADA) en de European Association for the Study of Diabetes (EASD). Alhoewel deze cardiovasculaire uitkomststudies noodzakelijke informatie bieden over de cardiovasculaire veiligheid van nieuwe bloedglucoseverlagende middelen, zullen beeldvormende studies belangrijk blijven voor onderzoek naar de biologische werking van antidiabetica op het cardiovasculaire systeem.

Cardiale magnetische resonantie technieken zoals '4D flow imaging', 'T1 mapping' en ^{1}H-MRS worden voortdurend doorontwikkeld. Deze technische verbeteringen zorgen ervoor dat magnetische resonantie steeds meer potentieel ontwikkelt voor risicostratificatie bij cardiometabole ziekte. Een toenemend aantal populatiestudies zoals de UK Biobank of MESA maakt inmiddels gebruik van gedetailleerde fenotypering via beeldvormende technieken. Mede gezien de ontwikkeling van cardiovasculaire protocollen zonder contrastmiddel zal magnetische resonantie in de toekomst waarschijnlijk steeds vaker ingezet worden voor cardiometabole fenotypering, zowel in populatieonderzoek als in klinische studies, en hopelijk zal dit bijdragen aan de ontwikkeling van 'geneeskunde op maat', niet alleen in de behandeling van hartfalen bij type 2 diabetes of andere cardiometabole ziekten, maar ook in de preventie.

DANKWOORD

Graag zou ik iedereen willen bedanken die heeft bijgedragen aan de totstandkoming van dit proefschrift: alle studiedeelnemers, mijn promotor en copromotores, collega-onderzoekers, alle coauteurs, de studenten die betrokken zijn geweest bij het onderzoek, familie en vrienden, en natuurlijk Daan.

Malou Paiman
6 april 2020